



**Uniwersytet Morski w Gdyni**  
**Wydział Mechaniczny**  
**Katedra Podstaw Techniki**



## **ROZPRAWA DOKTORSKA**

# **Influence of the numerical modelling methods on dispersions and errors of analysis results in chosen marine machines and structures**

**Promotor:**

**dr hab. inż. Lech Murawski**

**Promotor pomocniczy:**

**dr hab. inż. Hoang Nguyen**

**Pracę wykonał:**

**mgr inż. Đỗ Văn Đoàn**

# TABLE OF CONTENT

<b>Acknowledgment</b> .....	4
<b>Summary of the dissertation</b> .....	5
<b>1. Introduction</b> .....	9
1.1. Background and motivation.....	9
1.2. Thesis, purpose, and scope of work.....	13
1.3. Methodology of research.....	14
1.3.1. Numerical modelling method.....	16
1.3.2. Measurement position and measurement methodology.....	30
1.4. Summary of the results obtained.....	33
1.5. The layout of this dissertation.....	35
<b>2. Ship safety hazards and their prevention</b> .....	36
2.1. Loads and strength of ships.....	36
2.1.1. Ship structural loads.....	38
2.1.2. Strength of ships.....	40
2.1.3. Ship structures review.....	41
2.2. Ship vibration.....	42
2.2.1. Hull structure vibration.....	43
2.2.2. Vibration of major substructures.....	45
2.2.3. Vibration of main propulsion machinery.....	46
2.3. Simplified, analytical formulas for ship vibrations determination.....	53
2.3.1. Empirical formula for natural bending frequency of thin-walled beams..	53
2.3.2. Calculation formula of natural frequency of ship's vertical vibration....	54
2.4. Structural failures of marine structures.....	56
2.4.1. Structural failure causes.....	57
2.4.2. Failure mechanisms.....	57
2.4.3. Failure analysis and fatigue assessment.....	58
2.4.4. Ship failures.....	59
2.4.5. Tools used for failure analysis.....	60
2.5. Non-destructive testing and structural health monitoring.....	61
2.5.1. Non-destructive testing.....	61
2.5.2. Structural health monitoring.....	62
2.5.3. Structural health monitoring for ship Structures.....	64
<b>3. Numerical modelling for some of the local hull structures</b> .....	67
3.1. Study the vibration of the beams.....	68
3.1.1. Frequency of free vibration of beams in theory.....	69
3.1.2. Frequency of free vibration of the undamaged beam by numerical modelling .....	72
3.1.3. Frequency of free vibration of the damaged beam by numerical modelling .....	74
3.1.4. Comparison between theoretical method and numerical modelling method.....	76
3.2. Analysis the vibration of the thin plate.....	79
3.2.1. Numerical modelling of the thin plate.....	79

3.2.2.	Verify the results of numerical modelling of the real thin plate.....	88
3.3.	Study the vibrations of the stiffened plates.....	92
3.3.1.	Numerical modelling of the stiffened plate.....	93
3.3.2.	Verify the results of numerical modelling of the real stiffened plate.....	101
3.4.	Conclusions.....	105
<b>4.</b>	<b>Numerical modelling of ship hull and superstructure.....</b>	<b>106</b>
4.1.	The free vibration of ship hull and superstructure.....	108
4.1.1.	Empirical calculation procedures.....	108
4.1.2.	Natural vibration analysis of the ship hull.....	110
4.1.3.	Natural vibration analysis of the deckhouses structure.....	117
4.1.4.	Compare the natural vibration frequencies of different size container ships.....	121
4.1.5.	Ship hull vibration threaten using hull resonance diagram.....	124
4.2.	Forced vibration analysis.....	127
4.2.1.	The unbalanced excitation forces and moments of the main engine.....	128
4.2.2.	The forced vibrations with propeller hydrodynamic forces.....	138
4.2.3.	The forced vibrations with pressure impulses on the transom.....	141
4.2.4.	The total excitation forces from the main engine and the propeller.....	145
4.3.	Vibration limits for crew, passengers and local structures.....	149
4.4.	Conclusions.....	154
<b>5.</b>	<b>The operating parameter characteristics of the drive system.....</b>	<b>155</b>
5.1.	Stiffness characteristics of the ship's hull.....	157
5.2.	Shaft line alignment.....	171
5.2.1.	Influence of assumptions on the alignment of the shaft line.....	174
5.2.2.	Analysis of a typical propulsion system.....	177
5.2.3.	Analytical the shaft line alignment for measurement authentication.....	182
5.3.	Dynamic shaft line alignment.....	184
	<b>Conclusions and objectives of further research.....</b>	<b>187</b>
	<b>References.....</b>	<b>189</b>
	<b>List of figures.....</b>	<b>189</b>
	<b>List of tables.....</b>	<b>201</b>

## **Acknowledgment**

First of all, I would like to express my deep gratitude to my supervisor - Professor Lech Murawski for all the things he helped and supported me during the time I prepared this dissertation. I not only learned professional knowledge from my professor but also received the love and care of him like my family members for me. I could never successfully complete this job without his guidance. He was always there to listen, advise and encourage me to finish my work. I would also like to express my deep gratitude to Professor Hoang Nguyen - co-supervisor, who was always beside, motivating, encouraging, sharing his research experience and working in Poland for me, especially for Vietnamese. I do not forget to thank other colleagues in Professor's group who despite their overload work, with kindness and patience, have helped me a lot to conducted measurement experiments and providing invaluable assistance when working on specific software - numerical models and vibration calculations of chosen marine machinery and structures.

I am grateful to the Rectors - Professor Janusz Zarębski, Professor Ireneusz Czarnowski, and Professor Henryk Śniegocki and the staff of administrators of the Gdynia Maritime University for their enthusiastic help in the matters concerning my residence and accommodation in Poland. I also thank the Deans - Professor Andrzej Miszczak and Professor Adam Charchalis, professors and lecturers of the Marine Engineering Department for their kind help. Their open and friendly attitude has helped me feel as if I was working in my own department.

I also wish to thank all members of my extended family who always supported me in my work. I am grateful to all my friends who made my stay at Gdynia enjoyable. Last but not least, I send extremely hot thoughts to my wife Lê Thị Giang, who patiently endures both mental and physical inconvenience due to my frequent absences. The person who helped me raises and takes care of my two sons so that I can be assured to study in Poland. Only friendly and loving people can endure, sacrifice and overcome these difficult obstacles. I could not have completed this work without her support, love, and faith.

# Summary of the dissertation

## Influence of the numerical modelling methods on dispersions and errors of analysis results in chosen marine machines and structures

### Summary

A ship is a special device, operating independently on the sea, in extremely harsh conditions. Therefore, safety, durability, and vibration requirements are always a top priority when designing and manufacturing ships to reduce the risk of accidents that may cause damage to people and cargo. The basic question always raises how to design the details of marine machines and structures to meet basic safety criteria in different working conditions and environments. Initially, the solution to the problems of strength endurance, vibration was based on trial and error. But in recent times, the maritime field has been rapidly developing, structures are becoming more complex, and previous experience is no longer sufficient. In shipbuilding, classification societies have been established to form sets of rules - an empirical relationship that determines the extreme values of the main parameters of the structure. Almost parallel to the development of methods of analysis based on empirical relationships, progress is being made on the in-depth understanding of the physics of the phenomena we are interested in and the development of the mathematical description of these phenomena. The model of a device is described using a mathematical model that is usually simplified and saved using computerized procedures. The numerical modelling method is widely applied, but the degree of reliability, the effect of errors and the dispersion of the analysis results is unknown in detail for marine structures. In the dissertation the sources of calculation errors and the size of results desperations were considered of the modelling marine objects.

The basic method for reducing analysis error and dispersion is the use of correlation and mutual support between the numerical modelling method and the measurement method. In the doctoral thesis, the causes of computational errors and dispersion results are considered, depending on the model of the chosen marine machines and structures. Methods to minimize them are also analysed. The influence of computational conditions such as boundary conditions, density of meshing, type of finite elements, etc. on calculation imperfections are considered. The assessments are based on a comparison between results obtained from a numerical model and results obtained based on a number of empirical formulas verified by measurement methods. Based on the obtained results, the author asserts that the thesis has solved some initial contents of the thesis as follows:

1. Mathematical models of the small basic parts that make up the hull and superstructure such as beams, thin plates, stiffened plates has built. Analysis of selected structures takes into account factors that may cause errors and dispersion in calculations such as boundary conditions, density and finite element type to be applied. The structures are also calculated and analysed in two cases of liquid contact and non-liquid contact. The results obtained are compared with the results from some experience formulas and verified by a measurement method based on the measurements performed in the laboratory of Gdynia Maritime University.
2. Building the mathematical model for two container vessels of different sizes: an average container ship of 2000 TEU and a large container ship of 11400 TEU. One of

the most important parameters analysed is the ship's vibration. Global vibrations of the entire hull and local vibrations of the superstructure and main engine body are determined. The results obtained by numerical models are compared with the empirical formulas given by Brown and F. M. Lewis and F. H. Todd and some other authors. Since then, confirming the accuracy and advantages of the numerical modelling method based on the finite element method, the ability to applied numerical modelling methods to other structures in the maritime field. The reliability and confidence of engineering calculations was improved when applying numerical modelling methods for structural calculations and analysis.

3. Finally, the author has applied the numerical modelling method to the ship's propulsion system. The mathematical models for the ship's propulsion system with many different assumptions are built, choosing the most optimal ship propulsion model. Determined (point 2) stiffness of ship hull is used as the boundary conditions of power transmission system. Apply the most optimal mathematical model of the ship propulsion system to analyse and align the shaft line of the typical ship propulsion system. Static and dynamic calculations analysis of the propulsion system are carried out and compared with allowed values.

In the world's marine literature, there are a number of works confirming the occurrence of high errors and dispersions of computational analysis and measurement tests. Particularly the legitimacy of using numerical calculations seems to be limited due to their low level of confidence. The author has developed a number of calculation methods that allow a rational reduction of the levels of calculation errors, to an acceptable level while limiting the workload of numerical analysis. Within the dissertation obtained the following results:

1. The impact of calculation assumptions on errors and dispersion of analysis results in individual types of analyses (static, normal modes, forced vibrations) was estimated.
2. An optimal methodology for carrying out computational analyzes using the finite element method was developed for the ship's hull structure (including its superstructure and main engine body), taking into account the purpose of the calculations (static strength calculations, vibration analysis, thermal calculations, etc.).
3. An optimal methodology for conducting calculations using the finite element method was developed for the ship's power transmission system, taking into account the purpose of the calculations.
4. The developed calculation methods were verified by comparing them with experimental tests of selected elements of ship systems, together with determining the levels of measurement dispersions.

The author has proved that it is possible to limit dispersions and errors in numerical modelling of the marine structures and machines to an acceptable level and consistent with empirical research.

# **Wpływ metod modelowania numerycznego na rozrzuty i błędy analiz obliczeniowych wybranych urządzeń i konstrukcji okrętowych**

## **Streszczenie**

Statek to specyficzny wytwór ludzki, działający niezależnie na morzu w ekstremalnie trudnych warunkach środowiskowych. Z tego powodu wymogi bezpieczeństwa, wytrzymałości i odporności na drgania są najwyższym priorytetem przy projektowaniu i produkcji statków, tak aby zmniejszyć ryzyko wypadków, które mogą spowodować szkody dla ludzi i ładunku. Podstawowym pytaniem zawsze było jak w szczegółach zaprojektować konstrukcję morską, aby spełniała podstawowe kryteria bezpieczeństwa w różnych warunkach pracy. Początkowo rozwiązanie problemów wytrzymałościowych (statycznych i dynamicznych) opierano na podstawie prób i błędów. Ostatnimi czasami, rozwój przemysłu okrętowego gwałtownie przyspieszył. Konstrukcje okrętowe stają się coraz bardziej złożone i wcześniejsze doświadczenia projektowe już nie wystarczają. W budownictwie okrętowym, towarzystwa klasyfikacyjne ustalają specjalne zbiory przepisów, które opierają się głównie o empiryczne formuły, ustalające dopuszczalne wartości głównych parametrów konstrukcji. Równoległe z opracowywaniem metod analiz opartych na zależnościach empirycznych, poczyniono postępy w zakresie dogłębnego zrozumienia fizyki zjawisk, którymi jesteśmy zainteresowani, oraz opracowywania matematycznego opisu tych zjawisk. Urządzenia są opisywane modelami matematycznymi, który są zwykle upraszczane i zapisywane przy użyciu skomputeryzowanych procedur. Metody modelowania numerycznego są szeroko stosowane, ale stopień ich wiarygodności, wielkość błędów i rozrzutów wyników analiz nie jest szczegółowo znany w przypadku konstrukcji morskich.

Podstawową metodą, która pozwala na ograniczenie błędów i rozrzutów analiz jest wzajemna korelacja obliczeniowo-pomiarowa. W pracy doktorskiej rozważono przyczyny błędów i rozrzutów obliczeniowych w zależności od typu modelu wybranych maszyn i konstrukcji morskich. Rozważono również metody minimalizacji tych błędów. Zbadano wpływ różnych założeń obliczeniowych, takich jak warunki brzegowe, gęstość siatki, typów użytych elementów skończonych itp., na niedoskonałości wyników analiz. Ocena wyników opiera się na porównaniu rezultatów uzyskanych z modelu numerycznego z danymi uzyskanymi na podstawie szeregu zależności empirycznych, zweryfikowanych metodami pomiarowymi. Na podstawie uzyskanych wyników autor stwierdza, że rozprawa udowodniła początkowe założenia rozprawy. W szczególności wykonano:

1. Zbudowano modele matematyczne podstawowych części konstrukcji okrętowej, które składają się na kadłub i nadbudówkę, takich jak belki, cienkie płyty, płyty usztywnione. Analiza wybranych elementów uwzględnia czynniki, które mogą powodować błędy i rozrzuty obliczeń, takie jak warunki brzegowe, gęstość i rodzaj elementów skończonych. Badane modele były analizowane w dwóch przypadkach: z oddziaływaniem i bez oddziaływania wody. Wyniki obliczeń numerycznych były porównywane z wynikami wybranych zależności empirycznych a następnie weryfikowane badaniami pomiarowymi wykonanymi w laboratorium Uniwersytetu Morskiego w Gdyni.
2. Wykonano modele matematyczne dwóch kontenerowców o różnej wielkości: średniej wielkości statku o nośności 2000 TEU oraz dużego statku o nośności 11400 TEU.

Analizowano jeden z ważniejszych parametrów statków - drgania. Wyznaczono drgania globalne kadłuba oraz drgania lokalne nadbudówki i korpusu silnika głównego. Wyniki obliczeń numerycznych zostały porównane z zależnościami empirycznymi opracowanymi przez Brown, F. M. Lewis i F. H. Todd oraz niektórymi innymi autorami. Potwierdzono dokładność i zalety metody modelowania numerycznego opartego na metodzie elementów skończonych. A następnie zbadano możliwość zastosowania opracowanych metod modelowania do innych konstrukcji w branży okrętowej. Poprawiono niezawodność i pewność obliczeń inżynierskich, podczas stosowania metod modelowania numerycznego do obliczeń i analiz strukturalnych.

3. W końcowej części pracy autor zastosował modelowanie numeryczne do okrętowego układu napędowego. Zbudowano modele matematyczne układu napędowego z wykorzystaniem wielu różnych założeń. A następnie wybrano najkorzystniejszy model do obliczeń rozważanego układu. Wyznaczoną (wg punktu 2) sztywność kadłuba statku wykorzystano jako warunki brzegowe układu przeniesienia mocy. Zastosowano optymalny matematyczny model do analizy ułożenia linii wałów typowego okrętowego układu napędowego. Przeprowadzono statyczne i dynamiczne analizy obliczeniowe układu napędowego i porównano uzyskane wyniki z wielkościami dopuszczalnymi.

W literaturze światowej istnieje szereg prac potwierdzających występowanie tak wysokich błędów i rozrzutów wyników analiz obliczeniowych, że ich zasadność stosowania (poziom ufności) wydaje się być ograniczona. Autor opracował szereg metod obliczeniowych, które pozwalają na racjonalne obniżenie błędów obliczeniowych do akceptowalnego poziomu przy jednoczesnym ograniczeniu pracochłonności analiz numerycznych. W ramach prezentowanej rozprawy uzyskano następujące wyniki:

1. Oszacowano wpływ założeń obliczeniowych na błędy i rozrzuty wyników analiz w poszczególnych typach analiz (statyka, drgania własne, drgania wymuszone).
2. Opracowano optymalną metodologię przeprowadzania analiz obliczeniowych metodą elementów skończonych, dla konstrukcji kadłuba statku (wraz z jego nadbudówką i korpusem silnika głównego) z uwzględnieniem celu obliczeń (obliczenia wytrzymałości statycznej, analizy drgań, obliczenia termiczne itp.).
3. Opracowano optymalną metodologię przeprowadzania analiz obliczeniowych metodą elementów skończonych, dla okrętowego układu przeniesienia napędu z uwzględnieniem celu obliczeń.
4. Zweryfikowano opracowane metody obliczeń poprzez porównanie ich z badaniami eksperymentalnymi wybranych elementów układów okrętowych, wraz z określeniem poziomów rozrzutów pomiarowych.

Zdaniem autora udowodniono, że możliwe jest ograniczenie rozrzutów i błędów modelowania numerycznego konstrukcji i urządzeń okrętowych do akceptowalnego poziomu, tak żeby wyniki obliczeń były zgodne z badaniami pomiarowymi.

### **1. Introduction**

The maritime industry, including the shipbuilding industry in particular, plays a great role in the development of the world economy. Maritime transport is essential to the world's economy as over 90% of the world's trade is carried by sea and it is, by far, the most cost-effective way to move massive goods and raw materials around the world. With the rapid development of the maritime industry, the structures and machines have become increasingly large, modern and more complex. Along with the rapid development of computer technology, computational methods and numerical models have been applied in the design and manufacture of maritime structures and machines to ensure the strict requirements of durability, safety, and reliability as well as cost savings. But the reliability level, as well as the confidence of engineers when applying the numerical modelling method, is still limited. In this chapter, the author will discuss the background and motivation of the thesis, purpose, and scope of work, the methodology of research.

#### **1.1. Background and motivation**

Since the dawn of history, humanity has built more and more complex machines, devices and constructions (from simple machines such as levers, inclined plane...to more complex machines such as steam engines, diesel engines, nuclear engines...). Along with the development of machinery, the durability and reliability of these products also play an extremely important role and higher requirements for many reasons: from economics to human safety. The basic question has always been how to design structures and machines to meet basic safety criteria in different working conditions. Initially, the solution to the durability and reliability problems were based on trials and errors. Often, it was multi-generational work - knowledge was handed down "from father to son". However, the last 200-300 years are characterized by such a significant acceleration in the degree of development and complexity of the structures that the previous experiences have ceased to be sufficient. Maritime accidents often occur when people apply the experience unsuitable. This leads to a waste of resources and the safety of the crew. From that fact, shipbuilders have created classification societies that make up the set of rules - empirical relationships that define the extreme values of key structural parameters. Beginning to collect and generalize technical experience in a set of rules containing relatively simple empirical relationships describing the details of a device or structure. Not all issues can be generalized using simple empirical patterns. An example is the dynamics of ship structures; the rules of classification societies only set out general guidelines on how the level of vibration should be unchecked and what methods to analyse them. Almost parallel, to the development of analytical methods based on empirical relationships, analysis based on the in-depth understanding of the physics of the phenomena is also done. These physical phenomena are described under mathematical relationships for analysis. Analytical relationships are mostly based on linear and nonlinear differential equations. Despite the increasing complexity of these relationships, they are usually useful only for the description of relatively simple phenomena. Moreover, their solution is often impossible by analytical methods. Therefore, numerical methods have become indispensable for the analysis and testing of complex structures and components. There has also been the development of measuring techniques that check the structures and devices. Structural measurements are often irreplaceable. However, these methods are not

effective and expensive because they require the construction of many prototypes and/or models. In fact, empirical research to examine and evaluate marine structures is not always feasible, because too costly in terms of time, money, effort such as aerodynamic experiments of the engine, collision test, ship manoeuvring, vibration test and balance of deck beams, hull beams, hatch covers, shafts. For example, when testing the speed and manoeuvrability of sea-going ships, it may require model pools longer than 200 m.

Since the invention of computers, the ability to model devices and structures have been applied and developed - numerical models have begun. Nowadays, along with the development of computer science, numerical modelling methods have become useful solutions to solve the above problems. The numerical modelling is becoming an indispensable tool in the technical issues from the simulation, design, test, evaluation, and plays an increasingly large role in all fields of science, life, especially in the maritime field. The physical model of a marine structure is described using a mathematical model that is often simplified and processed on a computer by numerical software. There are many methods of numerical modelling, starting with the finite difference method, the boundary element method, the finite element method, the meshless, the weight residue or the energy method. The modelling process for real objects along with model verification is shown in Fig. 1.1.

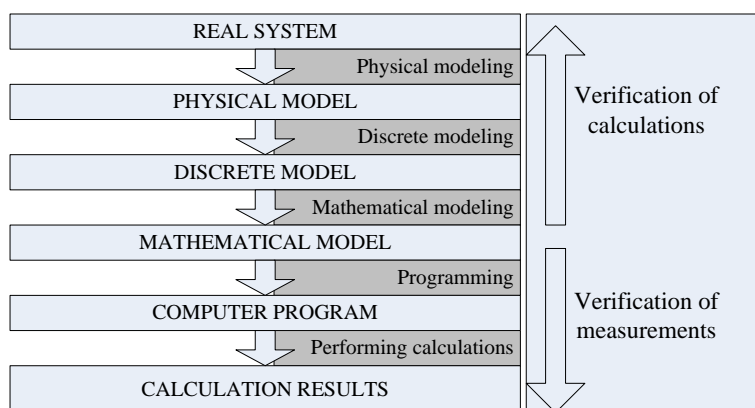


*Fig. 1.1. Modelling of real objects with their verification*

Although the method of numerical modelling is a technical tool extremely useful, indispensable in the field of science and technology. But modelling method is a method of approximation, so when using the numerical model method for calculating will lead to some errors and dispersions in the analysis results. There are many papers, scientific works acknowledge and study about the errors, dispersions of the numerical model to the results of analysis, specifically, the analysis by J. Priksaitisa et al. influence of the numerical dispersion effects in the modelling of ultrasonic measurements [86], numerical dispersion error in the finite element methods, O. Weckner, G. Brunk [110], modified integration rules for reducing dispersion error in finite element methods, M. N. Guddati and et al. [45], reduction of numerical dispersion in finite difference time domain (FDTD) method through artificial anisotropy, J. S. Juntunen and et al [57]. These documents refer to errors and dispersions in the results of the analysis when applying numerical modelling. Their applicability (degree of confidence) seems to be limited. This affects the confidence of engineers and designers when applying numerical methods for computation and structural analysis, especially among practice engineers, as illustrated in Fig. 1.2. It is true that measurements may also be subject to a number of errors and dispersions depending on the technique used. Measurement errors

are a problem for another job. In the proposed doctoral dissertation, the causes of computational errors and dispersions results will be considered depending on the modelling of chosen marine machines and structures.

**NO ONE BELIEVES IN THE CALCULATIONS APART FROM THE ONE WHO'S CALCULATING  
EVERYONE BELIEVES IN THE MEASUREMENTS APART FROM THE ONE WHO'S MEASURING**

*Fig. 1.2. A frequent view of engineers for computational and measurement errors*

The appearance and effect of errors and dispersions on the results of the analysis is described in detail by the International Ship and Offshore Structures Congress (ISSC). The ISSC has repeatedly and thoroughly investigated the problems of error and scattering of computational analysis. In one committee (Dynamic Response Committee, 16<sup>th</sup> edition of the ISSC) has done calculations on the water tank empty and partially filled with water to evaluate the influence of dispersions and errors on the analysis results. Calculations were conducted independently by experienced members of the committees from Great Britain, Germany, Italy, Japan, China, France, Turkey, and Poland. The first results showed an extremely large difference between the calculations of forced vibrations of the tanks; the results of the analysis are shown in Fig. 1.3. Only after defining the assumptions and calculation methods, the compatibility between the results of the members was much better. In particular, the identification of errors and the dispersion between measurements and numerical analysis (FEM) is shown in Fig. 1.4 of the Germanische Lloyd. Differences in the amplitude of forced vibrations reach even 3 orders of magnitude.

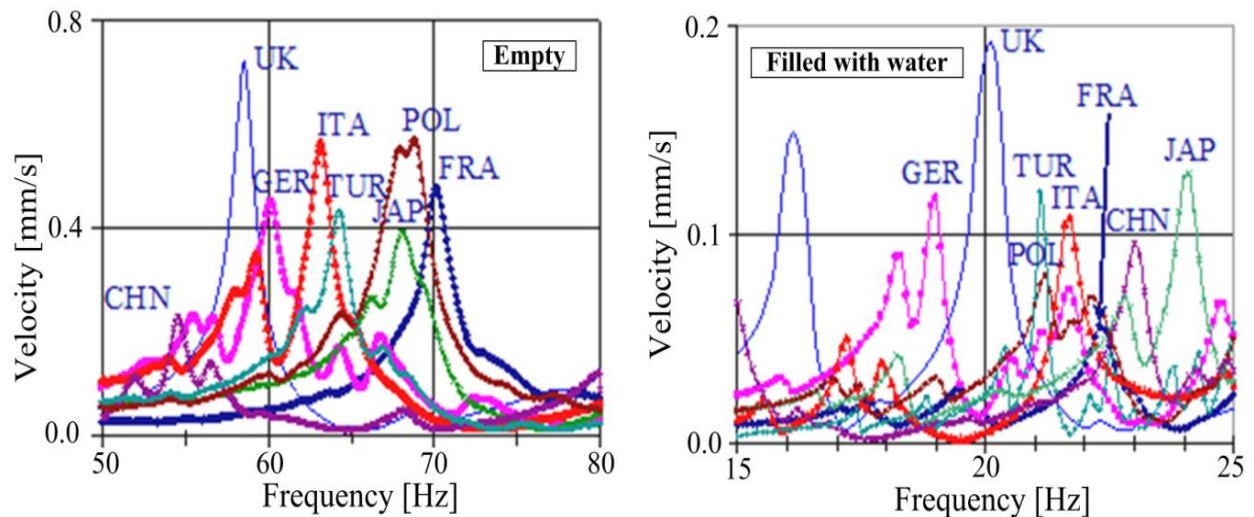


*Fig. 1.3. Dispersion of calculating a forced vibration empty tank and filled with water (source: ISSC 2006)*

In fact, for complex structures that require high technical requirements such as marine structures, using a single tool for analysis and evaluation is not enough to easily lead to errors, dispersion in the analysis results. Therefore, to reduce errors, dispersions in the analysis results are used the correlation and mutual support between the two methods: calculation method and measurement method. The measurement itself also has many errors, depending on the measuring technique, the person conducting the measurement and the measuring

device. The thesis focuses mainly on the influence of the numerical modelling method on errors and dispersions of analysis results in chosen marine machines and structures.

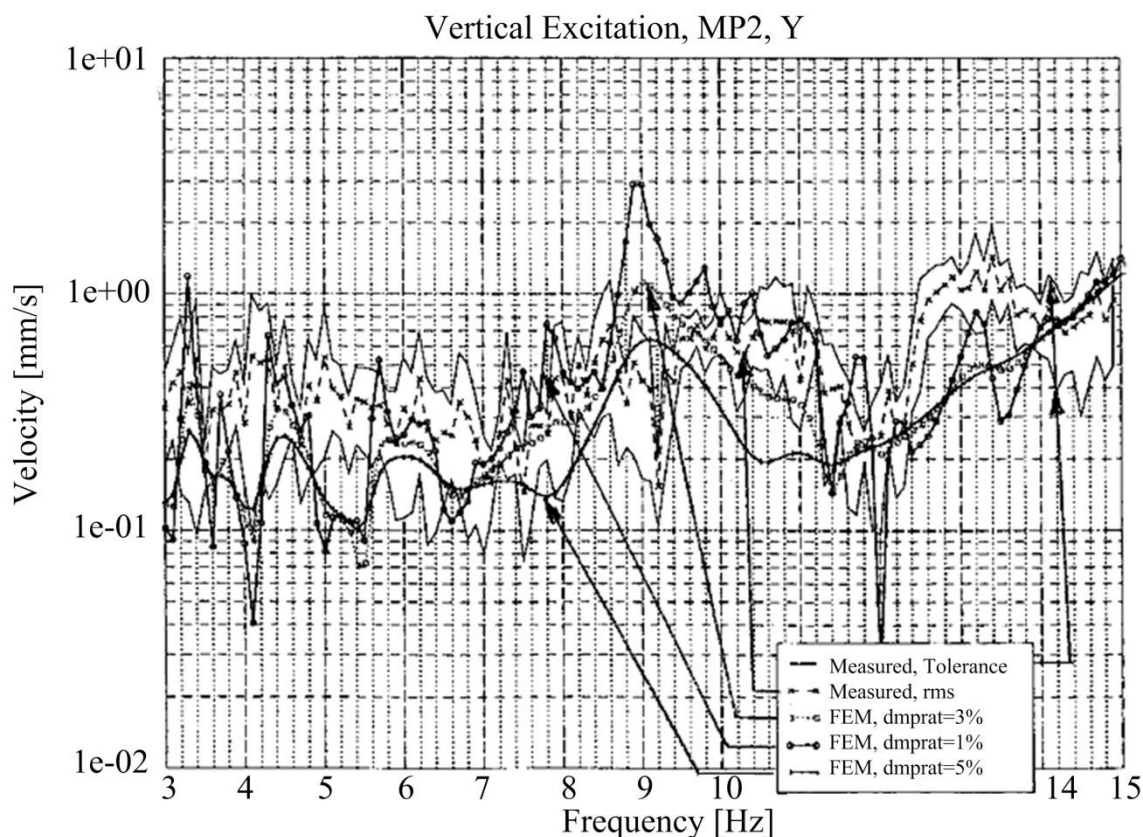


Fig. 1.4. Calculations and measurements of forced vibrations of the drive system (source: Germanischer Lloyd)

From the review of the literature, the question is how to promote the positive role of the numerical modelling method in modelling, inspection, assessment, monitoring, and predicting the technical state of the marine machines and structures. In addition, reduced errors and dispersions of the numerical modelling method on the analytical results of marine machines and structures to acceptable levels are consistent with empirical calculations. Therefore, the author has proposed the doctoral thesis titled “*Influence of the numerical modelling methods on dispersions and errors of analysis results in chosen marine machines and structures*”. The dissertation focused on analyzing the causes and effects of the numerical modelling on the errors and dispersions of the analysis results of chosen marine machines and structures. Analysis and evaluation are based on one of the important parameters affecting the reliability, safety, and longevity of the equipment, which is the vibration of chosen marine machines and structures. Methods to minimize the effects of the numerical modelling method on errors and dispersion of the analysis results of chosen marine machines and structures to conform with empirical calculation results also analyzed. From there, it is possible to choose the optimal and suitable numerical model for analyzing the numerical model of the selected maritime structures and machines in particular and the entire maritime structure and machinery in general, enhancing reliability and confidence of engineers when applying numerical modelling for analysis and calculation for marine machines and structures. The research was limited to the analysis of the most popular numerical modelling method - finite element method which is implemented in the famous commercial software Patran - Nastran. Details of the work have discussed in detail in the next chapters.

## 1.2. Thesis, purpose, and scope of work

Ships operate independently on the sea, in extremely rough conditions and harsh environments. Therefore, to ensure safety, marine machinery and structures must be tested and tested to meet the safety criteria set by the classification association at the design stage. The important criteria such as the strength, fatigue or vibration of marine machines and structures are tested. The testing and evaluation will be very laborious, money and time consuming when making many test samples and testing many times, especially not all test criteria can be conducted. Therefore, the model of numerical modelling was started, to model marine machines and structures to check and evaluate important parameters that meet critical values before designing and manufacturing. In recent years, many methods of numerical modelling have developed along with the development of computer science. But the errors and dispersion of the numerical modelling method to the analytical results are still large, depending on the experience and confidence of the design engineer. Therefore, errors and dispersion of numerical modelling methods are optimized, to improve the accuracy when applying numerical modelling methods for structural analysis and calculation, especially for marine machines and structures is a problem that is of great interest.

On the basis of literature research and own experiences, the author suggested that it is possible to develop optimal methods of numerical modelling of marine machines and structures. Optimization will allow the reduction of errors and dispersion of analytical results to an acceptable level consistent with empirical studies, reducing costs and laborious when creating test samples. For ships, there are two basic systems that can be distinguished in the structure of the ship: the hull with the superstructure and the main engine body and the transmission system (crankshaft, shaft, propeller). The doctoral thesis proposes a plan to develop research on the method of static-dynamic analysis of both systems above. The purpose of the doctoral thesis is to develop a package of numerical modelling analysis methods to assess the technical status of all-important ship safety components, one of which is vibration. Optimize and select the best numerical model for chosen maritime structures and machines to reduce errors and dispersion to acceptable levels. The reliability and confidence level of engineers are improved when applying numerical modelling methods analysis and calculation of structures and marine machinery. Therefore, the numerical modelling method must meet two basic criteria (partial contrast): criteria that ensure the accuracy and reliability of the assessment and the simple criteria of the applied numerical modelling methods. Literature studies and research is done so far show that methods of modelling shipbuilding equipment and structures have a significant impact on the degree of error and dispersion of numerical calculations. The study of selected components of maritime machinery and structures allows for a plausible assertion that an optimal calculation method can be found to limit the error and dispersion of the analysis results. In this context, it seems reasonable to place the following thesis:

***It is possible to decrease dispersions and to reduce a number of errors  
in the numerical modelling of a ship hull and superstructure  
and significant marine machines  
to the level that is both acceptable and in accordance with empirical tests***  
Specifically, the following objectives are identified:

1. Calculating and analyzing with important structures that make up ship hulls such as beams, thin plates, the thin stiffened plates with an important characteristic that greatly affects

durability, safety, and longevity of the structure (vibration), with particular regard to the influence of boundary conditions. Numerical modelling of chosen marine structures and machines is based on the finite element method, calculation and analysis results are compared with the results determined by empirical formulas and verified by measurement methods. Estimating the impact of the numerical modelling method taking into account the calculation purpose on errors and dispersion in the vibration analysis results of the selected structures, thereby determining the optimal numerical model for calculation and structural analysis.

2. Determine the optimal modelling to perform finite element method analysis for ship hull (including superstructure, main engine) related to the purpose of calculation (natural vibration, forced vibration, resonance region) and the influence of boundary conditions.

3. Determine the optimal model to perform a finite element method analysis for the ship's propulsion system (crankshaft, shaft line, propeller), taking into account the calculation purpose. Analysis of shaft line alignment by the selected numerical modelling method, optimizing the effect of numerical modelling on the errors and dispersion of the analysis results to an acceptable level.

4. Verify methods developed by comparing them with empirical studies of chosen marine machines and structures, including the determination of the degree of error and dispersion.

The objective of this thesis is to contribute to the improvement of efficiency and reliability, reduction of errors and dispersions on the calculation and analysis results for chosen marine machines and structures of numerical modelling methods. Optimization of the errors and dispersions of the numerical modelling method on the analysis results of chosen marine machines and structures to an acceptable level compared to the experimental results. This task is performed with the help of the most popular numerical modelling method - finite element method in software platform Patran - Nastran. Static-dynamic analysis of chosen marine machines and structures is modelled and calculated. Calculation results are compared with experimental results and verified by measurements. From that, evaluating the errors and dispersions of the selected numerical model, determine the optimal numerical model for the marine structures to be calculated in particular and the overall marine structure in general.

### **1.3. Methodology of research**

The research method is based on two methods: numerical modelling and empirical method verified by measurements. These methods are supported and complement each other, based on the results of calculations, comparison between these methods, can evaluate the influence of numerical modelling method on errors and dispersions of the analysis results of chosen marine machines and structures.

Computational analysis is based on the finite element method (FEM) implemented by MSC Software (Apex, Patran, Nastran). The finite element method implemented by Patran-Nastran software is currently the most widespread computer method used for numerical modelling analysis of structural strength and dynamics. The assumption of this method is to replace the mathematical model of the mechanical system (described in the form of the system of differential equations) with a discrete model of a simple mathematical description (the system of algebraic equations). The discrete model is created by dividing the continuously analysed object into a finite number of elements with a similar topological

shape. A very important element of the finite element method is to determine the shape function (interpolation), which is to guarantee the continuity of the function sought within the analysed structure. For the analysed structure, including boundary conditions, a system of algebraic equations is built. The result of their solution is to determine the sought function in a finite number of structure nodes, thanks to the assumed shape function, provide an approximate solution for the entire mechanical structure. The final result in the finite element method is a graphical presentation of the generated results. In which displays pre-and post-processing results made in Patran, computational analysis performed in Nastran software.

Selecting the interpolation method (shape and element functions), boundary conditions and mesh density are one of the main sources of errors and dispersions in computational results of marine structures. The Fig. 1.5 shows the results of calculating the static intensity of a simple T-beam (thin-wall structure as hull ship) supported at two ends: divided into two, four, and multiple finite elements. This is an extreme example of modelling errors that is considered in the thesis. An example of the source of the dispersion between measurements and calculations may be due to the dispersion of material properties, the method of modelling the properties of elements and the way of modelling the load and inciting force. An example of component modelling error is shown in Fig. 1.6. All critical sources of calculation results errors will be analysed in the dissertation.

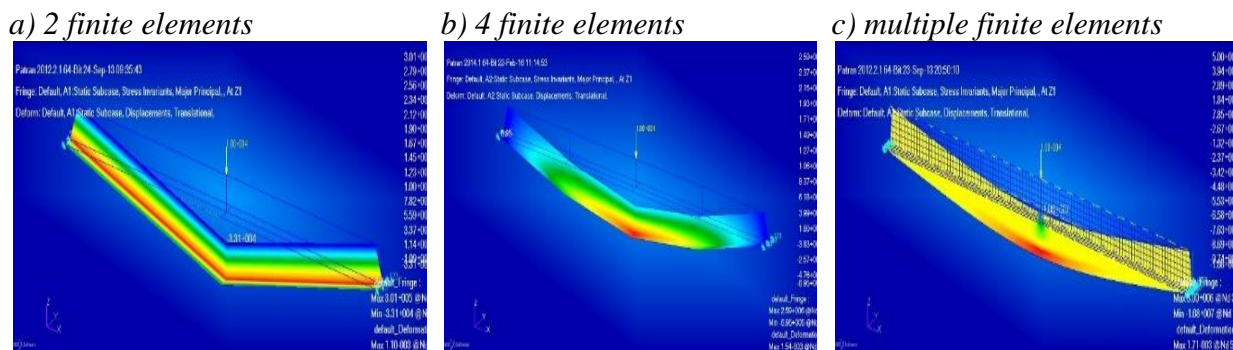


Fig. 1.5. The results of strength calculations of the T-beam with different finite elements

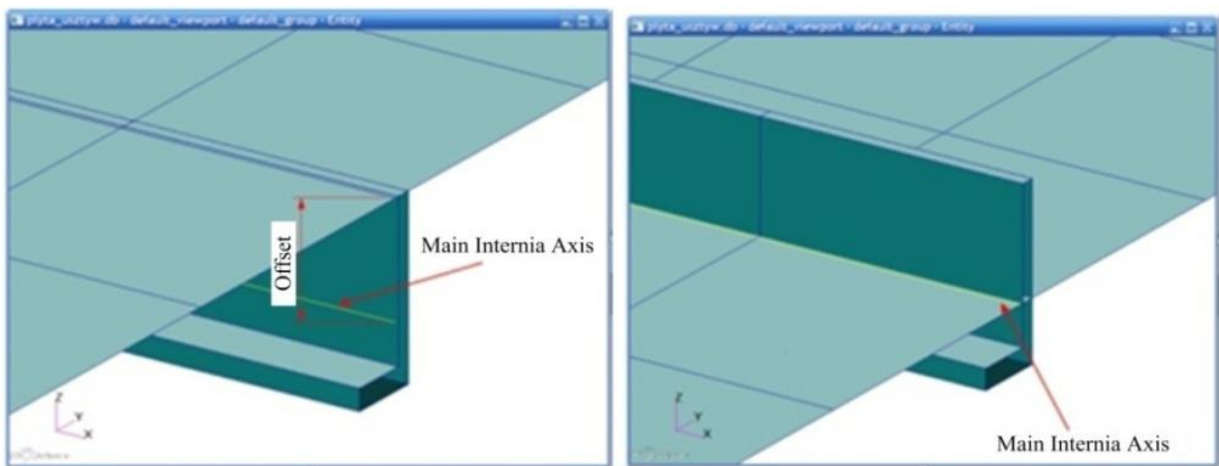


Fig. 1.6. Beam modelled without offset (left side - incorrect) and with offset (right side - correct)

The doctoral dissertation studied for static and dynamic analysis of chosen important marine machines and structures. Based on that, it is applied and developed to start working on other structures such as the hull model, and then consider the main engine models and power transmission models. An example of modelling some ship structures is shown in Fig. 1.7.

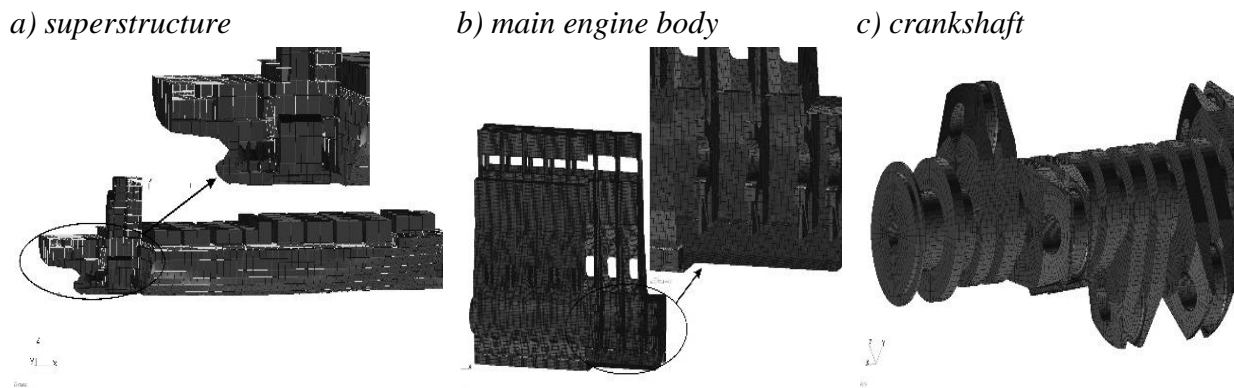


Fig. 1.7. Finite element model: superstructure, main engine body, and crankshaft

Empirical studies have been conducted at the laboratories of Gdynia Maritime University. The measurement methodology based on vibrodiagnostic techniques. Research is conducted with Bruel & Kjaer vibration analyser, piezoelectric accelerometers, modular impulse hammer, and laser displacement sensors. Surveying has carried out for typical ship hull structural elements as shaped beams and thin-walled plates with stiffeners, ship hull, superstructures, and propulsion systems.

### 1.3.1 Numerical modelling method

Nowadays, structures are becoming more and more complex, especially in the field of maritime and shipbuilding, so accurate analysis and calculations are often not feasible. In these cases, the numerical modelling method provides a model tool, numerical calculation based on approximate calculations to solve the problem. A brief history of numerical methods can be found in [113]. The development is shown in Fig. 1.8.

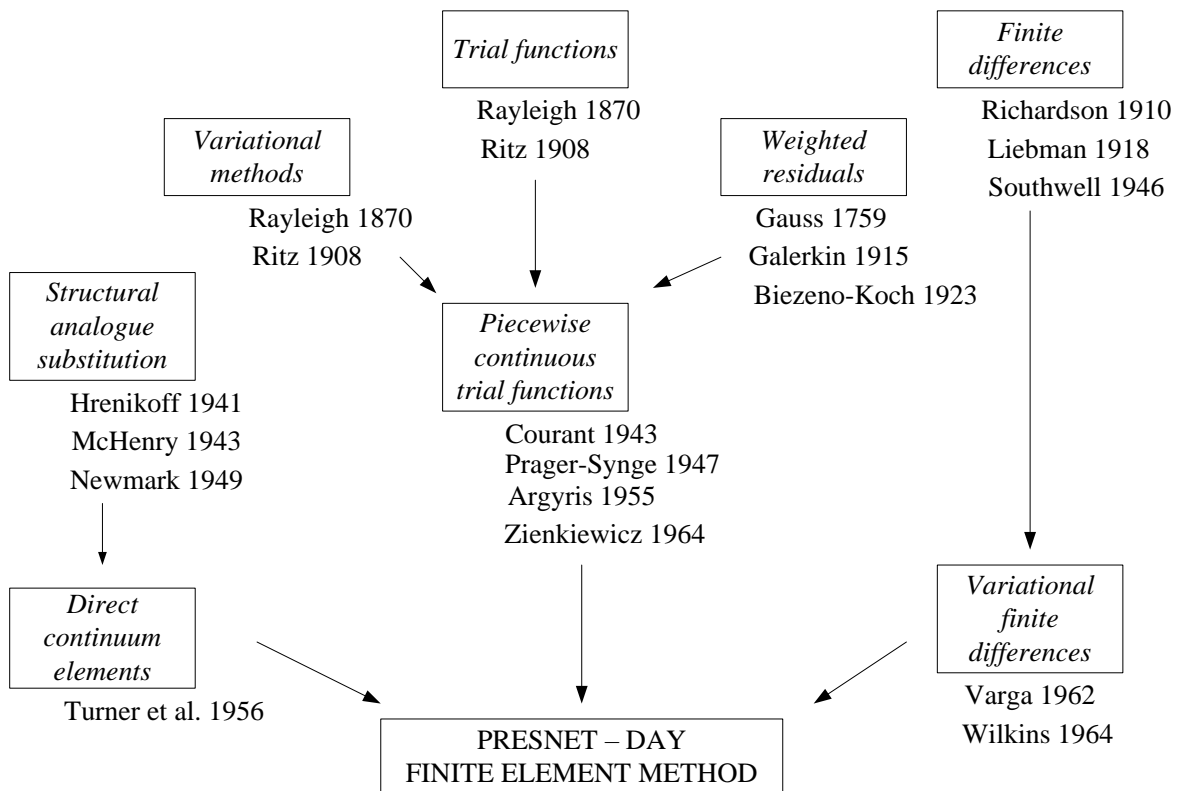


Fig. 1.8. History of numerical methods

The finite difference methods (see [92, 104]), the variational methods (see [89, 116]) have certain disadvantages. In the thesis, the author used the finite element method, the most popular numerical method today. Today finite element method is widely used because this method overcomes the disadvantage of the traditional variational methods by providing a systematic procedure for the derivation of the approximation functions over sub-regions of the domain. The method is endowed with some advantages that account for its superiority over other competing methods:

1. Modelling of complex geometries and irregular shapes are easier as varieties of finite elements are available for the discretization of the domain.
2. Boundary conditions can be easily incorporated in FEM.
3. Different types of material properties can be easily accommodated in modelling from element to element or even within an element.
4. Higher-order elements may be implemented.
5. FEM is simple, compact and result-oriented and hence widely popular among the engineering community.
6. The availability of a large number of computer software packages and literature makes FEM a versatile and powerful numerical method.

Thus, the FEM can be viewed, in particular, as an element-wise application of the Rayleigh-Ritz or weighted-residual methods. In the thesis, the author uses the finite element method for the modelling and analysis of chosen marine machines and structures. By modelling chosen marine machines and structures in the form of mathematical models, simplifying complex structures reduces the cost and time required for testing and evaluating the technical conditions of marine structures. Ensure the economy, stability, safety of marine structures before design, or during the exploitation. Finite element method, which is implemented in the Patran - Nastran software platform, applied to the static and dynamic analysis of chosen marine machines and structures.

### **1.3.1.1. History of finite element method**

The history of the finite element method is particularly interesting, especially because the method has only been in existence since the mid-1950s. The early work on the numerical solution of boundary-valued problems can be traced to the use of finite difference schemes; Southwell discusses the use of such methods in his book published in the mid-1940s [104]. The beginnings of the finite element method actually stem from these early numerical methods and the frustration associated with attempting to use finite difference methods on more difficult, geometrically irregular problems [94]. Beginning in the mid-1950s, efforts to solve continuum problems in elasticity using small, discrete "elements" to describe the overall behaviour of simple elastic bars began to appear. Argyris [3] and Turner, et al. [108] was the first to publish the use of such techniques for the aircraft industry. Actual coining of the term "finite element" appeared in a paper by Clough [16].

The early use of finite elements lay in the application of such techniques for structural-related problems. However, others soon recognized the versatility of the method and its underlying rich mathematical basis for application in non-structural areas. Zienkiewicz and Cheung [115] were among the first to apply the finite element method to field problems (e.g., heat conduction, irrotational fluid flow, etc.) involving the solution of Laplace and Poisson equations. Much of the early work on non-linear problems can be found in Oden [82]. Efforts

to model heat transfer problems with complex boundaries are discussed in Huebner [50]; a comprehensive 3-D finite element model for heat conduction is described by Heuser [47]. Early application of the finite element technique to viscous fluid flow is given in Baker [4].

Since these early works, rapid growth in usage of the method has continued since the mid-1970s. Numerous articles and texts have been published, and new applications appear routinely in the literature. Excellent reviews and descriptions of the method can be found in some of the earlier texts by Finlayson [38], Desai [21], Becker et al. [8], Baker [5], Fletcher [40], Reddy [89], Segerlind [100], Bickford [10] and Zienkiewicz and Taylor [116]. A vigorous mathematical discussion is given in the text by Johnson [56], and programming the finite element method is described by Smith [103]. A short monograph on the development of the finite element method is given by Owen and Hinton [84].

The underlying mathematical basis of the finite element method first lies with the classical Rayleigh-Ritz and variational calculus procedures introduced by Rayleigh [88] and Ritz [91]. These theories provided the reasons why the finite element method worked well for the class of problems in which variational statements could be obtained (e.g., linear diffusion type problems). However, as interest expanded in applying the finite element method to more types of problems, the use of classical theory to describe such problems became limited and could not be applied (this is particularly evident in fluid-related problems).

Extension of the mathematical basis to non-linear and non-structural problems was achieved through the method of weighted residuals, originally conceived by Galerkin [41] in the early 20th century. The method of weighted residuals was found to provide the ideal theoretical basis for a much wider basis of problems as opposed to the Rayleigh-Ritz method. Basically, the method requires the governing differential equation to be multiplied by a set of predetermined weights and the resulting product integrated over space; this integral is required to vanish. Galerkin's method is a subset of the general weighted residuals procedure, since various types of weights can be utilized; in the case of Galerkin's method, the weights are chosen to be the same as the functions used to define the unknown variables. Galerkin and Rayleigh-Ritz approximations yield identical results whenever a proper variational statement exists and the same basis functions are used. By using constant weights instead of functions, the weighted residual method yields the finite volume technique. A more vigorous description of the method of weighted residuals can be found in Finlayson [38]. Recent descriptions of the method are discussed in Chandrupatla and Belegundu [14], Liu and Quek [60], Hollig [49], Hutton [51], Solin et al [106], Reddy [90], Becker [9], and Ern and Guermond [37].

### **1.3.1.2. Analytical processes of the finite element method**

The FEM can be defined as a numerical method of obtaining approximate solutions of PDE's or their systems as well as integral equations. Essentially, the FEM can be described as a systematic procedure that approximates any continuous function by a discrete model, called the finite element model, which consists of a set of values of the given function at a finite number of points, called nodes, in its domain, together with piecewise approximations of the given function over a finite number of sub-domains, called finite elements or elements for short. The local approximation, called shape function or interpolation function, of the function over each element, is uniquely defined in terms of the discrete values of the function at nodes in its domain. The most distinctive feature of the FEM that separates it from others is the subdivision of the given domain into a set of elements. Other features of the method include

seeking continuous approximations of the solution over each element in terms of nodal values, assembly element equations by imposing the inter-element continuity of the solution.

Analytical Processes of Finite Method Element in solving a practical problem include eight steps can be distinguished as follow:

1. *Discretize and select the element types* involves dividing the body into an equivalent system of finite elements with associated nodes and choosing the most appropriate element type to model most closely the actual physical behaviour. The total number of elements used and their variation in size and type within a given body are primarily matters of engineering judgment. The elements must be made small enough to give usable results and yet large enough to reduce computational effort. Small elements (and possibly higher-order elements) are generally desirable where the results are changing rapidly, such as where changes in geometry occur; large elements can be used where results are relatively constant.

The choice of elements used in a finite element analysis depends on the physical makeup of the body under actual loading conditions and on how close to the actual behaviour the analyst wants the results to be. This choice concerning the appropriateness of one-, two-, or three-dimensional (1D, 2D, 3D) consideration is necessary. Moreover, the choice of the most appropriate element for a particular problem is one of the major tasks that must be carried out by the designer/analyst. Elements that are commonly employed in practice are shown in Fig. 1.9. Divide the domain into finite elements using appropriate element types (one-dimensional-1D, two-dimensional-2D, three-dimensional -3D).

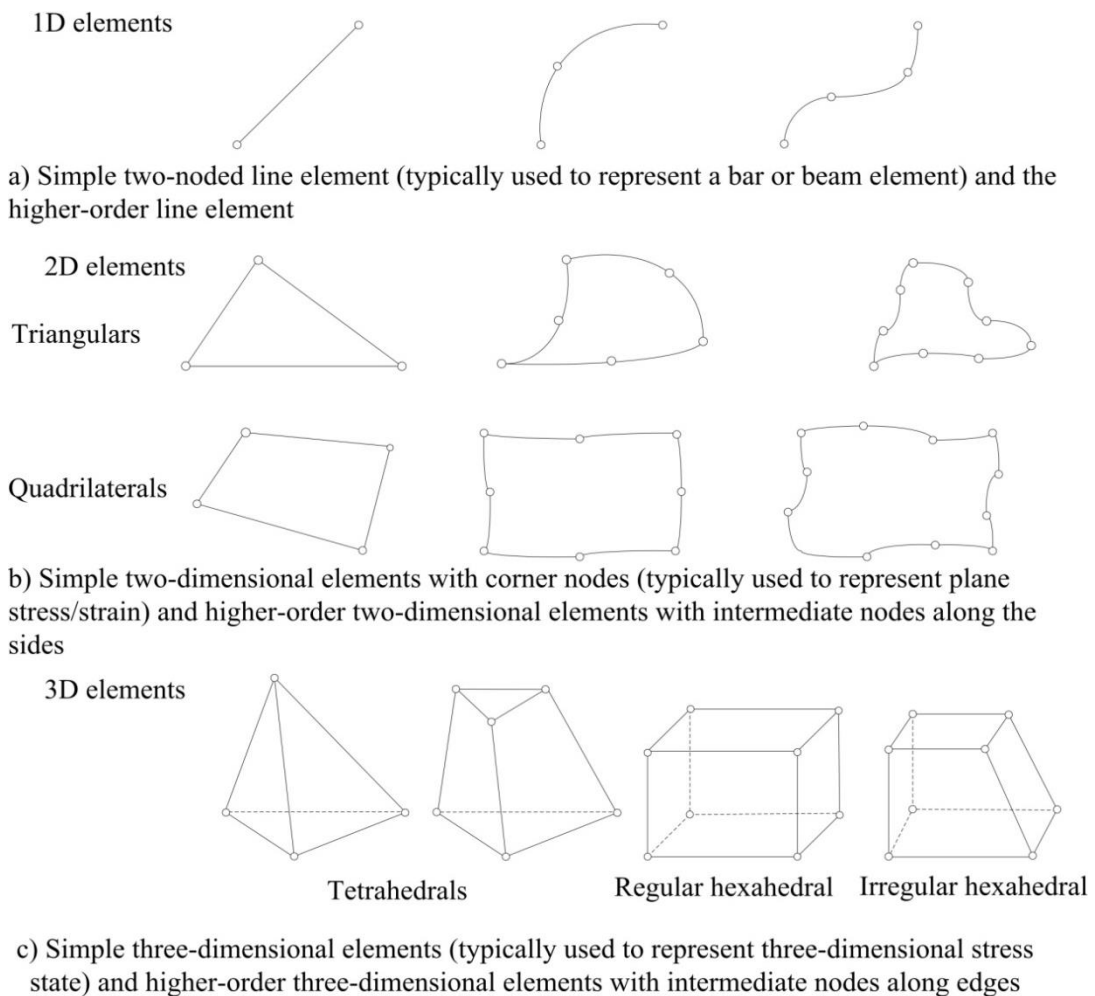


Fig. 1.9. Typical elements using in the FE analysis

2. *Select a displacement function* involves choosing a displacement function within each element. The function is defined within the element using the nodal values of the element. Linear, quadratic, and cubic polynomials are frequently used functions because they are simple to work within finite element formulation. However, the trigonometric series can also be used.

3. *Define the strain/displacement and stress/strain relationships:* Strain/displacement and stress/strain relationships are necessary for deriving the equations for each finite element. In the case of one-dimensional deformation, say, in the x-direction, we have strain  $\varepsilon_x$  related to displacement  $u$  by:

$$\varepsilon_x = \frac{du}{dx}. \quad (1.1)$$

This assumption applies to small strains. In addition, the stresses must be related to the strains through the stress/strain law-generally called the constitutive law. The ability to define the material behaviour accurately is most important in obtaining acceptable results. The simplest of stress/strain laws, Hooke's law, which is often used in stress analysis, is given by:

$$\sigma_x = E\varepsilon_x, \quad (1.2)$$

where  $\sigma_x$  is stress in the x direction and  $E$  is modulus of elasticity.

4. *Derive the element stiffness matrix and equations:* Derive the equations within each element. Initially, the development of element stiffness matrices and element equations was based on the concept of stiffness influence coefficients, which presupposes a background in structural analysis. Derive the equations within each element is done in the following ways:

- *Direct equilibrium or stiffness method:* According to this method, the stiffness matrix and element equations relating nodal forces to nodal displacements are obtained using force equilibrium conditions for a basic element, along with force/deformation relationships. Because this method is most easily adaptable to line or one-dimensional elements, respectively.
- *Work or energy methods:* To develop the stiffness matrix and equations for two- and three-dimensional elements, it is much easier to apply a work or energy method. The principle of virtual work (using virtual displacements), the principle of minimum potential energy, and Castigliano's theorem are methods frequently used for the purpose of the derivation of element equations. The principle of virtual work is applicable for any material behaviour, whereas the principle of minimum potential energy and Castigliano's theorem are applicable only to elastic materials. Furthermore, the principle of virtual work can be used even when a potential function does not exist. However, all three principles yield identical element equations for linear-elastic materials; thus which method to use for this kind of material in structural analysis is largely a matter of convenience and simplicity. For the purpose of extending the finite element method outside the structural stress analysis field, a functional (a function of another function or a function that takes functions as its argument) analogous to the one to be used with the principle of minimum potential energy is quite useful in deriving the element stiffness matrix and equations. For

instance, letting  $\pi$  denote the functional and  $f(x, y)$  denote a function  $f$  of two variables  $x$  and  $y$ , we then have  $\pi = \pi(f(x, y))$ , where  $\pi$  is a function of the function  $f$ . A more general form of a function depending on two independent variables  $u(x, y)$  and  $v(x, y)$ , where independent variables are  $x$  and  $y$  in Cartesian coordinates, is given by:

$$\pi = \iint F(x, y, u, v, u_x, u_y, v_x, v_y, u_{xx} \dots, v_{yy}) dx dy. \quad (1.3)$$

- *Methods of weighted residuals:* The methods of weighted residuals are useful for developing the element equations; particularly popular is Galerkin's method. These methods yield the same results as the energy methods wherever the energy methods are applicable. They are especially useful when a functional such as potential energy is not readily available. The weighted residual methods allow the finite element method to be applied directly to any differential equation. Galerkin's method, along with the collocation, the least squares, and the sub-domain weighted residual methods will be used to derive the bar element equations and the beam element equations and to solve the combined heat-conduction, convection, mass transport problem. For more information on the use of the methods of weighted residuals, see in [38], for additional applications to the finite element method, consult in [116] and [18]. Using any of the methods just outlined will produce the equations to describe the behaviour of an element. These equations are written conveniently in matrix form as

$$\begin{Bmatrix} f_1 \\ f_2 \\ f_3 \\ f_4 \\ \vdots \\ f_n \end{Bmatrix} = \begin{bmatrix} k_{11} & k_{12} & \dots & k_{1n} \\ k_{21} & k_{22} & \dots & k_{2n} \\ \dots & \dots & \dots & \dots \\ \dots & \dots & \dots & \dots \\ \dots & \dots & \dots & \dots \\ k_{n1} & k_{n2} & \dots & k_{nn} \end{bmatrix} \begin{Bmatrix} u_1 \\ u_2 \\ u_3 \\ u_4 \\ \vdots \\ u_n \end{Bmatrix}, \quad (1.4)$$

or in compact matrix form as

$$\{f\} = [k]\{u\}, \quad (1.5)$$

where  $\{f\}$  is the vector of element nodal forces,  $[k]$  is the element stiffness matrix (normally square and symmetric), and  $\{u\}$  is the vector of unknown element nodal degrees of freedom or generalized displacements,  $n$ . Here generalized displacements may include such quantities as actual displacements, slopes, or even curvatures.

5. *Assemble the element equations to obtain the global or total equations and introduce boundary conditions:* In this step, the individual element nodal equilibrium equations generated in step 4 are assembled into the global nodal equilibrium equations. Another more direct method of superposition (called the direct stiffness method), whose basis is nodal force equilibrium, can be used to obtain the global equations for the whole structure. Implicit in the direct stiffness method is the concept of continuity, or compatibility, which requires that the structure remain together and that no tears occur anywhere within the structure.

The final assembled or global equation written in matrix form is

$$M\ddot{u} + C\dot{u} + Ku = F, \quad (1.6)$$

Where  $F$  is the force matrix,  $K$  is the stiffness matrix,  $u$  is the displacement,  $C$  is the damping matrix, and  $M$  is the mass matrix. It can be shown that at this stage, the global stiffness matrix  $K$  is a singular matrix because its determinant is equal to zero. To remove this singularity problem, we must invoke certain boundary conditions (or constraints or supports) so that the structure remains in place instead of moving as a rigid body.

6. *Solve for the unknown degrees of freedom (i.e. primary unknowns)*: Equation (1.6) can be simplified to static strength analyses by expunction of elements with acceleration vector (mass matrix) and speed vector (damping matrix), modify to account for the boundary conditions, is a set of simultaneous algebraic equations that can be written in expanded matrix form as

$$\begin{Bmatrix} F_1 \\ F_2 \\ F_3 \\ F_4 \\ \vdots \\ F_n \end{Bmatrix} = \begin{bmatrix} K_{11} & K_{12} & \dots & K_{1n} \\ K_{21} & K_{22} & \dots & K_{2n} \\ \dots & \dots & \dots & \dots \\ \dots & \dots & \dots & \dots \\ \dots & \dots & \dots & \dots \\ K_{n1} & K_{n2} & \dots & K_{nn} \end{bmatrix} \cdot \begin{Bmatrix} u_1 \\ u_2 \\ u_3 \\ u_4 \\ \vdots \\ u_n \end{Bmatrix}, \quad (1.7)$$

where now  $n$  is the structure total number of unknown nodal degrees of freedom. These equations can be solved for the  $ds$  by using an elimination method (such as Gauss's method) or an iterative method (such as the Gauss-Seidel method). The  $ds$  is called the *primary unknowns* because they are the first quantities determined using the stiffness (or displacement) finite element method.

7. *Solve for the element strains and stresses*: The last step in solving any problem with the use of the FEM is to solve (1.7) for the values of the unknown solution  $u$  at nodes of the mesh. In general, the last equation obtained by the FEM is always a system of algebraic equations. There are many numerical methods to solve a system of linear equations. They are mainly divided into two groups:

- Exact (or direct) methods such as the Cramer's rule, the Gaussian method (also called Gaussian elimination), the method of principal elements, the method of square roots, etc. These methods allow finding the exact solution of a system of linear equations in the finite number of steps and are mostly used for small systems.

- Iterative methods, such as the method of iteration, the Seidel method, the method of relaxation, and others.

These methods have been systematically presented in detail in the literature related to linear algebra as well as the computational method, such as [24, 43]. In most software packages of finite element analysis, the solution of the linear system of equations has been programmed as the standard, built-in procedures and is available for use.

8. *Interpret the results*: The final goal is to interpret and analyse the results for use in the design/analysis process. Determination of locations in the structure where significant deformations and stresses occur is generally important in making design/analysis decisions. Postprocessor computer programs help the user to interpret the results by displaying them in graphical form.

### 1.3.1.3. Errors and dispersion of the numerical modelling method

The finite element method is an approximate numerical method, modelling complex marine structures into simple geometric forms in the form of mathematical models. This leads to discrete marine structures that are not fully compatible with the original marine structures, leading to errors and dispersions in the analysis results obtained. An example of the error and dispersion of the numerical model when discretizing the structure is given in Fig. 1.10. A real object with a boundary is a curve while a discrete element has triangles, with a boundary is a straight line so that when the finite elements are assembled there will be errors between the boundary line of the real object and the boundary created by the finite elements.

So, when we proceed to discrete marine structures, it is important to choose the appropriate finite one-dimensional-1D, two-dimensional-2D or three-dimensional-3D finite elements. The number, shape, and type (i.e., linear or quadratic) of elements should be chosen such that the geometry of the domain is approximated as accurately as necessary. For example, when the domain has a curved boundary is approximated by a mesh of straight edge triangles, then we have to use a large enough number of elements to ensure that the difference between the real and discrete boundary is small enough to be acceptable. Modelling chosen marine machines and structures such that the influence of numerical models on errors and dispersions to the analytical results of marine structures will be within acceptable limits, consistent with the results of experiment calculations.

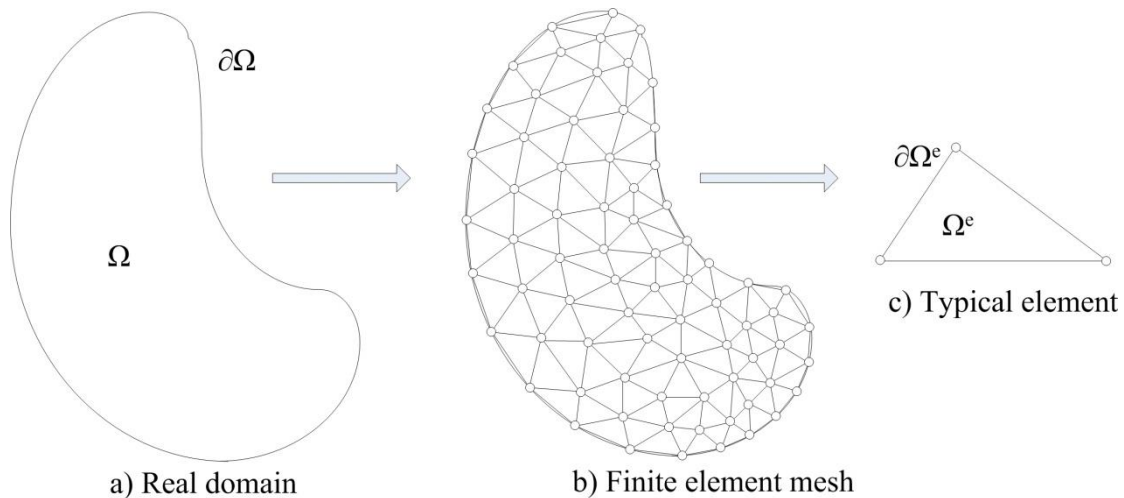


Fig. 1.10. Geometry error of discretization for the domain bounded by a curve

To simplify, marine structures are often modelled in the form of mathematical models, on which the algebraic polynomial functions can be applied. The assumed functions can be linear, quadratic or higher. But in reality, the distortion and displacement of marine structures are often more complex, may not follow a particular geometry. In addition, the errors and dispersion of the numerical modelling method to the analysis results of marine structures are due to the following reasons: incorrect meshing between element bar, plate element and solid element, and due to the choice of applying boundary conditions to incorrect elements. All of the causes leading to the error and dispersion of the analytical results of the marine structures will be analysed in detail in subsequent chapters, as well as providing solutions to optimize these errors and dispersions so as to ensure consistency with the experimental results to an acceptable level.

#### **1.3.1.4. Brief introduction of Patran-Nastran software**

MSC Software is one of the ten original software companies and the worldwide leader in multidiscipline simulation. The MSC Software incorporation (formerly MarcNeal-Schwendler incorporation) has been supplying sophisticated computer-aided engineering (CAE) tools since 1963. MSC Software is the developer, distributor, and supporter of the most complete and widely-used structural analysis program in the world, MSC.Nastran. As a trusted partner, MSC Software helps companies improve quality, save time and reduce costs associated with the design and test of manufactured products. MSC Software's engineering simulation technology is used by leading manufacturers for linear and nonlinear finite element analysis (FEA), acoustics, fluid-structure interaction (FSI), multi-physics, optimization, fatigue and durability, multi-body dynamics, and control systems simulation. The company's products accurately and reliably predict how products will behave in the real world to help engineers design more innovative products - quickly and cost-effectively.

MSC Software Milestones: Started in 1963 the company founded by Dr Richard MacNeal and Mr. Robert Schwendler. Developed the first program is called SADAM for structural analysis by digital simulation of Analog methods. This was the forerunner of MSC's flagship program, MSC.Nastran. In 1965, MSC participates in a NASA-sponsored project to develop a unified approach to computerized structural analysis. The program became known as Nastran (NASA Structural Analysis Program). In 1972, MSC releases a proprietary version of Nastran, called MSC.Nastran. In 1994, MSC merged with PDA Engineering (developer of Patran) to become the largest single provider of finite element analysis (FEA) software to the CAE market. In 1999, Company renamed as MSC Software Corporation with a wider focus on Engineering Simulation, detailed reference [65-69].

In software commercial packages, the author selects the Nastran (NASA Structural Analysis) software package using the finite element method for the modelling, analysis, and evaluation of marine structures and machinery. MSC.Nastran has highly efficient in using modern numerical analysis techniques. MSC.Nastran used extensively by aerospace, transportation, energy, biomedical, civil and other industries. MSC.Patran is a CAE (Computer-Aided Engineering) pre and post-processing software package. It consists of the following major components graphical user interface, direct geometry integration, robust meshing algorithms, workflow-based main menu, powerful results visualization, and analysis preferences.

#### **1.3.1.5. Analysis and calculation process in Patran-Nastran software**

In this section, the Analysis and calculation process in Patran-Nastran software is considered. MSC.Patran is a pre-processing software package by computer. The Patran software will perform the steps to determine the properties of elements such as geometry, meshing, material, properties, loads and boundary conditions. The numerical model of the structure is established in the Patran software with full properties, meshing, and then calculated in the Nastran software to determine deformation  $\{u\}$ , strain  $\epsilon$ , and stress  $\sigma$ . The results of the analysis, calculated in the software Nastran will be displayed in the Patran software in the form of graphics to convenience for evaluation. The workflow of the Patran and Nastran software and the problem-solving process using the finite element method is illustrated in Fig. 1.11÷1.12.

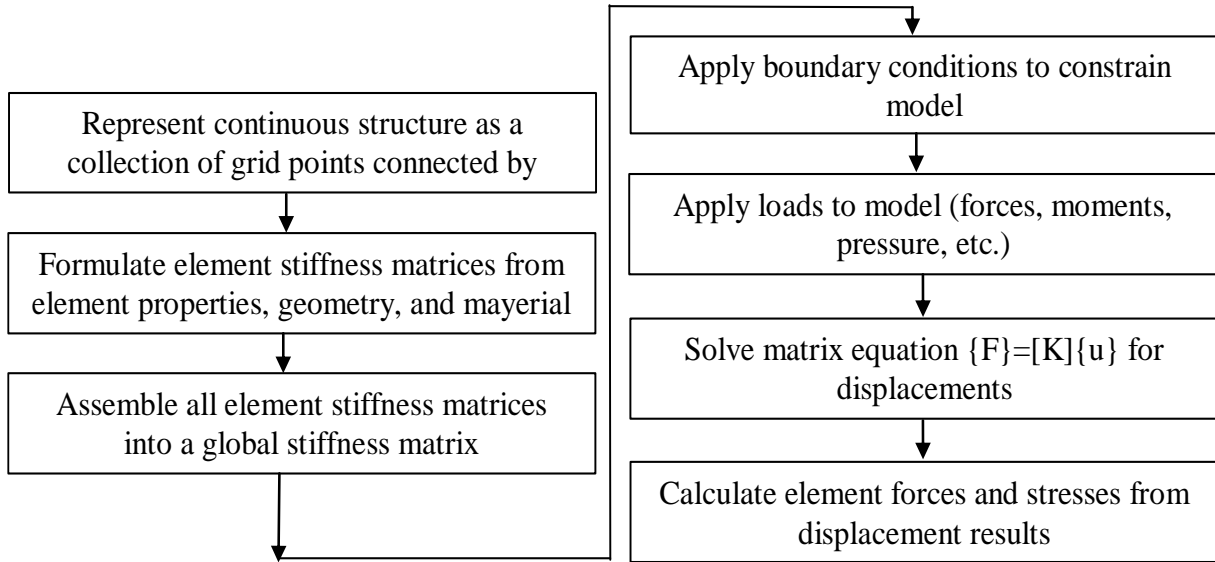


Fig. 1.11. MSC.Nastran solution flow

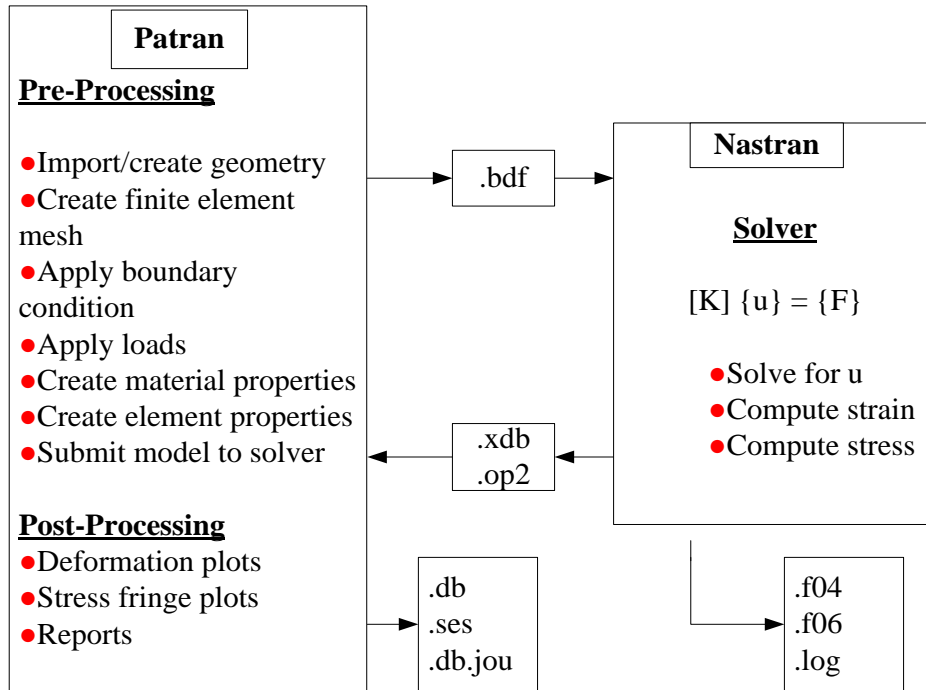


Fig. 1.12. Workflow and files of the Patran and Nastran software

The steps for building a finite element model in Patran software are discussed in detail below:

Step 1: Creating the finite element model in Patran software, the first look at the Patran software main interface as well as the main icons on the menu illustrated in Fig. 1.13. Determine the geometric shape of the chosen marine machines and structures. There are two ways to import the geometric shape of the structure. The first way is to import the available geometry shapes prepared in some software such as CAD-CAM by using "import file". The second way is to use points, lines, faces, cubes directly in the Patran software to determine the shape of the structure.

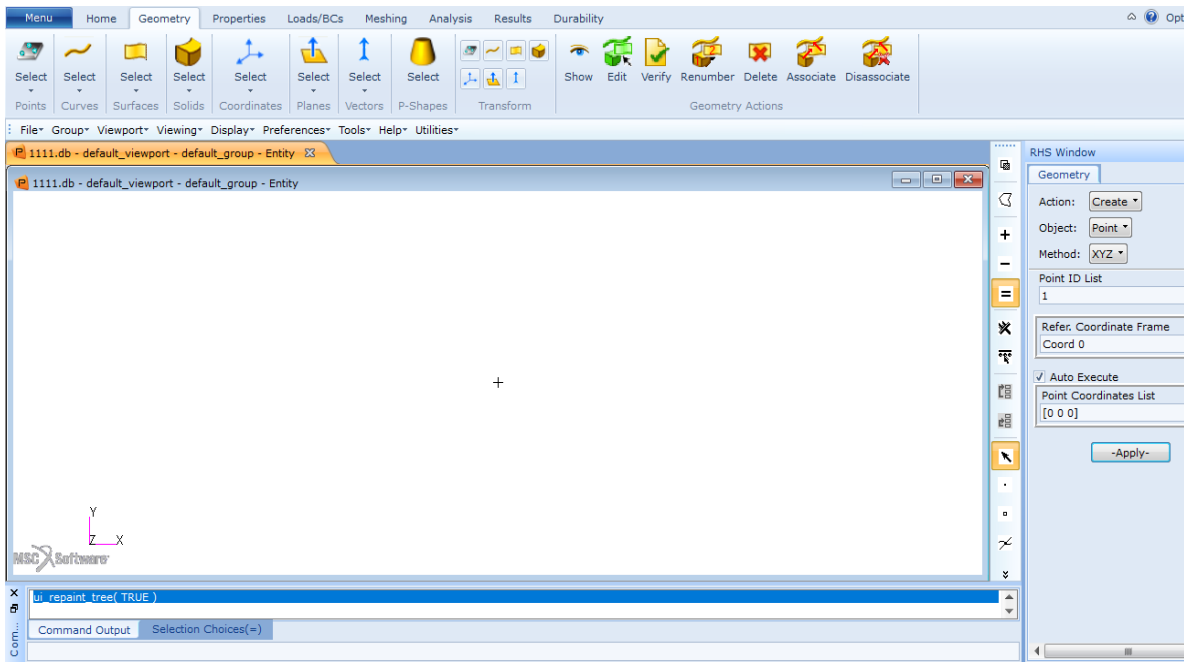


Fig. 1.13. Main menu and figure depicting the origin point and the geometry icon

Step 2: The next step is to determine the material properties of the elements. Nastran and Patran can support a variety of material definitions, including isotropic, 2D anisotropic, 2D orthotropic, 3D anisotropic, 3D orthotropic (a special case of 3D anisotropic), fluid, composite. Element properties define how the structural element behaves in the model. It serves two purposes. The first purpose it associates the material to the elements. The second purpose it defines the attributes of the element, including stiffness values (scalar elements), cross-sectional properties (1D element), element orientation (1D element), thickness (2D element), membrane, bending, transverse shear and membrane-bending coupling behaviour (2D element), material orientation (2D and 3D element). The material properties and material properties of the elements are illustrated in Fig. 1.14÷1.15.

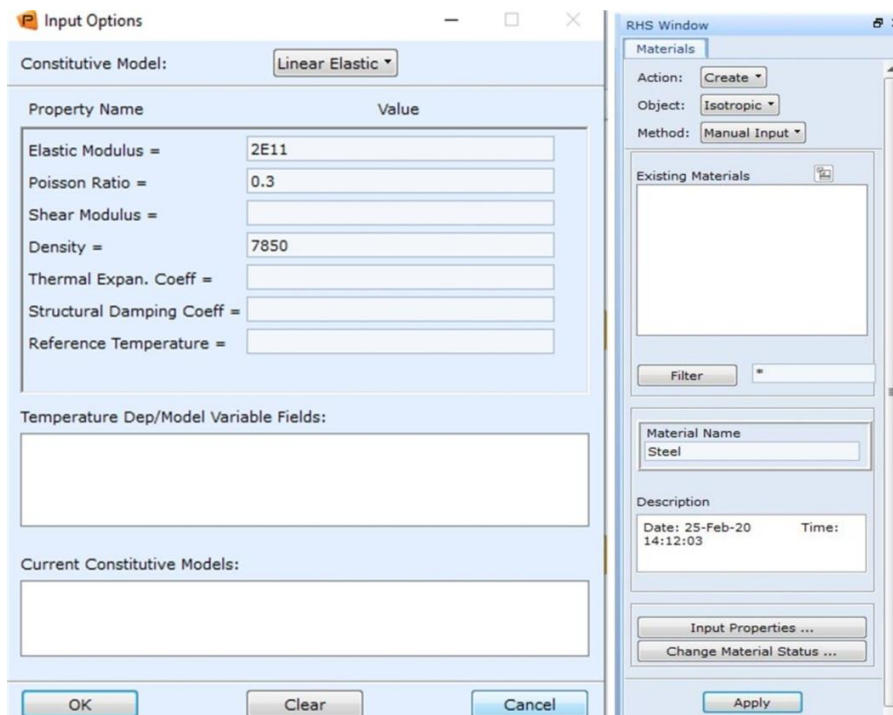


Fig. 1.14. Determination of material properties



Step 4: The next step is to assign the loads and boundary conditions to the elements. Many different loads and boundary conditions can be applied to the Nastran finite element model. Those supported by Patran include displacement (constraints or enforced motion), force, pressure, temperature (in a thermal analysis), inertial loads, initial conditions (displacement or velocity), velocity, acceleration, contact. Define the loads and boundary conditions for the element described in Fig. 1.17.

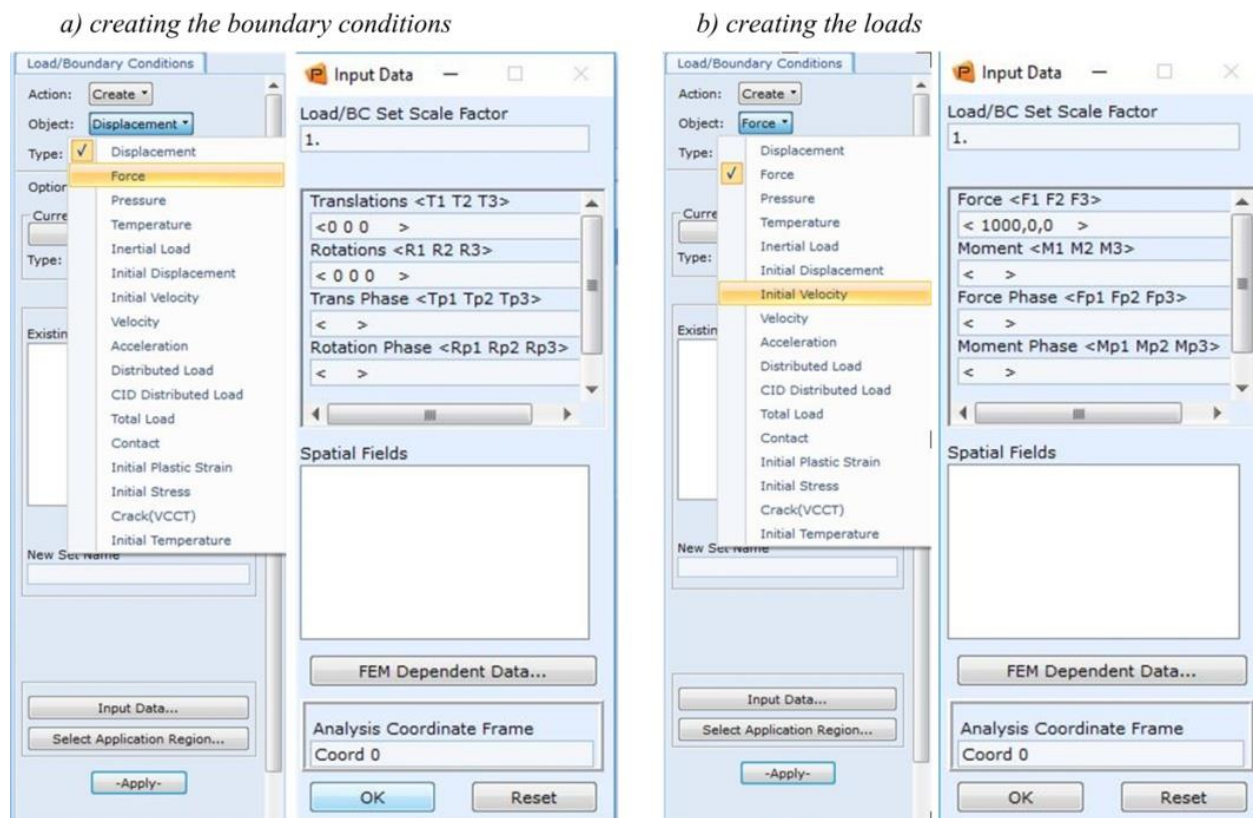


Fig. 1.17. Creating the loads and boundary conditions for the element

Step 5: Based on the purpose of calculation, we will choose the form of analysis: linear static, nonlinear static, normal modes, buckling, complex eigenvalue, frequency response, transient response, nonlinear transient, implicit nonlinear. After determining the form of analysis is complete, the file will be sent to analysis in the Nastran software. The process of identifying the analytical form and sending the analysis is described in Fig. 1.18.

Step 6: Both Nastran binary output files can be accessed by Patran for results post-processing. Each has advantages. The .xdb is a database that is accessed by Patran. The results do not become a part of the Patran database. Therefore, large results files can be attached without degradation in performance. The .xdb must be kept with the Patran database to view results. It does not support composite failure indices. The .op2 is a results file that is read into the Patran database. The results become part of the Patran database. As a result, the .op2 does not need to be maintained in order to view results. The Patran database size will expand due to the results data stored within. It does support composite failure indices. Results are not automatically attached to the Patran database. Fig. 1.19 shows attaching the results of Nastran to Patran software with the extension .xdb file.

# 1. INTRODUCTION

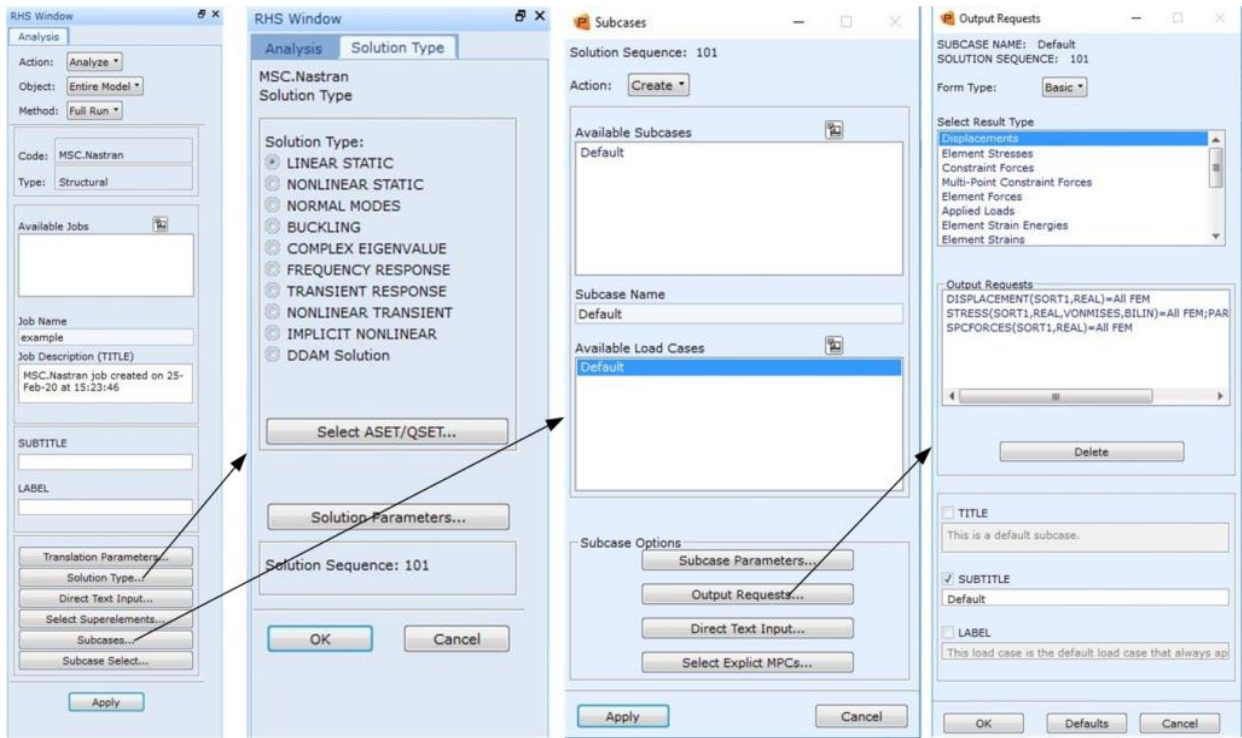


Fig. 1.18. Determining analysis form and submitting analysis

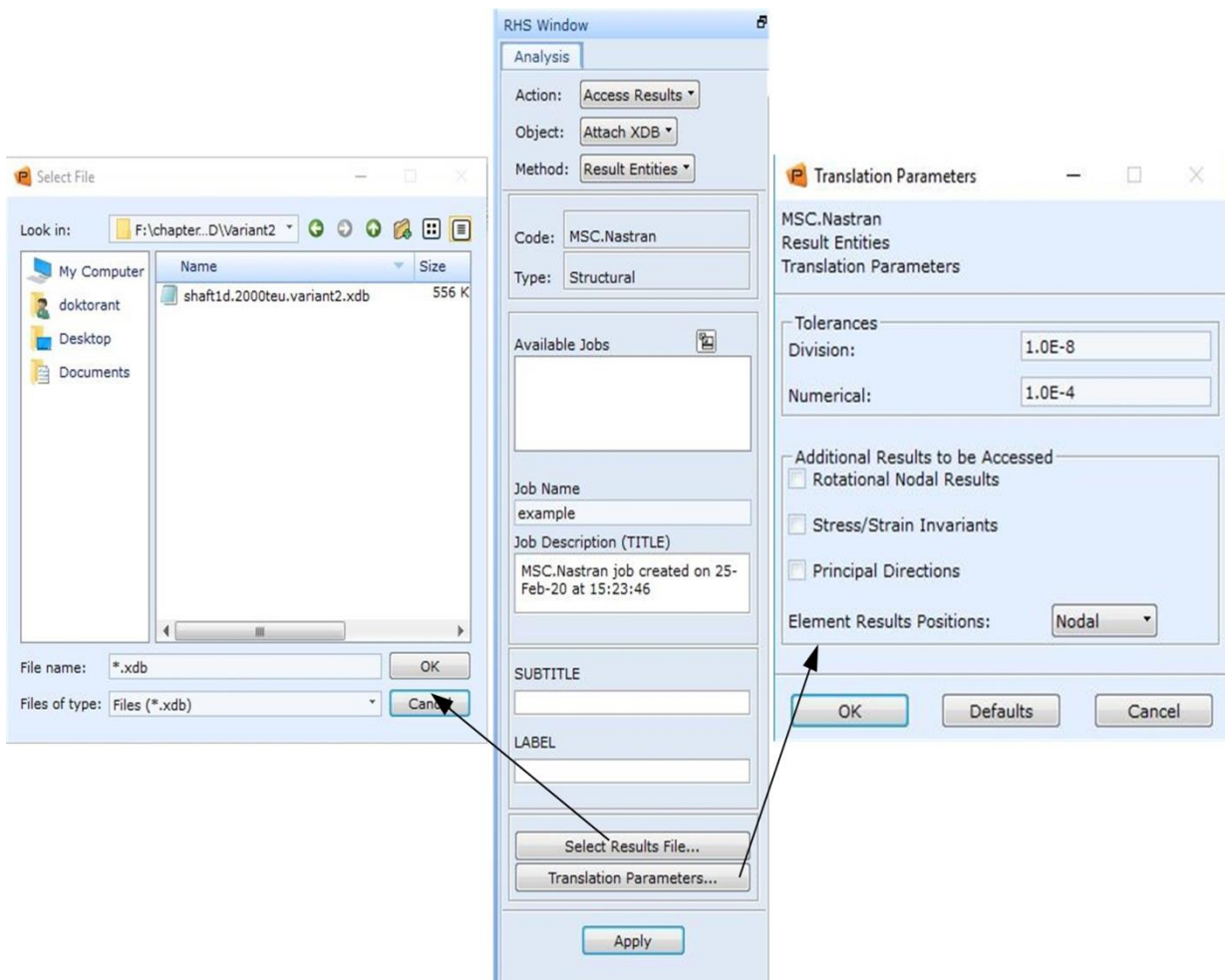


Fig. 1.19. Attaching the results from the Nastran file to the Patran software

Step 7: Post-processing: The Patran Results menu provides options for a variety of result plots or reports. The more commonly used plots include: quick Plot including combined fringe and deformation plot and fringe results are averaged at the nodes, deformation, fringe including contoured plot and provides significant control for result averaging and extrapolation, marker including plots individual markers for scalar, vector or tensor data, graph, reports, free-body including provides tools to generate free-body and interface plots. The resulting processing in the Patran software is described in Fig. 1.20.

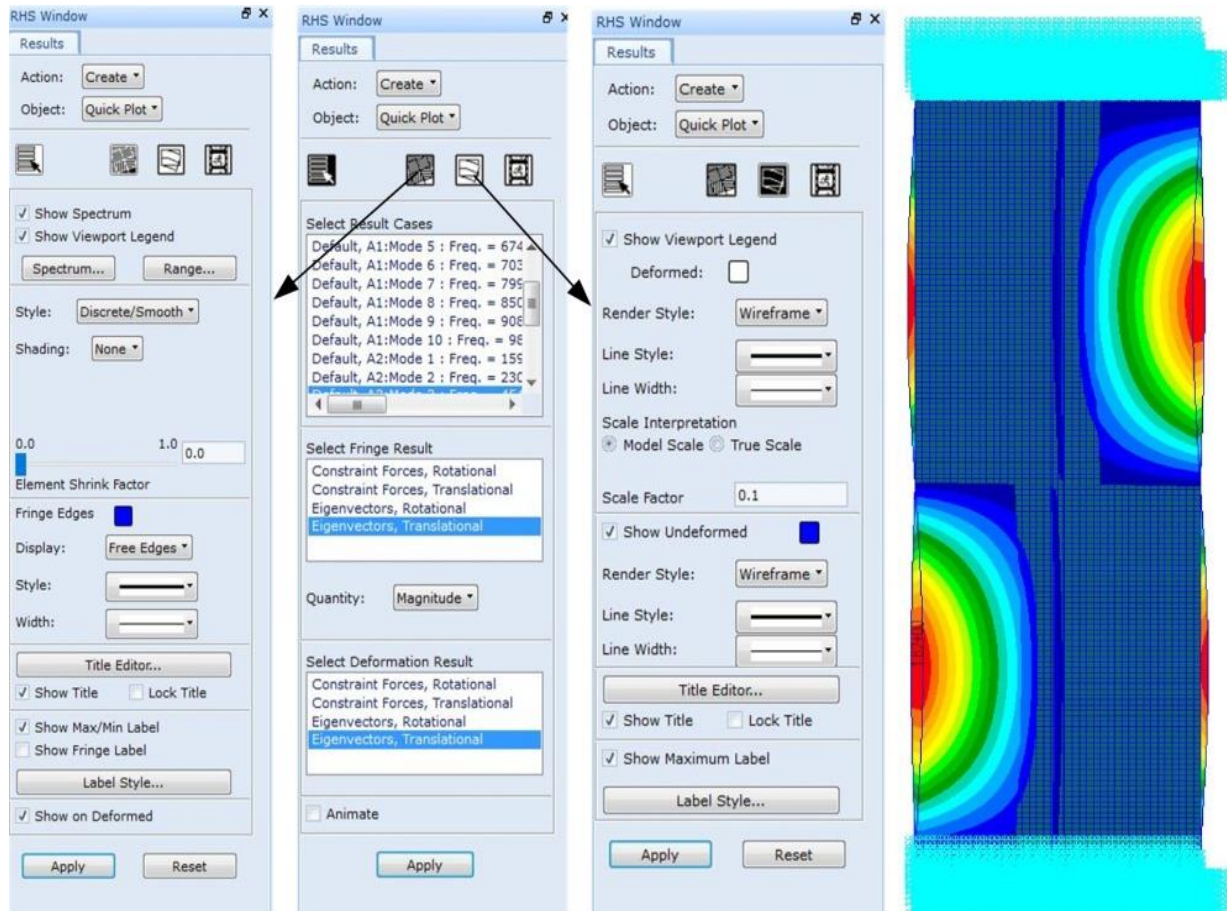


Fig. 1.20. Post-processing in the Patran-Nastran software

### 1.3.2. Measurement position and measurement methodology

Experimental research was carried out in the laboratories of the Faculty Marine Engineering of the Maritime University in Gdynia. The methodology of measuring research was based on the most promising and economical techniques, from the point of view of the analysis of static-dynamic characteristics of the selected structure. The tests were carried out mainly with the use of a Bruel & Kjaer vibration analyser, piezoelectric accelerometers, a modal hammer for impulse excitation. They were supplemented with measurements of displacement amplitudes carried out with the help of laser displacement sensors. The tests were carried out on a series of thin-walled plates with different parameters in two cases without and with water. Algorithms for determining new parameters and dynamic characteristics of objects implemented for the Matlab program. Scripts have been developed enabling automatic loading of measurement data, determination of diagnostic parameters and their graphical presentation.

In order to implement the adopted research plan, the author developed and constructed a laboratory stand. The measuring stand for testing thin plate and thin stiffened plate in two cases without and with water using vibration methods consist of: a stand, a Bruel & Kjaer type 3050-A-60 type vibration analyser, four 4514-B accelerometers, a modal hammer (8206 - 002). The construction of the stand allows mounting thin plates or thin stiffened plates vertically (two-point clamping). The described stand with an indication of the most important elements is shown in Fig. 1.21.

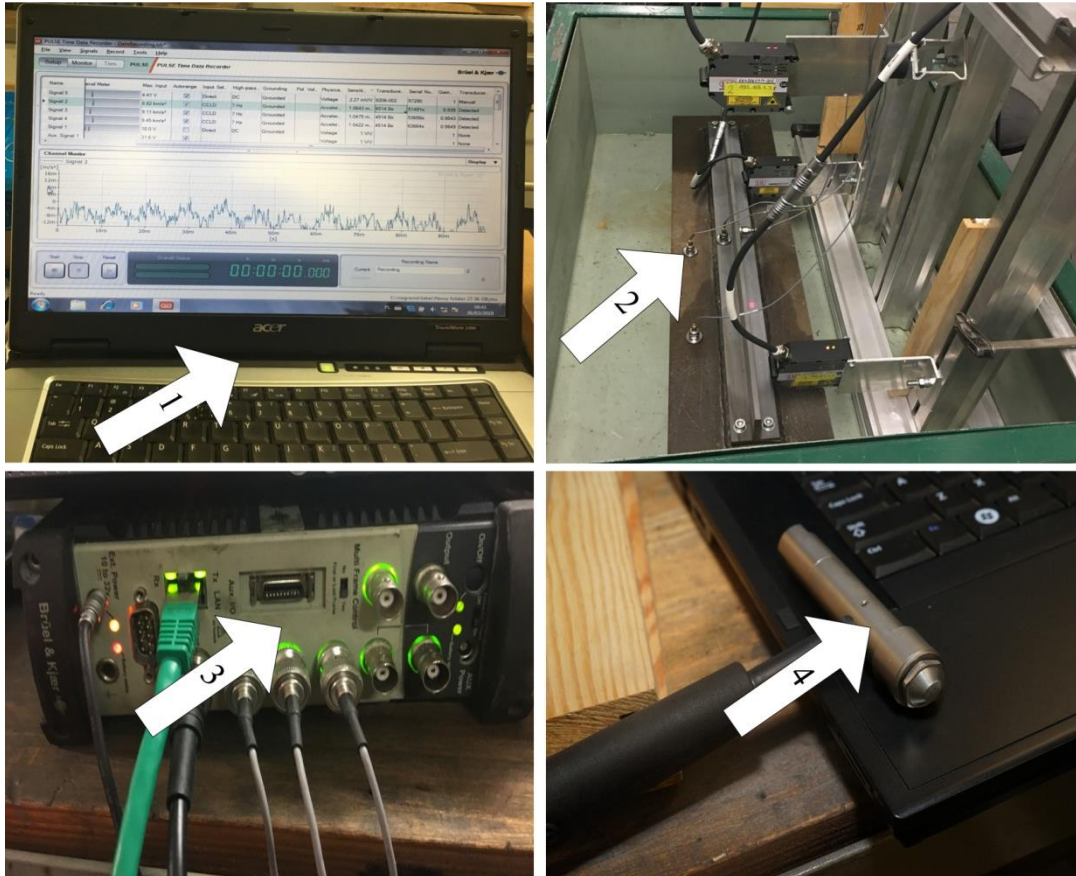


Fig. 1.21. Equipment for testing stiffened plates using vibration methods: 1 – Laptop, 2 - 4514B accelerometers, 3 - vibration analyser by Bruel & Kjaer type 3050A60, 4 - modal hammer (8206-002)

Vibrodiagnostic tests were carried out using measuring equipment shown in Fig. 1.21. The B&K 3050-A-60 measuring cassette is a measuring device that allows simultaneous measurement with 1 to 6 sensors. The device used has a maximum measuring band of 51.2 kHz/channel with a sampling rate of 131.072 kHz/channel, these values are independent of the number of connected channels. The device is equipped with a switchable high-pass analog filter with cut-off frequencies of 0.1, 0.7 Hz, 1 and 7 Hz, and 22.4 Hz. In the range up to 1 kHz and input signal voltage up to 1 V, the amplitude linearity is maintained at  $\pm 0.05$  dB. Noise in the range of 10 Hz to 25.6 kHz depends on the input voltage and range from 4  $\mu\text{V}_{\text{rms}}$  to 13  $\mu\text{V}_{\text{rms}}$  for an input voltage of 10 V. The dynamic range of the device is 160 dB, it is also equipped with a Butterworth type third-order anti-aliasing filter. The cassette is equipped with a 24-bit analog-to-digital converter.

The B&K 4514 B transducers are piezoelectric accelerometers of the DeltaTron type made in the IEPE (integrated electronic piezoelectric) standard - with built-in electronics (preamplifier). In the case of B&K products, IEPE standard transducers are known as CCLD

(Constant Current Line Drive). The use of the IEPE standard means that we get a voltage signal at the transducer output, thanks to which it is possible to use ordinary cables with one signal wire, for which there are no special requirements regarding impedance or low noise. Another advantage of this standard is the ability to remotely monitor the condition of the cable and connections between the transducer and the measuring instrument. The Pulse system used during measurements automatically detects any disturbances between the measuring cassette and the transducer and in case of their occurrence signals overdrive. The possibility of placing the transducer of its data (TEDS – Transducer Electronic Data Sheet) in the electronic module is also significant, which allows the system to automatically identify it, thus avoiding errors related to e.g. defining the incorrect sensitivity of the transducer. The measuring range of the transducers used is in the range from 1 Hz to 10 kHz, the declared sensitivity is 1 mV/ms<sup>-2</sup>. The transducer, as well as the entire measuring system, meets the requirements of all standards regarding the measurement of vibration parameters, including PN-ISO 10816-1.

The B&K modal hammer type B&K 2270 was used as the element forcing the impulse stimulating the tested panels to their own vibrations. This device is also made in the CCLD standard. The sensitivity of the modal hammer used is 2.27 mV/N and the maximum force that can be correctly registered with its use is 2200 N. The hammer was used in configurations with metal (aluminum) tips.

This measurement standard, as well as good measurement practice, imposes the obligation to calibrate entire measurement paths before and after measurements. The calibration procedure was carried out using the B&K 4294 calibrator –Fig. 1.22, which is an electro-dynamic exciter of vibrations with a maximum permissible load of 70 grams. The calibrator at 159.2 Hz generates a vibration signal with the following parameters: acceleration of vibrations with  $a_{rms}$  amplitude = 10 mm/s<sup>2</sup>, velocities with amplitude  $v_{rms}$  = 10 mm/s and displacement  $x_{rms}$  = 10 μm.



*Fig. 1.22. B&K calibrator [www.bksv.com access time 20.12.2018]*

During the measurements, time courses of vibration accelerations were recorded using the Pulse measuring system by Bruel & Kjaer. For the acquisition of vibration data, the Time Data Recorder program was used, which allows data to be exported to Matlab. During the analysis of signals recorded during vibration tests, the FFT (Fast Fourier Transformation) is

most often used. It is an algorithm that converts a digital signal from the time domain to the frequency. Digital signal processing requires analog-to-digital conversion of the input signal. The first step in the conversion is to sample the instantaneous amplitudes of the input signal at specific intervals, according to the sampling frequency selected. The tested (expected) device frequency cannot exceed half of the sampling frequency, because higher input frequencies contain false components, creating the phenomenon of Aliasing. As a consequence of the occurrence of aliasing in the spectrum reproduced from the incorrectly recorded signal, components with false frequencies appear.

The measurement was conducted by applying an arbitrary force of the hammer to the plates. After that, data were collected with the measurements. The sampling frequency with the accelerometers is 800 Hz. During the experiment, the measurement was repeated 20 times, to ensure accuracy. The vibration signal is received as a digital signal by the accelerometers, which are then amplified. Then, the amplified signal is received in the data acquisition thanks to the vibration analyser by Bruel & Kjaer type 3050A60, the final signal is analysed in the computer. The data collected will be frequency-analysed and graphed based on the Matlab software platform, thereby obtaining the natural vibration frequency of the thin plates and thin stiffened plates. Matlab is the program used in this thesis to analyse the data received from the experiment. Through the use of Matlab, it is possible to apply a Fast Fourier Transform to the sound data, in order to display graphically the resonance frequency of the selected structures is studied. After analysing the FFT of the vibration signals in the Matlab software, the spectral spectrum and the natural frequency values of the measurements are obtained. The spectra obtained from the measurements after FFT analysis in the Matlab software is analysed and compared with the results obtained from the numerical modelling method.

### **1.4. Summary of the results obtained**

A ship is a special device, operating independently on the sea, under extremely harsh conditions. Therefore, safety requirements are always the top priority when designing and manufacturing ships to reduce the risk of accidents that can cause damage to people and goods. To ensure that these requirements of marine machinery and structures before manufacturing need to be modelled, tested many times to meet the standards of safety, durability, reliability due to the ship registry association is launched. But marine structures and structures are often very complex, the cost of making samples is often very expensive, time-consuming, and even some tests may be deemed impossible to do. To solve that problem, numerical modelling methods based on numerical computation methods are increasingly developed and widely applied in industries in general and in the maritime industry in particular. The numerical modelling methods are widely applied, but the degree of reliability, the effect of errors and the dispersion on the analytical results depend very much on the confidence level and experience of implementation engineers.

In this thesis, the author evaluated the effects of the numerical model method based on the finite element method implemented in the Patran-Nastran digital software platform for a number of chosen maritime machines and structures. The influence of numerical models on the error and dispersion of the results of the analysis of selected maritime structures and machines, taking into account the computational conditions such as boundary conditions, the density of finite elements and finite element type are selected one-dimensional (1D), two-dimensional (2D) or three-dimensional (3D). The assessments are based on a comparison

between results obtained from numerical modelling and results obtained based on a number of empirical formulas verified by measurement methods. From there, assessing the accuracy of the selected numerical modelling method, selecting the most optimal numerical model for the selected structures, the scalability applies to the entire structure of the ship.

Based on the obtained results, the author asserts that the thesis has solved some initial contents of the thesis as follows:

1. Mathematical models of the small basic parts that make up the hull and superstructure such as beams, thin plates, stiffened plates has built. Analysis of selected structures takes into account factors that may cause errors and dispersion in calculations such as boundary conditions, density and finite element type to be applied.

2. Building the mathematical model for two container vessels of different sizes: an average container ship of 2000 TEU and a large container ship of 11400 TEU. One of the most important parameters analysed is the ship's vibration. Global vibrations of the entire hull and local vibrations of the superstructure and main engine body are determined. The results obtained by numerical models are compared with the empirical formulas given by Brown and F. M. Lewis and F. H. Todd and some other authors. Since then, confirming the accuracy and advantages of the numerical modelling method based on the finite element method, the ability to applied numerical modelling methods to other structures in the maritime field. The reliability and confidence of engineering calculations was improved when applying numerical modelling methods for structural calculations and analysis.

3. Finally, the author has applied the numerical modelling method to the ship's propulsion system. The mathematical models for the ship's propulsion system with many different assumptions are built, choosing the most optimal ship propulsion model. Determined (point 2) stiffness of ship hull is used as the boundary conditions of power transmission system. Apply the most optimal mathematical model of the ship propulsion system to analyse and align the shaft line of the typical ship propulsion system. Static and dynamic calculations analysis of the propulsion system are carried out and compared with allowed values.

The author has developed a number of calculation methods that allow a rational reduction of the levels of calculation errors, to an acceptable level while limiting the workload of numerical analyses. Within the dissertation obtained the following results:

1. The impact of calculation assumptions on errors and dispersion of analysis results in individual types of analyses (static, normal modes, forced vibrations) was estimated.

2. An optimal methodology for carrying out computational analyses using the finite element method was developed for the ship's hull structure (including its superstructure and main engine body), taking into account the purpose of the calculations (static strength calculations, vibration analysis, thermal calculations, etc.).

3. An optimal methodology for conducting calculations using the finite element method was developed for the ship's power transmission system, taking into account the purpose of the calculations.

4. The developed calculation methods were verified by comparing them with experimental tests of selected elements of ship systems, together with determining the levels of measurement dispersions.

The author has proved that it is possible to limit dispersions and errors in numerical modelling of the marine structures and machines to an acceptable level and consistent with empirical research.

### **1.5. The layout of this dissertation**

This dissertation comprises five chapters and general conclusions:

Chapter 1 presents an overview of the research thesis, research purposes, and research methodology. The method used in the thesis is based on the finite element method - performed on the Patran-Natsran software platform, the measurement method is based on vibration diagnosis techniques conducted in the laboratory of the Faculty of Marine Engineering, Gdynia Maritime University.

Chapter 2 is devoted entirely to the presentation of theories about ship strength, the vibration of the ship's hull and machinery, the sources of ship vibration, and empirical formulas for determining the vibration of thin beams and hull.

Chapter 3 presents mathematical models of the small basic parts that make up the hull and superstructure such as beams, thin plates, stiffened plates has built. Analysis of selected structures takes into account factors that may cause errors and dispersion in calculations such as boundary conditions, density and finite element type to be applied. The structures are also calculated and analysed in two cases of liquid contact and non-liquid contact. The results obtained are compared with the results from some experience formulas and verified by a measurement method based on the measurements performed in the laboratory of Gdynia Maritime University.

Chapter 4 built the mathematical model for two container vessels of different sizes: an average container ship of 2000 TEU and a large container ship of 11400 TEU. One of the most important parameters analysed is the ship's vibration. Global vibrations of the entire hull and local vibrations of the superstructure and main engine body are determined. The results obtained by numerical models are compared with the empirical formulas given by Brown and F. M. Lewis and F. H. Todd and some other authors. Since then, confirming the accuracy and advantages of the numerical modelling method based on the finite element method, the ability to applied numerical modelling methods to other structures in the maritime field. The reliability and confidence of engineering calculations was improved when applying numerical modelling methods for structural calculations and analysis

Chapter 5 has applied the numerical modelling method to the ship's propulsion system. The mathematical models for the ship's propulsion system with many different assumptions are built, choosing the most optimal ship propulsion model. Determined stiffness of the ship hull is used as the boundary conditions of the power transmission system. Apply the most optimal mathematical model of the ship propulsion system to analyse and align the shaft line of the typical ship propulsion system. Static and dynamic calculations analysis of the propulsion system is carried out and compared with allowed values.

The final section is the general conclusion of the thesis and further research and development proposals of the dissertation.

## **2. Ship safety hazards and their prevention**

A ship is a very special device, operating independently on the sea, in high-risk environments such as waves, storms or extreme weather conditions. These environmental factors greatly affect the durability, safety, longevity, and strength of ships. In this chapter, the author discussed some basic theories about the load and strength of ships. Besides, the author also analyzes some causes of damage to equipment and the structure of ships. The analysis and collection of fault data often occur to marine structures and equipment that play an important role in monitoring the health and diagnosing the condition of the equipment. This is a regular work on board to prevent possible failures as well as make predictions about the remaining workability of the device. Chapter 2 also provides some empirical formulas for calculating ship vibration, these empirical formulas will be used to calculate ship vibration and be compared with the results calculated by the numerical modelling in the next chapters.

### **2.1. Loads and strength of ships**

Ships are a very complex structure, whose main purpose is to transport goods by sea. Nowadays, the size of the ships is getting bigger, with the purpose of carrying more goods. Therefore, the load and strength of the ship are one of the very important parameters that need to be taken into account when designing a ship. The load of a vessel can vary and be divided into various cases such as the load of the cargo, waves, vibrations, which will be studied in detail in the next section. In order to accommodate such different types of loads, the ship's strength must also be designed to ensure consistency with all types of ship's load.

#### **2.1.1. Ship structural loads**

It is convenient to study and analysis, when the load on the ship structure is divided into four categories as follows: (i) static loads as fixed weights, (ii) low-frequency dynamic loads as quasi-static load, wave loads), (iii) high-frequency dynamic loads as vibrations, (iv) impact loads as blast, collisions. This division is based partly upon the nature of the load and partly upon the nature of the ship's response. Since the loads on the ship structure are very complex, in this section we refer only to the static load affecting the ship structure. Static loads are loads that vary slowly with time and change when the total weight of the ship changes, as a result of loading or discharge of cargo, consumption of fuel, or modification to the ship itself. Static loads are influenced by the weight of the ship and its contents, static buoyancy of the ship when at rest or moving, thermal loads resulting from nonlinear temperature gradients within the hull, concentrated loads caused by dry-docking and grounding. The static loads acting on a ship afloat in still water consist of two parts: buoyancy forces and gravity forces, or weights. The buoyancy force is the resultant of the hydrostatic pressure distribution over the immersed external area of the ship. This pressure is a surface force per unit area whose direction is everywhere normal to the hull. However, the buoyant force is the resultant perpendicular to the water surface and directed upward. The weights are body forces distributed throughout the ship and its contents, and the direction of the weight forces is always vertically downward. These component force systems are illustrated schematically in Fig. 2.1.

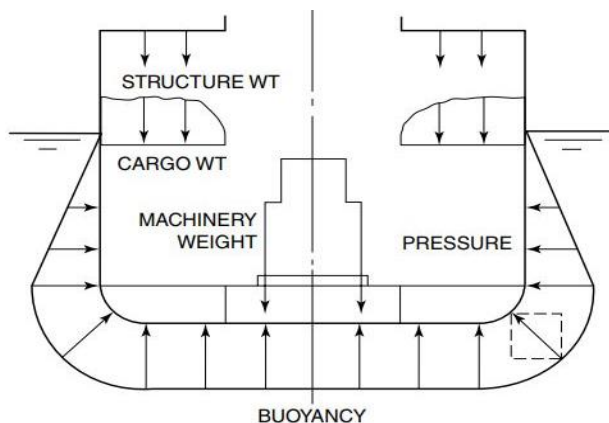


Fig. 2.1. Static load components on hull

If we integrate the local buoyant pressures over a unit ship length around a cross-section at a given longitudinal position, the resultant is a vertical buoyant force per unit length whose magnitude is given by  $\rho g A$ , where  $\rho g$  is the weight density of water ( $\rho$  is the mass density or mass per unit volume) and  $A$  is the immersed sectional area. Similarly, we may add all the weights contained in a unit length of the ship at this same section, resulting in a total weight per unit length. The net structural load per unit length is the algebraic sum of the unit buoyancy and the unit weight. The individual loads can have both local and overall structural effects. A very heavy machinery item induces large local loads at its points of attachment to the ship, and its foundations must be designed to distribute these loads evenly into the hull structure. At the same time, the weight of this item contributes to the distribution of shear forces and bending moments acting at all locations along the length of the hull. If a part of the content of the ship is made up of liquids (e.g., fuel or liquid cargo), there will be hydrostatic pressure forces exerted by such liquids that are normal to the boundary surfaces of the tanks within which they are contained. These internal pressure loads can have important local structural effects and must be considered when designing the bulkheads and other tank boundary members.

The conditions of static equilibrium require that the total weight and buoyancy be equal and that the center of buoyancy is on the same vertical line as the center of gravity. Two resultant forces act on a free-floating body, the force of weight acting downwards and the force of buoyancy acting upwards. The force of weight ( $W$ ), acts through a point known as the center of gravity ( $CG$ ), and the force of buoyancy ( $B$ ) acts through what is known as the center of buoyancy ( $CB$ ). By Archimedes' Principle, we know that the force of buoyancy equals the weight of the liquid displaced by the floating body, and thus the center of buoyancy is the center of gravity of the displaced liquid. Two forces are equal in magnitude, the centroid of the forces are vertically in line.

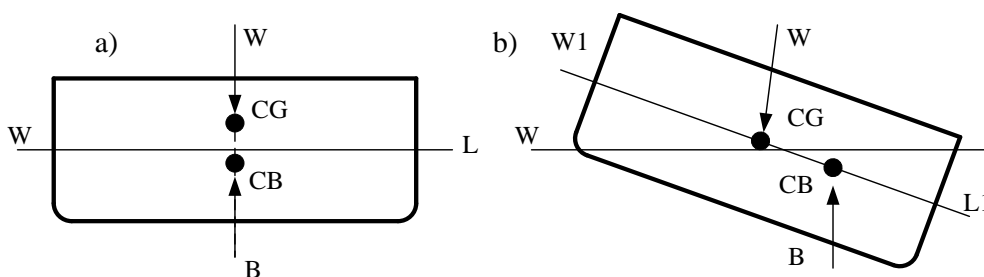


Fig. 2.2. Interaction of Weight and Buoyancy

When a floating body is in equilibrium and is displaced slightly from its original position, three conditions may apply. As shown in Fig. 2.2 [85], the body may:

1. Return to its original position, a situation known as positive stability,
2. Remain in its new position, and this is known as neutral stability,
3. Move further from its original position, known as negative stability.

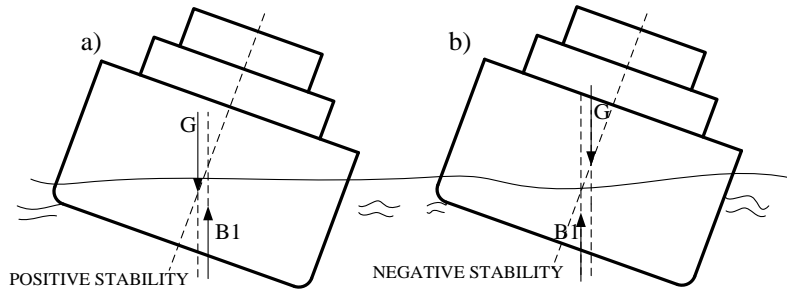


Fig. 2.3. Positive and negative stability

A ship should be positively stable so that it can return to its original position without overturning when displaced from its original position, say by a wave. The stability of a floating body such as a ship is determined by the interaction between the forces of weight,  $W$ , and buoyancy,  $B$ , as seen in Fig. 2.2. When in equilibrium, the two forces acting through the centers of gravity,  $CG$ , and buoyancy,  $CB$ , are aligned (Fig. 2.2a). If the body rotates from  $WL$  to  $W1L1$ , (Fig. 2.2b and Fig. 2.3a), a righting moment is created by the interaction of the two forces and the body returns to its original equilibrium state, as shown in Fig. 2.2a. This is a case of positive stability. If the interaction between the weight and buoyancy forces led to a moment that would have displaced the floating body further from its original position, it would have been a case of negative stability, as shown in Fig. 2.3b. Thus, when designing a ship, it is very important to ensure that the centers of gravity and buoyancy are placed in a position that results in positive stability for the ship.

### 2.1.2. Strength of ships

Another essential aspect of ship design is the strength of the ship. This refers to the ability of the ship structure to withstand the loads imposed on it. One of the most important strength parameters is the longitudinal strength of the ship, which is estimated by using the maximum longitudinal stress that the hull may withstand. The shear stress is another relevant parameter. The longitudinal strength of the ship's hull is evaluated based on the bending moments and shear forces acting on the ship. Considering a ship as a beam under distributed load, the shear force at location  $X$ ,  $V(X)$ , may be expressed as

$$V(X) = \int_0^X (b(x) - w(x))dx, \quad (2.1)$$

where  $b(x)$  and  $w(x)$  denote buoyancy force and weight at location  $x$  respectively. The bending moment at location  $X$ ,  $M(X)$  is the integral of the shear curve,

$$M(X) = \int_0^X V(x)dx. \quad (2.2)$$

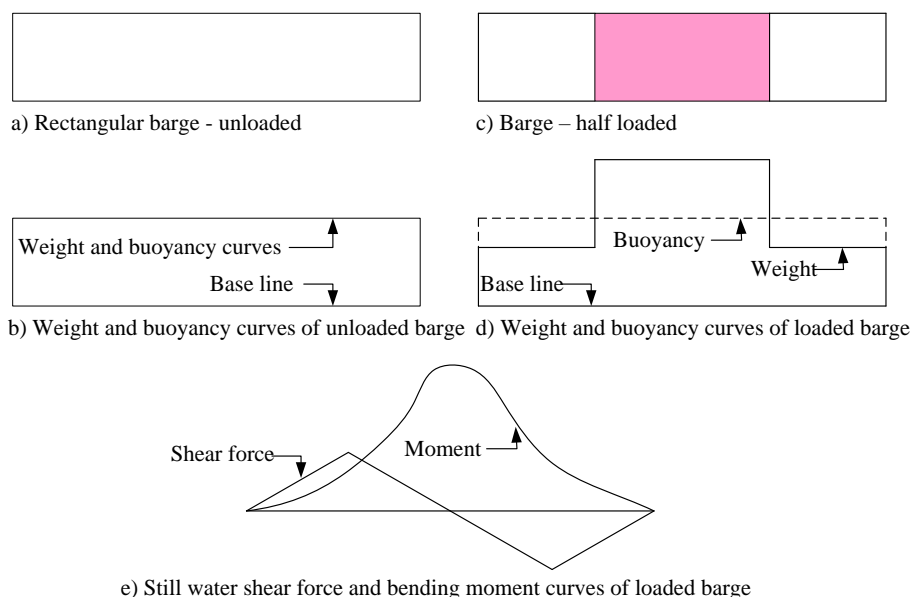


Fig. 2.4. Bending moment development of a rectangular barge in stillwater

This is further illustrated in Fig. 2.4 [85] for a ship in still-water (e.g. in harbors). As may be seen in Fig. 2.4a, an unloaded barge of constant cross-section and density, floating in water would have an equally distributed weight and buoyancy force over the length of the barge. This is represented by the weight and buoyancy curves, seen in Fig. 2.4b. If the barge were loaded in the middle in Fig. 2.4c, the weight distribution would change and the resulting curve is shown in Fig. 2.4d. This difference between the weight and buoyancy curves results in a bending moment distribution over the length of the ship. This bending moment is known as the still water bending moment,  $M_s$ , as seen for a loaded barge in Fig. 2.4e.

Longitudinal bending moment and stress for a ship in waves, the bending moment is further separated into two terms:

$$M = M_s + M_w , \quad (2.3)$$

where  $M_s$  and  $M_w$  denote still water and wave bending moment, respectively.

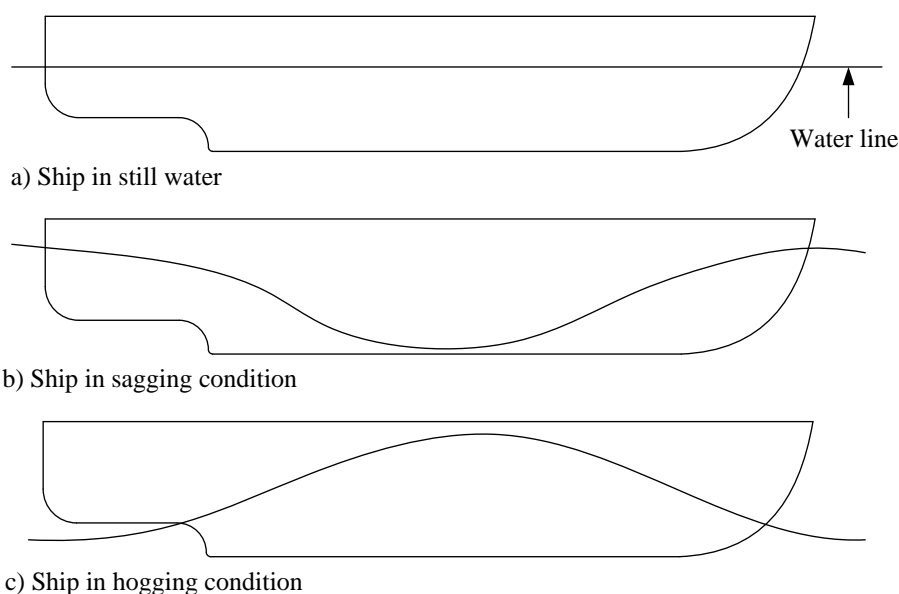


Fig. 2.5. Wave bending moment in a regular wave

Fig. 2.5 [83] illustrates a ship in a wave equal to its own length. Fig. 2.5a shows the still water condition where the only bending moment acting on the ship is the still water bending moment. Fig. 2.5b shows the condition when the wave hollow is amidships. This results in a larger buoyancy distribution near the ends of the ship and thus the ship experiences a sagging condition. In a ‘sagging’ condition, the deck of the ship is in compression while the bottom is in tension. Fig. 2.5c shows a wave crest amidships. In this case, the buoyancy force is more pronounced in the amidships section than at the ends of the ship thus resulting in a hogging condition. ‘Hogging’ means that the ship is arching up in the middle. Thus, the deck of the ship will be in tension while the bottom will be in compression.

In order to compute the primary stress or deflection due to vertical and horizontal bending moments, the elementary Bernoulli-Euler beam theory is used. When assessing the applicability of this beam theory to ship structures, it is useful to restate the following assumptions:

1. The beam is prismatic, i.e. all cross-sections are uniform,
2. Plane cross-sections remain plane and merely rotate as the beam deflects,
3. Transverse (Poisson) effects on the strain are neglected,
4. The material behaves elastically,
5. Shear effects can be separated from and not influence bending stresses or strains.

This gives the following well-known formula:

$$\sigma = \frac{M}{SM} = \frac{M_S + M_W}{SM}, \quad (2.4)$$

where  $SM$  is the section modulus of the ship. The maximum stress obtained from Eq.(2.4) is compared to the maximum allowable stress that is defined in the rules provided by Classification Societies for ship design. If the maximum stress is larger than the maximum allowable stress, the ship’s section modulus should be increased, and the drawing changed. The maximum bending moment is usually found in the mid-section of the ship, and thus the longitudinal strength at the mid-section of the ship is usually the most critical.

In general, the maximum shear stress is given by Eq.(2.5):

$$\tau = \frac{F_T S}{tI}, \quad (2.5)$$

where  $F_T$  is the total shear force,  $t$  and  $I$  denote the web thickness of the hull girder and the moment of inertia of the hull,  $S$  is the first moment of the effective longitudinal area above or below the horizontal neutral axis, taken about this axis. The distribution of the shear force on the sides and on the bulkheads is very complicated, and hence the required thickness is not easily expressed with a simple formula. Each classification society has its own empirically-based formulae for shear force and its distribution along the longitudinal direction. In conclusion, the static loading must be computed for several different distributions of cargo and other variable weights to obtain the extreme values of shear and bending moment. These extreme values will then be combined with other loads upon which the design of structural members will be based.

### 2.1.3. Ship structures review

A ship structure usually consists of a network of plates and supporting structures. The supporting structure consists of large members running both longitudinally and transversely and is often known as the Frame. The ship plating is attached to the frame. The structural components of the ship are described in the Fig. 2.6 [27].

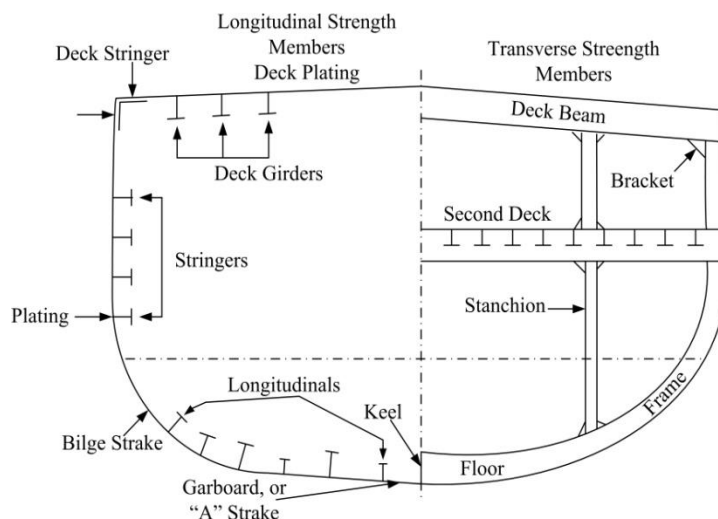


Fig. 2.6. Typical transverse and longitudinal strength members

The *keel* is a large center plane girder running longitudinally along the bottom of the ship. Plating is thin pieces closing in the top, bottom, and sides of the structure. *Plating* makes a significant contribution to longitudinal hull strength and resists the hydrostatic pressure load. The *frame* is a transverse member running continuously from the keel to the deck. Resists transverse loads (ie. waves hitting the side of the ship). The floor is deep frames running from the keel to the turn of the bilge. Frames may be attached to floors - the frame would be that part above the turn of the bilge. *Longitudinal* is girders that run parallel to the keel along the bottom of the ship. Longitudinal intersect floors at right angles and provide longitudinal strength. *Stringers* are girders running along the sides of the ship. Typically smaller than longitudinal, they also provide longitudinal strength. *Deck beams* are transverse members of the deck frame. *Deck girders* are longitudinal members of the deck frame.

1. *Framing systems*: The number and size of the different framing elements used in the construction of the frame of a ship is dependent upon a number of different factors. Clearly, it would be possible to make a ship very strong simply by adding more and more framing elements and increasing the thickness of its plating. However, this would make the ship increasingly inefficient in terms of space utilization and eventually cause it to sink when its displacement exceeded its possible buoyant force! There has to be a compromise between the requirements of strength and the conflicting but equally important requirements of buoyancy, space utilization, and cost. This compromise is to use an appropriate framing system to combat the types of load a particular ship is likely to encounter.

2. *Longitudinal strength members*: The longitudinal elements such as the keel, longitudinal, stringers and deck girders have a primary role in combating the longitudinal bending stress created by the ship sagging and hogging. These conditions are maximized when the ship's length is equal to the wavelength of a wave. A typical wavelength associated with an ocean wave is about 300 ft; consequently, ships of this length and greater are likely to

experience considerable longitudinal bending. Shorter ships experience much lower levels of bending because they tend to “terrain follow” a wave-like roller coaster. Consequently, ships that are longer than about 300 ft tend to have a greater number of longitudinal elements to their structures than transverse elements. This is taken to extremes in very long ships where their structure is almost totally based upon longitudinal elements. A ship framed in this manner is said to be - longitudinally framed.

3. *Transverse strength members*: The transverse elements such as frames and hull plating have a primary role to combat the hydrostatic load. For ships shorter than 300 ft and those designed to operate at large depths, this is the primary load of concern. Hence short ships and submarines have structures consisting of many frames and fairly thick plating. A ship structured in this manner is said to be – transversely framed.

4. *Combination framing system*: Modern Naval vessels typically use a Combination Framing System which combines the other two methods in some creative manner. A typical combination framing network might consist of longitudinal and stringers with shallow web frames. Every third or fourth frame would be a deep web frame. The purpose of such a system is to optimize the structural arrangement for the expected loading while minimizing weight and cost.

5. *Double bottoms* are just that, two watertight bottoms with a void space in between. They are strong and can withstand the upward pressure of the sea in addition to the bending stresses. Double bottoms provide a space for storing fuel oil, fresh water (not potable), and salt water ballast. The structure can withstand considerable bottom damage caused by grounding or underwater blasts without flooding the ship provided the inner bottom remains intact. Also, a double bottom provides a smooth inner bottom. This makes it easier to arrange cargo and equipment while providing better accessibility for cleaning.

6. *Watertight bulkheads*: The structural element that has not been mentioned so far is the watertight bulkhead. These are large bulkheads that split the hull of a ship into separate sections. In addition to their stiffening of the overall ship structure, they have a primary role in reducing the effects of damage on a ship. Ships are designed so that they can withstand specified levels of damage before water creeps onto the weather deck. The careful positioning of these watertight bulkheads allows the ship to fulfill these rules and withstand certain damage conditions. To enable watertight bulkheads to fulfill their role and withstand the pressures associated with flooded compartments, they are stiffened by steel members in the vertical and horizontal directions.

### **2.2. Ship vibration**

With the increase of ship size and speed, shipboard vibration becomes a great concern in the design and construction of the vessels. Vibration aboard ship can result in fatigue failure of structural members or major machinery components, can adversely affect the performance of vital shipboard equipment and increase maintenance costs, and result in discomfort or annoyance to passengers and crew. Determining the effect of structural dynamics and the causes of vibration will provide users, specifically shipyards, naval architects, and ship owners, to use the concept design to avoid excessive ship vibration at an early design stage. If ship vibrations are determined with insight and good judgment in the concept design stage, then the difficult countermeasures and corrections at the subsequent stages may be avoided in most cases. This will help to reduce the cost of fabrication,

exploitation as well as increase the reliability of the equipment and the safety of the crew while working on the ship.

The Ship hull can be seen as a system composed of multiple beams with stiffeners. The hull of the ship has a dense natural frequency spectrum. The hull is excited by a large number of exciting forces with such dense frequency spectrum these are the source of the vibrations. These vibrations are a complex mix of different frequencies. Thus, the phenomenon of resonant vibration is unavoidable. On ships, to ensure the safety, reliability, longevity of the equipment, as well as the comfort of passengers and sailors when working on ship, undesirable vibrations must be suppressed or reduced. In order to minimize the impact of ship dynamic, especially the resonant vibrations, when designing, engineers need to calculate and pay attention to some important issues. Calculating the natural vibrations frequencies, the forced vibrations of the structure, helps the designer limit resonant areas. The propulsion system design of the vessel is most suitable, preliminary calculations of the hull vibrations and its structures, measurement, and analysis of measurement results. The design and layout of the ship's systems must ensure that the hydraulic excited is at the lowest possible level, through the appropriate arrangement of the propulsion system and the shape of the vessel. The equilibrium loss of inertia forces and inertia moments are the sources of vibrations for the engine. Typically, when designing motors, engineers will try to limit these vibrations at the lowest possible level.

The vibration of ships is very complex. The complexity of the phenomena ranges from piping vibration to total vibration of the hull, the failure of a reduction gear, a propeller shaft, or the global movement of a deckhouse. So when studying the vibration as well as the reaction of the parts on board, we tend to simplify them - we only consider a number of factors, important equipment. Therefore, it has been found to be convenient in both design studies and shipboard evaluation to divide the complete ship system into the following basic elements: hull structure, major structural substructures like deckhouse, main engine body, main propulsion machinery system: power transmission system.

### **2.2.1. Hull structure vibration**

The ship's hull structure includes the girders, the shell plating like broadside, main deck, and double bottom, and all internal members, which collectively provide the necessary strength to satisfactorily perform the design functions of the ship in the expected sea environment. The hull girder responds as a free-free beam (both ends free) when subjected to dynamic loads. Although the surrounding water and loading of the hull influences its response, the hull girder will always responds as a free-free beam. The vibration of the hull girder, excited by alternating propeller forces, represents the most frequent source of troublesome vibration encountered aboard ship. The vibration characteristics of the ship are primarily established by the propeller and stern configuration. In addition, the vibration of the hull girder will provide the excitation to the major substructures, local structural elements, and shipboard equipment. Main propulsion machinery and auxiliary machinery can also contribute to general hull vibration and the vibration of local structural components. Primary excitation sources are shown in Fig. 2.7 [27].

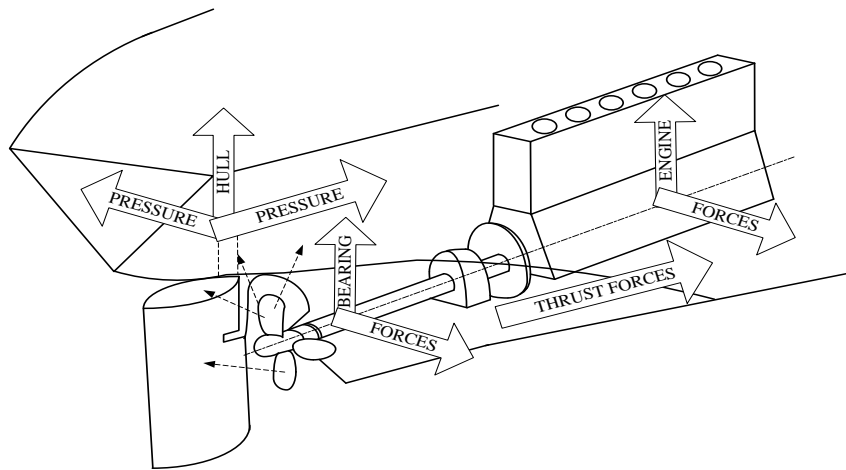
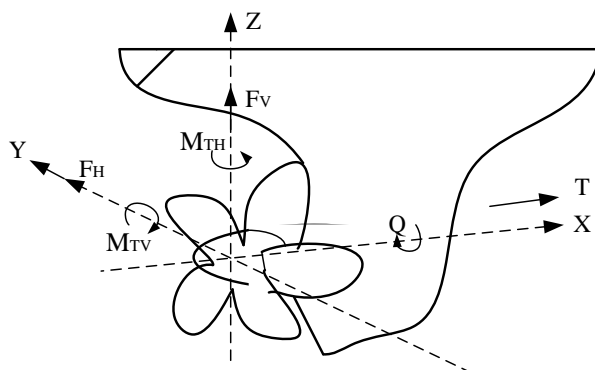


Fig. 2.7. Main excitation sources (taken from [27])

1. *Shaft frequency forces:* Mechanical forces that are associated with shaft rotational speed may result from one or more of the following causes (i) shaft unbalance, (ii) propeller unbalance, (iii) propeller pitch error, (iv) engine unbalanced, (v) coupling or flange misalignment. Shaft frequency forces occur within a low-frequency range. They are, however, of considerable concern since they may be of large magnitude and may excite one of the lower hull modes at or near full power, thus producing a significant resonant effect.

2. *Propeller forces:* In addition to the basic design purpose of generating steady thrust for the ship's propulsion, the marine propeller also generates undesired fluctuating dynamic forces and moments due to its operation in a non-uniform wake caused by the passage of the blades close to the hull and appendages. These fluctuating forces and moments are usually referred to as propeller forces and are at fundamental blade frequency and higher harmonics. The higher harmonics are normally of secondary importance. These propeller forces are in turn categorized as either bearing or hull pressure forces.

*Bearing forces* excite the ship through the propulsion shafting/bearing system and are fully described by six components illustrated in Fig. 2.8. As shown in Fig. 2.8 [27], with the origin of axes at the center of the propeller, these components are the thrust and torque in and about the longitudinal or fore and aft axis; the horizontal bearing force and the vertical bending moment in and about the horizontal or athwart-ship axis; and the vertical bearing force and horizontal bending moment in and about the vertical axis. Fluctuating vertical and horizontal bearing forces result from differences in torsional forces on the blades of the propeller, while the vertical and horizontal bending moments are due to the propeller thrust vector-center at a point that is eccentric to the center of the propeller.



X, Y, Z axes are fore aft, athwartship, and vertical axes, respectively,  
 T is thrust,  
 $F_H$  is horizontal bearing torque,  
 $F_V$  is vertical bearing torque,  
 Q is torque,  
 $M_{TH}$  is horizontal bending moment,  
 $M_{TV}$  is vertical bending moment.

Fig. 2.8. Description of bearing forces and moments

*Hull pressure forces* originate from the pressure variation caused by the passage of propeller blade tips close to the hull and appendages. The hull pressure forces are affected by propeller-hull clearance, by blade loading, and by changes in the local pressure field around the blade. The occurrence of blade cavitation will drastically increase the pressure forces. The pressure forces excite the ship through the hull bottom surface in way of and adjacent to the propeller. The pressure forces are fully described by six components: the longitudinal force and moment in and about the fore-aft axis, the horizontal force and vertical moment in and about the athwart-ship axis, and the vertical force and horizontal moment in and about the vertical axis illustrated in Fig. 2.9 [27].

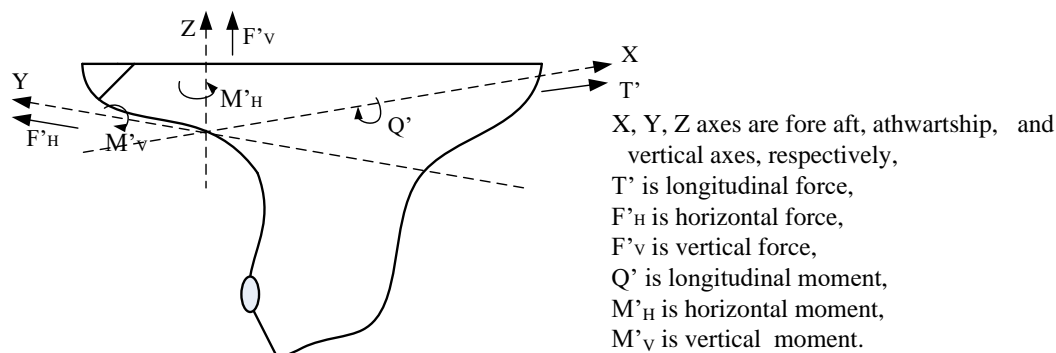


Fig. 2.9. Description of hull pressure forces and moments

*Effect of propeller forces:* The alternating blade frequency thrust of the bearing forces provides the principal excitation to the propulsion system in the longitudinal mode, while the blade frequency torque constitutes the principal excitation to the propulsion system in the torsional mode. The blade frequency vertical bearing force, when victory combined with the blade frequency vertical pressure force, provides the total vertical force, which excites the hull in the vertical direction. Similarly, the horizontal bearing forces, when combined with the blade frequency horizontal pressure forces, provide the major contribution for exciting the hull in the horizontal direction. The vertical and horizontal forces and their distance from the neutral axis of the hull combine to excite the hull torsionally. Longitudinal hull pressure forces and alternating thrust entering the hull through the thrust bearing will combine to excite the hull in the longitudinal direction.

### 2.2.2. Vibration of major substructures

For purposes of evaluation, major substructures are defined as secondary structures of sufficient mass or are capable of developing sufficient force to have dynamic characteristics of their own, which, because of the direct coupling with the vibration of the hull girder, can significantly influence the total or global pattern of vibration of the ship. In analyzing vibration patterns of such large complex structures it is necessary to identify the principal reason for excessive vibration when observed. Although the excitation of the substructure generally originates at its attachment to the hull structure, excitation can come from machinery or active equipment mounted in the major substructure. Excessive vibration of a major substructure may result from structural resonances in the substructure or in the method of attachment of the substructure to the hull girder. Because of the mass involved and method of attachment, the major substructure can amplify the response of the hull structure.

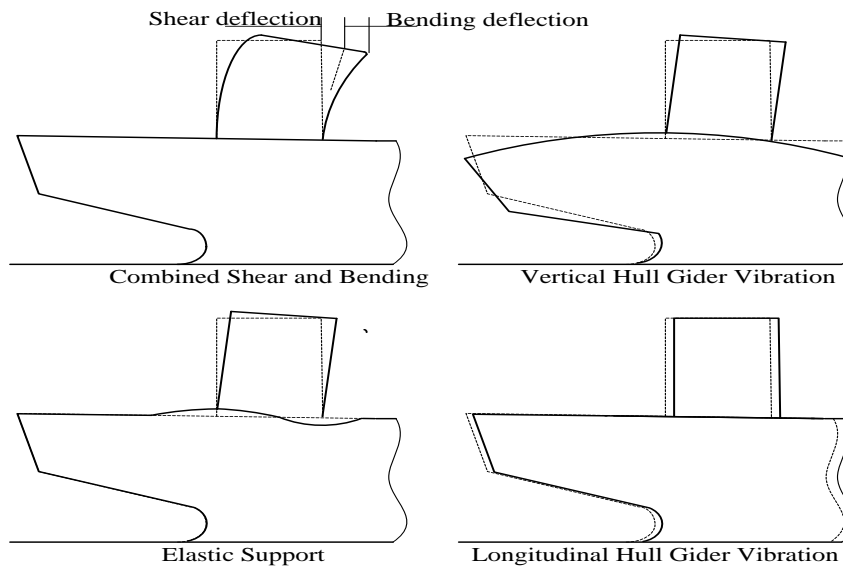


Fig. 2.10. Superstructure longitudinal vibration

Typical major substructures would include deckhouses; main deck structures; large propulsion machinery systems, particularly large slow-speed diesel; and other heavy installations, including their foundations, such as boilers, reactors, rudders, etc. The Fig. 2.10 shows some possible modal patterns of vibration frequently found in aft deckhouse structures when excited by flexural and longitudinal vibration of the hull girder. Those shown indicate longitudinal vibration and include: superstructure shear deflection, superstructure bending deflection, superstructure support deflection with rigid body motion, vertical hull girder vibration, longitudinal hull girder vibration. The dynamic response characteristic of the superstructure is primarily a function of superstructure shear stiffness and supporting structure vertical stiffness and the degree of coupling to hull girder modes. The superstructure rigid body motion is mostly due to the hull girder response.

### 2.2.3. Vibration of main propulsion machinery

The main propulsion system consists of all parts of the shaft system and main engine. The vibration of the main propulsion machinery contributes to the vibration of the vessel. Dynamic stresses within the system and within the system components are a major concern. The control of dynamic forces generated by the propulsion system contributes to the vibratory characteristics of the total ship. Although the vibration of both the ship's hull and main propulsion machinery are interrelated, it is convenient, both in preliminary design studies and in the control of shipboard vibration, to conduct independent studies on the propulsion system. It is necessary, however, to include actual or empirical factors related to the ship's structure, which form an important part of the effective mass-elastic system under study. In particular, the stiffness of the thrust bearing foundation is critical when evaluating the response of the longitudinal vibration of the propulsion system. The main areas of concern that can give rise to troublesome vibration or dynamic stresses include: dynamic unbalance and misalignment, shaft line alignment, dynamic shaft stresses, longitudinal vibration, torsional vibration, lateral vibration, excitation of the main engine.

*1. Shaft line alignment:* Proper shaft line alignment is one of the most important actions during the design of the propulsion system [118, 75]. It consists of determining the location of the main engine driving axis, intermediate bearings axis and stern tube bearing

axis. The propulsion system bearing is usually mutually moved in the vertical plane. An example of the typical shaft line alignment of a container ship is shown in Fig. 2.11.

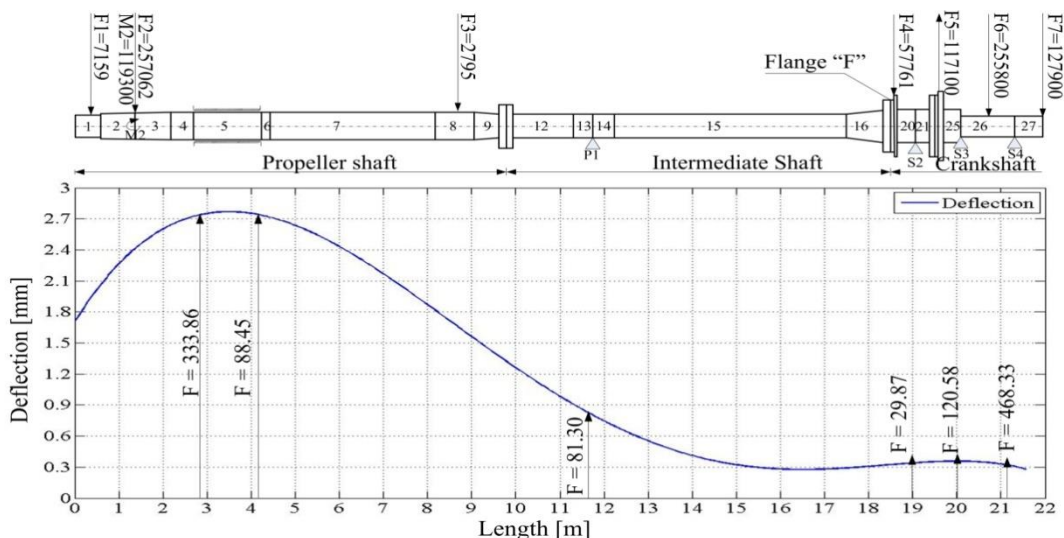


Fig. 2.11. Shaft line alignment for the container ship

Appropriate loadings of the shaft line and crankshaft bearing are the main targets of the shaft line alignment. Firstly, reactions in the stern tube and intermediate bearings do not have to be high or too small in all the propulsion's service conditions. In the case of low static bearing's reactions, the possible influence on lateral vibrations (dynamic reactions) should be considered. If the static reaction is similar to the dynamic one, the loading direction might be changeable. Impact loading might be the cause of a quick deterioration of the bearing. The bending stresses of the shaft line in the given final alignment should be checked. Usually (for most typical marine power transmissions systems) these quasi-static stresses are not very high for all service conditions.

2. *Dynamic unbalance and misalignment:* Dynamic and hydrodynamic unbalance of the propeller, dynamic unbalance of shafting, bull gears, and other large components of the propulsion system operating at propeller shaft speed may contribute to objectionable hull vibration, particularly if the exciting frequency falls in resonance with a natural frequency of the hull. Such difficulties may also arise from the primary or higher-order unbalanced forces in large, slow-speed diesel engines or from serious shaft misalignment. It is generally true, however, that the vibration occurring at these low frequencies will be particularly objectionable to humans when operating at the lower hull resonances. The vibration that exceeds the recommended criteria should be corrected to prevent local damage and excessive bearing wear. Specific corrective action may be required to control primary and secondary unbalances in slow-speed diesel engines.

3. *Dynamic shaft stresses:* Propulsion shafting is normally designed in accordance with Classification Society Rules (ABS, Lloyds, etc.), and in some instances, by Navy rules [22]. With normal design practice, periodic inspections, and proper maintenance procedures no difficulty should be experienced with propulsion shafting during the life of the ship. However, experience has indicated serious difficulties, including shaft failure, which can happen under normal operating conditions [81]. Shaft problems are related to dynamic stresses that in most cases are exacerbated by corrosion fatigue. Such problems may be caused by the eccentric thrust, precipitated by adverse flow conditions at the propeller, and

aggravated by misalignment and faulty shaft seals. Excessive stresses associated with torsional vibration in slow-speed diesel engine drives are also a potential problem area. As a minimum, the complete propulsion system should be evaluated for acceptable steady and dynamic stress levels during the design phase, and verified during ship trials. Maintenance procedures should check for corrosion and fatigue cracks at the propeller keyway and at the shaft near the forward end of the propeller hub.

4. *Longitudinal vibration:* The propulsion system may exhibit excessive longitudinal vibration caused by alternating thrust generated by the propeller at blade frequency or harmonics of blade frequency. The vibration is considered excessive if it exceeds machinery criteria and can be particularly damaging to thrust bearings and/or reduction gears. Depending on structural characteristics, the alternating thrust forces transmitted to the ship through the thrust bearing can cause serious local vibrations in the engine room and to serious superstructure fore and aft response. Fig. 2.12 shows the longitudinal vibration of a typical propulsion shaft. The forces transmitted to the ship's structure are dependent on the total mass of the system shown in Fig. 2.12 and the combined thrust bearing and foundation stiffness.

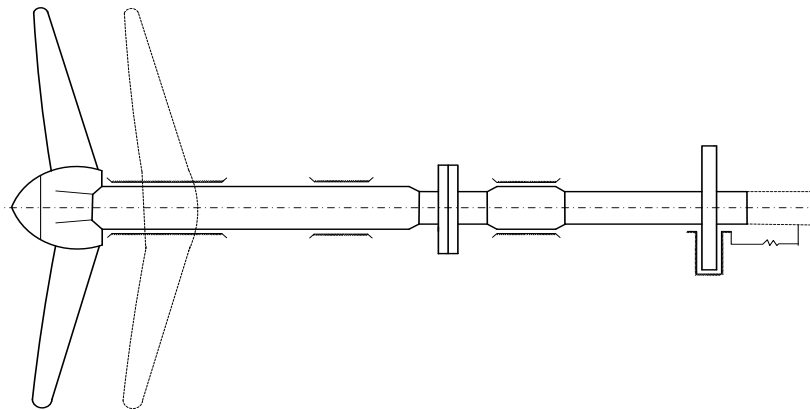


Fig. 2.12. Longitudinal vibration of shafting system

5. *Torsional vibration:* Torsional vibrations are the result of the pulsing torque of the reciprocating combustion engine and the torsional elasticity of the power transmission system. All system components like the crankshaft, intermediate shaft, propeller shaft, and optional couplings and gears have to transmit the static torque and the additional vibratory torque. Ordinarily torsional resonances within the shafting system are shown in Fig. 2.13. Torsional vibrations of the marine power transmission system are usually the most dangerous for the shaft line and the crankshaft. Vibratory stresses, torques and/or angular amplitudes have to be analysed by calculations and very often by measurements for all marine propulsion systems. In diesel engine drive systems of all types, torque reactions can be a major structural vibration concern. Additionally, torsional resonances can be damaging to system components. Although the evaluation of the torsional vibration of the shafting is subject to classification rule requirements, it is also considered necessary to carry out a torsional vibration analysis of the complete propulsion system in the design phase and verify the system response characteristics during ship trials. The research methods have been developed since the 1950s [80] and are well known [112].

The design formulas (determined dimensions of shaft line and crankshaft) do not take into consideration the possibility of dangerous torsional vibration and where the propulsion critical speed is located. Danger torsional vibration stresses may occur within the operating range. Calculations should be submitted, including tables of natural frequencies and vector

summations for critical speeds of all significant orders up to 120% of the rated speed. The classification societies defined the stress limits for the crankshaft is a constant and for shaft line is defined as a rotating speed function (for higher speeds the limit is lower). When torsional stresses exceed the limits, at revolutions within the operating range, a barred speed range should be provided. Continuous operating of the main engine is prohibited in the barred range; main engine revolution has to be changed as quickly as possible. In the barred speed range a higher vibratory stress level is allowable. Barred ranges are not acceptable in a speed range between 0.8 and 1.05 of the rated speed. The existence of a barred speed range should also be defined; it should be equal to about  $\pm 10\%$  with respect to the critical engine speed.

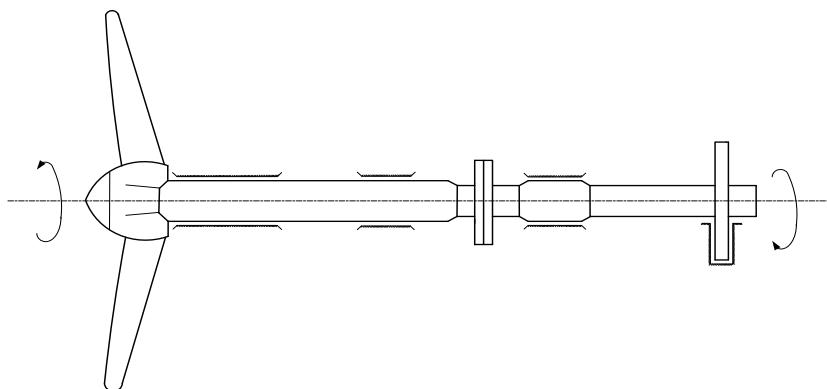


Fig. 2.13. Torsional vibration of typical shafting system

6. *Lateral vibration:* The propulsion shaft system, Fig. 2.14, is designed so that the fundamental lateral or whirling critical speed is well above the running speed. Dynamic, bending stresses, shear forces and lateral vibration amplitudes of the shaft line are negligible in comparison to a shaft line torsional vibration.

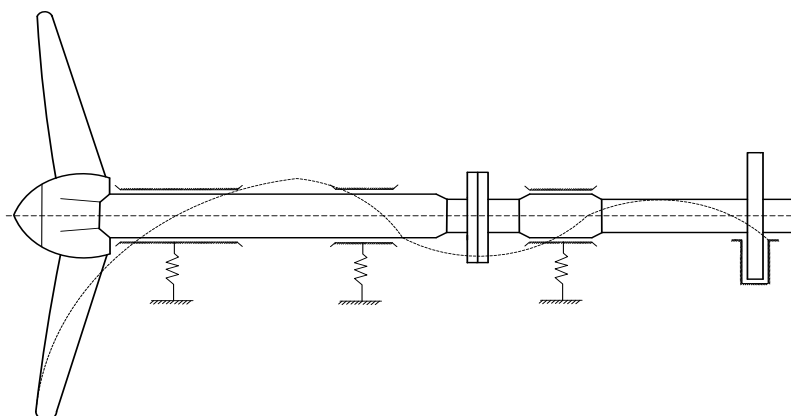


Fig. 2.14. Whirling vibration of shafting

The lateral vibration analysis should be treated as the second part of the shaft line alignment calculations. The lateral vibration calculation's correctness depends totally on the proper boundary condition's determination. Shaft line alignment has a strong influence on the bearing's stiffness and damping characteristics. The dynamic component of the bearings' reactions and crankshaft flange loading were taken into account during shaft line alignment analysis. However, it is not only the dynamic behaviour of the propulsion system which should be analysed during the ships designing. The ship hull and superstructure vibrations calculations are nearly as important as the dynamic analyses of the power transmission

system. These are not separate problems. The bearings' reaction (coming from the lateral and longitudinal propulsion system vibrations) is one of a ship hull and deckhouse excitation forces. Therefore, the bearings' dynamic reactions should be determined. The Fig. 2.14 taken from Det Norske Veritas guidelines [27] shows the influence of the position of the aft bearing support on the frequency of the whirling critical. Misalignment or serious bearing wear can result in high dynamic stresses in the shaft, dynamic magnification of bearing reactions and increased hull vibration, and overheating. On the assumption that the design was satisfactory initially, good maintenance is required to keep it that way. The use of roller bearings or self-aligning bearings and attention to dynamic balance will minimize potential problems.

7. *Main engine excitations:* The principle of operation of piston combustion engines causes the formation of unbalanced, external forces and dynamic moments. Marine engines have balanced all external forces and moments of main orders. However, always some of the moments remain unbalanced. They cause longitudinal, transverse and torsional vibrations of the engine body, which are transferred to other ship structures. Unbalanced torque values are given in the engine documentation. The unbalanced moments of the main engine, generated by gas and inertia forces of the piston-crank system. There are internal and external excitation forces and moments of the engine. Internal forces and moments will deform the engine. The most important internal moments for the ship structure vibrations are the lateral X-type moments of a different order. External forces and moments acted on the ship through the foundation. External forces and moments are external moments (order 1 and 2), lateral H-type moments (different order). There are three important vibration modes of the engine: the H-mode, which is the torsional vibration mode around the longitudinal axis, the X-mode, which is the 'twisting' vibration mode around the vertical axis, and the L-mode [76, 15, 42].

External horizontal moments are presented as Fig. 2.15.

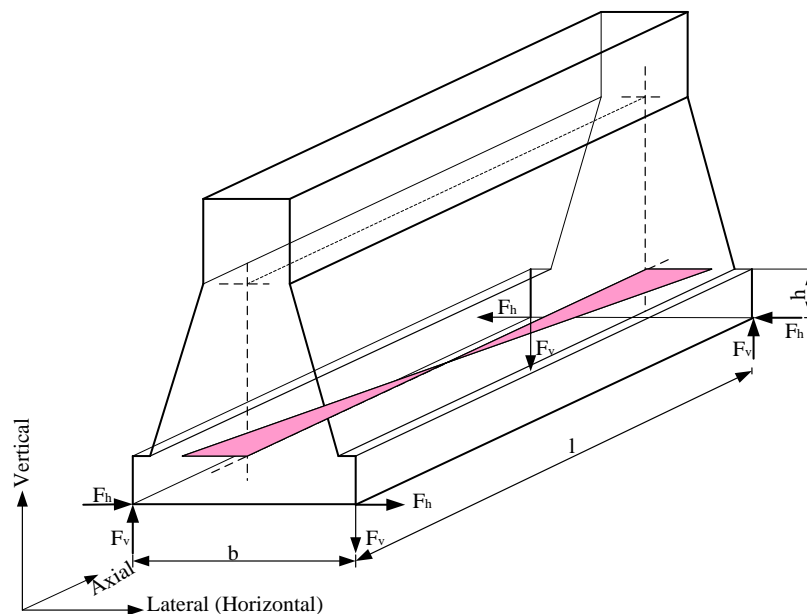


Fig. 2.15. External horizontal moments

The external horizontal moments depend on the firing order and the rotating masses of the running gear. In in-line engines, there is only a first-order horizontal moment. The horizontal and vertical foundation forces can approximately be calculated as follows:

$$F_{1h} = \frac{M_{1h}}{2b}, \quad (2.6)$$

$$F_{1v} = \frac{h}{2bl} M_{1h}. \quad (2.7)$$

External vertical moments are illustrated as Fig. 2.16.

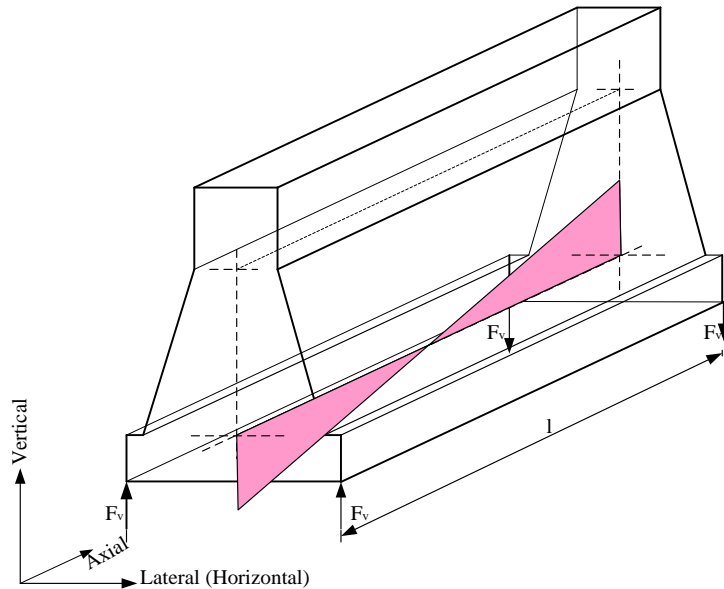


Fig. 2.16. External vertical moments

The external vertical moments depend on the firing order, the geometry of the running gear, and the oscillating and rotating masses. The vertical foundation forces of 1<sup>st</sup> and 2<sup>nd</sup> order can be calculated as follows:

$$F_{1v} = \frac{M_{1v}}{2l}, \quad (2.8)$$

$$F_{2v} = \frac{M_{2v}}{2l}. \quad (2.9)$$

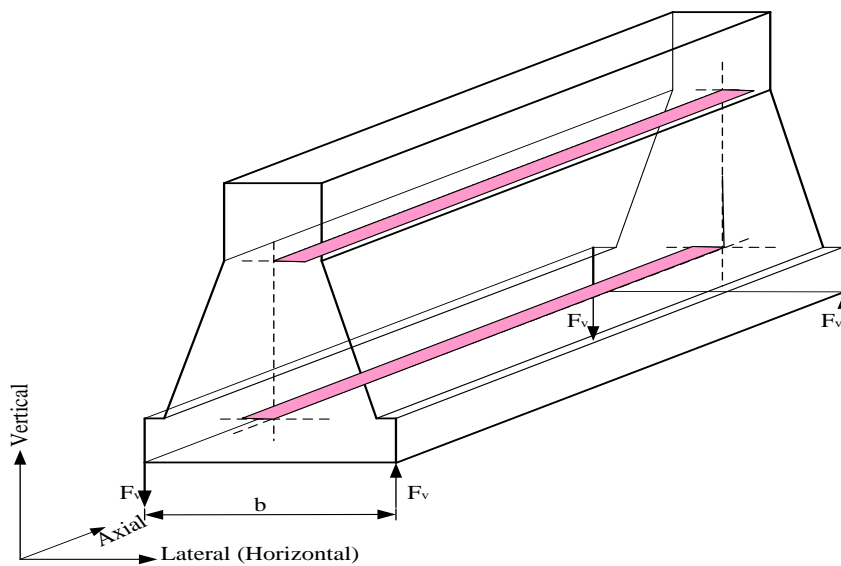


Fig. 2.17. Lateral H-type moments

The lateral components of the gas and inertia forces acted on the cylinder lines through the piston in four-stroke engines and on the cylinder block through the crosshead bearing in two-stroke engines. They find their reaction forces in the journal bearings at the bedplate. The vector sum of the harmonic forces for a given order depends mainly on the firing order. The lateral forces can generate engine vibration in either the H-mode as Fig. 2.17 or X-mode as Fig. 2.18.

When the lateral guide forces all act in phase, they generate a moment about the longitudinal axis. The lateral H-type moment of order 0 is equal to the nominal torque and can be calculated from the values for power and speed. The resulting torque variation as given in our documentation is nearly the same as the lateral H-type moment for the main order (order = cylinder number). The vertical foundation forces can be calculated as follows:

$$F_{iv} = \frac{T_i}{2b}. \quad (2.10)$$

### Lateral X-type moments

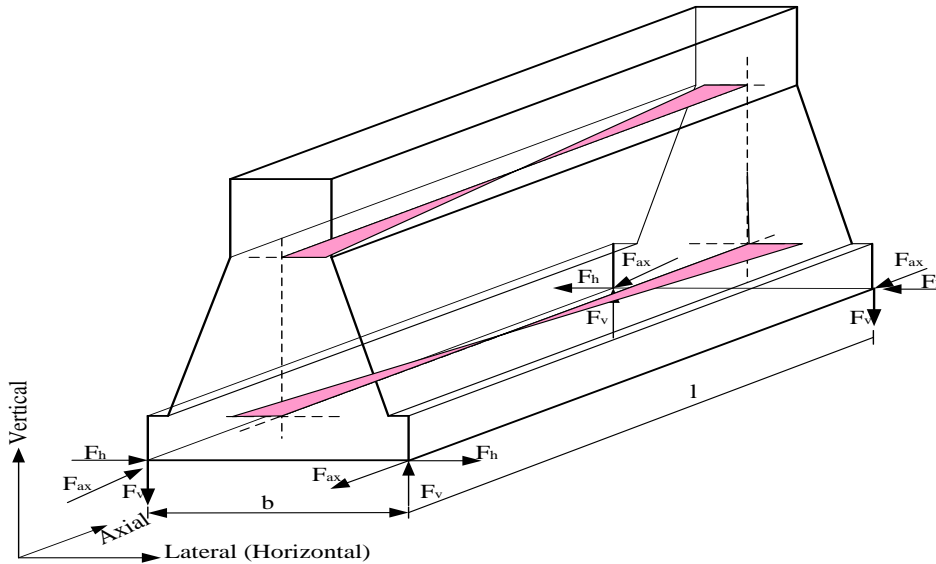


Fig. 2.18. Lateral X-type moments

The lateral forces also induce lateral moments of various harmonic orders about the vertical axis of the engine, when they do not act in the same phase. Lateral moments are internal moments. Their reaction forces on the ship structure depend on the stiffness and the natural frequencies of the engine fitted to the ship foundation. A good approximation for the foundation forces for the ship structure calculation is given as follows:

$$F_{ih} \approx 0.15 \frac{M_{il}}{l}, \quad (2.11)$$

$$F_{iv} \approx 0.08 \frac{M_{il}}{b}, \quad (2.12)$$

$$F_{iax} = \frac{l}{b} F_{ih} \approx 0.15 \frac{M_{il}}{b}, \quad (2.13)$$

where  $l$  is the length of the bedplate of the main engine,  $b$  is the width of the bedplate of the main engine,  $h$  is the height of the bedplate of the main engine.

### 2.3. Simplified, analytical formulas for ship vibrations determination

The ship is a kind of complex elastic structures. During ship sailing operation, it will be encountered with the external exciting forces from main engine, propellers and wave loads. These incentives will cause the hull vibration issue and even ship structural damage. Excessive vibration may lead to structural fatigue failure affect shipping efficiency, human-being health, and the service life of equipment [55]. So, to forecast the ship's hull natural frequencies accurately at the design stage is very important for avoiding harmful vibration especially the overall vertical vibration. In general, empirical formulas are widely and efficiently used to predict the ship-hull vertical vibration at the design stage. The empirical formula method is simple and practical. Many professionals have done a lot of work in the study of empirical formulas for the prediction of the natural frequency of the ship's overall vertical vibration [48, 58, 79, 117, 118, 111]. Schlick formula and Todd formula are earliest used as the empirical formulas. In recent years, the focus of the ship's overall vibration study is mainly cantered on the ship overall vibration analysis by 3D FEM methods [95, 113] and computation of added mass in ship vibration analysis. Specifically, Ivo SENJANOVIĆ et al [96÷98] systematically study on the coupled horizontal and torsional vibration of the ship hull with large hatch openings such as container ship et al; Josip BAŠIĆ and Joško PARUNOV [6] make an in-depth study on the calculation method of added mass in ship vibration analysis and compare the result of each calculation method. Determining the vertical natural frequency using empirical formulas plays an important role in evaluating the FEM models used.

#### 2.3.1. Empirical formula for natural bending frequency of thin-walled beams

The bending vibration equation of thin-walled uniform beam in consideration of the effect of shear deformation and moment of inertia is [118]:

$$EI \frac{\partial^4 y}{\partial x^4} + \rho A \frac{\partial^2 y}{\partial t^2} - \rho I \left(1 + \frac{E}{kG}\right) \frac{\partial^4 y}{\partial x^2 \partial t^2} + \frac{\rho^2 I}{kG} \frac{\partial^4 y}{\partial t^4} = 0. \quad (2.14)$$

Where  $I$  is beam section moment of inertia.  $E$  is elastic modulus.  $G$  is shear modulus of material.  $A$  is the cross-section area of beam,  $\rho$  is density of the material,  $k$  is coefficient related to the cross-sectional shape which had been sufficient studied by G. R. Cowper [17].

Timoshenko beam theory assumes that when the beam bending deformation occurs, the cross-section perpendicular to the middle section originally remain as the plane; so, the assumption of uniform distribution of shear stress and shear strain on the section can be introduced. Actually, Shear stress and shear strain on the cross-section is not evenly distributed. In G. R. Cowper [17] has carried on the correction of Timoshenko beam theory, derived equation of shear coefficient, and numerical solution of series of beam cross section is given. Among them calculation formula of straight thin-walled box beam shear coefficient is:

$$k = \frac{10(1 + \nu)(1 + 3m)^2}{(12 + 72m + 150m^2 + 90m^3) + \nu(11 + 66m + 135m^2 + 90m^3) + 10n^2[(3 + \nu)m + 3m^2]}, \quad (2.15)$$

where  $m = Bt_1/Ht$ ,  $n = B/H$ ,  $B$  is the height of beam,  $H$  is the width of beam,  $t_1$  is the thickness of upper and lower wing plate,  $t$  is the thickness of web,  $\nu$  is Poisson ratio.

For simply supported boundary conditions at both ends, the solution of equation (2.14) is  $y = A_j \sin \frac{j\pi x}{l} \sin(\omega_j t + \varphi_j)$ .

Bring it into Eq.(2.14), the equation can be re-written as follows:

$$EI \left( \frac{j\pi}{l} \right)^4 - \rho A \omega_j^2 - \rho I \left( 1 + \frac{E}{kG} \right) \left( \frac{j\pi}{l} \right)^2 \omega_j^2 + \frac{\rho^2 I}{kG} \omega_j^4 = 0. \quad (2.16)$$

Compared with the first item, the last item is a coupling term of shear deformation and the moment of inertia is a small amount, which can be neglected.

$$EI \left( \frac{j\pi}{l} \right)^4 - \rho A \omega_j^2 - \rho I \left( 1 + \frac{E}{kG} \right) \left( \frac{j\pi}{l} \right)^2 \omega_j^2 = 0. \quad (2.17)$$

For simply supported boundary conditions at both ends, Eq.(2.17) has its analytical solution, whose bending vibration natural frequency of simply supported beam is [118]

$$\omega = \frac{j^2 \pi^2}{L^2} \sqrt{\frac{EI}{\rho A}} \sqrt{\frac{1}{1 + \frac{j^2 \pi^2 I}{L^2 A} \left( 1 + \frac{E}{kG} \right)}}, \quad (2.18)$$

where  $L$  is the length of the beam,  $j$  is the vibration order number. For simply supported at both ends boundary conditions, bending vibration natural frequency of Euler beam is [119]

$$\omega = \frac{j^2 \pi^2}{L^2} \sqrt{\frac{EI}{\rho A}}. \quad (2.19)$$

For free at two ends boundary conditions, Euler beam natural frequency of bending vibration is

$$\omega = \frac{(j + 0.5)^2 \pi^2}{L^2} \sqrt{\frac{EI}{\rho A}}. \quad (2.20)$$

According to Eq.(2.18)÷(2.20), the approximate formula for natural frequency of bending vibration of free at two ends Timoshenko beam considering the effect of shear deformation and moment of inertia are given:

$$\omega = \frac{(j + 0.5)^2 \pi^2}{L^2} \sqrt{\frac{EI}{\rho A}} \sqrt{\frac{1}{1 + \frac{(j+0.5)^2 \pi^2 I}{L^2 A} \left( 1 + \frac{E}{kG} \right)}}. \quad (2.21)$$

### 2.3.2. Calculation formula of natural frequency of ship's vertical vibration

In general, the ship structure is considered as the variable cross-section beam floating freely in the water for the prediction of its overall vertical natural frequencies. Its natural frequencies usually depend on their stiffness and mass of ship structure (including the added mass of surrounding water). When the principal dimensions and weight of the ship are

determined, the natural frequency of vertical vibration ship will be governed by geometrical characteristics of parallel middle sections (moment of inertia and shear area). As the variable cross-section beam, the mass and moment of inertia are non-uniform distributed along the ship length. So the natural frequency of vibration cannot be directly calculated by the formula (2.21). According to the structural characteristics of the ship and the formula (2.21), the calculation formula of the natural frequency of overall vibration of the ship in consideration of the effect of shear deformation and moment of inertia is:

$$f_n = A_n \sqrt{\frac{I_v}{\Delta_v L^3 (1 + \alpha)}}, \quad (2.22)$$

where  $A_n$  is natural frequency coefficient of vertical vibration of ship,  $L$  is length,  $I_v$  is mid-ship section moment of inertia for horizontal axis,  $\alpha$  is shear and rotational inertia influence coefficient,  $\alpha = \frac{I}{A} \left(1 + \frac{E}{kG}\right) \left(\frac{(j+0.5)\pi}{L}\right)^2$ ,  $k$  is shear coefficient, obtained by the formula (2.7),  $\Delta_v$  is mass of ship structure including added mass,  $\Delta_v = (1 + \tau)\Delta$ ,  $\tau$  is added mass coefficient using Todd formula calculate added mass coefficient in vertical vibration,  $\tau = (0.2 + \frac{B}{3d})$ ,  $\Delta$  is ship displacement.

Considering the superstructure are short but high of the large oil tanker, bulk carrier, and container ship, the impact on the overall vertical vibration due to superstructure can be ignored. Based on the over 90 ships' measured data which has been collected by the author for years, the value of coefficient  $A_n$  can be obtained by the least square regression. The value of coefficient  $A_n$  are shown in Tab. 2.1.

*Tab. 2.1. Coefficient  $A_n$  of natural of the ship overall vertical vibration*

Ship type	First order coefficient	Second order coefficient	Third order coefficient
Bulk carrier	$0.677 \times 10^5$	$0.155 \times 10^6$	$0.255 \times 10^6$
Tanker	$0.690 \times 10^5$	$0.165 \times 10^6$	$0.30 \times 10^6$
Container ship	$0.655 \times 10^5$	$0.150 \times 10^6$	$0.250 \times 10^6$

At the very beginning design stage of the ship, the moment of inertia of the mid-ship section is often lacking. Therefore, the approximate calculation formula of the moment of inertia in this article is proposed:

$$I = cBD^2L, \quad (2.23)$$

where  $L$  is the length,  $B$  is the breadth,  $D$  is the depth. By statistical analysis of over ninety different type ships, the coefficient  $c$  can be taken as  $c = 1.07 \times 10^{-4}$ ; for container ship and large opening bulk carrier,  $c$  can be taken as  $0.95 \times 10^{-4}$  because their moment of inertia are relatively lower. When the length, breadth and depth were designed, the moment of inertia of the mid-ship section can be estimated.

For the approximate prediction, the effect term of shear and moment of inertia  $\sqrt{1/(1 + \alpha)}$  in formula (2.22) will be taken an approximate value, through statistical analysis of over ninety different type ships, the effect can be taken as 0.909, 0.781 and 0.671 respectively for the first three orders vertical vibration.

Therefore, formula (2.22) can be transformed into the following form:

$$f_n = A_n \sqrt{\frac{I_v}{\Delta_v L^3 (1 + \alpha)}} \approx A_n \sqrt{\frac{cBD^2L}{\Delta_v L^3 (1 + \alpha)}} = C_n \sqrt{\frac{BD^2}{\Delta_v L^2}}$$

Namely simplified formula suitable for initial design stage of ship is as follows:

$$f_n = C_n \sqrt{\frac{BD^2}{\Delta_v L^2}}, \tag{2.24}$$

where coefficient  $C_n$  value is shown in Tab. 2.2.

*Tab. 2.2. Coefficient  $C_n$  of natural of the ship overall vertical vibration*

Ship type	First order coefficient	Second order coefficient	Third order coefficient
Bulk carrier	620.6	1212.2	1735.6
Tanker	639.5	1373.8	2082.7
Container ship	560.6	1111.7	1592.6

In this part, the simplified formula for the natural frequency of the ship's overall vertical vibration is derived. Together with the results obtained from these formulas will be compared with the results obtained by the measurements and the results obtained by the numerical modelling method. Based on these comparisons, we evaluated the accuracy and optimization of the numerical model used for the simulation of chosen marine structures.

## 2.4. Structural failures of marine structures

To limit the occurrence of faults that damage the marine structure, economic losses, marine structures must be designed, built and operated to ensure stability, errors and damage are minimized. Extensive research into catastrophic accidents that serve as a basic source of knowledge for future design processes will help make marine structures safer and more lasting. Fatigue is considered a critical limit state which must be taken into account in the design of the marine structure. Today, the theoretical basis for a fatigue analysis is largely based on data and procedures developed from empirical research. Due to fatigue damage (cracks) cause physical damage at the microscopic scale, difficult to identify with the normal methods. Therefore, various fatigue assessment methods have been developed for marine structure details. Studies and analyses of marine structural failures have shown that a significant failure rate is the result of inappropriate design due to lack of operational considerations, and assessment of inadequate structural factors, and Using incorrect calculation methods. During a specific marine structure design stage, the level of structural safety is chosen by determining the individual structural elements, materials used and functional requirements based on the expected structural life of the structure (higher safety factor) and cost of failures. An important factor that must be taken into account is the time dependence of strength and load. The strength of the structure decreases with time and is strongly dependent on inspection and maintenance procedures, while the load itself varies throughout the life of the structure [99].

### **2.4.1. Structural failure causes**

The strength of a structure represents the limited state of the load conditions on which the structure loses its ability to achieve the required function. Structural failures may be defined as the loss of load capacity of a component or member within a structure or of the structure itself (including global failure modes such as overturning, sinking, or failure of the positioning system, etc.). Failure may result in catastrophic damage (i.e., complete structural damage) or partial structural damage when the structure can be repaired or restored. Global failures can often result in serious casualties while smaller and local structural damage can lead to pollution and recoverable structural damage. Structural failure is initiated when the material in a structure is stressed to its strength limit, thereby causing excessive cracking or deformation. The structural integrity of the sea structure depends on the load condition, the strength of the structure itself, the level of quality of production and materials, the severity of service conditions, the design quality as well as various human factors have influence in the process of structural exploitation. There are two different groups of causes of failure. The first group includes unforeseen external or environmental impacts that cause additional loads on the structure leading to overload. Such effects are extreme weather (overload), random loads (collisions, explosions, fires, etc.) and operating errors. The second group includes the causes of faults in the design and construction phase (size errors, poor construction workmanship, material imperfections) or due to increase over time (fatigue), both reduce the actual power of design value. All listed causes may be partly or wholly attributable to the human factor.

### **2.4.2. Failure mechanisms**

The process of fatigue failure itself is highly complex in nature and it is dependent on a large number of parameters. The factors are numerous and perhaps the most significant are mean stress (distribution), residual stresses, loading characteristics and sequence, structural dimensions, corrosion parameters, environmental temperature, design criteria fabrication methods, and quality. Failure mechanisms that usually occur in marine structures can be progressive (excessive yielding, buckling, excessive deformations) or sudden (brittle and fatigue fractures). Excessive yielding and brittle fractures occur when the load exceeds critical strength, whilst buckling and fatigue fractures depend on time and specific load conditions. Fatigue can be defined as a process of damage accumulated during each cycle of the dynamic load that the structure is subjected to with an important characteristic of load intensity lower than the values that would cause immediate failure. This fatigue crack evolution model was a starting point for further analysis. Further development in fatigue analysis resulted in more detailed models of fatigue crack growth [102]. Various authors tried to standardize crack types [93]. Cui proposes a division of the failure fatigue process in five stages, namely crack nucleation, micro-structurally small crack propagation, physically small crack propagation, long crack propagation final fracture [19]. The process which occurs before long crack propagation is usually named “fatigue crack initiation,” while long crack propagation is called “fatigue crack propagation”. Cui also emphasizes that the above listed five stages of the fatigue process only exist in “defect-free” metal components.

One of the most common structural elements that will manifest as the crack starting point is the weld joint. The fatigue failure behaviour of welded joints is complex in its nature and often represents a problem for fracture mechanics approach modelling and description of

the phenomena. New models, where fatigue life and fatigue limit are treated as random variables have been developed [59], [20] resulting in a two-phase model (TPM) for fatigue process in fillet weld joints.

### 2.4.3. Failure analysis and fatigue assessment

Structural failure analysis can be defined as the process of collecting and analysing data to determine the cause of a failure. The actual failure analysis is dependent on the type of the marine structure to be analysed as the characteristics of loads and environmental factors vary for each type. Failure analysis and prediction are based on fatigue analysis and lifetime prediction methods. Fatigue analysis should be done based on all relevant forces and factors for non-operational and operational conditions alike. If the structure is insensitive to dynamic effects (shallow waters) a deterministic analysis is satisfactory. On the other hand, when the dynamic character of the loading is present a stochastic analysis is recommendable.

1. *Classical approach:* Attempting to perform failure analysis of marine structures, designers have encountered problems in the prediction of load dynamics, determining stress concentration factors and physically modelling fatigue damage accumulation processes and effects [99]. The first approaches for fatigue failure analysis were based on S-N data, collected experimentally, which define the stress capacity  $S_{in}$  relation to specific structural detail and the number constant amplitude load cycles  $N$ , hence the name stress-based approach. There are 3 sub-categories for this stress approach for fatigue assessment dependent on the type of stress used in the analysis, namely nominal stress approach (using general stress in the structure calculated by beam theory based on the structure loads and the cross-sectional properties), hot spot stress approach (using a local stress on the point with highest stress taking into account structural discontinuity and geometry) and notch stress approach (using peak stresses in stress concentration areas).

2. *Recent development:* In the past decade, research has been focused on solving persistent fundamental problems of fatigue analysis and fatigue life prediction. Some main issues in the area are prediction of fatigue life under variable amplitude loading, applying fatigue data obtained from small specimens to actual structural components (multi-scaling), corrosion effects on fatigue, the influence of creep on fatigue, multi-axial fatigue stresses under variable amplitude and obtaining a scientifically and practically correct calculation of fatigue life at very low probabilities of failure.

The deterministic method uses discrete values in order to simulate the energy state of the environmental loading factors and structural responses and stresses causing fatigue damage are summarized to obtain the damage accumulated during the lifetime of the structure. If the long-term stress range from the wave environment is of interest spectral fatigue analysis methodology [25], [26], [61]. This approach assumes linear load effects and linear stress response and is performed in the frequency domain. A simplified spectral analysis is the design wave approach where each load is defined by an equivalent wave. The purpose of such analysis is to assess whether fatigue crack sizes will not reach sizes of unstable fractures during the lifetime of a structure. The procedure comprises of crack growth factors determination, evaluation of initial structural defects by NDT inspection methods. The standard analysis method is characterized by large uncertainties when assessing the probability of failure during the lifetime of a structure. Constant inspection of the structure during exploitation is necessary in order to compare calculated values with the actual state of

failure advancement. As stated above, the classical approach to fatigue life assessments is based on the linearity assumption (Miner's rule). In order to apply this rule the complex stress time history is divided into blocks (intervals) of constant stress amplitude (or range). The most used method for this purpose is the rain flow counting method. Recently, cycle counting methods were in this field assessed and tested in practical applications proving the rain flow counting method as valid [62].

#### 2.4.4. Ship failures

This section will deal with ship structural elements failures (hull, stiffeners, masts, stanchions, etc.) and main propulsion system failures (shaft lines, crankshaft, bearings, foundations, etc.). The causes of ship structure failure can be external (impact, bad weather) or internal (inadequate dimensioning, material grade, fatigue, etc.).

1. *Structural failures:* Bilge keel structures are used to enhance the transverse stability of ships. Cracks have been noticed in various ships in the internal structure of the bilge keels and on the connecting points to the ship's hull. Failure analysis of the damage can identify the causes of failure and the analysis results serve as the basis for design improvements. It has been shown, both theoretically and applying FEM analysis, that the failure locations in bilge keels structures occur in the stress concentration regions that are present due to the structure geometry commonly used, therefore new structural elements are proposed that significantly reduce the possibility of failure occurrence. Corrosively aggressive cargo (acids, alkalis, etc.) can represent a danger to the integrity of ship structures. Marine engines and propellers produce dynamic loads on their supportive structures which can lead to fatigue failures. One of the most stressed components of the engine structure is the bearing bushing (or shell). A state-of-the-art design procedure for the bearing girders is comprised of essential procedures such as bearing loads determination, stresses calculation and bearing girder fatigue strength assessment. The fatigue and structural durability analysis is conducted for multi-axial stresses and opens the possibility to construct lightweight engines.

2. *Propulsion system failures:* Ship propulsion systems are subjected to vibration loads, torsion [77], coupled longitudinal (axial) [70] and lateral [71]. These vibrations can cause a fracture, failure in system components or on the ship's structure, resulting in complete destruction of the propulsion system, reduction of the service life of shafts and/or their components, fatigue fracture on support brackets and/or engine mountings. The shafts line's misalignment [75] or bend represents one of the most frequent reasons for this kind of damages. Cracks usually occur in flanges, shaft liners, shaft end, and keyways. The causing factors can be grouped in design, workmanship, and operation cause groups. Propulsion shaft elements can fail while running at low speed due to fatigue caused by torsion stress [12]. The cause of the failure in this particular case was exposure to corrosive environments without any protective coating that resulted in pitting corrosion. The crack grew with multiple starting points due to torsion force (moment) with high-stress concentrations, i.e. the failure cause was fatigue and corrosion.

Engine crankshafts are subjected to bending, stretch-compression, and torsion dynamic loads. Thermal displacement (caused by normal engine working conditions) of the crankshaft and thermal interaction between the main engine body and ship hull is another source of variable loads acting on the power transmission system. Therefore the crankshafts are prone to fatigue failures under multi-axial loading. Fatigue analysis for a typical marine

crankshaft has shown that a combination of rotating bending with steady torsion stress caused the formation of a crack initiated by rotating bending, whilst the effect of the steady torsion became itself significant in the later phases of crack growth. The fact that the propagation was fast in comparison with the total number of the engine work hours indicates that the failure was caused by fatigue.

### 2.4.5. Tools used for failure analysis

The latest trend in failure analysis development is the unification of analysis methods and procedures in order to obtain a comprehensive procedure of structural failure analysis that would cover main failure modes and enable a safer and more efficient design, manufacture and maintenance processes.

1. Experimental: Non-destructive testing and examination (NDT, NDE), as well as structural health monitoring (SHM), of structures, play a significant role in fracture analysis and control procedures. Any method used must not alter, change or modify the failed condition but must survey the failure in a non-destructive mode so as to not impact, change or further degrade the failure zone. This kind of examination provides input values for fracture analysis which yields results that define inspection and maintenance intervals for the structure and represent input values for life prediction estimates. Structures are inspected at the beginning of their service life in order to document initial flaws which determine the starting point of the structure fatigue life prediction. The most commonly used procedures for marine structures are optical microscopy, scanning electron microscopy (SEM), GDS and acoustic emission (AE) testing. Should we just mention SHM methods like vibration-based methods, electrical strain gauges, fiber optic strain-stress sensors (e.g. Fibre Bragg Grating FBG), Lamb waves, comparative Vacuum Monitoring, electromagnetic layer.

Optical microscopy is a common and most widely used NDT analysis method which enables rapid location and identification of most external material defects. This technique is often used in conjunction with micro-sectioning to broaden the application. One of the main disadvantages is the narrow depth-of-field especially at higher magnifications. Scanning electron microscopy is an extension of optical microscopy in failure analysis. The use of electrons instead of a light source provides much higher magnification and much better depth of field, unique imaging, and the opportunity to perform elemental analysis and phase identification. The examined item is placed in a vacuum enclosure and exposed with a finely focused electron beam. The main advantage of this method is minimal specimen preparation activity due to the fact that the thickness of the specimen does not pose any influence to the analysis, ultra-high resolution and 3D resulting appearance of the test object.

2. Analytical: Although various analytical models have been proposed by a number of authors no comprehensive model exists. Analytical methods have been developed for the prediction of progressive structural failures of marine structures [7]. The finite element modelling approach for prediction of the development of failures is accurate but can be time-consuming. Analytical procedures, based on spectral fatigue analysis, beam theory, fracture mechanics and structural factors, can provide solutions in considerably less time when needed. The goal is to define approaches for computing the fracture driving force in structural components that contain cracks. The most appropriate analytical methodology for a given situation depends on geometry, loading, and material properties. The decisive choice factor is the character of stress. If the structure behaviour is predominantly elastic, linear elastic

fracture mechanics can yield acceptable results. On the other hand, when significant yielding precedes fracture elastic-plastic methods such as referent stress approach (RSA) and failure assessment diagram (FAD) need to be used. Since a purely linear elastic fracture analysis can yield invalid and inaccurate results [2], the safest approach is to adopt an analysis that spans the entire range from linear elastic to fully plastic behaviour. One of the methodologies that can be applied is the failure assessment diagram (FAD) approach.

3. Numerical: The effective application of numerical methods in fracture mechanics and fatigue analysis begun with the development of computer science in the second half of the 20th century. Various methods were used (finite difference method, collocation methods, Fourier-transformations) but the finite elements method (FEM) has been established as a standard due to its universality and efficiency. FEM enables complicated crack configuration analysis under complex loads and non-linear material behaviour. Recent years have brought a significant development and increase in accessibility of commercial computational software and hardware for finite element analysis applications, marine structures included. This enables more advanced and detailed fatigue and fractures analysis even for more complex large scale structures. As the extent of scientific material published on this matter is very ample, here recently developed methods will be briefly described and referenced.

Various computer software packages for fatigue crack growth analysis have been developed by NASA. Nastran is a life-prediction code based on the crack-closure concept and is used to predict crack length against cycles from a specified initial crack size to failure for many common crack configurations found in structural components. NASA FLAGRO v2 fatigue cracks growth computer program developed as an aid in predicting the growth of pre-existing flaws and cracks in structural components using a two-dimensional model which predicts growth independently in two directions based on the calculation of stress intensity factors. PFAFAT probabilistic failure assessment for fatigue and flaw propagation software package is utilizing probabilistic failure-assessment (PFA) methodology to model flaw-propagation and low-cycle-fatigue modes of failure of structural components.

## **2.5. Nondestructive testing and Structural health monitoring**

The structures and equipment of marine machinery are more and more modern and complex. Maintenance and repair work must be done periodically to avoid causing damage to the equipment. But sometimes unnecessary disassembly and assembly can cause problems, errors for parts and equipment. Therefore, non-destructive testing (NDT) and structural health monitoring (SHM) are very important to help the operator make appropriate and timely maintenance and repair decisions. It is also one of the advanced techniques for predictive maintenance and accurate maintenance technology in the future.

### **2.5.1. Non-destructive testing**

All structural materials contain imperfections, and the greater their complexity, the more likely flaws will be introduced during manufacture. The sophisticated nature of composite materials employed in the marine environment increases the likelihood of the introduction of flaws within these structures. These can arise both during manufacture and in-service, and range from human error in design or preparation, to the introduction of anomalies by high temperature and pressure cure of polymer matrices, or damage sustained in the

operating environment. A means of assuring that a component will perform to specification (i.e. that it contains no flaws above a certain size) is to inspect it non-destructively. Non-destructive testing (NDT) is a maturing technology field comprising a variety of mainly physics-based techniques that are used to detect or characterize defects in engineering structures. NDT techniques employ mechanical, chemical and electromagnetic energies to introduce a disturbance into the structure and measure the response, on the basis that an internal anomaly will effect a change in the returned signal.

The original NDT techniques, of unassisted visual and aural (acoustic) inspection, have been performed by people for centuries. The five traditional NDT techniques developed mainly for the steel industry were radiography, dye penetrant testing, eddy-current testing, ultrasonic, and magnetic particle testing. Additionally, many inspection techniques that fall within the purview of NDT have been developed, mostly during the twentieth century. Of the original techniques, only ultrasonic and radiography have any significant application to marine structures. This section discusses the application of advanced NDT techniques to the inspection of marine structures.

1. *Vibration analysis:* Vibration techniques acquire a global acoustic response for a structure over a broad frequency spectrum and repeat measurements at specified intervals, or in conjunction with dynamic analyses of the entire structure, where the characteristic response will change over time due to changes in structural stiffness. These techniques are performed at relatively low elastic-wave frequencies (<20 kHz).

2. *Conventional ultrasonic:* Ultrasonic testing (UT) utilizes the piezoelectric effect, in which a permanently polarised and appropriately cut crystal can be used to both generate elastic waves in structures at specific frequencies and convert those waves into electrical energy upon return. The original transducers employed quartz crystals, which were later replaced by piezoceramics such as barium titanate and lead zirconate titanate ('PZT'). UT relies on a mismatch in acoustic impedance between structures and internal defects, to detect the presence of anomalies. Transducers may be arranged in a variety of geometries, though the most common configurations are the 'through-transmission', in which two axially aligned transducers measure the degree of attenuation of the signal through the specimen, and 'pulse-echo', in which a single transducer both sends and receives the elastic waves. The advantage of the latter is that the time of each echo may be used to determine the depth in the structure at which a defect occurs, and thus the precise location of the damage in the through-thickness direction may be inferred.

3. *Optical interferometry:* The application of laser light to study component surfaces has resulted in a range of NDT techniques, useful in determining local strain and stiffness in thin structures.

4. *Electrical and magnetic techniques:* A range of NDT techniques that exploit electrical conductivity, or permittivity have been demonstrated for composite inspection, though in most cases, they require either an electrically conductive (i.e. carbon-fibre) composite, or they are used to detect the presence of moisture.

### 2.5.2. Structural health monitoring

The effective application of NDT measurements typically requires knowledge about the component being inspected, including (i) its structural geometry, (ii) its behaviour under load, and hence the regions of stress concentration and likely damage initiation and (iii) its

history of damage, and the location of such events. The more contextual information that is available to the inspector, the higher the inspection reliability. SHM employs a different methodology; of attaching a large number of permanently mounted sensors and monitoring them at routine intervals. This provides general information about the behaviour of the structure over time, which can yield an indication of its useful life, in addition to detecting damage events that might happen within the measurement zone of the sensors. The boundary between the two philosophies is not entirely sharp, and in some cases, both methodologies employ identical measurement physics. A major factor in SHM is the need for long-term in-service stability of sensors and systems in order to maintain calibration when exposed to the elements over many months or years.

Structural health monitoring (SHM) is a process in which certain strategies are implemented for determining the presence, location, and severity of damages and the remaining life of structure after the occurrence of damage. Health monitoring is typically used to track and evaluate the performance, symptoms of operational incidents and anomalies due to deterioration or damage as well as health during and after extreme events [1]. Damage identification is the basic objective of SHM. SHM involves the observation of a system over time using periodically sampled dynamic response measurements from an array of sensors, the extraction of damage-sensitive features from these measurements, and the statistical analysis of these features to determine the current state of the system health. For long term SHM, the output of this process is periodically updated to provide information regarding the ability of the structure to perform its intended function in the inevitable aging and degradation resulting from operational environments. After extreme events, such as earthquakes or blast loading, SHM is used for quick condition screening and aims to provide, in near real-time, reliable information regarding the integrity of the structure [30].

Generally, the SHM techniques split into two main categories, namely active and passive ones. In the first case, there have to be used some additional elements, which play the role of actuators of the vibrations. A frequently used piezoelectric element is applied in order to generate the required signal. In the latter method the vibrations, which are generated by the analysed machine itself are used to detect the changes in the dynamic response of the structure. The detected possible changes could be interpreted as caused by the damage. However, the detection of the existence of the flaw is not the only aim of the SHM methods. The SHM process [31] can be divided into five following levels. In the first level, the presence of damage is confirmed. It can be done by monitoring the change of some mechanical properties of the structure, like fundamental natural frequency, strain energy, phase information, stiffness reduction or impedance. Next, in level 2, it is necessary to estimate the location, extent, and orientation of the detected damage. It can be performed by a trigger experimentally high-frequency content signal through the tested structure. The measured output in some locations will have an additional wave reflection caused by the existence of the damage. The appropriate analysis of the received signal makes it possible to locate the flaw. This part of the SHM process is the most difficult. It is necessary to develop a very accurate theoretical model of the considered structure and the expected damage. Here it is very useful the finite element method (FEM) due to its versatile character. However, the accuracy of the numerical estimation of the dynamic response of the structure strictly depends on the element size. The higher frequencies of the input signal require the smaller element size. Thus, very often the number of necessary elements is enormously large. The alternative algorithm is the Spectral Finite Element Method (SFEM) and its variants. This method

enables one to obtain highly accurate results with the use of a very small number of elements. Unfortunately, it is not so universal as FEM. The main limitation is connected with the geometry of the modelled structure. Further, the received experimentally signal can be noise polluted. Hence, the appropriate algorithm of signal processing has to be applied.

The main aim of level 3 of the SHM process is to estimate the severity of the detected damage on the safety of the whole structure. The uncontrolled growth of the discovered damage can be very dangerous for the whole structure, especially in the case of delaminations, which grow very fast. That way in level 4 an appropriate action should be performed in order to arrest or stop the growth of the flaw. The methods of repair the damaged structure are very different and strictly depend on the considered material and structure. Level 5 is strictly associated with level 4, wherein the fatigue analysis is performed in order to estimate the remaining time of the safe exploitation of the machine. This analysis is based mainly on statistical data. In order to summarize, every real SHM system consists of the following components [42]: the analysed structure where the SHM system is installed, contact or non-contact sensors, data acquisition system, signal processing, theoretical damage modelling, and damage detection algorithm, data transfer and storage mechanisms and data handling and management.

1. *Strain monitoring*: Strain gauges are a common feature of many structural test articles. The ability to monitor strain at a large number of sites on a component's surface gives the operator an indication of the likelihood of early failure and its location on the structure. Strain gauges are commonly small, planar metallic foils that are adhesively bonded to the test surface. As the surface is strained, the resistivity of the gauge either increases (tension) or decreases (compression), and the degree of change can be related to the surface strain measurement. An innovative application of strain sensing utilizes fibre-Bragg gratings (FBGs) rather than resistivity sensors to measure the strain variation at the test surface. Many FBG can be scribed onto a single optic fibre and these act as a notch filter on the incident laser light. Changes in the local strain can then be correlated with a shift in reflectance or transmittance of the light, to give a sensing resolution  $<1$  microstrain.

2. *Acoustic emission*: Acoustic emission (AE) is the passive version of UT, in which a series of piezoelectric transducers are permanently attached to a structure and monitored. The difference is in the source of the acoustic waves, which, rather than emanating from a driver transducer, come from the internal structure itself: matrix cracking and fiber breakage both give rise to ultrasonic-frequency disturbances, and the rate and frequency of occurrence are measured to assess the rate of damage growth, often in a structure experiencing dynamic loading. An algorithm is then used to measure the timing of receipt of the signal at the various transducers, and estimate the location of the source.

### 2.5.3. Structural health monitoring for ship Structures

The current practice for marine structural surveys generally involves an initial overall visual survey, in which a trained surveyor accesses the structure, focusing on known problem areas and on any noted anomalies. Depending on the type of structure, this overall visual survey may be followed by close-up visual surveys and inspections and the investigation of critical areas using non-destructive testing (NDT) methods (liquid penetrant, magnetic particle, eddy current, ultrasonic inspection, etc.). Real-time structural health monitoring can be advantageous in helping survey efficiency (e.g. directing Surveyors to areas of interest,

locating new discontinuities, validating repairs, etc.). An early warning system that provides information about the crack activity and/or corrosion can reduce unscheduled maintenance and help to avoid catastrophic failure by monitoring the growth of known flaws, and capturing a ship's structural condition in critical areas.

Continuous knowledge of the ship's structural condition is needed to verify the reliability of structural integrity. Real-time structural health monitoring can be advantageous in helping survey efficiency (e.g. directing Surveyors to areas of interest, locating new discontinuities, validating repairs, etc.). An early warning system that provides information about the crack activity and/or corrosion can reduce unscheduled maintenance and help to avoid catastrophic failure by monitoring the growth of known flaws, and capturing a ship's structural condition in critical areas. Although no standard process currently exists for Structural Health Monitoring (SHM), a process (Fig. 2.19) was proposed by Muravin [78] and adopted for the current study. This process is divided into four stages (Procedure Development, Sensing, Diagnosis, and Monitoring).

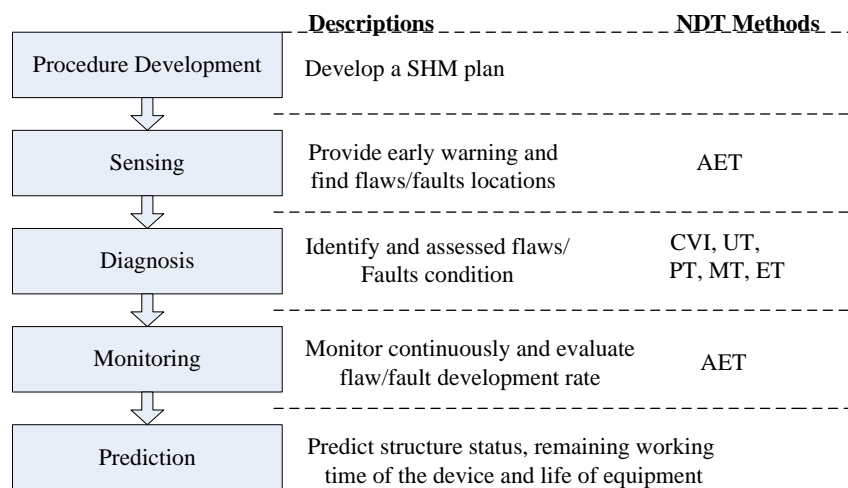


*Fig. 2.19. Overall process of structural health monitoring*

1. *Procedure Development*: The development of new SHM applications is essentially based on a learning process. This includes collection and analysis of information about:

- Material properties,
- Structural design, history of operation, repairs and results of previous inspections,
- Applied loads, operational and environmental conditions,
- Typical flaws/faults to be detected, assessed and monitored,
- Characteristics of flaws/faults to be detected, assessed and monitored,
- Wave propagation characteristics in the material and geometry of the inspected structure including propagation modes, attenuation, dispersion, scattering and other characteristics,
- SHM instrumentation appropriate for the particular application.

An SHM plan is developed based on the collection and analysis of information about structural design, history of operation, repairs, survey results, applied loads and environmental conditions. In this plan, the critical areas of the structure are identified.

2. *Sensing*: Sensing is a process of data measurement. It involves measurement of parametric data like pressure, temperature, strain and other according to the developed SHM procedure. There are several important aspects to address during the sensing stage. First, it is an important to check that data collected during the data acquisition process is valid and can

be satisfactorily used for the purposes defined in the developed SHM procedure. If this is not a case, additional measurements with different setup or loading, operational and/or environmental conditions may be required. Second, and the most important, it is an express evaluation of structure condition based on the measured data for major conditions that may threaten the structure immediately or in a short term.

Sensors are installed in the identified critical areas and to collect in-service data which is analysed and used to provide an early warning of structural failures and locate the flaw/defect. For this stage, AET is the proposed NDT method to conduct the structural condition assessment at critical areas and is used as a screening tool for survey planning.

3. *Diagnosis*: Diagnosis is one of the primary goals of SHM. Diagnosis in SHM is a process of detection, identification, and assessment of flaws/faults in a structure or system. To achieve these objectives special development efforts are required including material research, numerical modelling, and small or full-scale samples tests. Numerical modelling, analysis of stress conditions, history of the inspected structure, local application of different NDE (non-destructive evaluation) methods, material investigations and other may be required to crystallize the most correct diagnostic picture regarding the condition of an examined structure.

Diagnosis performed based on collected data using methods of statistical pattern recognition. Pattern recognition is a branch of artificial intelligence concerned with the classification or description of observations. From the Sensing stage results, the flaws/defects are identified, located, and assessed using close-up visual inspection (CVI), ultrasonic testing (UT), liquid penetrant (PT), magnetic particle (MT), eddy current (ET) and/or other NDT methods.

4. *Monitoring*: Monitoring is essential for evaluation:

- Flaw/fault development rate,
- Next repetitive inspection interval,
- Distinguishing between developing and non-developing flaws/faults.

Monitoring is performed continuously to evaluate flaw development rates and to distinguish between propagating and non-propagating flaws. For this stage, an AET system is proposed for monitoring the growth of flaws.

By locating and identifying flaws as they occur, a monitoring system could potentially yield a large reduction in risk. Additionally, an effective continuous monitoring system should:

- Be readily available to marine and offshore industries,
- Provide early detection of flaws and corrosion,
- Have limited or no disturbance to operation,
- Support screening tools that assist survey and maintenance planning.

5. *Prediction*: The goals of prediction are to:

- Identify the useful a remaining lifetime of a component or structure,
- Define an appropriate re-inspection/monitoring policy based on diagnostic and monitoring data.

Prediction normally done based on diagnostic results, several monitoring and in conjunction with all information about the structure, its history and all know measurable or not risk factors.

### **3. Numerical modelling for some of the local hull structures**

Beams, plates, stiffened plates are the main components that make up the hull structure as well as other real parts of the ship. Therefore, the study of hull structure and superstructure will be taken to study the beams, thin plates and thin plates with stiffened. The purpose of this chapter is to study and analyse the vibration of the real structures of ship hull and superstructure such as beams, thin plates, plates with stiffened by numerical modelling methods, theoretical method and verified by measurement method. From there, evaluate the accuracy of the chosen numerical modelling method, the effect of errors and dispersion on the analysis results of some selected ship's structures. From the evaluation of the errors and the dispersion of the selected numerical modelling method, the author made some recommendations for selecting the optimal numerical model for calculating, analysing vibration of ship structure, improving the confidence level of architects and designers in applying the numerical modelling method for ship structure calculation and design. The numerical model method used is the finite element method implemented on the Patran - Nastran famous numerical commercial software platform (see chapter 1). The theoretical method is based on a number of empirical formulas given for the structure of beams, thin plates [32, 41, 36, 107]. The verification and measurement method was carried out for thin plate and stiffened plate structures carry out in the laboratory of the Marine Engineering Faculty - Maritime University of Gdynia. The measured vibration signals will be processed and graphed in the Matlab software.

Vibrations in the maritime structure are always a matter of primary concern for marine designers and structural engineers. Because, vibrations are the cause of the uncomfortable feeling of passengers, crews on the ship as well as causing damage, deformation of marine structures such as ships, bridges, and offshore structures. Especially when resonance occurs, only a small impact force can cause serious damage to marine structures. The problem of hull vibration and superstructures are not new, but always the interest of marine engineers, operators, and exploiters of ships. They want to minimize the harmful effects of vibration on ships, improve the reliability, the safety of marine structures as well as the comfort of passengers and crews while working on the ship. Resonant vibration occurs when the natural frequencies vibration of the structures coincide with the frequencies of the forces. Thus, determining the natural vibration frequencies are the first and most important problem of vibration analysis. Determining the natural vibration frequency of the structures will help marine engineers solve the vibration resonance problem of equipment. This helps to increase the lifespan, the reliability of the ship hull and deckhouse, the safety and comfort of the crews as well as passengers on board. Structural vibration analysis is a mandatory and important requirement in engineering.

The vibration of real parts of ship structure such as beams, thin plates, stiffened plates is analysed in two cases, the first case in the air (without water) and the second case coupled with water. The author uses the finite element method in Patran - Nastran software platform is the only numerical modelling method in the calculation and analysis of ship structures in this dissertation. The specific analysis for the real structures of the ship hull is made in the next sections in this chapter.

### 3.1. Study the vibration of the beams

In this section, the T-beam with 1308 mm in length, of which 308 mm is mounted on the plate, is considered. The damaged and undamaged aluminium beams of the same dimensions are mounted on the plate, with the mathematical model illustrated in Fig. 3.1. The natural vibration frequency of the beams is calculated for aluminium material. The theoretical calculations of the natural vibration frequency of the beams are considered for different boundary conditions. Calculate the natural vibration frequency of the beam according to the numerical modelling method to be considered for different boundary conditions, the density of the mesh, and finite elements. Then compare the natural frequency values of the beams obtained from the two theoretical and numerical methods. The materials, properties of the T-beam and the plate are presented in the Tab. 3.1.

Tab. 3.1. Geometric properties of the T-beam model mounted on the plate

	Length [mm]	Width [mm]	Thickness [mm]	Height [mm]	Young Modulus $E$ [GPa]	The density of the material $\rho$ [kg/m <sup>3</sup> ]	Poisson's ratio $\nu$
T-beam	1308	49.8	5.1	50	70	2800	0.34
Plate	352	220	12.5	-	70	2800	0.34

Here is the mathematical model of the T-beam.

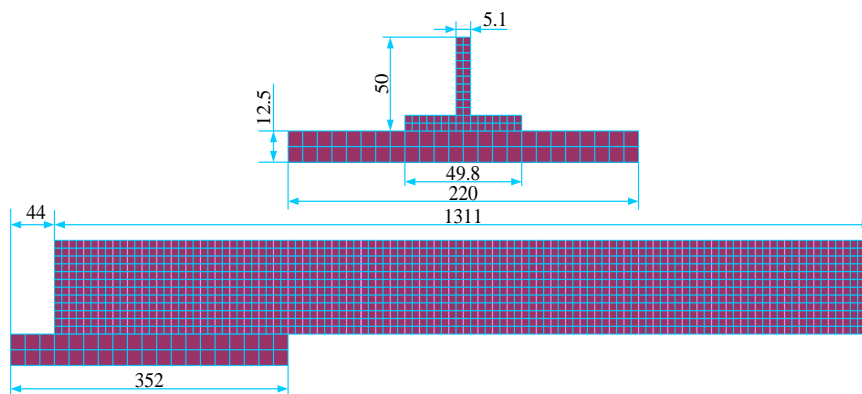


Fig. 3.1. Mathematical model of the undamaged beam mounted on the plate

With the known parameters of the T beams as shown in Fig. 3.1, the inertial moment of the T beam is calculated. The moment of inertia  $I$  in the x-axis is calculated and presented in Fig. 3.2 [32].

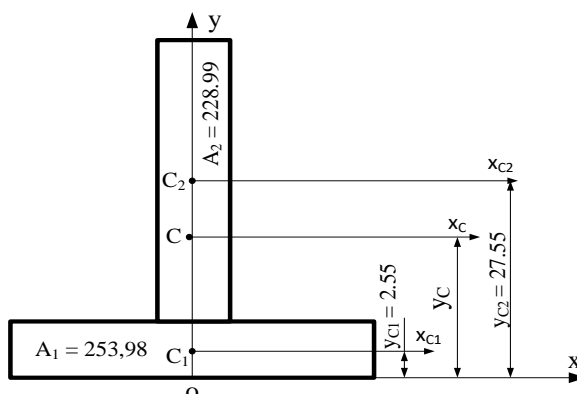


Fig. 3.2. Model for calculating the moment of inertia of the beam cross section

Where  $C_1$  is the centroid of rectangle number 1,  $C_2$  is the centroid of rectangle number 2,  $C$  is the centroid of the cross-section of the T-beam. The moment of inertia of the T-beam cross-section:  $I = 114289.058 \text{ mm}^4 = 1.14289 \cdot 10^{-7} \text{ m}^4$ , for details see [32].

### 3.1.1. Frequency of free vibration of beams in theory

Consider the free-body diagram of an element of a beam shown in Fig. 3.3, where  $M(x, t)$  is the bending moment,  $V(x, t)$  is the shear force, and  $f(x, t)$  is the external force per unit length of the beam. Since the inertia force acting on the element of the beam is  $\rho A(x) dx \frac{\partial^2 w}{\partial t^2}(x, t)$ .

The force equation of motion in the z-direction gives

$$-(V + dV) + f(x, t)dx + V = \rho A(x) dx \frac{\partial^2 w}{\partial t^2}(x, t), \quad (3.1)$$

where  $\rho$  is the mass density and  $A(x)$  is the cross-sectional area of the beam. The moment equation of motion about the y-axis passing through point  $O$  in Fig. 3.3 leads to

$$(M + dM) - (V + dV)dx + f(x, t)dx \frac{dx}{2} - M = 0. \quad (3.2)$$

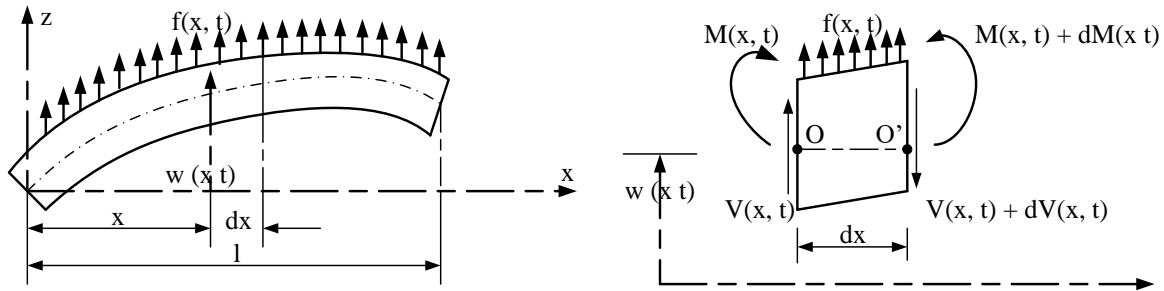


Fig. 3.3. A beam in bending

By writing

$$dV = \frac{\partial V}{\partial x} dx \quad \text{and} \quad dM = \frac{\partial M}{\partial x} dx$$

and disregarding terms involving second powers in  $dx$ , Eq.(3.1) and Eq.(3.2) can be written as

$$-\frac{\partial V}{\partial x}(x, t) + f(x, t) = \rho A(x) \frac{\partial^2 w}{\partial t^2}(x, t), \quad (3.3)$$

$$\frac{\partial M}{\partial x}(x, t) - V(x, t) = 0. \quad (3.4)$$

By using the relation  $V = \partial M / \partial x$  from Eq.(3.4), Eq.(3.3) becomes

$$-\frac{\partial^2 M}{\partial x^2}(x, t) + f(x, t) = \rho A(x) \frac{\partial^2 w}{\partial t^2}(x, t). \quad (3.5)$$

From the elementary theory of bending of beams (the Euler-Bernoulli or thin beam theory), the relationship between bending moment and deflection can be expressed as [32]

$$M(x, t) = EI(x) \frac{\partial^2 w}{\partial x^2}(x, t), \quad (3.6)$$

where  $E$  is Young's modulus and  $I(x)$  is the moment of inertia of the beam cross-section about the  $y$ -axis. Inserting Eq.(3.6) into Eq.(3.5), obtain the equation of motion for the forced lateral vibration of a non-uniform beam

$$\frac{\partial^2}{\partial x^2} \left[ EI(x) \frac{\partial^2 w}{\partial x^2}(x, t) \right] + \rho A(x) \frac{\partial^2 w}{\partial t^2}(x, t) = f(x, t). \quad (3.7)$$

For a uniform beam, Eq.(3.7) reduces to

$$EI \frac{\partial^4 w}{\partial x^4}(x, t) + \rho A \frac{\partial^2 w}{\partial t^2}(x, t) = f(x, t). \quad (3.8)$$

For free vibration,  $f(x, t) = 0$ , and so the equation of motion becomes

$$c^2 \frac{\partial^4 w}{\partial x^4}(x, t) + \frac{\partial^2 w}{\partial t^2}(x, t) = 0, \quad (3.9)$$

where

$$c = \sqrt{\frac{EI}{\rho A}}. \quad (3.10)$$

Since the equation of motion involves a second-order derivative with respect to time and a fourth-order derivative with respect to  $x$ , two initial conditions and four boundary conditions are needed for finding a unique solution for  $w(x, t)$ . Usually, the values of lateral displacement and velocity are specified as  $w_0(x)$  and  $\dot{w}_0(x)$  at  $t = 0$ , so that the initial conditions become

$$\begin{aligned} w(x, t = 0) &= w_0(x), \\ \frac{\partial w}{\partial t}(x, t = 0) &= \dot{w}_0(x). \end{aligned} \quad (3.11)$$

The free vibration solution can be found using the method of separation of variables as

$$w(x, t) = W(x)T(t). \quad (3.12)$$

Substituting Eq.(3.12) into Eq.(3.9)

$$\frac{c^2}{W(x)} \frac{d^4 W(x)}{dx^4} = -\frac{1}{T(t)} \frac{d^2 T(t)}{dt^2} = a = w^2, \quad (3.13)$$

where  $a = w^2$  is a positive constant. Equation (3.13) can be written as two equations

$$\frac{d^4 W(x)}{dx^4} - \beta^4 W(x) = 0, \quad (3.14)$$

$$\frac{d^2T(t)}{dt^2} + w^2T(t) = 0, \quad (3.15)$$

where

$$\beta^4 = \frac{w^2}{c^2} = \frac{\rho Aw^2}{EI}. \quad (3.16)$$

To solution of Eq.(3.15) can be expressed as

$$T(t) = A\cos wt + B\sin wt, \quad (3.17)$$

where  $A$  and  $B$  are constants that can found from the initial conditions. For the solution of Eq.(3.14), we assume

$$W(x) = Ce^{sx}, \quad (3.18)$$

where  $c$  and  $s$  are constants and derive the auxiliary equation as

$$s^4 - \beta^4 = 0. \quad (3.19)$$

The roots of this equation are

$$s_{1,2} = \pm\beta, \quad s_{3,4} = \pm i\beta. \quad (3.20)$$

Hence the solution of Eq.(3.14) becomes

$$W(x) = C_1e^{\beta x} + C_2e^{-\beta x} + C_3e^{i\beta x} + C_4e^{-i\beta x}, \quad (3.21)$$

where  $C_1, C_2, C_3$  and  $C_4$  are constants. Equation (3.21) can also be expressed as

$$W(x) = C_1\cos\beta x + C_2\sin\beta x + C_3\cosh\beta x + C_4\sinh\beta x. \quad (3.22)$$

The constants  $C_1, C_2, C_3,$  and  $C_4$  can be found from the boundary conditions. The natural frequencies of the beam are computed from Eq.(3.16) as

$$w = \beta^2 \sqrt{\frac{EI}{\rho A}} = (\beta l)^2 \sqrt{\frac{EI}{\rho Al^4}}. \quad (3.23)$$

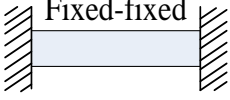
Finally, using Eq.(3.23) the natural frequency  $f_n$  (Hz) of the beam is found as follows:

$$f_n = \frac{\omega}{2\pi} = \frac{(\beta l)^2}{2\pi} \sqrt{\frac{EI}{\rho Al^4}}. \quad (3.24)$$

The function  $W(x)$  is known as *the normal mode or characteristic function of the beam* and  $w, f_n$  are called *the natural frequency of vibration*. For any beam, there will be an infinite number of normal modes with one natural frequency associated with each normal mode. The unknown constants  $C_1$  to  $C_4$  in Eq.(3.22) and value of  $\beta$  in Eq.(3.23) can be determined from the boundary conditions of the beam.

The frequency equations, the mode shapes (normal functions), and the natural frequencies for beams with common boundary conditions are given in Tab. 3.2 [46, 28, 87].

*Tab. 3.2. Common boundary conditions for the transverse vibration of a beam*

Conditions of beam	Frequency Equation	Mode shape (Normal Function)	Value of $\beta_n l$
 Fixed-fixed	$\cos \beta_n l \cosh \beta_n l = 1$	$W_n = C_n[\sinh \beta_n x - \sin \beta_n x + \alpha_n(\cosh \beta_n x - \cos \beta_n x)]$ Where $\alpha_n = \left( \frac{\sinh \beta_n l - \sin \beta_n l}{\cos \beta_n l - \cosh \beta_n l} \right)$	$\beta_1 l = 4.730041$ $\beta_2 l = 7.853205$ $\beta_3 l = 10.99561$ $\beta_4 l = 14.13717$
 Fixed-free	$\cos \beta_n l \cosh \beta_n l = -1$	$W_n = C_n[\sin \beta_n x - \sinh \beta_n x - \alpha_n(\cos \beta_n x - \cosh \beta_n x)]$ where $\alpha_n = \left( \frac{\sin \beta_n l + \sinh \beta_n l}{\cosh \beta_n l + \cos \beta_n l} \right)$	$\beta_1 l = 1.875104$ $\beta_2 l = 4.694091$ $\beta_3 l = 7.854757$ $\beta_4 l = 10.99554$
 Fixed-pinned	$\tan \beta_n l - \tanh \beta_n l = 0$	$W_n = C_n[\sin \beta_n x - \sinh \beta_n x + \alpha_n(\cosh \beta_n x - \cos \beta_n x)]$ where $\alpha_n = \left( \frac{\sin \beta_n l - \sinh \beta_n l}{\cos \beta_n l - \cosh \beta_n l} \right)$	$\beta_1 l = 3.926602$ $\beta_2 l = 7.068583$ $\beta_3 l = 10.21018$ $\beta_4 l = 13.35177$

Calculate the natural vibration frequency of the beams as Fig. 3.1 for different boundary conditions with the aluminium material. From the Eq.(3.24) and Tab. 3.2, the frequencies of the aluminum beam, with different boundary conditions by the theoretical method were calculated. These frequencies are illustrated in Tab. 3.3.

*Tab. 3.3. Natural frequencies of the beam with different boundary conditions in theory*

Shapes/ Models	Natural frequencies [Hz]		
	Clamped-Clamped	Clamped-Free	Clamped-Simply Supported
1	274.02	43.063	188.84
2	755.35	269.87	611.95
3	1480.80	755.65	1276.8

### 3.1.2. Frequency of free vibration of the undamaged beam by numerical modelling

The numerical modelling of aluminum beams with geometric parameters was presented in Tab. 3.1. In this section, the natural vibration frequency for T-beams with the variable boundary conditions, mesh density, finite element types are calculated. The T-beam model in the Patran-Nastran software is illustrated in Fig. 3.4. In this section, the author calculates the natural vibration frequency of the undamaged beams with different boundary conditions, mesh density and finite element types. The natural vibration frequency is only considered for vertical bending cases, corresponding to the first three modes. Because of the vibration modes for different conditions are relatively similar. Therefore, the author illustrates the vibrations of the undamaged beams for different cases of finite element density: one-dimensional (1D), two-dimensional (2D), three-dimensional (3D). The vibration modes are illustrated in Fig. 3.5÷3.7.

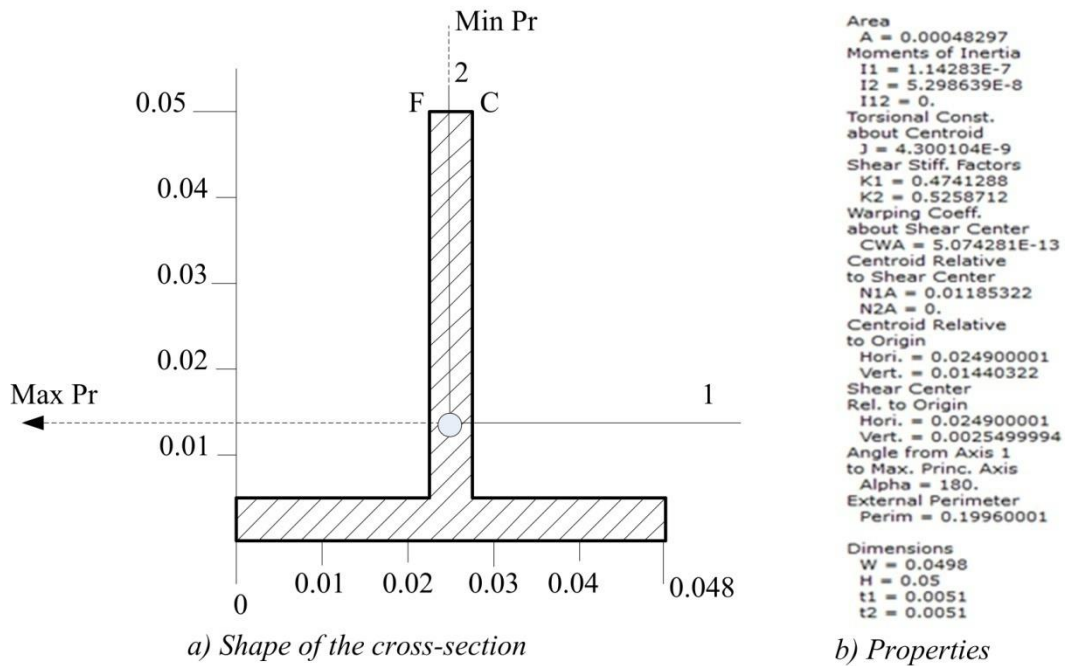


Fig. 3.4. Beam property analysis by Patran software

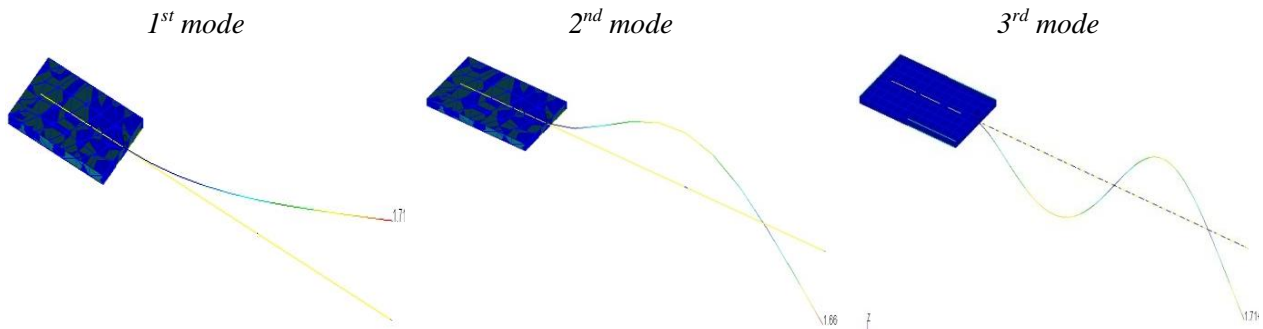


Fig. 3.5. Modes of vibration for the undamaged aluminum T-beam of 1D model

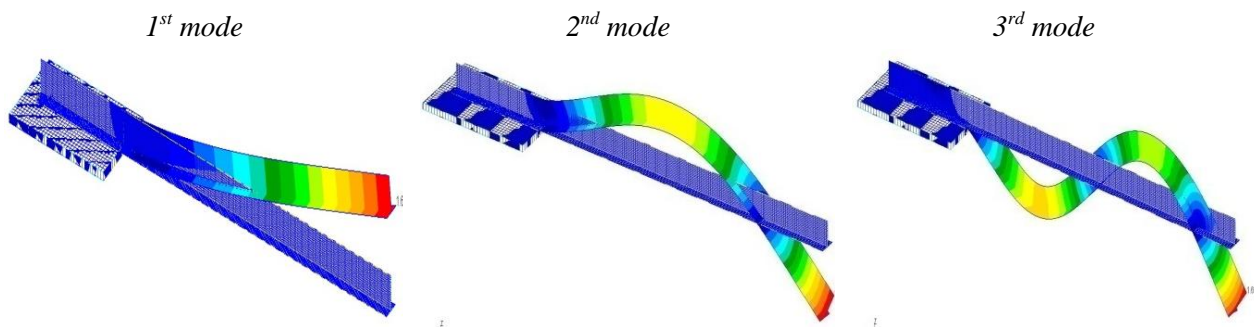


Fig. 3.6. Modes of vibration for the undamaged aluminum T-beam of 2D model

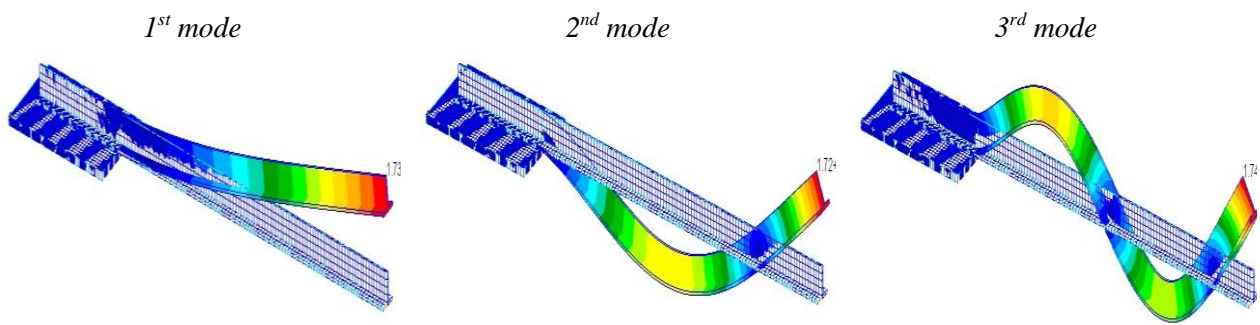


Fig. 3.7. Modes of vibration for the undamaged aluminum T-beam of 3D model

Below is the natural frequency of undamaged beams corresponding to different boundary conditions, meshing density and finite element. The natural frequency of aluminium beams with different boundary conditions as clamped-clamped (C-C), clamped-free (C-F), clamped-simply support (C-SS) are illustrated in Tab. 3.4.

*Tab. 3.4. Natural frequencies of the undamaged beam with different boundary conditions according to the numerical model-FEM*

Shapes\ Models	Natural frequencies [Hz]		
	Clamped-Clamped	Clamped-Free	Clamped-Simply Supported
1	268.97	43.674	197.48
2	712.02	268.11	598.69
3	1330	727.45	1185.2

Calculate the natural vibration frequency of the aluminium beam for different mesh densities. In this section, the cantilever beam, a fixed end, a free end, for finite element one-dimensional (1D) is considered with only one boundary condition. Natural frequency for different mode shapes for T-beam mounted on the plate with the different density of element finite. The results of the natural vibration frequency and mode shapes of the aluminium beam for the different mesh densities are presented in Tab. 3.5.

*Tab. 3.5. Natural frequencies of the undamaged beam with different mesh densities according to the numerical model-FEM*

Shapes\ Models	Natural frequencies [Hz]	
	10 elements	132 elements
1	42.694	43.674
2	259.29	268.11
3	696.44	727.45

Calculate the natural vibration frequency of the beams for different finite elements (1D, 2D, 3D). In this section, the cantilever beam, a fixed end, a free end is considered with a boundary condition. Natural frequency for different mode shapes for T-beam mounted on the plate with the different element finite 1D, 2D, 3D. This section has been calculated and presented in the author's paper, for details see [32]. The natural frequencies and mode shapes of the beam with different finite elements are presented in Tab. 3.6.

*Tab. 3.6. Natural frequencies of the undamaged aluminum beam with the different finite element according to the numerical model-FEM*

Shapes\ Models	Natural frequencies [Hz]		
	One dimensional-1D	Two dimensional-2D	Three dimensional-3D
1	43.674	42.829	41.173
2	268.11	263.24	253.66
3	727.45	712.2	689.3

### 3.1.3. Frequency of free vibration of the damaged beam by numerical modelling

To evaluate the influence of the numerical model on the errors and dispersions of the analysis results, the beam has been modelled by different boundary conditions, mesh density, and finite element. In addition, the numerical model of the damaged beam for the evaluation

### 3. NUMERICAL MODELLING FOR SOME OF THE LOCAL HULL STRUCTURES

of the influence of the numerical model to the results of the analysis more accurate is considered. In this section, the natural vibration frequency of damaged beams is presented. In it, the author reviews two numerical models as two-dimensional (2D) and three-dimensional (3D) with the open gap. The mathematical model of the damaged beam with the open gap is presented in Fig. 3.8. The results of the frequency vibration of the damaged beams are shown in Tab. 3.7 and the corresponding vibration modes are illustrated in Fig. 3.9÷3.10.

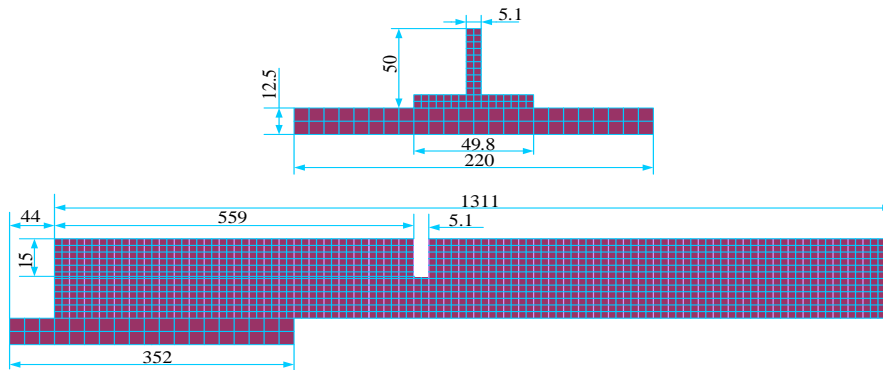


Fig. 3.8. Mathematical model of the damaged beam with an open gap

Tab. 3.7. Natural frequencies of the damaged aluminium beam with 2D and 3D elements according to the numerical model-FEM

Shapes\ Models	Natural frequencies [Hz]	
	Two dimensional-2D	Three dimensional-3D
1	39.9	37.9
2	251.6	239.2
3	664.3	638.9

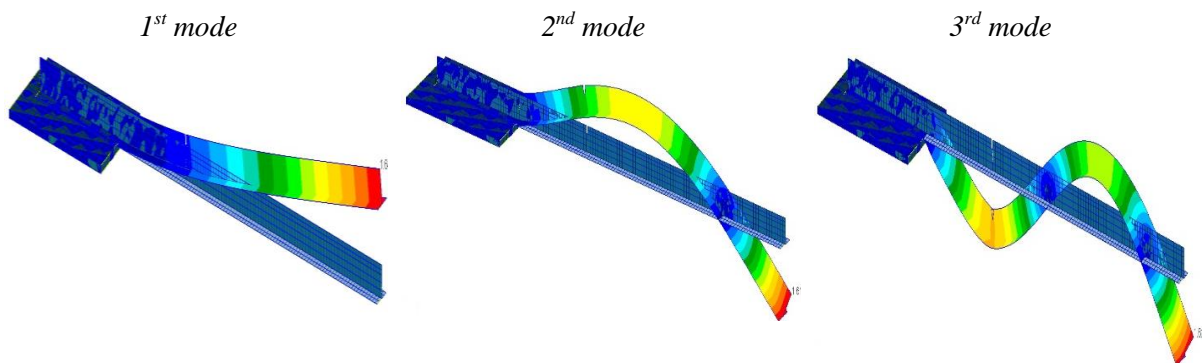


Fig. 3.9. Modes of vibration for damaged T-beam of two-dimensional model

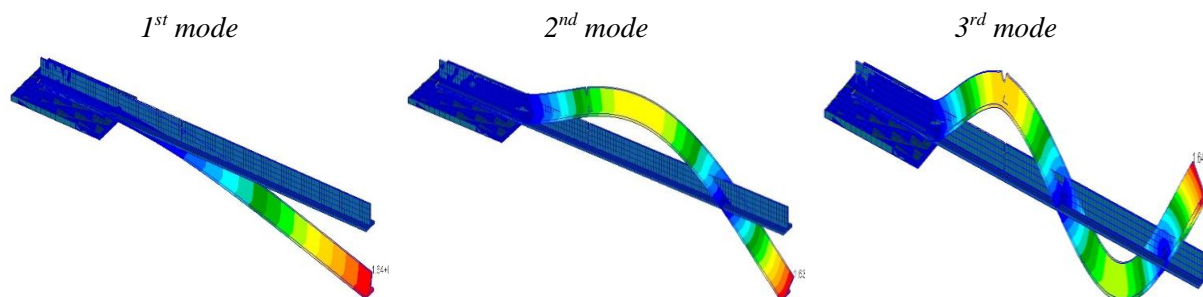


Fig. 3.10. Modes of vibration for damaged T-beam of three-dimensional model

### 3.1.4. Comparison between theoretical method and numerical modelling method

In this section, the author compares the natural frequencies obtained between the theoretical method and numerical modelling method of damaged and undamaged beams. Based on these comparisons, error and dispersion in the analysis of the results are presented. Thus, the conclusion on numerical models gives the most accurate results and the error is within the allowable range.

*The first step, comparison of the natural vibration frequencies of the undamaged beams with different boundary conditions between the theoretical method and the numerical modelling method is presented.*

From the data in the Tab. 3.3 and the Tab. 3.4 in the sections 3.1.1 and 3.1.2, the natural frequency data table of the undamaged beam is obtained with different boundary conditions calculated by the theoretical method and numerical modelling method. The errors and dispersions of the natural frequencies of the undamaged aluminum beams are presented in Tab. 3.8, and illustrated in Fig. 3.11.

*Tab. 3.8. Relative errors of natural frequencies of the undamaged beam with different boundary conditions*

Normal mode	Clamped-Clamped			Clamped-Free			Clamped-Simply Supported		
	Theory f1(Hz)	FEM f2(Hz)	( $\Delta f/f$ ) [%]	Theory f1(Hz)	FEM f1(Hz)	( $\Delta f/f$ ) [%]	Theory f1(Hz)	FEM f2(Hz)	( $\Delta f/f$ ) [%]
1	274.0	269.0	1.8	43.1	43.7	1.4	188.8	197.5	4.6
2	755.4	712.0	5.7	269.9	268.1	0.7	612.0	598.7	2.2
3	1480.8	1330	10.2	755.7	727.5	3.7	1276.8	1185.2	7.2

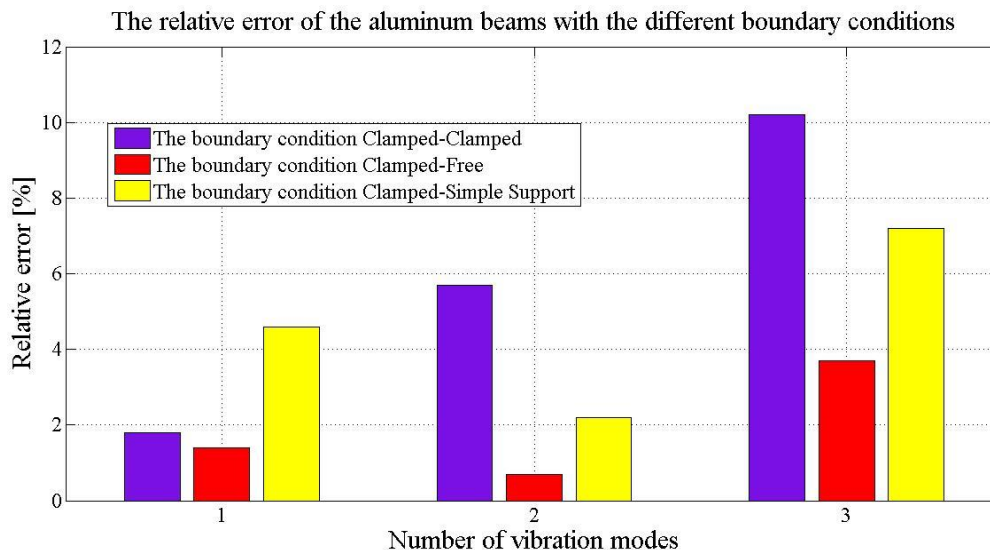


*Fig. 3.11. The relative error of the natural frequencies of the undamaged beams with different boundary conditions*

From the data presented in Tab. 3.8 and Fig. 3.11, the author found that the higher mode, the higher the frequency, and the bigger the error, respectively. In the case of the undamaged beams, the maximum error is 10.2%, corresponding to the mode 3 and the clamped-clamped boundary condition, the smallest error is 0.7%, corresponding to mode 2 and the clamped-free boundary condition. The errors between the theoretical method and the selected numerical model method are not too large. With different boundary conditions, error may vary, but usually less than 10%.

### 3. NUMERICAL MODELLING FOR SOME OF THE LOCAL HULL STRUCTURES

Next step, natural frequencies of the undamaged beams obtained by two theoretical and numerical methods with different mesh density and finite elements are compared.

From the data obtained in the Tab. 3.3 and the Tab. 3.5 in section 3.1.2, the natural frequency data table of the undamaged beam, with different mesh densities calculated by the theoretical method and numerical modelling method is presented. The natural frequency of the undamaged beams with different mesh densities under the two theoretical and numerical methods is illustrated in Tab. 3.9 and Fig. 3.12.

Tab. 3.9. Relative error of natural frequencies of the undamaged beam with different mesh densities

Normal mode	Hand calculation		10 elements $f_1$ (Hz)	$(\Delta f/f)$ [%]	132 elements $f_2$ (Hz)	$(\Delta f/f)$ [%]
	Frequency (Radian/sec)	Frequency $f$ (Hz)				
1	270.5	43.1	42.7	0.87	43.7	1.4
2	1694.7	269.9	259.3	3.92	268.1	0.6
3	4745.3	755.6	696.4	7.83	727.5	3.7

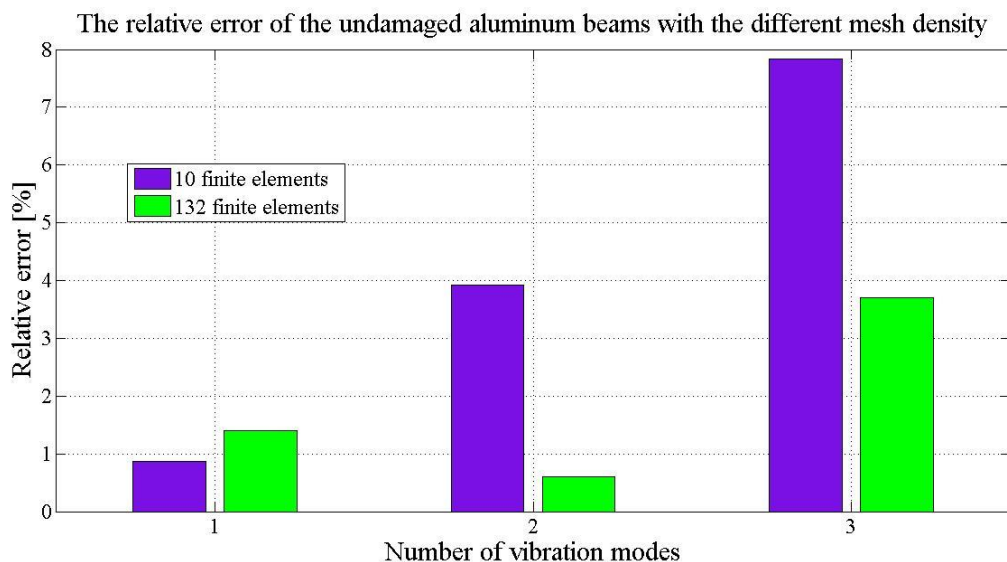


Fig. 3.12. The relative error of the natural frequencies of the undamaged beam models with different mesh densities

From the data obtained in the Tab. 3.3 and the Tab. 3.6 section 3.1.2, the natural frequency data table of the undamaged beam is presented with different finite element calculated by the theoretical method and numerical modelling method. The error of natural frequencies of the undamaged aluminium beam with the different finite element is obtained from the numerical modelling method with the theoretical method, is illustrated in Tab. 3.10 and Fig. 3.13.

Tab. 3.10. Relative error of natural frequencies of the undamaged beam with the different finite element

Normal mode	Hand calculation		Model 1D $f_1$ (Hz)	$(\Delta f/f)$ [%]	Model 2D $f_2$ (Hz)	$(\Delta f/f)$ [%]	Model 3D $f_3$ (Hz)	$(\Delta f/f)$ [%]
	Frequency (Radian/sec)	Frequency $f$ (Hz)						
1	270.467	43.068	43.674	1.407	42.829	0.555	41.173	5.726
2	1694.739	269.863	268.11	0.637	263.24	2.442	253.66	6.004
3	4745.331	755.626	727.45	3.729	712.2	5.747	689.3	8.777

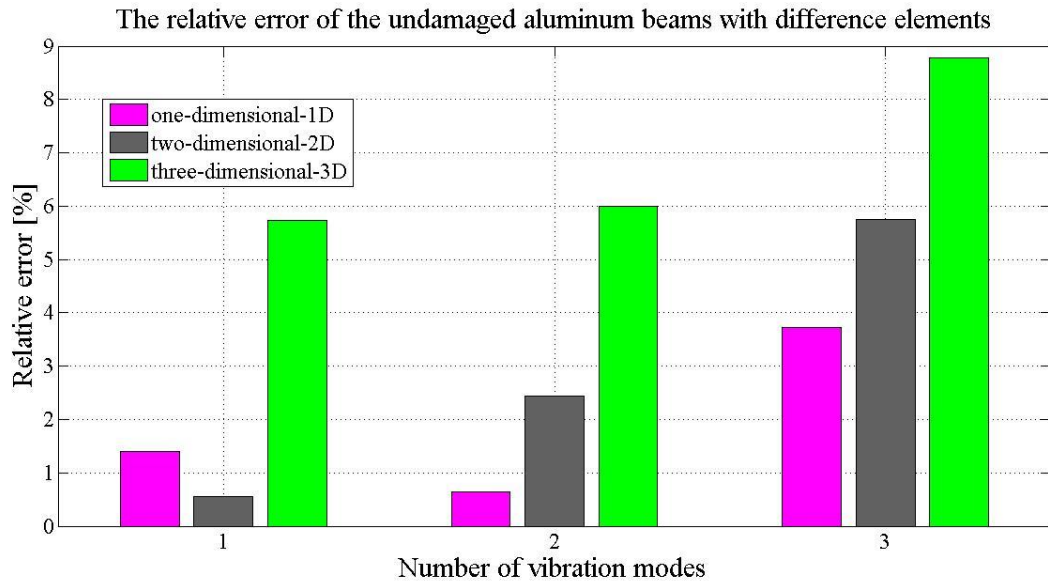


Fig. 3.13. The relative error of the natural frequencies of the undamaged beam models with the different finite elements

From Tab. 3.9 and Fig. 3.12, when the mesh density is higher, the error is smaller, the higher the accuracy of the calculation results. As the mesh density increases, the graph is smoother. The smallest error is 0.6%, corresponding to mode 2 and the highest error is 7.83%, corresponding to mode 3. Thus, as the mesh density increases, the accuracy of the resulting increases, but at the same time, it increases the computational time and requires a higher configuration computer, increasing the computational cost. Therefore, it is necessary to choose an appropriate mesh density, to ensure accuracy as well as reduce the time and the cost. Applying the different finite element types, 1D, 2D, 3D, also affects the accuracy of the calculation results. The biggest error, in this case, is 8.8%, corresponding to mode 3, the 3D finite element, the minimum error of 0.6%, corresponding to mode 1, the 2D finite element. The comparisons and error calculations of the undamaged beams with the different finite elements are presented in Tab. 3.10 and Fig. 3.13.

*Final step, natural frequencies of the damaged beams obtained by two theoretical and numerical methods with different finite elements is compared.*

From the data obtained in the Tab. 3.3 and the Tab. 3.7 section 3.1.2, the natural frequency data table of the damaged aluminium beam is presented with different finite element calculated by the theoretical method and numerical modelling method. The error of natural frequencies of the damaged aluminium beam with the different finite element is obtained from the numerical modelling method with the theoretical method, is illustrated in Tab. 3.11 and Fig. 3.14.

Tab. 3.11. Error of natural frequencies of the damaged beam with different finite element

Normal mode	Hand calculation		Model 2D f <sub>1</sub> (Hz)	(Δf/f) [%]	Model 3D f <sub>2</sub> (Hz)	(Δf/f) [%]
	Frequency (Radian/sec)	Frequency f (Hz)				
1	270.5	43.1	39.9	7.4	37.9	12.1
2	1694.7	269.9	251.6	6.8	239.2	11.4
3	4745.3	755.6	664.3	12.1	638.9	15.4

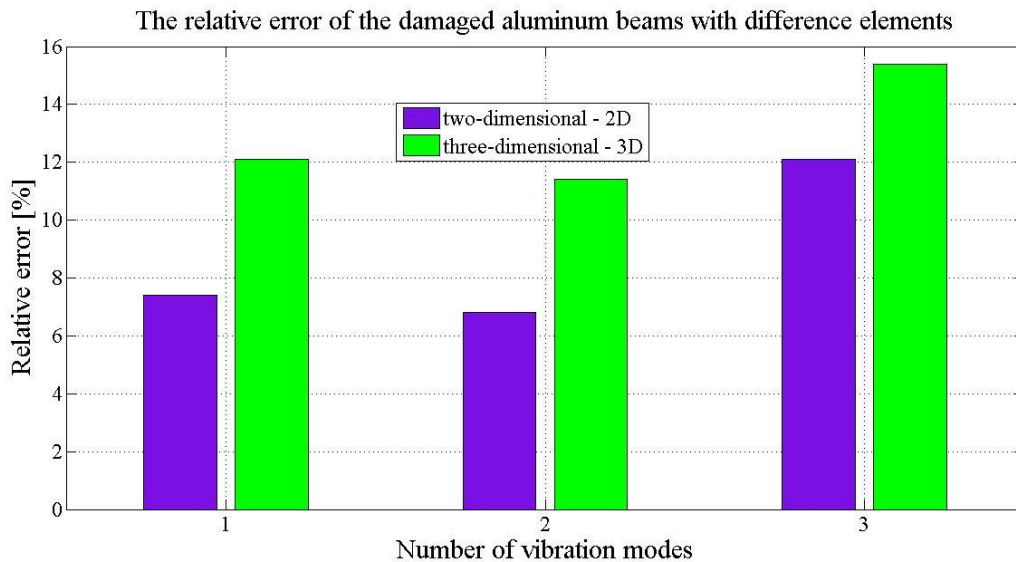


Fig. 3.14. The relative error of the natural frequencies of the damaged beam models with different finite element

When the beam was damaged, an open gap, the error in the calculation results of the numerical model increased very fast. The error is 0.55% with the undamaged beam, the error is 7.4% with the damaged beam, with mode 1 and the corresponding the finite element 2D. The maximum error, in this case, is 15.4%, corresponding to mode 3, the 3D finite element, the minimum error of 6.8%, corresponding to mode 2, the finite element 2D. The error of the damaged aluminium beams is presented in Tab. 3.11 and Fig. 3.14.

### 3.2. Analysis the vibration of the thin plate

The hull is made up of many parts, including important components such as beams and thin plates, stiffened plates. Previously section, the author has studied beams with boundary conditions, mesh density and different finite element types. In this section, the author continues to study another important structure of hulls that are thin plates with assumptions of boundary conditions suitable for the model. Then, the numerical results of the numerical model were verified by the method of measuring real objects at the laboratory in Marine engineering department of Gdynia Maritime University. The thin plate model was analysed and determined the natural vibration frequency in two cases without water (in the air) and coupled with the water. Thin plates are modelled with 1-dimensional (1D), 2-dimensional (2D), 3-dimensional (3D) finite elements as well as various finite element densities, to evaluate the accuracy of the chosen numerical modelling method.

#### 3.2.1. Numerical modelling of the thin plate

In this section, the author built a mathematical model of the thin plate 800x200x8 mm and 720x60x60 mm fixed at both ends in two cases: the first one has no contact with the fluid (in the air), in the second case the thin plate has the lower side in contact with the fluid. Models are built using numerical modelling in the Patran-Nastran software platform. The model of the thin plate with the lower side in contact with the fluid is made using the Mfluid element in the Nastran software. The real model of the thin plate studied in this section has the parameters as shown in Tab. 3.12. The process of prototyping, displaying results in pre- and post-processing software Patran was been detailed in chapter 1.

*Tab. 3.12. Geometric properties of the thin plate*

Dimensions	Length [mm]	Width [mm]	Thickness [mm]	Young Modulus $E$ [GPa]	The density of the material $\rho$ [kg/m <sup>3</sup> ]	Poisson's ratio $\nu$
Thin plate - steel	800	200	8	21	7850	0.3
	720	60	60	21	7850	0.3

*The first case: vibration analysis of the thin plate without water (in the air):*

The numerical calculation was based on the finite element method implemented in the Patran-Nastran software. These programs are based on the finite element method. The natural vibration frequency of thin plates, as well as the influence of numerical models on the accuracy of calculation results, is determined. In this section, the author calculates with four numerical models with the following boundary conditions:

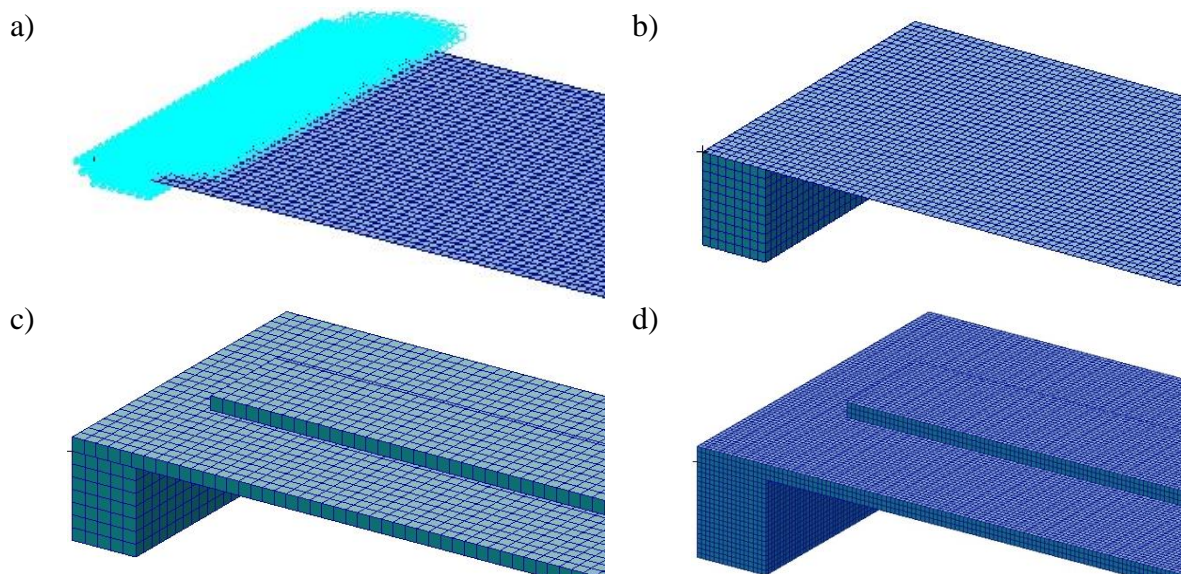


*Fig. 3.15. Computational models of the thin plate, respectively: 2D, 2-3D, 3-D and 3-D det.*

Model 2-D (two-dimensional): the thin plate is modelled by 2D finite element, number of elements 6400 (Quad 4), number of nodes 6601, number of degrees of freedom 36162. The 2D model with corresponding boundary conditions described as Fig. 3.15a.

Model 2-3D: the thin plate is modelled with 2D finite elements 6400 (Quad 4), the thin plate is fixed at both ends with two plates. The two fixed plates at the ends of the thin plate are modelled with 3D elements 6400 (Hex8), the number of nodes 13981, degrees of freedom 35178. The 2-3D model with boundary conditions is described as Fig. 3.15b.

Model 3-D (three-dimensional): Both thin plate and two fixed plates are simulated by three-dimensional elements 19200 (Hex8), number of nodes 27183, degrees of freedom 57195. The 3D models with boundary conditions described as in Fig. 3.15c.

Model 3-D det.: the thin plate model and two fixed plates with 3D finite elements. In this case, the number of finite elements is very large 128000 elements (Hex8) to increase the calculation accuracy, number of nodes 159084, degrees of freedom 303750. Model 3-D det. described as Fig. 3.15d.

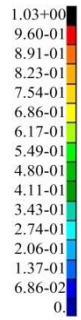
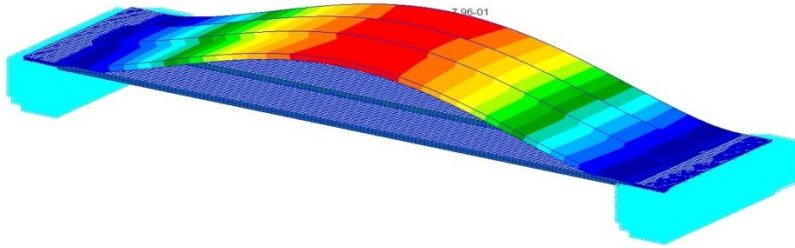
Because the natural vibration of the cases is relatively similar, the author only illustrates the natural vibration graphics of thin plates with the case of 3-D det. model. The natural vibration of the 3-D model det. described in Fig. 3.16.

### 3. NUMERICAL MODELLING FOR SOME OF THE LOCAL HULL STRUCTURES

MSC.Patran 2018 01-Jan-20 22:10:00

Fringe: Default, A1:Mode 1:Freq. = 135.58, Eigenvectors, Translational, Magnitude, (NON-LAYEDRED)

Deform: Default, A1:Mode 1:Freq. = 135.58, Eigenvectors, Translational,

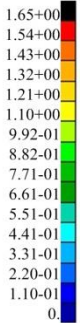
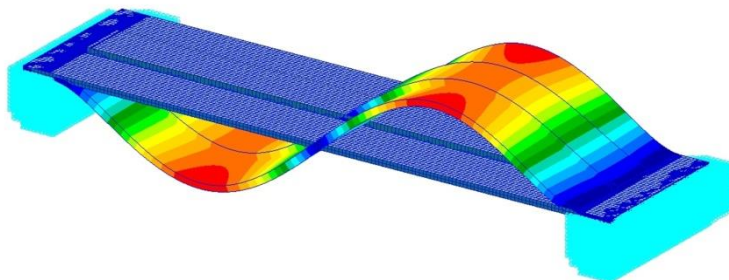


default\_Fringe:  
Max 1.03+00@Nd 6682  
Min 0.@Nd 1  
default\_Deformation:  
Max 1.03+00@Nd 6682

MSC.Patran 2018 01-Jan-20 22:10:32

Fringe: Default, A1:Mode 2:Freq. = 260.56, Eigenvectors, Translational, Magnitude, (NON-LAYEDRED)

Deform: Default, A1:Mode 2:Freq. = 260.56, Eigenvectors, Translational,

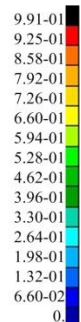
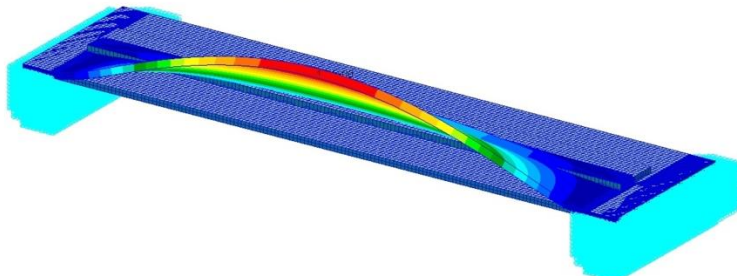


default\_Fringe:  
Max 1.65+00@Nd 81  
Min 0.@Nd 1  
default\_Deformation:  
Max 1.65+00@Nd 81

MSC.Patran 2018 01-Jan-20 22:10:42

Fringe: Default, A1:Mode 3:Freq. = 375.68, Eigenvectors, Translational, Magnitude, (NON-LAYEDRED)

Deform: Default, A1:Mode 3:Freq. = 375.68, Eigenvectors, Translational,

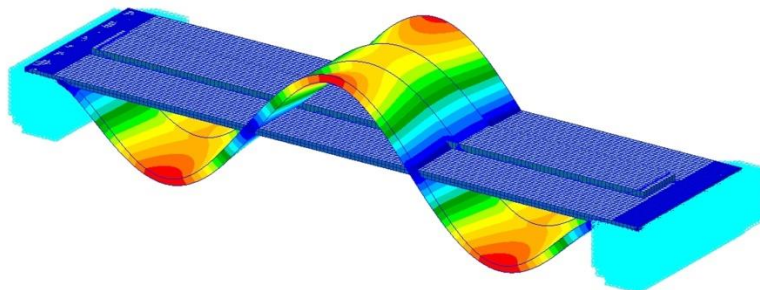


default\_Fringe:  
Max 9.91-01@Nd 6652  
Min 0.@Nd 1  
default\_Deformation:  
Max 9.91-01@Nd 6652

MSC.Patran 2018 01-Jan-20 22:11:13

Fringe: Default, A1:Mode 4:Freq. = 455.77, Eigenvectors, Translational, Magnitude, (NON-LAYEDRED)

Deform: Default, A1:Mode 4:Freq. = 455.77, Eigenvectors, Translational,



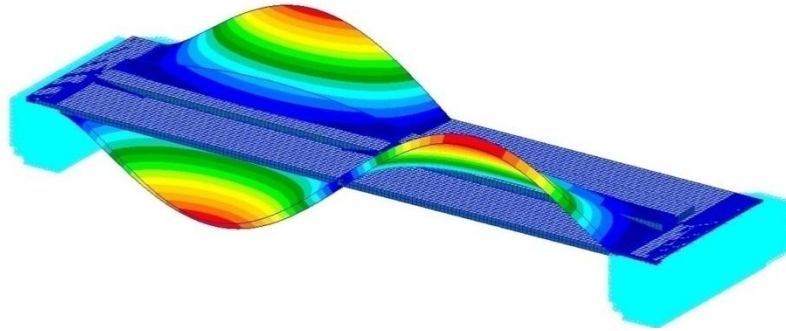
default\_Fringe:  
Max 1.00+00@Nd 6640  
Min 0.@Nd 1  
default\_Deformation:  
Max 1.00+00@Nd 6640

# INFLUENCE OF THE NUMERICAL MODELLING METHODS ON DISPERSIONS AND ERRORS OF ANALYSIS RESULTS IN CHOSEN MARINE MACHINES AND STRUCTURES

MSC.Patran 2018 01-Jan-20 22:11:22

Fringe: Default, A1:Mode 5:Freq. =577.72, Eigenvectors, Translational, Magnitude, (NON-LAYEDRED)

Deform: Default, A1:Mode 5:Freq. = 577.72, Eigenvectors, Translational,

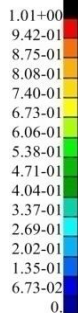
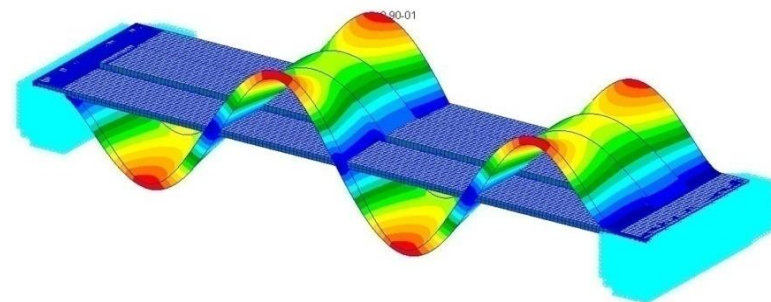


default Fringe:  
Max 1.61+00@Nd 114  
Min 0.@Nd 1  
default\_Deformation:  
Max 1.61+00@Nd 114

MSC.Patran 2018 01-Jan-20 22:11:29

Fringe: Default, A1:Mode 6:Freq. =638.6, Eigenvectors, Translational, Magnitude, (NON-LAYEDRED)

Deform: Default, A1:Mode 6:Freq. = 638.6, Eigenvectors, Translational,

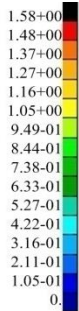
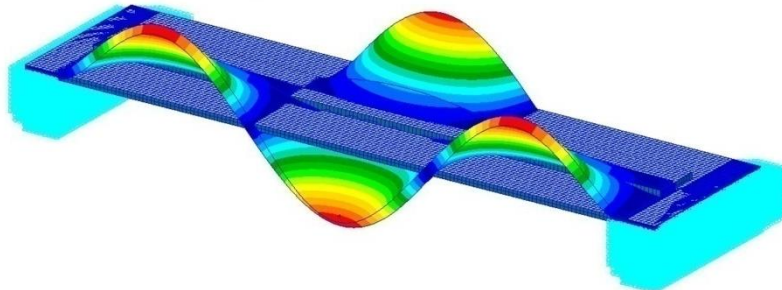


default Fringe:  
Max 1.01+00@Nd 6633  
Min 0.@Nd 1  
default\_Deformation:  
Max 1.01+00@Nd 6633

MSC.Patran 2018 01-Jan-20 22:11:38

Fringe: Default, A1:Mode 7:Freq. =681.83, Eigenvectors, Translational, Magnitude, (NON-LAYEDRED)

Deform: Default, A1:Mode 7:Freq. = 681.83, Eigenvectors, Translational,

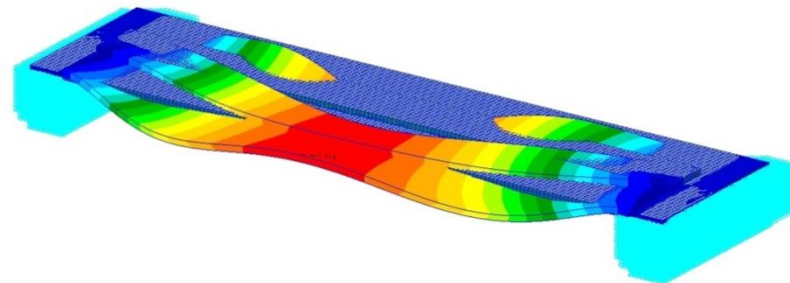


default Fringe:  
Max 1.58+00@Nd 37  
Min 0.@Nd 1  
default\_Deformation:  
Max 1.58+00@Nd 37

MSC.Patran 2018 01-Jan-20 22:11:45

Fringe: Default, A1:Mode 8:Freq. =778.25, Eigenvectors, Translational, Magnitude, (NON-LAYEDRED)

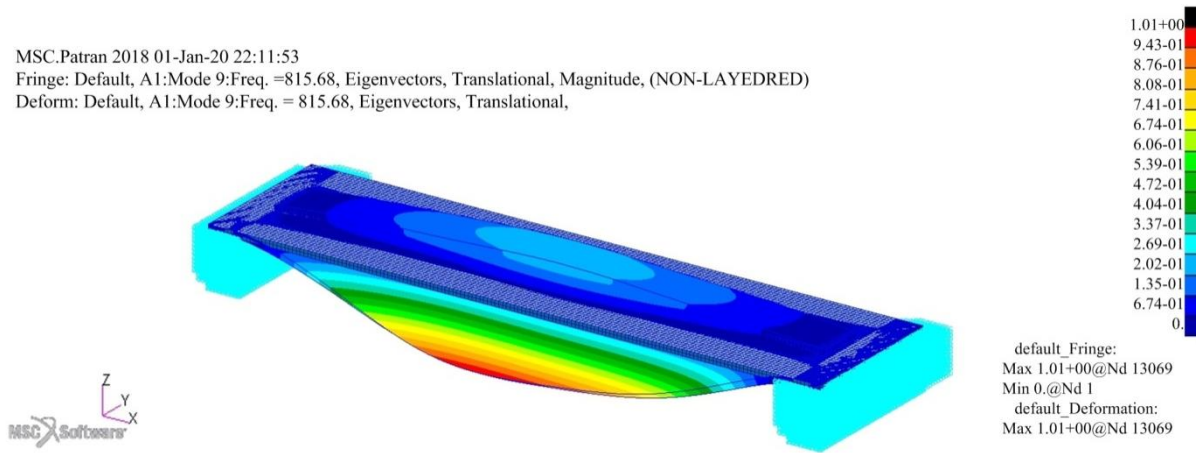
Deform: Default, A1:Mode 8:Freq. = 778.25, Eigenvectors, Translational,



default Fringe:  
Max 1.56+00@Nd 31  
Min 0.@Nd 1  
default\_Deformation:  
Max 1.56+00@Nd 31

### 3. NUMERICAL MODELLING FOR SOME OF THE LOCAL HULL STRUCTURES

MSC.Patran 2018 01-Jan-20 22:11:53  
 Fringe: Default, A1:Mode 9:Freq. =815.68, Eigenvectors, Translational, Magnitude, (NON-LAYEDRED)  
 Deform: Default, A1:Mode 9:Freq. = 815.68, Eigenvectors, Translational,



MSC.Patran 2018 01-Jan-20 22:12:15  
 Fringe: Default, A1:Mode 10:Freq. =906.77, Eigenvectors, Translational, Magnitude, (NON-LAYEDRED)  
 Deform: Default, A1:Mode 10:Freq. =906.77, Eigenvectors, Translational,

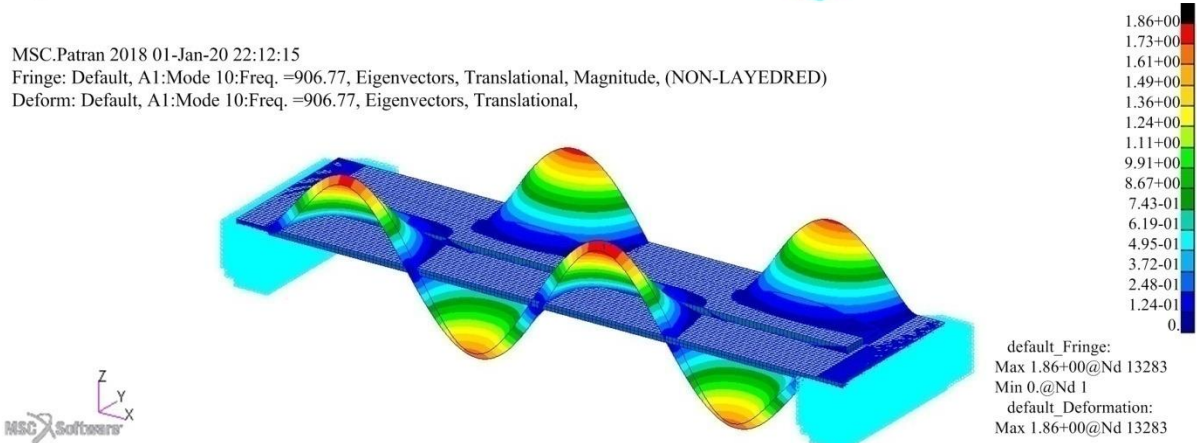


Fig. 3.16. Natural vibration modes of analytical thin plates without water

In fact, the natural vibration frequency of the ship is not too large, usually below 500 Hz. It can be seen that vibration forms, starting with the fifth vibration mode, are very unlikely to resonate, with much higher frequencies (exceeding 500 Hz). Therefore, in the deeper analysis, only the first four vibration modes will be considered. The results of calculating the natural frequencies of each model are presented in Tab. 3.16 and Fig. 3.17.

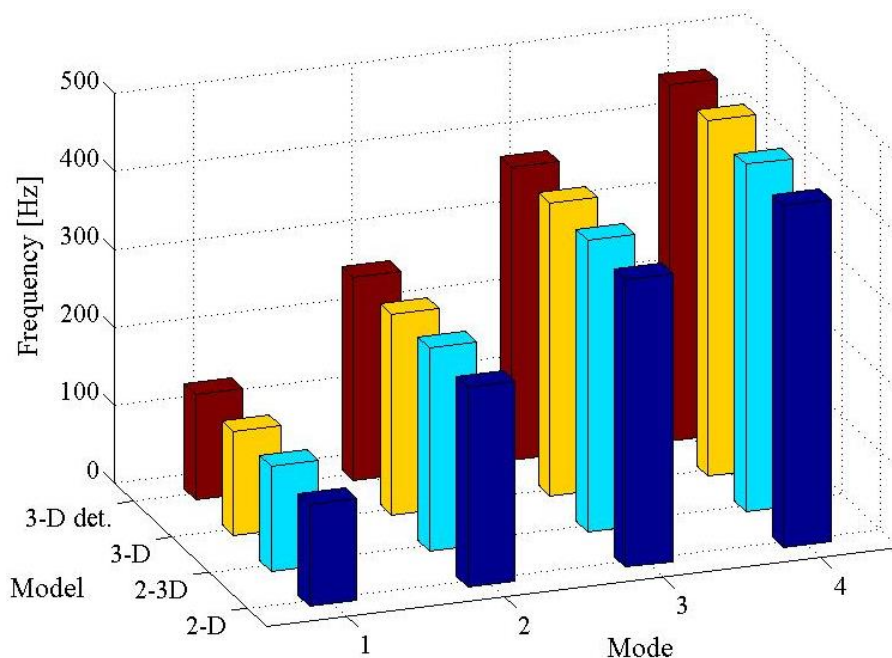


Fig. 3.17. Natural frequencies of the thin plate without water

*Tab. 3.13. Natural frequencies of calculation models without water (in the air)*

Normal mode	The natural frequency of the model f [Hz]			
	Model 2D	Model 2-3D	Model 3-D	Model 3-D det.
Mode No. 1	130.45	133.67	132.75	135.58
Mode No. 2	255.5	260.89	258.34	260.56
Mode No. 3	368.79	373.28	374.89	375.68
Mode No. 4	437.98	445.76	456.45	455.77

*The second case: vibration analysis of the thin plate coupled with fluid:*

In this section, the natural vibration frequency of the thin plate combined with water is calculated by method numerical modelling method. The numerical model method is based on the virtual mass method - Mfluid method in Nastran software. The virtual liquid mass method is used for small movements of liquids that cannot be compressed. Fluids can be coupled with internal and external surfaces (with infinite fluid boundaries). There is no clear liquid model; only wet structures (elements) must be identified. Since the liquid is represented by a combined block matrix directly attached to the structural points. A virtual liquid volume creates a block matrix representing the liquid to be coupled with a boundary consisting of structural elements and other effects, such as free surfaces, symmetrical planes, and liquids infinite. Uncompressed fluids create a defined block matrix with full coupling between acceleration and pressure on flexible structural interfaces.

The following is a brief overview of the virtual mass approach. For more information, refer to the documentation [65÷69]. The MSC Nastran software uses the Helmholtz method to solve Laplace's equation by distributing the set of sources on the outer boundary, each creating a simple solution to the differential equation. By connecting the assumed known boundary motions to the effective motion caused by the sources, the linear matrix equation for the magnitude of the sources is solved. Combining all these steps into a matrix equation leads to a virtual mass matrix as derived below

$$\dot{u}_i = \sum_j \int_{A_j} \frac{\sigma_j e_{ij}}{|r_i - r_j|^2} dA_j, \quad (3.25)$$

where  $\dot{u}_i$  is velocity vector of fluid at any other point  $r_i$ ,  $\sigma_j$  is value of a point source of fluid (units are volume flow rate per area),  $r_i$  is location of the fluid source,  $A_j$  is assumed action area of the fluid source,  $e_{ij}$  is the unit vector in the direction from point  $j$  to point  $i$ .

The other set of necessary equations are the pressures,  $p_i$ , at any point,  $i$ , in terms of the density  $\rho$ , sources and geometry, namely

$$p_i = \sum_j \int_{A_j} \frac{\rho \dot{\sigma}_j e_{ij}}{|r_i - r_j|} dA_j. \quad (3.26)$$

The results of integrating Eq.(3.25) and Eq.(3.26) over the finite element surfaces are collected respectively in two matrices,  $[\chi]$  and  $[\Lambda]$  where

$$\dot{u}_i = [\chi]\{\sigma\}, \quad (3.27)$$

and

$$\{F\} = [\Lambda]\{\sigma\}, \quad (3.28)$$

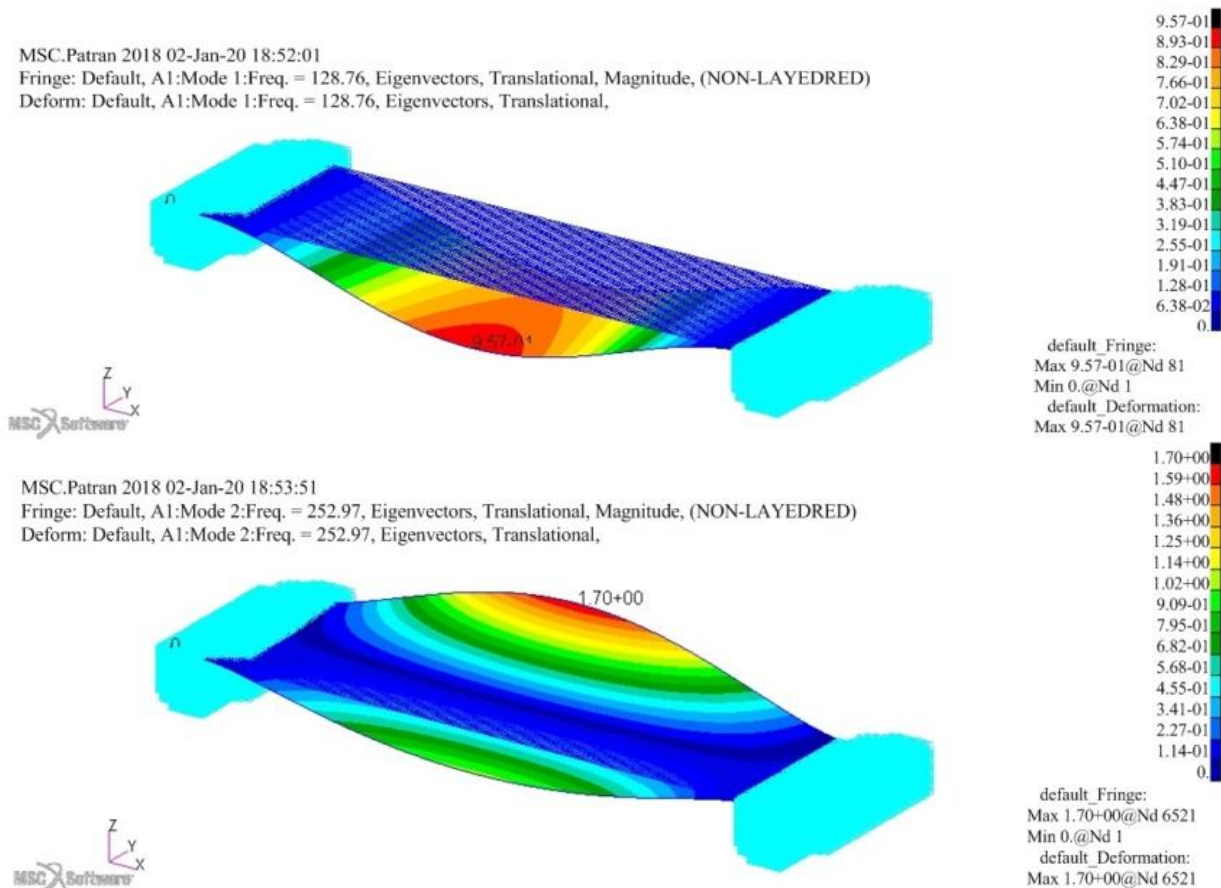
where  $F$  are the forces at the grid points. The matrix  $[\Lambda]$  is obtained by integrating Eq.(3.26). An additional area integration is necessary to convert the pressures to forces. A mass matrix may now be defined using Eq.(3.27) and Eq.(3.28) as

$$\{F\} = [M^f]\{\ddot{u}\}, \quad (3.29)$$

where the virtual fluid mass matrix,  $[M^f]$  is

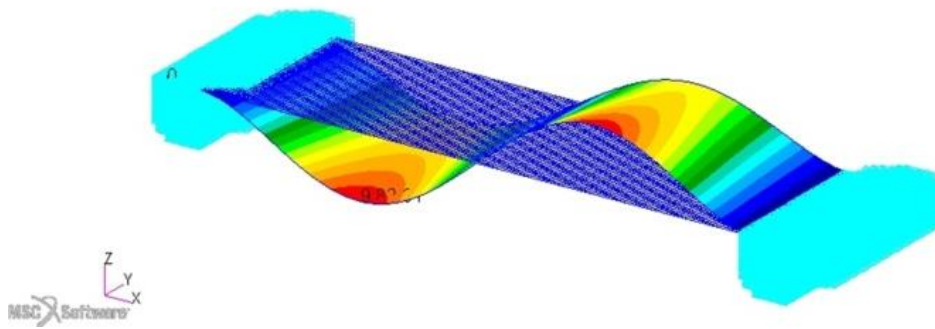
$$[M^f] = [\Lambda][\chi]^{-1}. \quad (3.30)$$

The above equations are built and solved in the Nastran software to find the desired eigenvalues. Because the Mfluid method of solving fluid and structural interactions that cannot be done directly in Patran pre-processing software. Therefore, the stiffened plate model is built with full geometry, material, meshing, and boundary conditions. After that, Patran software will create the file ending with \*.bdf. To analyse the interaction between structure and fluid, the segment of codes will be added to the \*.bdf file. The final file is analysed and processed in the Nastran software. After calculation, the author obtained the natural vibration frequencies of the thin plate for different cases of finite elements: one-dimensional, two-dimensional, three-dimensional, different finite element density for thin plates with one side coupled with fluid. The Fig. 3.18 shows an example of vibration modes of thin plates with the fluid contact surface.



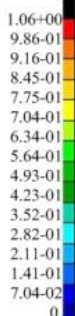
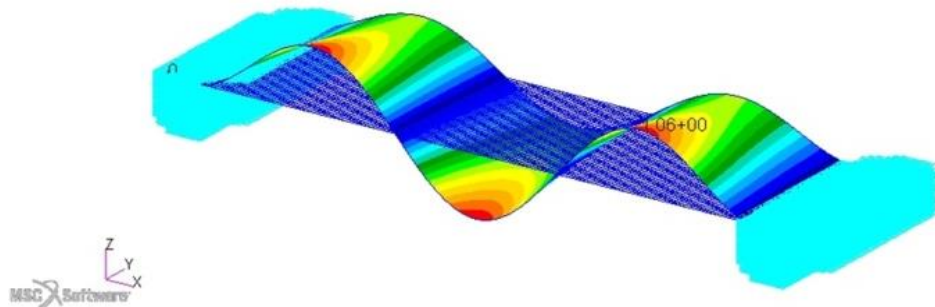
# INFLUENCE OF THE NUMERICAL MODELLING METHODS ON DISPERSIONS AND ERRORS OF ANALYSIS RESULTS IN CHOSEN MARINE MACHINES AND STRUCTURES

MSC.Patran 2018 02-Jan-20 18:54:01  
 Fringe: Default, A1:Mode 3:Freq. =368.49, Eigenvectors, Translational, Magnitude, (NON-LAYEDRED)  
 Deform: Default, A1:Mode 3:Freq. = 368.49, Eigenvectors, Translational,



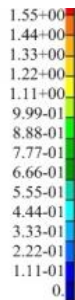
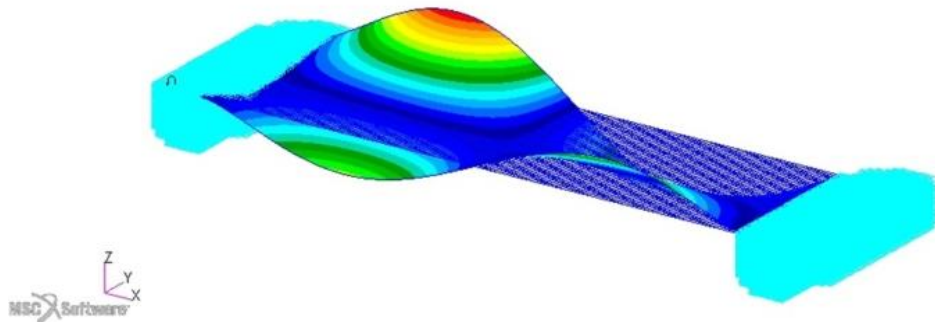
default Fringe:  
 Max 9.82-01@Nd 51  
 Min 0.@Nd 1  
 default\_Deformation:  
 Max 9.82-01@Nd 51

MSC.Patran 2018 02-Jan-20 18:54:11  
 Fringe: Default, A1:Mode 4:Freq. =453.76, Eigenvectors, Translational, Magnitude, (NON-LAYEDRED)  
 Deform: Default, A1:Mode 4:Freq. = 453.76, Eigenvectors, Translational,



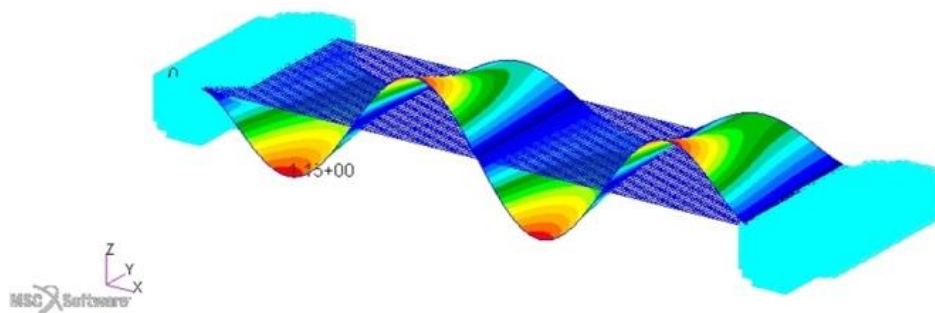
default Fringe:  
 Max 1.06+00@Nd 124  
 Min 0.@Nd 1  
 default\_Deformation:  
 Max 1.06+00@Nd 124

MSC.Patran 2018 02-Jan-20 18:54:19  
 Fringe: Default, A1:Mode 5:Freq. =545.22, Eigenvectors, Translational, Magnitude, (NON-LAYEDRED)  
 Deform: Default, A1:Mode 5:Freq. = 545.22, Eigenvectors, Translational,



default Fringe:  
 Max 1.67+00@Nd 6553  
 Min 0.@Nd 1  
 default\_Deformation:  
 Max 1.67+00@Nd 6553

MSC.Patran 2018 02-Jan-20 18:54:27  
 Fringe: Default, A1:Mode 6:Freq. =606.68, Eigenvectors, Translational, Magnitude, (NON-LAYEDRED)  
 Deform: Default, A1:Mode 6:Freq. = 606.68, Eigenvectors, Translational,



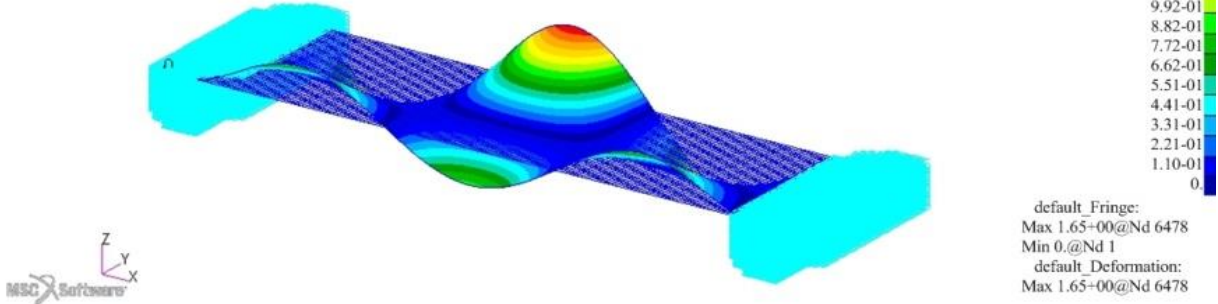
default Fringe:  
 Max 1.15+00@Nd 32  
 Min 0.@Nd 1  
 default\_Deformation:  
 Max 1.15+00@Nd 32

### 3. NUMERICAL MODELLING FOR SOME OF THE LOCAL HULL STRUCTURES

MSC.Patran 2018 02-Jan-20 18:54:40

Fringe: Default, A1:Mode 7:Freq. =635.87, Eigenvectors, Translational, Magnitude, (NON-LAYEDRED)

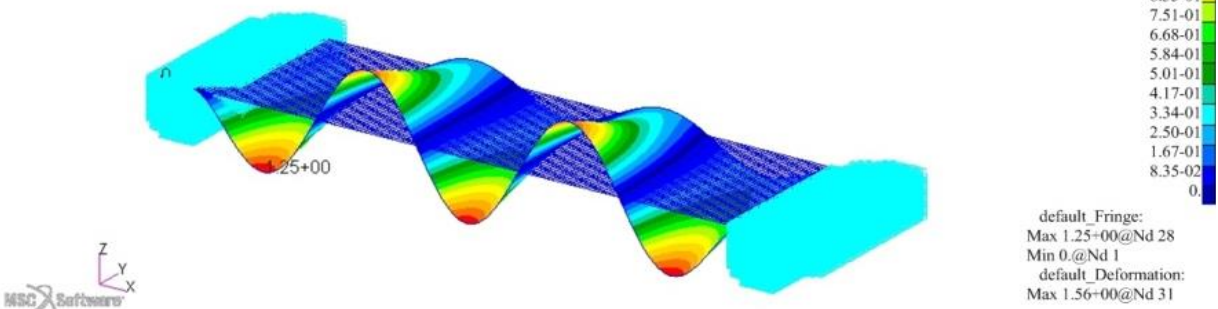
Deform: Default, A1:Mode 7:Freq. = 635.87, Eigenvectors, Translational,



MSC.Patran 2018 02-Jan-20 18:54:48

Fringe: Default, A1:Mode 8:Freq. =718.56, Eigenvectors, Translational, Magnitude, (NON-LAYEDRED)

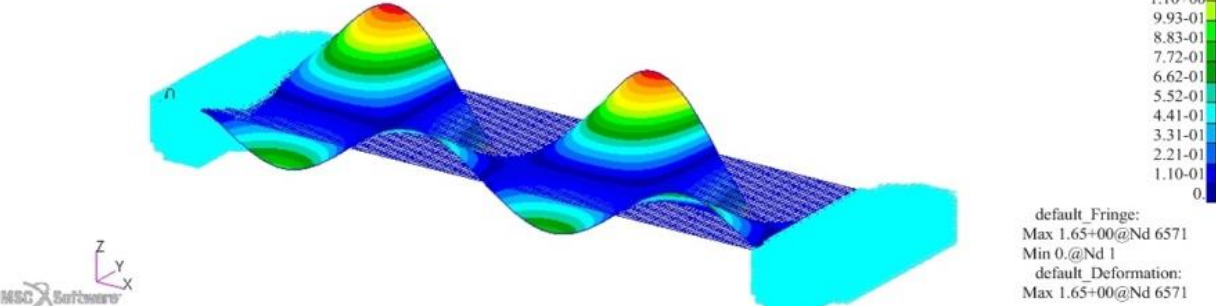
Deform: Default, A1:Mode 8:Freq. = 718.56, Eigenvectors, Translational,



MSC.Patran 2018 02-Jan-20 18:54:56

Fringe: Default, A1:Mode 9:Freq. =771.45, Eigenvectors, Translational, Magnitude, (NON-LAYEDRED)

Deform: Default, A1:Mode 9:Freq. = 771.45, Eigenvectors, Translational,



MSC.Patran 2018 02-Jan-20 18:55:05

Fringe: Default, A1:Mode 10:Freq. =826.44, Eigenvectors, Translational, Magnitude, (NON-LAYEDRED)

Deform: Default, A1:Mode 10:Freq. =826.44, Eigenvectors, Translational,

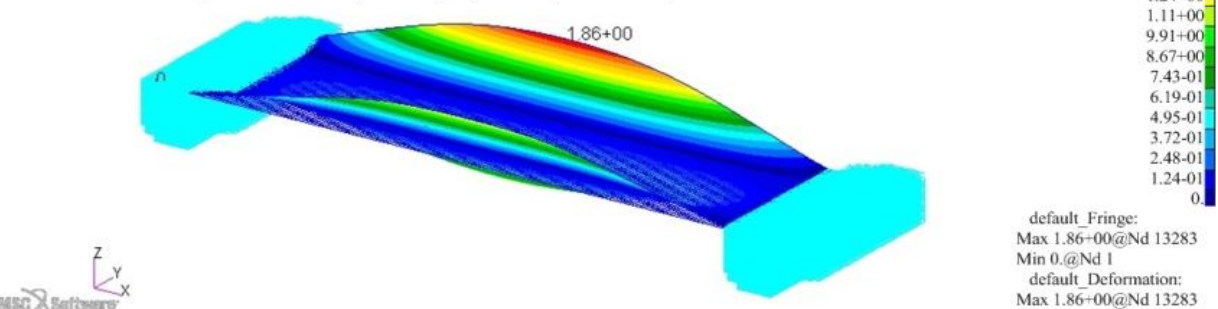


Fig. 3.18. Natural vibration modes of analytical thin plates coupled with fluid

The Tab. 3.14 and Fig. 3.19 show the four natural vibration modes of thin plates with a fluid contact surface.

Tab. 3.14. Natural frequencies of the thin plate coupled with fluid

Normal mode	The natural frequency of the model f [Hz]			
	Model 2D	Model 2-3D	Model 3-D	Model 3-D det.
Mode No. 1	125.55	128.76	128.75	130.34
Mode No. 2	252.58	252.97	253.34	255.67
Mode No. 3	365.28	368.49	375.97	375.46
Mode No. 4	435.77	453.76	453.45	450.58

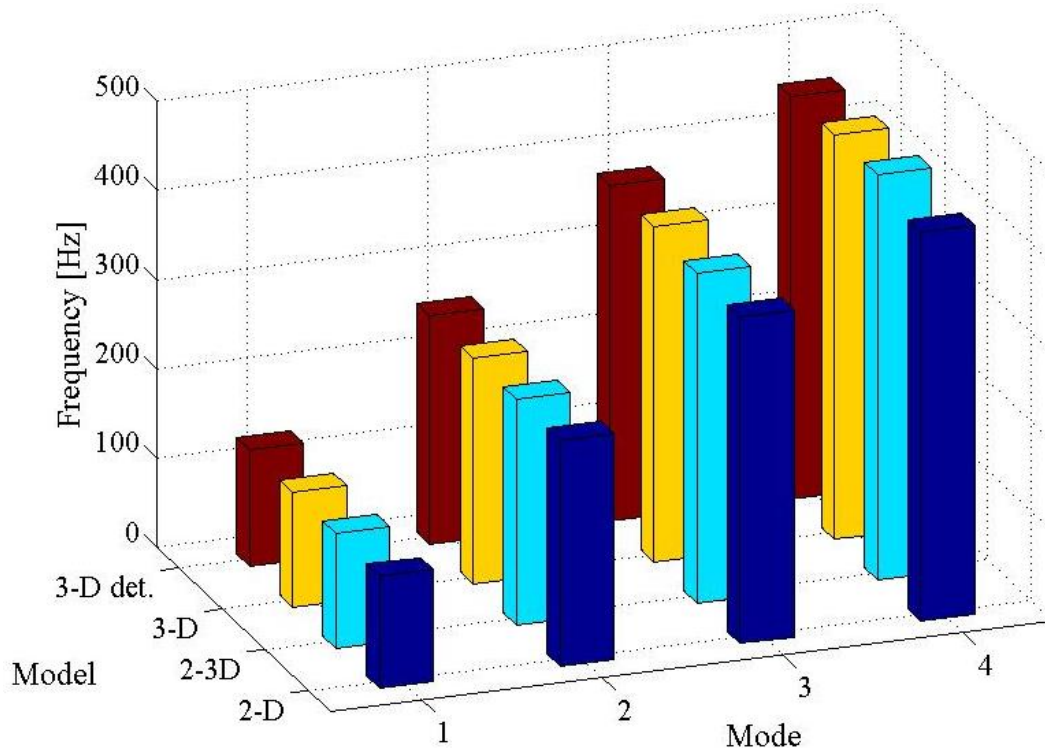


Fig. 3.19. Natural frequency of the thin plate coupled with fluid

After calculating results, natural vibration analysis of thin plates for two cases combined with fluid and not with fluid by numerical modelling on the Patran-Nastran software platform. The results will be verified by measurement and analysis of the vibration of real objects in the laboratory of the Marine Engineering Faculty - Maritime University of Gdynia. Comparing analysis results, calculated by numerical modelling method and measurement results, assessing the degree of error and dispersion of the selected numerical modelling method.

### 3.2.2. Verify the results of numerical modelling of the real thin plate

In this section, measurement with a real model of the thin plate in steel material with boundary conditions with two cases with and without fluid as shown in Fig. 3.20. In tests, the equipment is attached according to the diagram as shown in Fig. 3.21. During the measurement of the real thin plate, two accelerometers 4514-B were used ch4, and ch5. During the study, the displacement of the plate was also registered with the use of laser sensors however, the interpretation of the results is still unclear and requires further analysis, so they cannot be more detailed here.

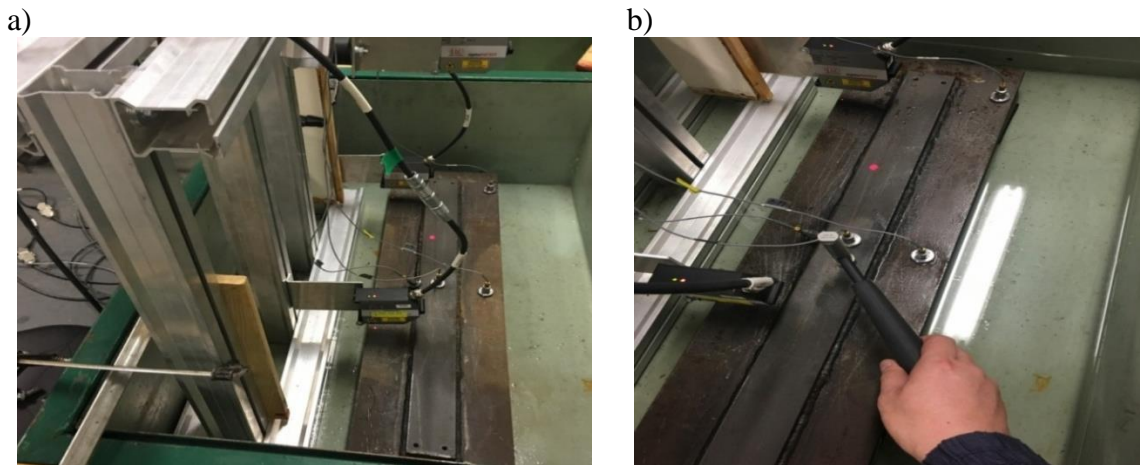


Fig. 3.20. Photograph of measuring model of thin plate, a) without water, b) with water

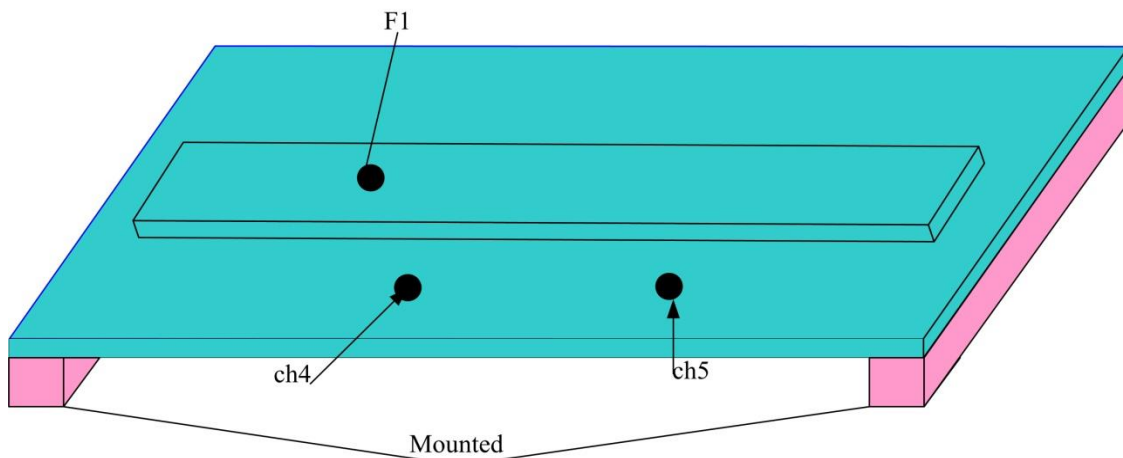


Fig. 3.21. Location of the transmitters during the tests, ch4 - accelerometer (channel 4 - direction V on the plate), ch5- accelerometer (channel 5 - direction V on the plate)  
F1 - the place of impact with a modal hammer

The vibration parameters obtained by the results of the measurements are carried out on the actual thin plate with the above boundary conditions. All tests have been done according to good practice principles. They include the calibration of the equipment used to

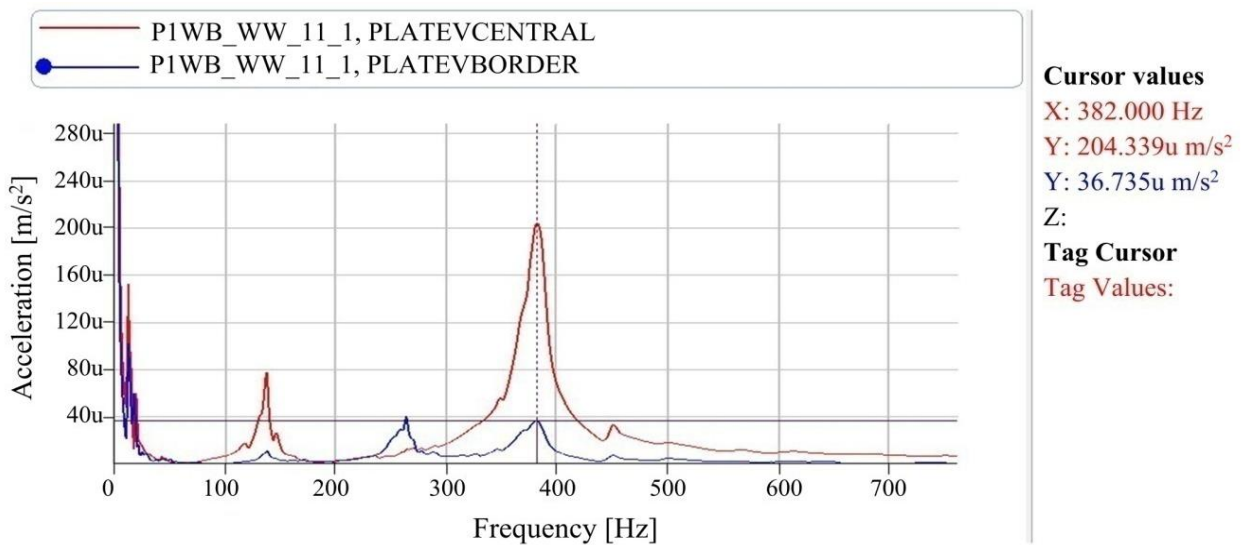


Fig. 3.22. Response of the acceleration spectrum vibrates with the impact of the hammer of thin plate without water

increase the accuracy of the measurement. The number of repetitions of the results obtained in the pre-defined frequency domain is large enough to meet the accuracy requirement (the lack of repeatability may indicate incorrect assembly of the test subject). The frequencies in the measurement tests were determined with a resolution of 0.125 Hz, allowing relative measurement errors of up to 0.6% for the first natural frequency. It should be emphasized that all computational errors lower measurement errors should be considered as 0. The vibration signals are performed Fourier-FFT fast analysis in the Matlab software to obtain the accelerated spectral response of vibration. On the graph, the acceleration response of the vibration determines the natural frequency values at the vertices of the graph. The response of thin plate spectra without water with the modal hammer is shown in Fig. 3.22.

The Fig. 3.23 illustrates the response of the acceleration spectrum of vibration on the impact of the modal hammer on the thin plate coupled with water.

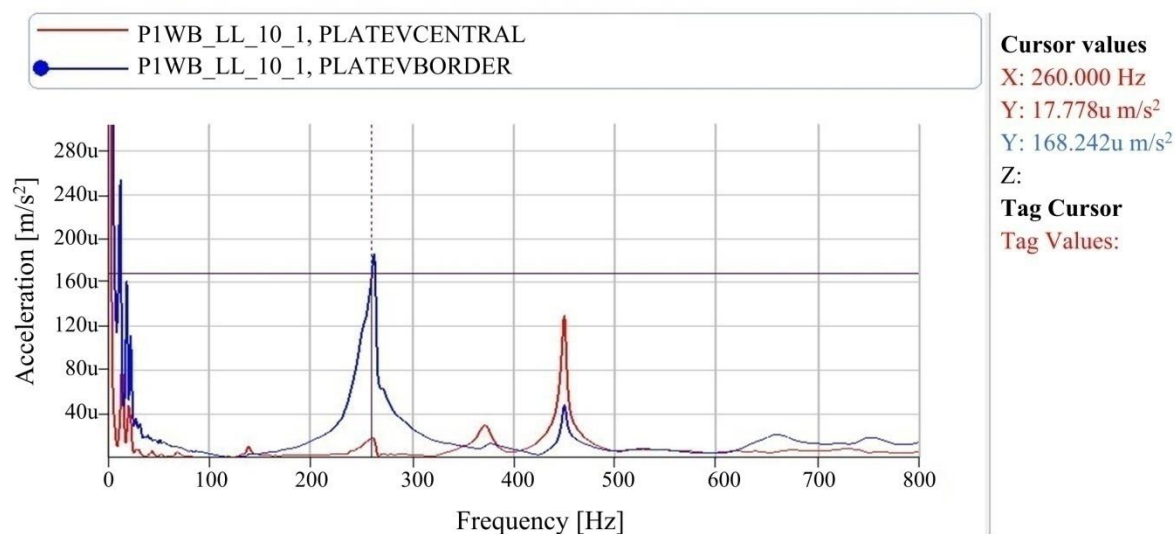


Fig. 3.23. Response of the acceleration spectrum vibrates with the impact of the hammer of thin plate coupled with water

In Fig. 3.22÷3.23, the author presented the approximation of the spectra of the thin plate without and with water, thanks to which it is possible to read the value of the mode of the natural vibrations of the thin plate without and with water. They are 138 Hz, 264 Hz, 382 Hz, and 451 Hz, respectively for the thin plate without water. They are 132 Hz, 260 Hz, 371 Hz, and 448 Hz, respectively for the thin plate with water. The values of the frequencies of the further forms were not read because in conditions of the normal operation of vessels there is no excitation at such high frequencies.

Thereafter, the result of measuring the natural vibration frequency of the thin plate is determined for two cases: without and with water. The next section presents a comparison between the natural vibration frequency value of the thin plate between two methods: numerical modelling method implemented on the Patran-Nastran software platform and measurement method. Thereby, assess the accuracy of the numerical modelling method and select the optimal numerical model applied to thin structures.

The natural frequency results obtained by numerical model analysis - finite element method implemented on Patran-Nastran software and measurement methods are presented for two cases without and with water. The natural frequencies and correlation error between natural frequencies obtained by numerical modelling and natural frequencies obtained by the measurement method for the thin plate without water is described in Tab. 3.15 and Fig. 3.24.

Tab. 3.15. Parameters of calculation model for the thin plate without water

	The natural frequency of the model: [Hz]				Measurement tests [Hz]
	Model 2D	Model 2-3D	Model 3-D	Model 3-D det.	
Mode No. 1	130.45	133.67	132.75	135.58	<b>138,00</b>
Mode No. 2	255.5	260.89	258.34	260.56	<b>264,00</b>
Mode No. 3	368.79	373.28	374.89	375.68	<b>382,00</b>
Mode No. 4	437.98	445.76	456.45	455.77	<b>451,00</b>

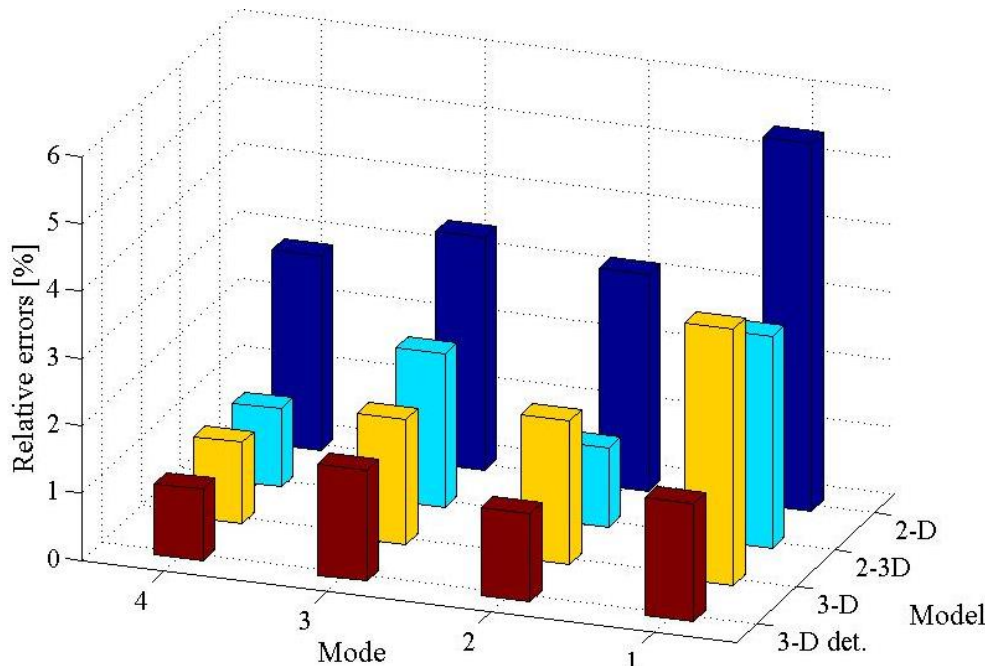


Fig. 3.24. Relative errors of calculations of the natural frequency of the thin plate without water

Correlation error between natural frequencies obtained by numerical modelling and natural frequencies obtained by the measurement method for the thin plate coupled with the fluid is described in Tab. 3.16 and Fig. 3.25.

Tab. 3.16. Parameters of calculation model for the thin plate with water

	The natural frequency of the model: [Hz]				Measurement tests [Hz]
	Model 2D	Model 2-3D	Model 3-D	Model 3-D det.	
Mode No. 1	125.55	128.76	128.75	130.34	<b>132,00</b>
Mode No. 2	252.58	252.97	253.34	255.67	<b>260,00</b>
Mode No. 3	365.28	368.49	375.97	375.46	<b>371,00</b>
Mode No. 4	435.77	453.76	453.45	450.58	<b>448,00</b>

The results of calculating the natural frequencies of the individual models together with the comparison with the measurement tests are shown in Tab. 3.15÷3.16, the thin plate without and with water, respectively. Computational errors (related to measurement tests) and numerical modelling methods are shown in Fig. 3.24÷3.25. All numerical models, including the simplest 2D model, perfectly reflect the dynamic characteristics of the real plate, although each model has its own disadvantages. First, considering the 2D model, the basic plate model is most often used with selected boundary conditions suitable for constraints, respectively. This model may be too simple to accurately reproduce the dynamic properties of thin plates.

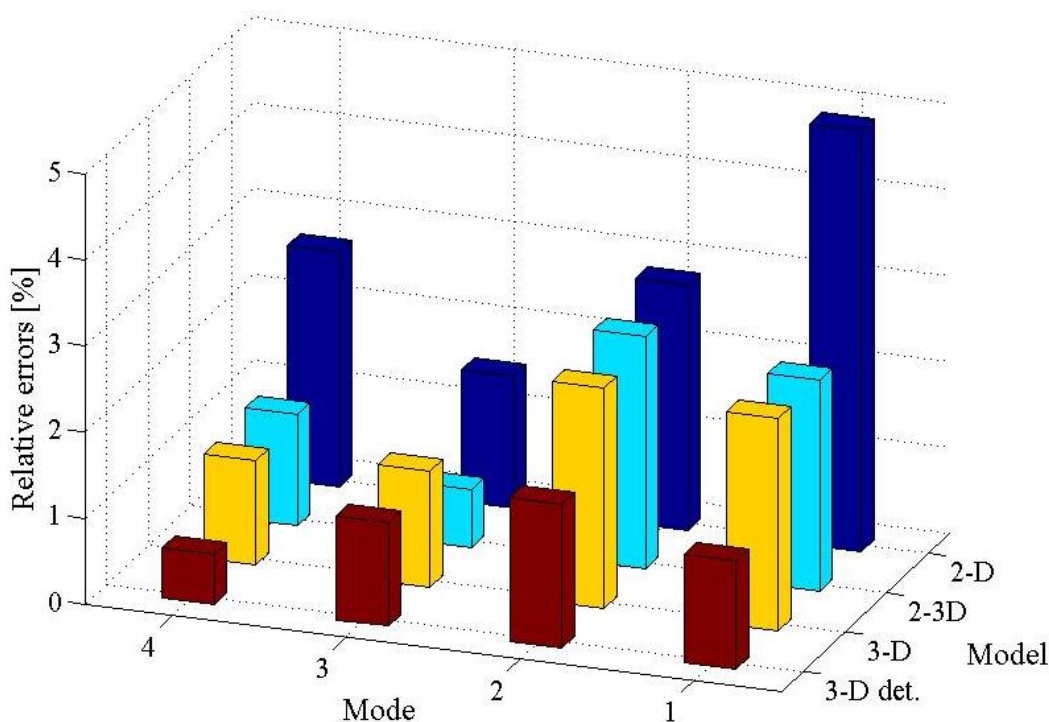


Fig. 3.25. Relative errors of calculations of the natural frequency of the thin plate coupled with water

In particular, boundary conditions have a large impact on the accuracy of the results. The simplest 2D model does not take into account the rigidity of the mounting plate. Therefore, the relatively large error of calculations occurs for the simplest 2D model and for the first natural vibration form is 5.47% and 4.89% for the thin plate without and with water, respectively. In the 2-3D model, problems occur when connecting plate elements to solid elements; plate elements are characterized by six degrees of freedom on each node, while solid elements do not include rotation degrees of freedom (three degrees of freedom for each node). This results in a relatively large error for vibration form first and third for the thin plate without water and forms first, second and third for the thin plate coupled with water, relative errors of 3.22% and 2.14% for the thin plate without water, relative errors of 2.85%, 2.70%, and 2.56% for the thin plate coupled with water, respectively. The disadvantages of the 3D model are completely the weak expression of the deformation distribution on the thickness of the plate due to its linear shape function and an element on each sheet thickness. The exact 3D det. model does not have any of the above disadvantages however it is many times larger than other models. It should be noted that the model 3-D det. has more than 0.33 million degrees of freedom. A 3-D det. model cannot analyse without using the connected supercomputer in the network. A significant increase in computing costs does not include the increased accuracy of the calculation. Therefore, the 2-3D model is evaluated as optimal according to the viewpoint of technical practice. The measurement method has additionally verified and proved the correctness of the selected 2-3D model.

### 3.3. Study the vibrations of the stiffened plates

In the previous section, the author studied dynamic properties, especially the vibrations of the beam and thin plate structures separately. In this section, the author studies the dynamic properties, the vibration of thin plate structures with reinforced beams called off stiffened plates. The stiffened plates are widely used in modern technical fields such as

construction, aerospace, aircraft manufacturing, shipbuilding. Especially in the shipbuilding industry, the stiffened plates are the main components that make up the ship walls, decks, hulls. Therefore, it is very important to study the static and dynamic behaviour of the stiffened plates under different load conditions. Understanding the effect of changing loads on the vibrations of the stiffened plates will help design engineers take measures to improve the safety of structures and equipment when applying the stiffened plates to the structure.

The structure of ships especially ship hulls often works in water environments. The natural frequencies of structures, when in contact with the fluid, differ from the frequency of the structure in the air. Therefore, the calculation and understanding of natural frequency changes due to the presence of fluid are important to design structures which in contact with or immersed in the fluid meet safety conditions. In general, the effect of fluid force on the structure is expressed in terms of mass added to the structure, increasing the mass and reducing the natural frequency of the structure when measured in the air. In this section, the vibration analysis of the stiffened plates is calculated in both air and fluid environments. Analytical calculations based on the finite element method are performed on the Patran-Nastran software platform and verified by the measurement method. The natural vibration of the stiffened plates in the air is considered for different finite element densities and finite element types (one-dimensional, two-dimensional and three-dimensional). Thereby assess the effect of boundary conditions, finite element types on the error and dispersion of the analytical results. On that basis, optimizing the selected numerical model for calculating the natural vibration frequency of the stiffened plate coupled with fluid.

### 3.3.1. Numerical modelling of the stiffened plate

The numerical modelling of the stiffened plate with geometric parameters is presented in the Tab. 3.17. In this section, the natural vibration frequency for the stiffened plate coupled with and without water for the variable mesh density, finite element types are calculated. The stiffened plate model in the Patran-Nastran software is illustrated in Fig. 3.26. The vibration analysis of the stiffened plate is also considered for two cases: the first case, the stiffened plate does not contact fluid (in the air), the second case, the stiffened plate coupled with the liquid at the underside of the plate.

Tab. 3.17. Geometric properties of the stiffened plate

Dimensions	Length [mm]	Width [mm]	Height [mm]	Thickness [mm]	Young Modulus $E$ [GPa]	The density of the material $\rho$ [kg/m <sup>3</sup> ]	Poisson's ratio $\nu$
Thin plate	800	200	-	8	21	7850	0.3
Beam	720	60	60	8			

*The first case: vibration analysis of the stiffened plate in the air:*

The numerical calculation was done with the help of the MSC Software package: Patran-Nastran. These programs are based on the finite element method. The natural vibration frequency of the stiffened plates, as well as the influence of numerical models on the accuracy of calculation results, is determined. In this section, the author calculates with four numerical models with the following boundary conditions:

Model 2-D (two-dimensional): the stiffened plate is modelled by two-dimensional finite elements, number of elements 9856 (Quad 4), number of nodes 8341, number of

degrees of freedom 46110. The two-dimensional model with corresponding boundary conditions described as Fig. 3.26a.

Model 2-3D: the stiffened plate is modelled with two-dimensional finite elements 9856 (Quad 4), the stiffened plate is fixed at both ends with two plates. The two fixed plates at the ends of the thin plate are modelled with three-dimensional elements 6400 (Hex8), number of nodes 15721, degrees of freedom 45618. The 2-3D model with boundary conditions is described as Fig. 3.26b.

Model 3-D (three-dimensional): Both the stiffened plate and two fixed plates are simulated by three-dimensional elements 19200 (Hex8), number of nodes 27183, degrees of freedom 57195. The 3D models with boundary conditions described as in Fig. 3.26c.

Model 3-D det.: the stiffened plate model and two clamps with three-dimensional finite elements. In this case, the number of finite elements is very large 192800 elements (Hex8) to increase the calculation accuracy, number of nodes 210657, degrees of freedom 458451. Model 3-D det. described as Fig. 3.26d.

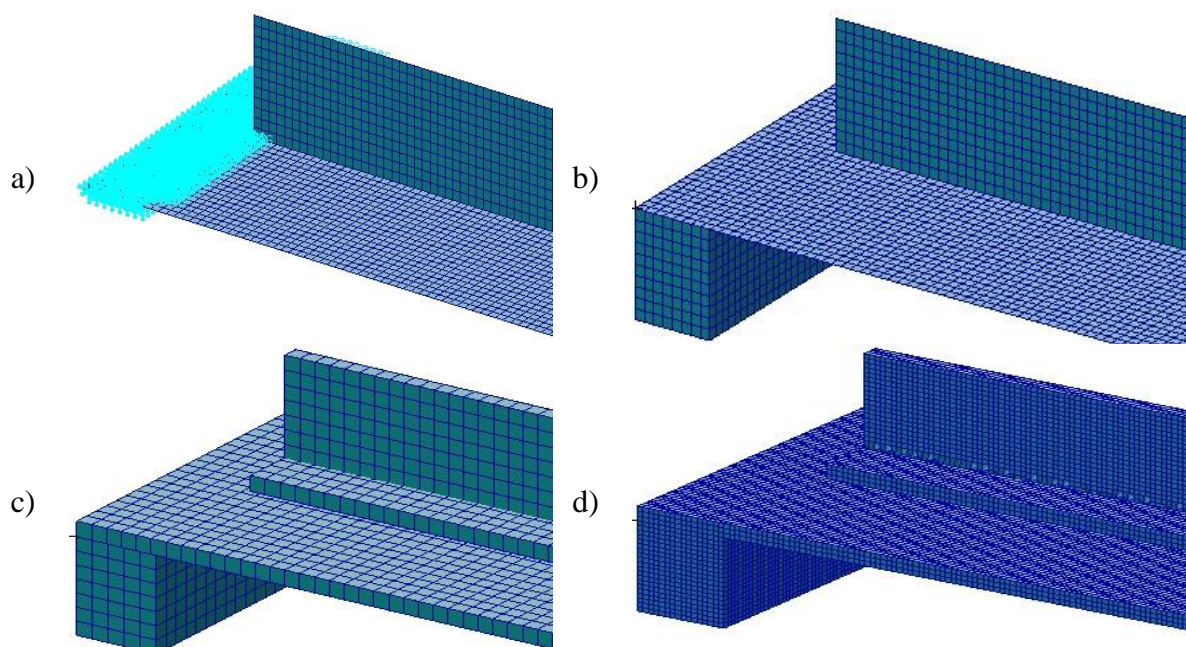
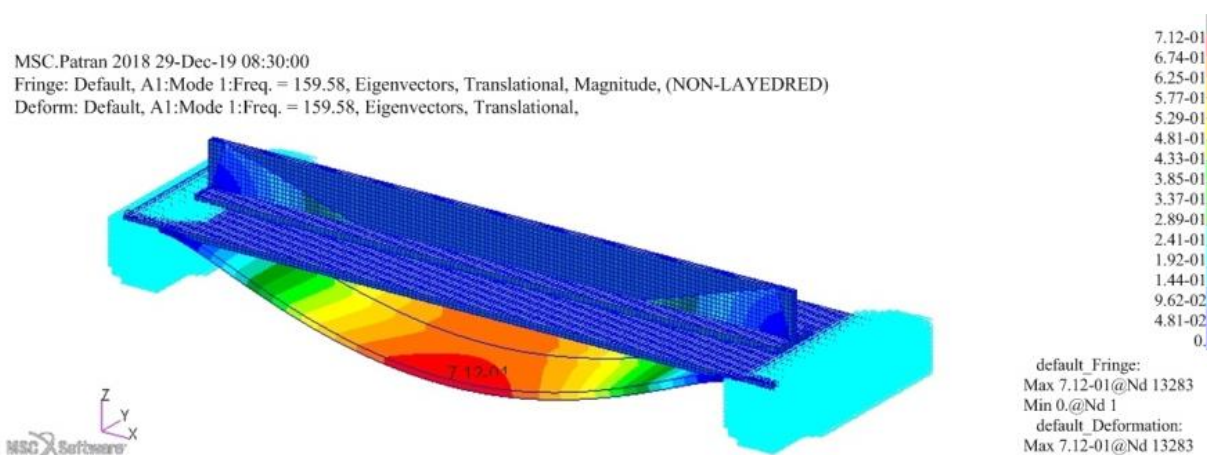


Fig. 3.26. Computational models of the stiffened plate, respectively: 2D, 2-3D, 3-D and 3-D det.

The natural vibration mode of three-dimensional model det. is described in Fig. 3.27.

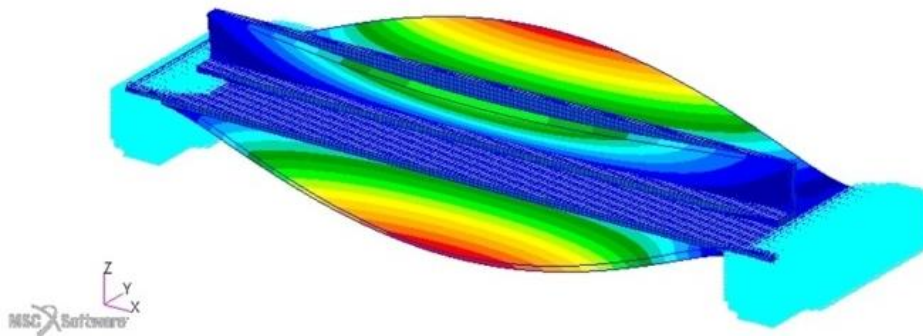


### 3. NUMERICAL MODELLING FOR SOME OF THE LOCAL HULL STRUCTURES

MSC.Patran 2018 29-Dec-19 08:31:55

Fringe: Default, A1:Mode 2:Freq. = 275.47, Eigenvectors, Translational, Magnitude, (NON-LAYEDRED)

Deform: Default, A1:Mode 2:Freq. = 275.47, Eigenvectors, Translational,

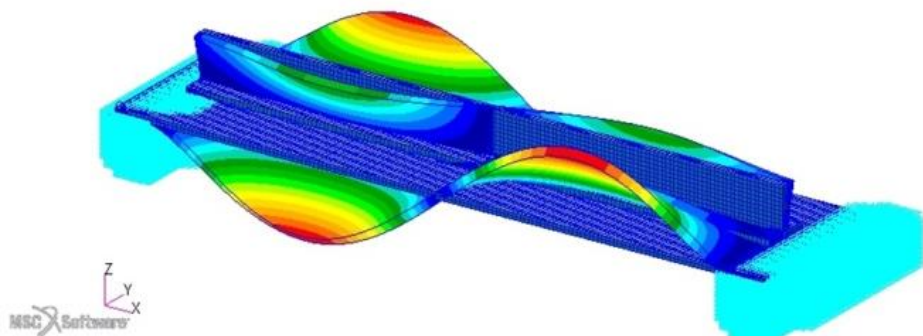


default Fringe:  
Max 1.53+00@Nd 6521  
Min 0.@Nd 1  
default\_Deformation:  
Max 1.53+00@Nd 6521

MSC.Patran 2018 29-Dec-19 08:32:06

Fringe: Default, A1:Mode 3:Freq. =331.08, Eigenvectors, Translational, Magnitude, (NON-LAYEDRED)

Deform: Default, A1:Mode 3:Freq. = 331.08, Eigenvectors, Translational,

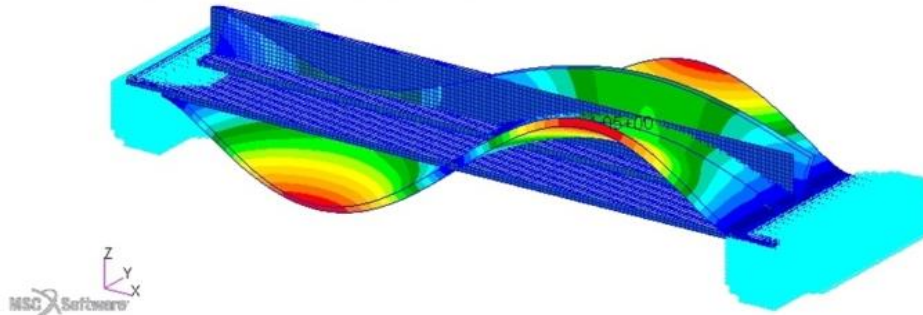


default Fringe:  
Max 1.62+00@Nd 6487  
Min 0.@Nd 1  
default\_Deformation:  
Max 1.62+00@Nd 6487

MSC.Patran 2018 29-Dec-19 08:32:16

Fringe: Default, A1:Mode 4:Freq. =400.62, Eigenvectors, Translational, Magnitude, (NON-LAYEDRED)

Deform: Default, A1:Mode 4:Freq. = 400.62, Eigenvectors, Translational,

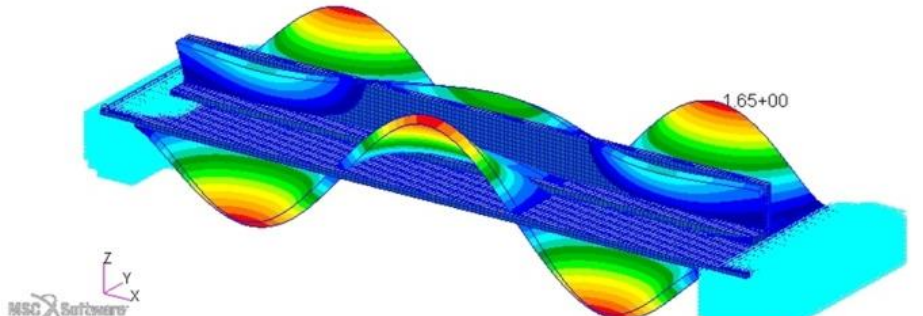


default Fringe:  
Max 1.05+00@Nd 6487  
Min 0.@Nd 1  
default\_Deformation:  
Max 1.05+00@Nd 6487

MSC.Patran 2018 29-Dec-19 08:32:24

Fringe: Default, A1:Mode 5:Freq. =462.38, Eigenvectors, Translational, Magnitude, (NON-LAYEDRED)

Deform: Default, A1:Mode 5:Freq. = 462.38, Eigenvectors, Translational,



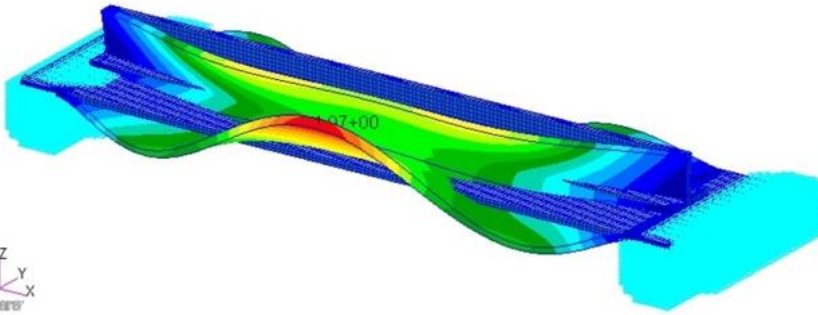
default Fringe:  
Max 1.65+00@Nd 126  
Min 0.@Nd 1  
default\_Deformation:  
Max 1.65+00@Nd 126

# INFLUENCE OF THE NUMERICAL MODELLING METHODS ON DISPERSIONS AND ERRORS OF ANALYSIS RESULTS IN CHOSEN MARINE MACHINES AND STRUCTURES

MSC.Patran 2018 29-Dec-19 08:32:35

Fringe: Default, A1:Mode 6:Freq. =688.6, Eigenvectors, Translational, Magnitude, (NON-LAYEDRED)

Deform: Default, A1:Mode 6:Freq. = 688.6, Eigenvectors, Translational,

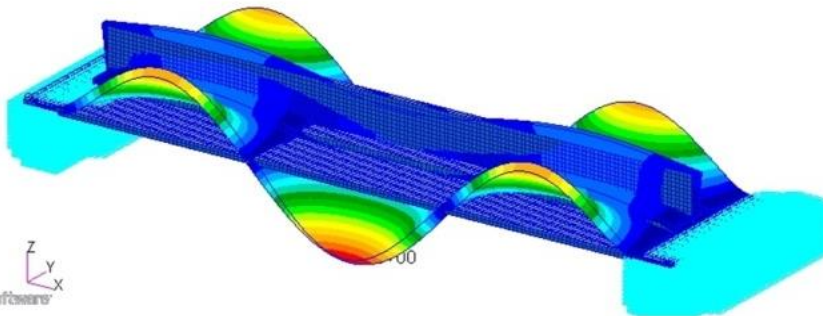


default Fringe:  
Max 1.07+00@Nd 81  
Min 0.@Nd 1  
default Deformation:  
Max 1.07+00@Nd 81

MSC.Patran 2018 29-Dec-19 08:32:45

Fringe: Default, A1:Mode 7:Freq. =781.23, Eigenvectors, Translational, Magnitude, (NON-LAYEDRED)

Deform: Default, A1:Mode 7:Freq. = 781.23, Eigenvectors, Translational,

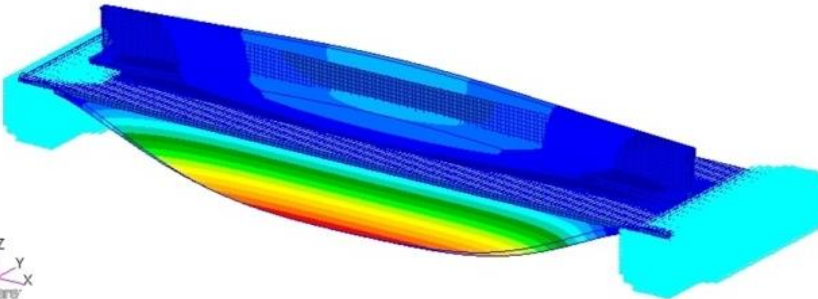


default Fringe:  
Max 1.85+00@Nd 81  
Min 0.@Nd 1  
default Deformation:  
Max 1.85+00@Nd 81

MSC.Patran 2018 29-Dec-19 08:32:54

Fringe: Default, A1:Mode 8:Freq. =871.02, Eigenvectors, Translational, Magnitude, (NON-LAYEDRED)

Deform: Default, A1:Mode 8:Freq. = 871.02, Eigenvectors, Translational,

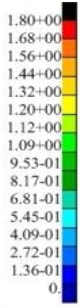
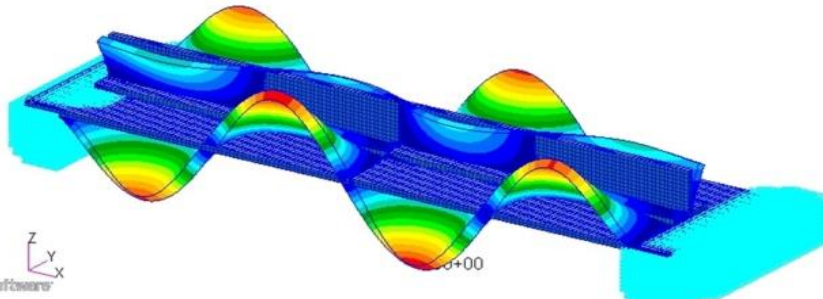


default Fringe:  
Max 1.88+00@Nd 6529  
Min 0.@Nd 1  
default Deformation:  
Max 1.88+00@Nd 6529

MSC.Patran 2018 29-Dec-19 08:33:04

Fringe: Default, A1:Mode 9:Freq. =875.86, Eigenvectors, Translational, Magnitude, (NON-LAYEDRED)

Deform: Default, A1:Mode 9:Freq. = 875.86, Eigenvectors, Translational,



default Fringe:  
Max 1.80+00@Nd 98  
Min 0.@Nd 1  
default Deformation:  
Max 1.80+00@Nd 98

### 3. NUMERICAL MODELLING FOR SOME OF THE LOCAL HULL STRUCTURES

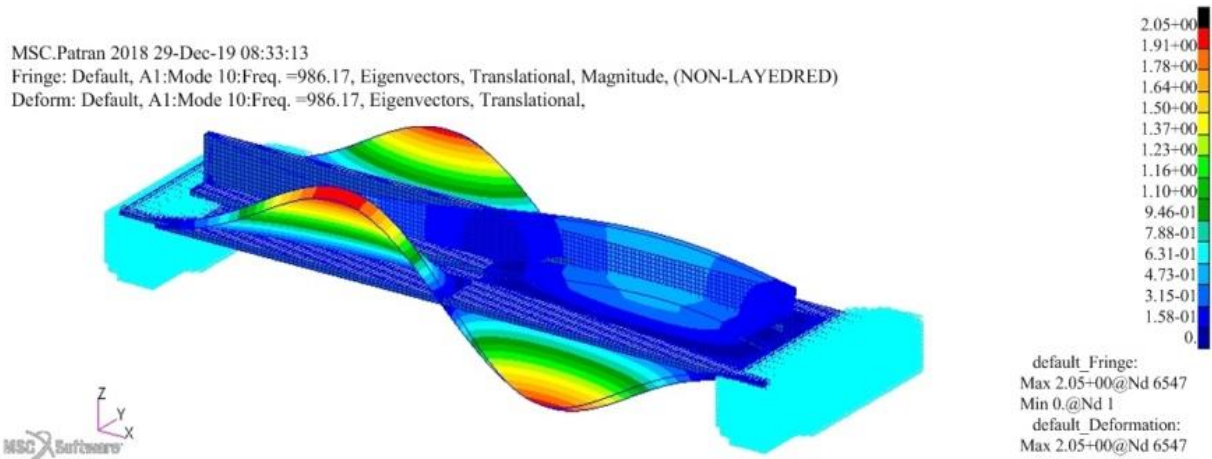


Fig. 3.27. Natural vibration modes of analytical stiffened plates without fluid

The Tab. 3.18 and Fig. 3.28 show the five natural vibration modes of the stiffened plate without fluid.

Tab. 3.18. Natural frequencies of the stiffened plate without fluid

Normal mode	The natural frequency of the model f [Hz]			
	Model 2D	Model 2-3D	Model 3-D	Model 3-D det.
Mode No. 1	153.52	157.56	155.36	159.58
Mode No. 2	259.65	275.15	278.55	275.47
Mode No. 3	317.16	323.35	335.47	331.08
Mode No. 4	408.98	405.55	403.75	400.02
Mode No. 5	474.61	465.43	470.68	462.38

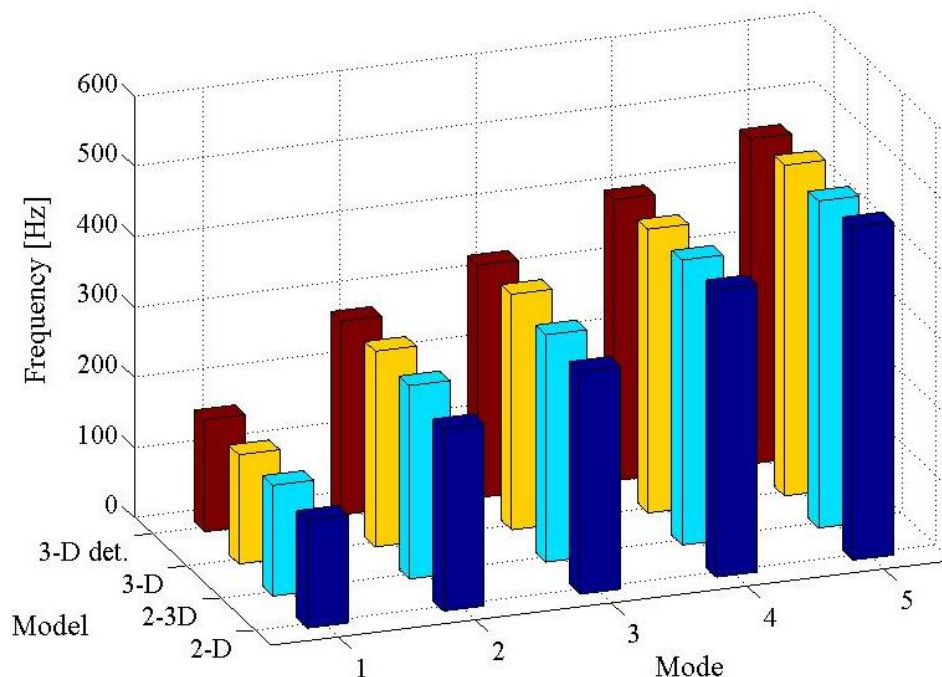
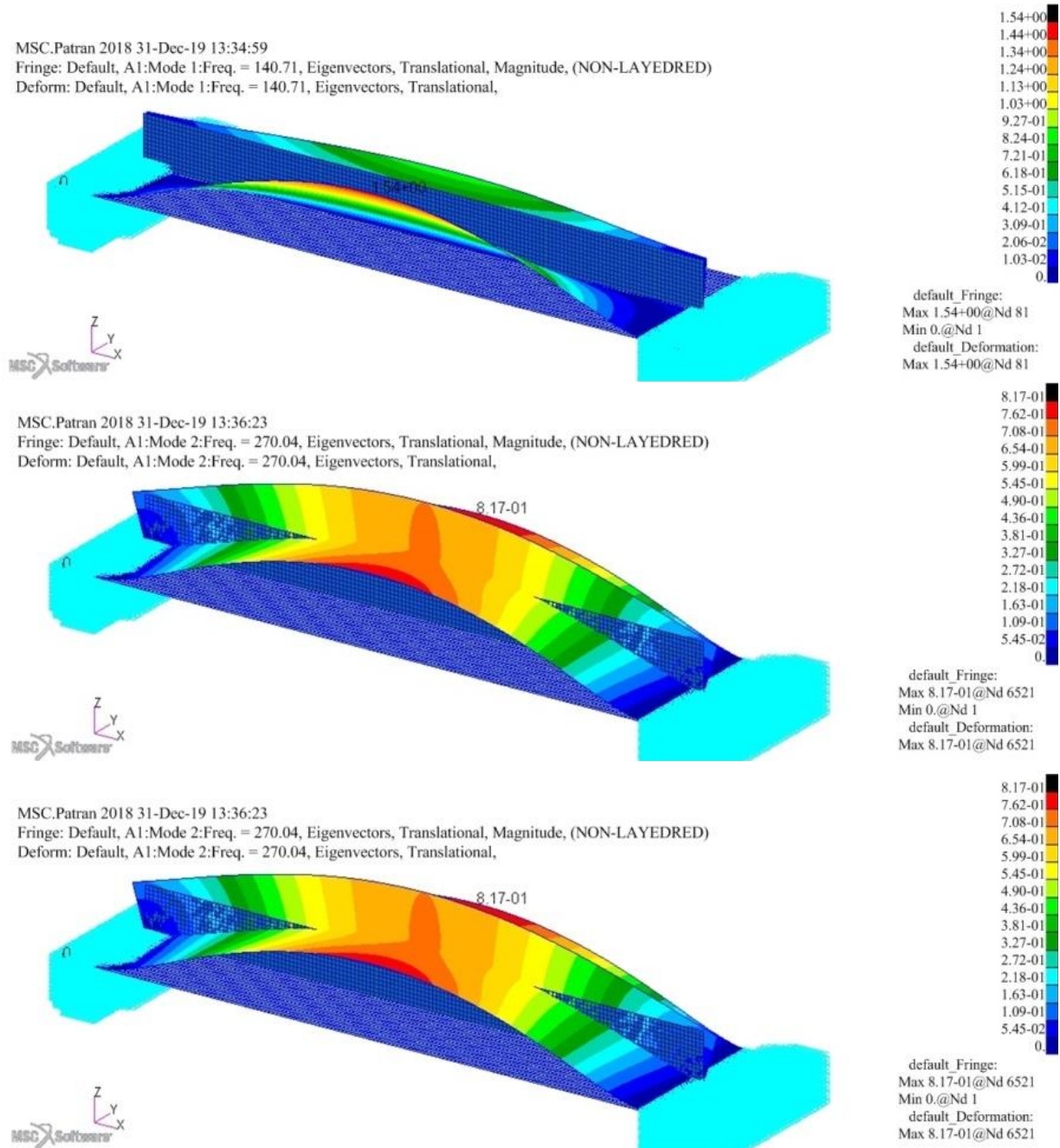


Fig. 3.28. Natural frequency of the stiffened plate without fluid

*The second case: vibration analysis of the stiffened plate coupled with fluid:*

In this section, the natural vibration frequency of the stiffened plate combined with water is calculated by method numerical modelling method. The numerical model method is based on the virtual mass method - Mfluid method in Nastran software. The calculation steps

are the same as in the calculation for thin plates in contact with the fluid. After calculation, the author obtained the natural vibration frequency of the stiffened plate for different finite elements: one-dimensional (1D), two-dimensional (2D), three-dimensional (3D) and different finite element density for the stiffened plate with one side contact with the fluid. The Fig. 3.29 shows an example of the vibration modes of the stiffened plate coupled with fluid.

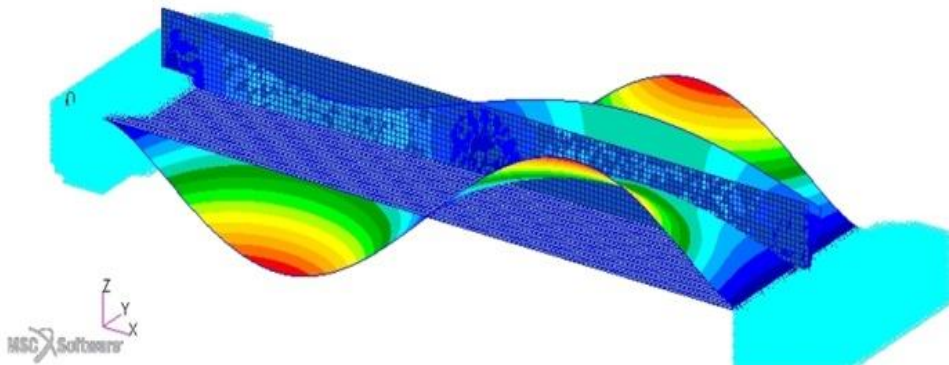


### 3. NUMERICAL MODELLING FOR SOME OF THE LOCAL HULL STRUCTURES

MSC.Patran 2018 31-Dec-19 13:36:41

Fringe: Default, A1:Mode 4:Freq. =392.01, Eigenvectors, Translational, Magnitude, (NON-LAYEDRED)

Deform: Default, A1:Mode 4:Freq. = 392.01, Eigenvectors, Translational,

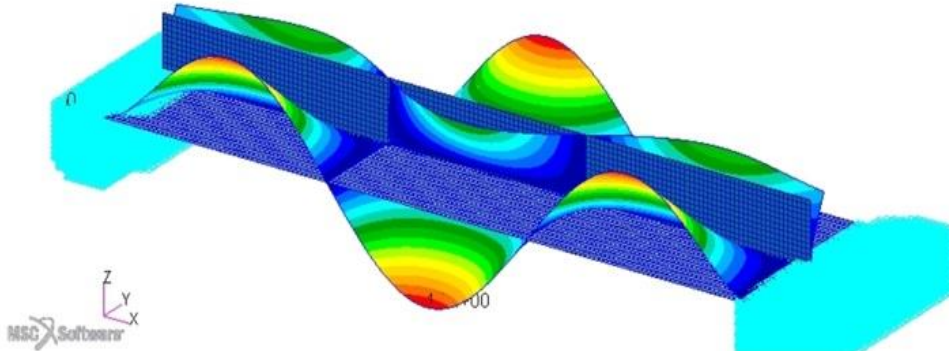


default\_Fringe:  
Max 1.28+00@Nd 6488  
Min 0.@Nd 1  
default\_Deformation:  
Max 1.28+00@Nd 6488

MSC.Patran 2018 31-Dec-19 13:36:49

Fringe: Default, A1:Mode 5:Freq. =462.32, Eigenvectors, Translational, Magnitude, (NON-LAYEDRED)

Deform: Default, A1:Mode 5:Freq. = 462.32, Eigenvectors, Translational,

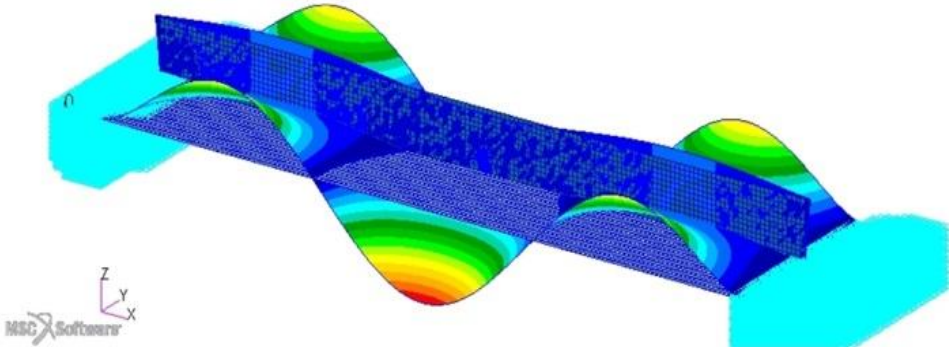


default\_Fringe:  
Max 1.54+00@Nd 81  
Min 0.@Nd 1  
default\_Deformation:  
Max 1.54+00@Nd 81

MSC.Patran 2018 31-Dec-19 13:36:56

Fringe: Default, A1:Mode 6:Freq. =671.35, Eigenvectors, Translational, Magnitude, (NON-LAYEDRED)

Deform: Default, A1:Mode 6:Freq. = 671.35, Eigenvectors, Translational,

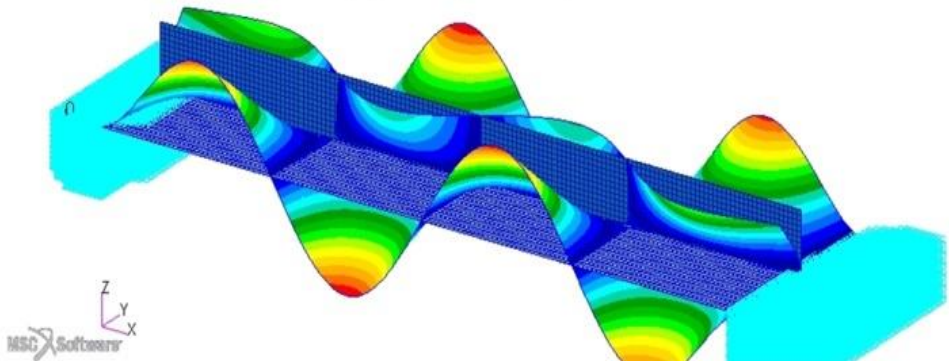


default\_Fringe:  
Max 1.96+00@Nd 6521  
Min 0.@Nd 1  
default\_Deformation:  
Max 1.96+00@Nd 6521

MSC.Patran 2018 31-Dec-19 13:37:03

Fringe: Default, A1:Mode 7:Freq. =701.23, Eigenvectors, Translational, Magnitude, (NON-LAYEDRED)

Deform: Default, A1:Mode 7:Freq. = 701.23, Eigenvectors, Translational,



default\_Fringe:  
Max 1.53+00@Nd 6538  
Min 0.@Nd 1  
default\_Deformation:  
Max 1.53+00@Nd 6538

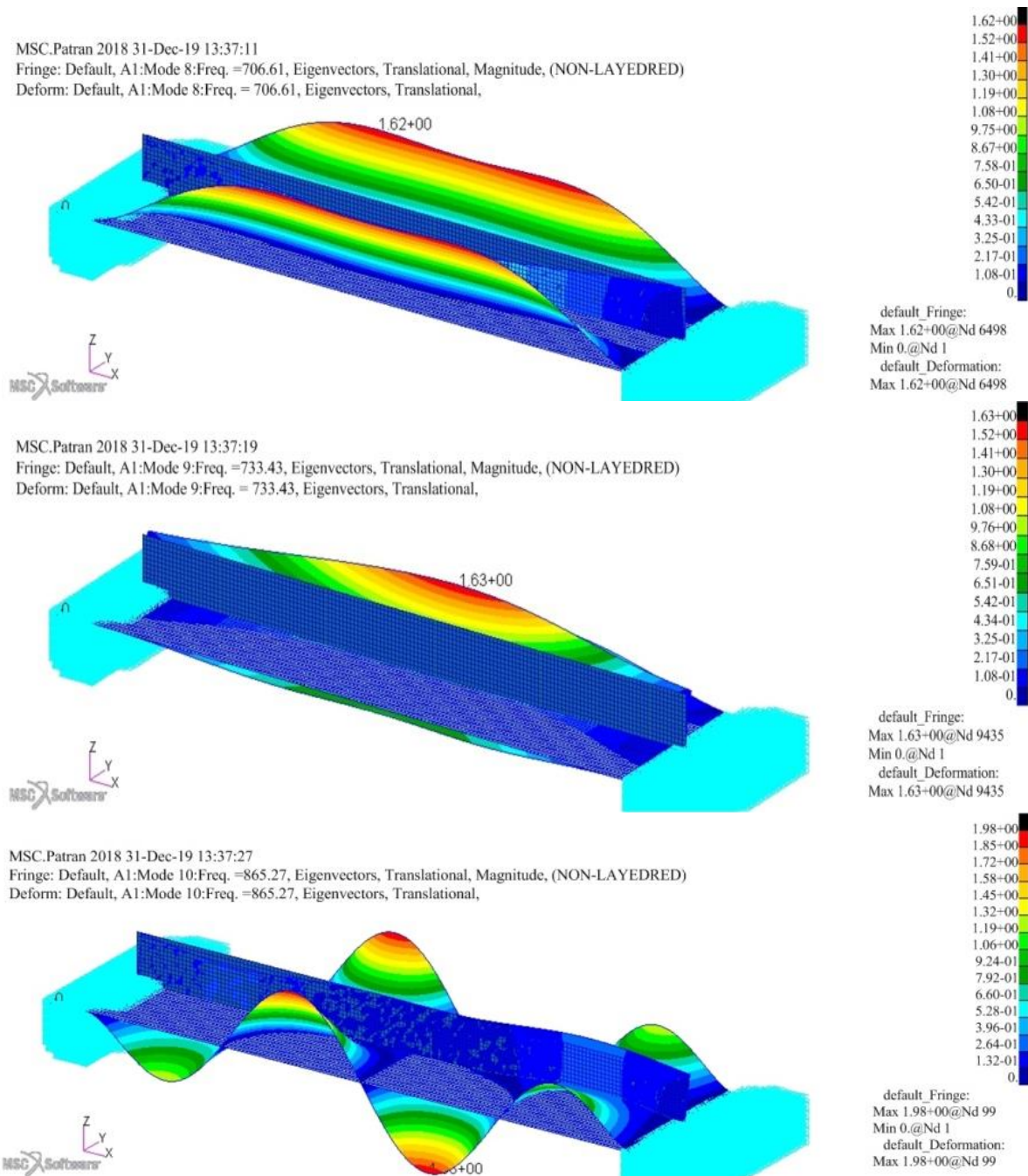


Fig. 3.29. Natural vibration modes of analytical stiffened plates coupled with fluid

The Tab. 3.19 and Fig. 3.30 show the five natural vibration modes of the stiffened plate coupled with fluid on one side surface.

Tab. 3.19. Natural frequencies of the stiffened plate coupled with fluid

Normal mode	The natural frequency of the model f [Hz]			
	Model 2D	Model 2-3D	Model 3-D	Model 3-D det.
Mode No. 1	135.11	140.71	137.75	142.52
Mode No. 2	256.88	270.04	272.36	269.35
Mode No. 3	285.15	295.78	305.79	300.80
Mode No. 4	395.34	392.01	392.27	387.65
Mode No. 5	465.38	462.32	464.50	456.31

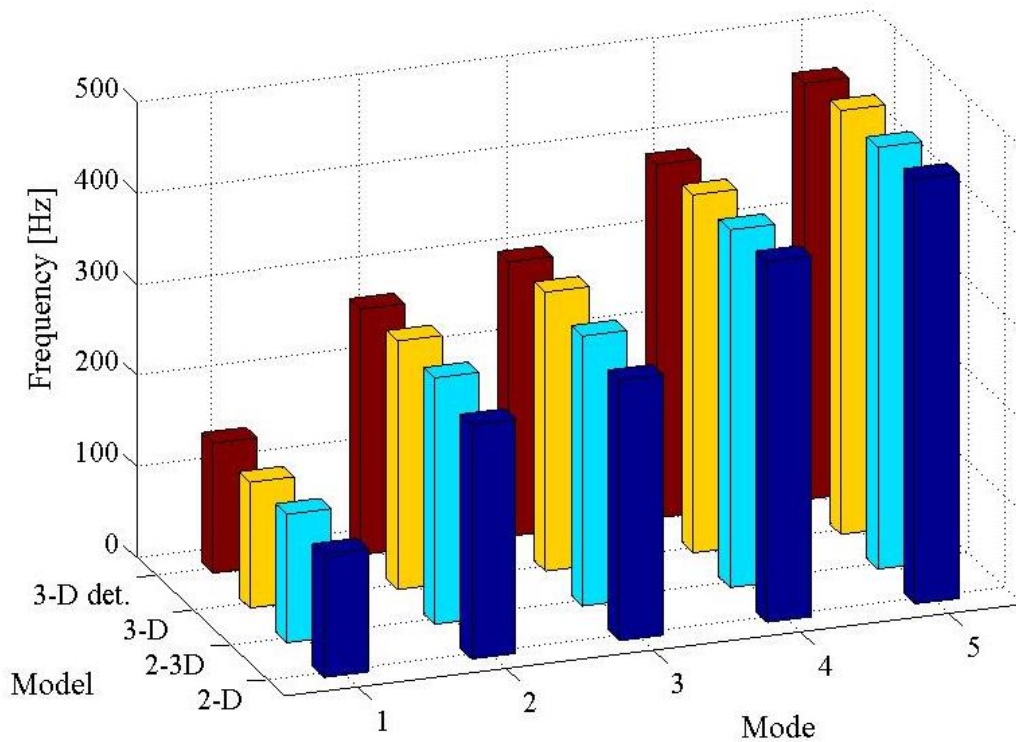


Fig. 3.30. Natural frequency of the analysed stiffened plate coupled with water

After calculating results, natural vibration analysis of the stiffened plate for two cases combined with fluid and not with fluid by numerical modelling method on the Patran-Nastran software platform. The results are verified by measurement and analysis of vibration of real objects in the laboratory of the Marine engineering Faculty - Maritime University of Gdynia.

### 3.3.2. Verify the results of numerical modelling of the real stiffened plate

In this section, experiment with a real model of the stiffened plate, size 800x200x8 mm, beam 720x60x60x8 mm in steel material with boundary conditions with the second case with and without fluid as shown in Fig. 3.31.

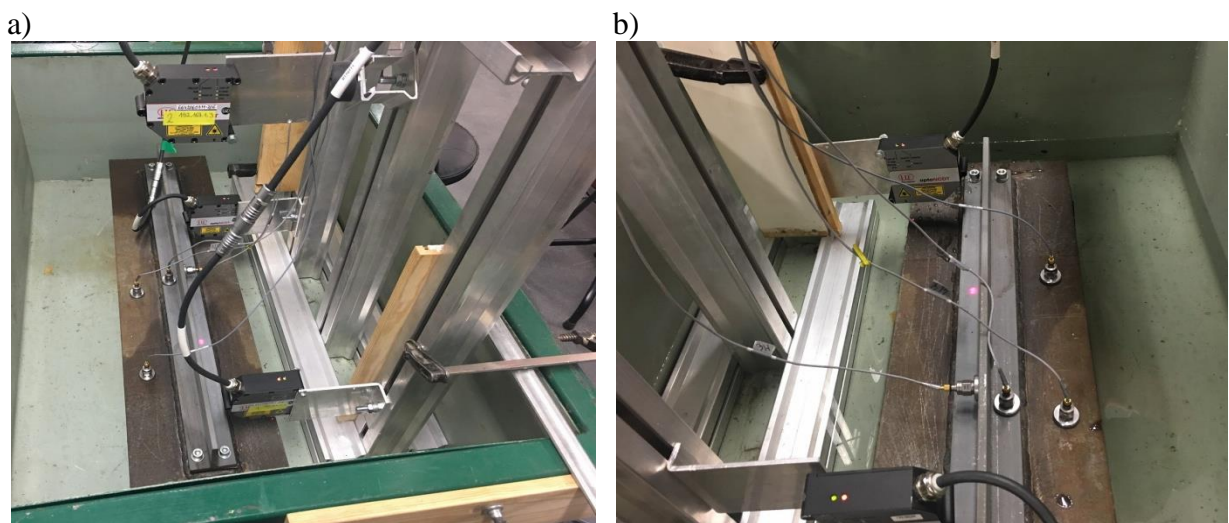


Fig. 3.31. Photograph of measuring model of stiffened plate, a) without water, b) with water

In tests, the equipment of the test is attached according to the diagram as shown in Fig. 3.32 is similar to the diagram for measurement the stiffened plate.

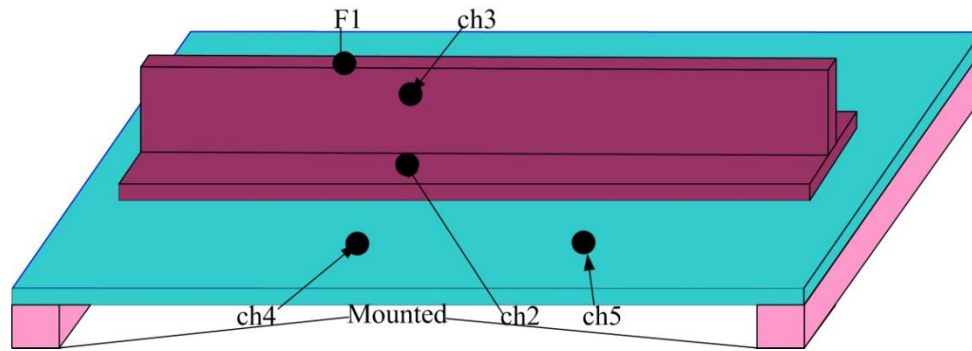


Fig. 3.32. Location of the transmitters during the tests for stiffened plate, ch2 - accelerometer (channel 2 - direction V on the beam), ch3 - accelerometer (channel 3 - direction H on the beam), ch4 - accelerometer (channel 4 - direction V on the plate), ch5- accelerometer (channel 5 - direction V on the plate), F1 - the place of impact with a modal hammer

After the measurement and calculation by FFT in Matlab software, the response of stiffened plate spectra without water with the modal hammer is shown in Fig. 3.33. On the graph, the acceleration response of the vibration determines the natural frequency values at the vertices of the graph. Fig. 3.34 illustrates the response of the acceleration spectrum of vibration to force of the modal hammer of the thin plate with water.

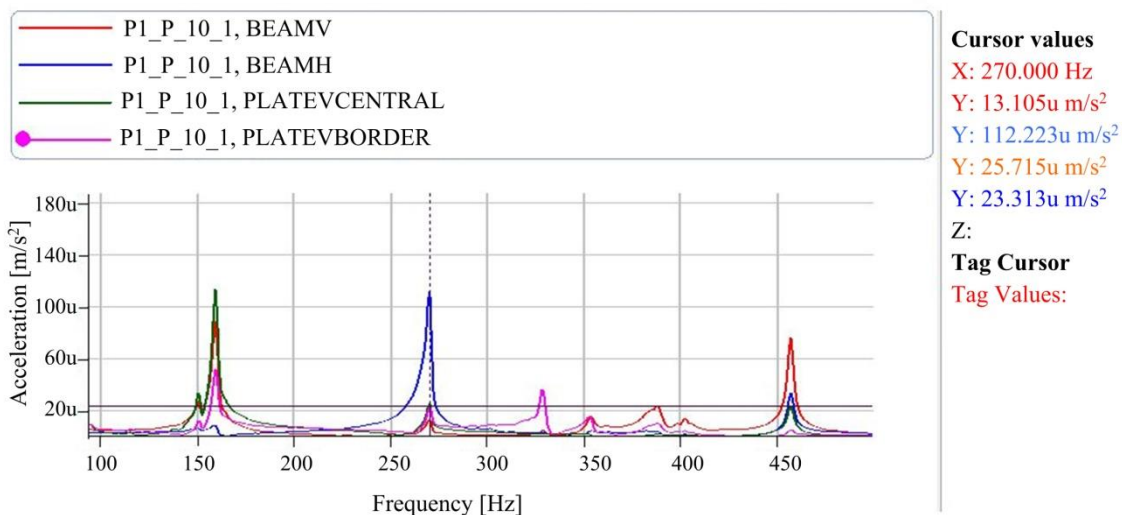


Fig. 3.33. Response of the acceleration spectrum vibrates with the impact of the hammer of the stiffened plate without water

In Fig. 3.33÷3.34, the author presented the approximation of the spectra of the stiffened plate without and with water, thanks to which it is possible to read the value of the mode of the natural vibrations of the stiffened plate without and with water. They are 159 Hz, 270 Hz, 328 Hz, 388 Hz and 457 Hz, respectively for the stiffened plate without water. They are 142 Hz, 264 Hz, 298 Hz, 376 Hz and 451 Hz, respectively for the stiffened plate with water. The values of the frequencies of the further forms were not read because in conditions of the normal operation of vessels there is no excitation at such high frequencies. Thereafter, the result of measuring the natural vibration frequency of the stiffened plate is determined for two cases: without and with water. The next section presents a comparison between the natural vibration frequency values of the stiffened plate between two methods: numerical simulation method implemented on the Patran-Nastran software platform and measurement method. Thereby, assess the accuracy of the numerical modelling method and select the optimal numerical model applied to stiffened structures.

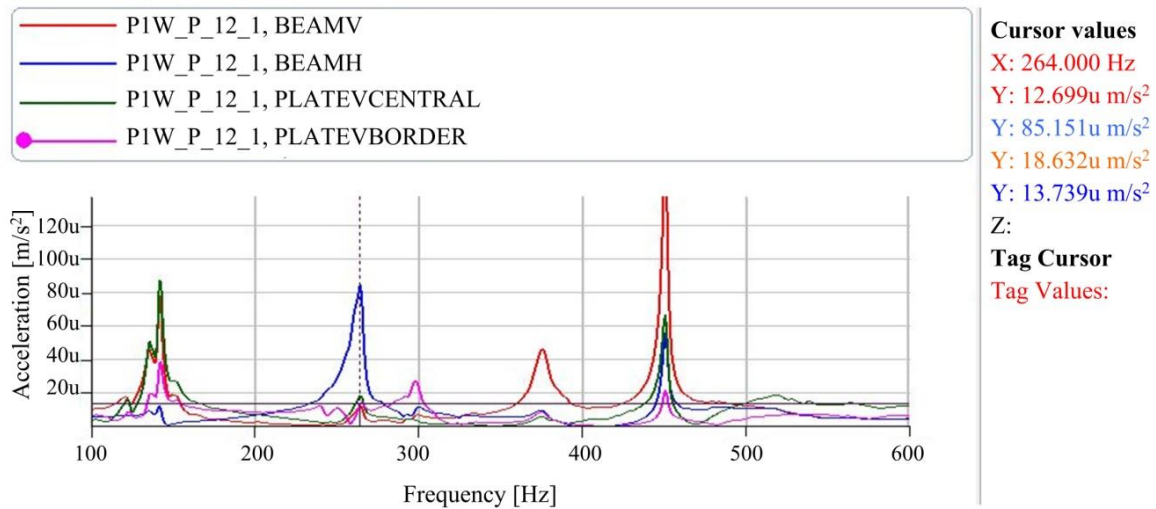


Fig. 3.34. Response of the acceleration spectrum vibrates with the impact of the hammer of the stiffened plate coupled with water

The natural frequency results obtained by numerical model analysis - finite element method implemented on Patran-Nastran software and experimental methods are presented for two cases without and with water are illustrated as the Tab. 3.20 and Fig. 3.35.

Tab. 3.20. Parameters of calculation model for the stiffened plate without water

	The natural frequency of the model: [Hz]				Measurement tests [Hz]
	Model 2D	Model 2-3D	Model 3-D	Model 3-D det.	
Mode No. 1	153.52	157.56	155.36	159.58	<b>159,00</b>
Mode No. 2	259.65	275.15	278.55	275.47	<b>270,125</b>
Mode No. 3	317.16	323.35	335.47	331.08	<b>328,00</b>
Mode No. 4	408.98	405.55	403.75	400.02	<b>388,125</b>
Mode No. 5	474.61	465.43	470.68	462.38	<b>457.125</b>

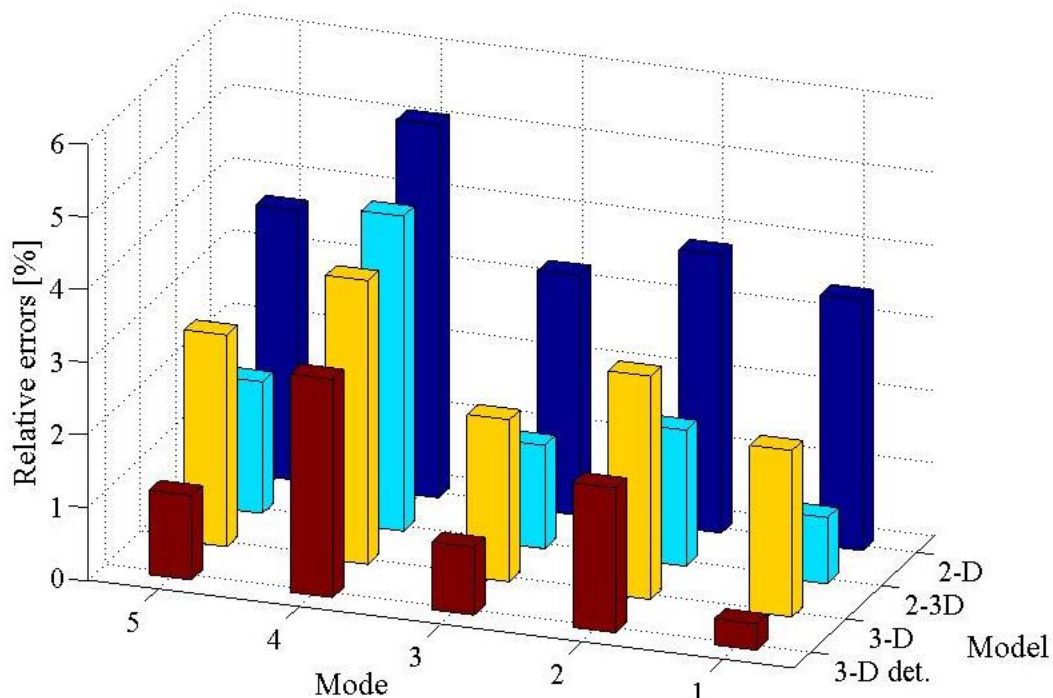


Fig. 3.35. Relative errors of calculations of the natural frequency of the stiffened plate without water

Correlation error between natural frequencies obtained by numerical modelling and the measurement method is described in Tab. 3.21 and Fig. 3.36.

Tab. 3.21. Parameters of calculation model for the stiffened plate with water

	The natural frequency of the model: [Hz]				Measurement tests [Hz]
	Model 2D	Model 2-3D	Model 3-D	Model 3-D det.	
Mode No. 1	135.11	140.71	137.75	142.52	<b>142.00</b>
Mode No. 2	256.88	270.04	272.36	269.35	<b>264.00</b>
Mode No. 3	285.15	295.78	305.79	300.80	<b>298.00</b>
Mode No. 4	395.34	392.01	392.27	387.65	<b>376.0</b>
Mode No. 5	465.38	462.32	464.50	456.31	<b>451.125</b>

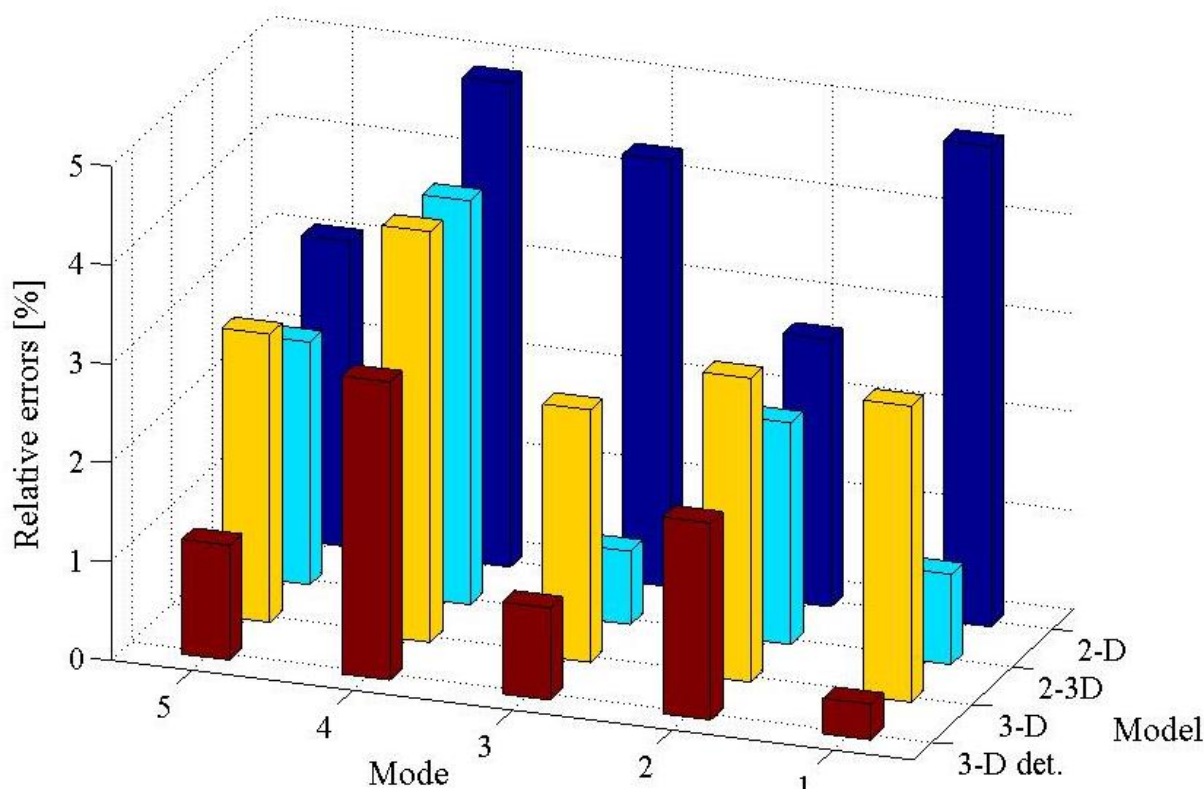


Fig. 3.36. Relative errors of calculations of the natural frequency of the stiffened plate with water

The results of calculating the natural frequencies of the individual models together with the comparison with the measurement tests are shown in Tab. 3.20÷3.21, the stiffened plate without and with water, respectively. Computational errors (related to measurement tests) and numerical modelling methods are shown in Fig. 3.35÷3.36. First, considering the 2D model, this model has a relatively large error of calculations that occurs for the simplest 2D model and for the first natural vibration form is 3.45% and 4.85% for the stiffened plate without and with water, respectively. In the 2-3D model has relatively large error for vibration form first and third for the stiffened plate without and with water, relative errors of 3.83% and 3.07% for the stiffened plate without water, relative errors of 2.70%, and 3.07% for the stiffened plate coupled with water, respectively. The exact 3D det. model does not have any of the above disadvantages, however, it is many times larger than other models. It should be noted that the model 3-D det. has more than 0.5 million degrees of freedom. A 3-D det. Model cannot analyse without using the connected supercomputer in the network. A

significant increase in computing costs does not include the increased accuracy of the calculation. Therefore, the 2-3D model is evaluated as optimal according to the viewpoint of technical practice.

#### 3.4. Conclusions

The author has conducted a vibration analysis of some selected real parts that make up the hull structure, superstructure such as beams, thin plates, stiffened plates. The analysis and calculations are performed by numerical modelling based on the famous Patran-Nastran digital software platform. Calculations and analyses for the selected structures are carried out for two cases, the first in the air, the second coupled with the fluid. The results of the calculation and analysis of the selected structures have been verified by measurement methods, conducted in the laboratory of the Marine Engineering Faculty of the Maritime University of Gdynia. Thereby, assessing the influence of error and the dispersion on the analysis results of the selected structures when applying the numerical modelling method for calculation, particularly here is the numerical modelling method based the finite element method implemented in the Patran-Nastran software. Here are some of the conclusions summarized after the end of chapter 3.

The selected numerical model method - finite element method on the Patran-Nastran software platform gives relatively accurate calculation results, has errors in the acceptable range, especially applied for calculations, structural analysis in the initial design stage. Help architects and designers reduce the testing time and prototype making time, saving costs and time.

Boundary conditions (constraint conditions), different types of finite elements (one-dimensional - 1D, two-dimensional - 2D, three-dimensional - 3D), different finite element densities, have a large effect on errors and dispersions on analysis results for selected structures. When the mesh density is higher, the error is smaller, the higher the accuracy of the calculation results. As the mesh density increases, the graph is smoother. The model of selected structures with three-dimensional elements and large element densities results in high accuracy and the error is usually less than 2% compared to the corresponding measurement results. Thus, as the mesh density increases, the accuracy of the resulting increases, but at the same time, it increases the computational time and requires a higher configuration computer, increasing the computational cost. Therefore, it is necessary to choose an appropriate mesh density, to ensure accuracy as well as reduce the time and the cost.

Through measurement verification, the numerical modelling is approached implemented in the Patran-Nastran software platform for the 2-3D finite element results in relatively accurate results. The highest error in both experimental cases for the selected structures without and with water was 5.47% and 4.85%, respectively. These errors may be within tolerable limits, especially in the design phase.

#### 4. Numerical modelling of ship hull and superstructure

The ship hull vibration has a great impact on the performance, safety of the devices, structures and the sailor's comfort when working on the ship. Therefore, designing a ship without any excessive vibration is an important issue and should be studied through analysis right in the design phase. To ensure minimum vibration in a proposed new design; avoid damage to structures, machinery or equipment (mechanically suitable); meeting the requirements of the crew's living environment and working conditions. The basic elements of a hull vibration system include basic mass elastic properties as well as damping and exciting forces. In order to control or limit the vibration response, it is necessary to modify the mass elastic properties by increasing damping, reducing excitation forces or changing the excitation frequency. Increasing damping may be useful in solutions to local structural vibration problems and in some machine and equipment problems but not as a practical solution to reduce hull vibration.

It is very important to determine the vibration of the ship hull in the design phase, in order to evaluate as well as make adjustments right in the design phase. Previously, the analysis of these vibrations was mainly based on empirical formulas. The global vibration of a ship, including the natural frequency and mode of the complete hull structure, is analysed by strip theory in which the natural frequency of the entire ship is calculated from beam theory and estimated weight and moment distribution at each hull. A method of such an approach is given by Todd [109]. While the formulas recommended by DNV [27], Japanese shipbuilding design handbook [83] and the shipping industry standard of the People's Republic of China [120], Yumei et. [114] are used to calculate the natural frequencies of the first three orders vertical vibration. Today, due to the rapid development of computer technology and the increasing speed and capacity of modern computers, hull vibrations are analysed by the finite element method (FEM). FEM is increasingly used in analysing and designing complex ship structures [52, 33, 34]. The three-dimensional finite element method is a common procedure to obtain the main vibration characteristics of ships. Therefore, the resonant frequency can be obtained and through forced vibration analysis, the maximum values of displacement, velocity or acceleration can be tested by the ISO-standards for vibration value allows the shipbuilding association of the world. The reaction of the hull structure may be resonant or non-resonant. The hull structure will often vibrate in the following modes: vertical bending mode, horizontal bending mode, twisting mode, coupling mode between horizontal and twisted mode (especially for container ships).

In this section, calculating and analysing the free vibration of ship hull and forced vibration caused by on board vibrating sources is carried out for medium size container ships of 2000 TEU and large container ships 11400 TEU. Calculation and analysis are done in two ways: firstly, empirical calculations of some countries such as Japan, China, and the DNV registry, the second is a calculation based on numerical model analysis using the finite element method. The first is to determine the free vibration characteristics of the ship hull to determine if the ship hull may be related to the resonance of the main excitation force under normal operating conditions. The second is to determine the characteristics of force vibration (velocity and stresses) of the ship hull and superstructure caused by the hull excitation source under normal operating conditions. To compare the vibration values obtained between the two methods, evaluate the accuracy of the applicable numerical modelling method. The parameters of 2000 TEU and 11400 TEU container ships are illustrated as Tab. 4.1÷ 4.2.

*Tab. 4.1. Properties of the modelled ship 2000 TEU*

<b>Number</b>	<b>Property</b>	<b>Value</b>
1	Type of ship	Container ship
2	Length overall	182.85 m
3	Length between perpendiculars	171 m
4	Breadth	28 m
5	Depth	16.1 m
6	Draught	11 m
7	Deadweight	27244 tons
8	Main Engine	MAN B&W 8S70MC-C
9	Engine power	24840 kW
10	Ship speed	19.5 kn
11	Engine RPM	91 rpm
12	Propeller	Rolls Royce CPP
13	Diameter	7600 mm
14	Number of blades	5
15	Propeller RPM	91 rpm

*Tab. 4.2. Properties of the modelled ship 11400 TEU*

<b>Number</b>	<b>Property</b>	<b>Value</b>
1	Type of ship	Container ship
2	Length overall	364.7 m
3	Length between perpendiculars	348 m
4	Breadth	45.6 m
5	Depth	29.74 m
6	Draught	15.5 m
7	Displacement, full load	171445 tons
8	Displacement, ballast	74977 tons
9	Displacement, light weight	37151 tons
10	Main Engine	MAN B&W 12K98ME-C(Mk7)
11	Engine power	72240 kW
12	Ship speed	24.7 kn
13	Engine RPM	100 rpm
14	Propeller	Rolls Royce CPP
15	Diameter	8900 mm
16	Number of blades	6
17	Propeller RPM	100 rpm

The evaluation model of the hull vibration and structures developed on the real ship. Fig. 4.1 is an illustration of the overall structure of the medium size container ship of 2000 TEU and large container ship 11400 TEU.



Fig. 4.1. Real model of the container ships: a) 2000 TEU, b) 11400 TEU

#### 4.1. The free vibration of ship hull and superstructure

One of the dangers to durability, safety, and longevity of a ship is the resonant vibration that occurs when the natural frequency of the hull and superstructure is compatible with the frequency of excitation. In this section, the natural vibration frequencies of the hull and superstructure are determined by two methods: calculation method by empirical formula and numerical modelling method using the finite element method.

##### 4.1.1. Empirical calculation procedures

In this section, some empirical calculations determine the natural vibration frequency of vertical bending vibrations to be carried out. Experimental formulas were developed by Yumei et. Verifying the vibration of hull ships by measurement method in the design phase is not feasible. Therefore, the author uses empirical calculation results to determine the correctness of the numerical model method. The approximate formulas of Yumei .et. were used to calculate the first three natural frequencies of the ship. The Todd's formula will be used to calculate the added mass of water for container ship, Eq.(4.1)÷(4.2). In the calculation of vertical vibration, the added water mass is calculated according to the formula proposed by F. M. Lewis and F. H. Todd [109]:

$$m_{av} = \frac{1}{2} \pi a_v C_v K_i \rho b^2, \quad (4.1)$$

added mass formula in horizontal vibration is:

$$m_{aH} = \frac{1}{2} \pi a_H C_H K_i \rho d^2, \quad (4.2)$$

where:

$m_{av}$  is added mass according to the vertical,

$m_{aH}$  is added mass according to the horizontal,  
 $a_v$  is natural frequency coefficient of vertical vibration of ship,  
 $a_H$  is natural frequency coefficient of horizontal vibration of ship,  
 $C_v$  is coefficient of added mass for vertical vibration,  
 $C_H$  is coefficient of added mass for horizontal vibration,  
 $\rho$  is density of material,  
 $b$  is the half breadth,  
 $d$  is the depth of submerged portion.

Horizontal vibration frequency calculation formula suggested by Brown [11] and reported by Todd [109]:

$$N_{2H} = 11.38 \times 10^4 \sqrt{\frac{DB^3}{\Delta_1 L^3}} - 0.8, \quad (4.3)$$

and

$$\Delta_1 = \Delta \left( 1.2 + \frac{1}{3} \cdot \frac{B}{d} \right), \quad (4.4)$$

where:

$N_{2H}$  is the natural frequency of horizontal 2 node (cycles per minutes – cpm),  
 $L$  is length of ship (m),  
 $B$  is breadth of ship (m),  
 $D$  is depth of ship (m),  
 $\Delta$  is displacement of ship (ton),  
 $\Delta_1$  is adjusting for entrained mass of water and adding a shear correction factor,  
 $d$  is the draft (m).

The following formula is also frequently used for estimating the higher modes:

$$N_{nH} = N_{2H}(n - 1)\mu_H, \quad (4.5)$$

where  $\mu_H = 1.02$  for tankers, 1.0 for container ships and 0.85 for cargo ships.

From the parameters of the medium-sized container ship with the capacity of 2000 TEU and the large size container ship of 11400 TEU capacity are shown in Tab. 4.1 and Tab. 4.2, the vertical natural vibration frequency according to the formula Eq.(2.22) and Eq.(2.24) (see chapter 2) are determined and horizontal natural vibration frequencies according to formula Eq.(4.3) are determined. The values of natural vibration frequencies of the two above container ships are illustrated in Tab. 4.3.

*Tab. 4.3. Natural frequency of two container ships 2000 TEU and 11400 TEU*

Ship type	Order	Vertical natural frequency [Hz]		Horizontal natural frequency [Hz]
		Experimental formula Eq.(2.22)	Experimental formula Eq.(2.24)	Experimental formula Eq.(4.3)
Container 2000 TEU	1	1.200	1.182	2.121
	2	2.548	2.344	4.252
	3	3 937	3.358	6.363
Container 11400 TEU	1	0.574	0.529	0.510
	2	1.219	1.049	1.020
	3	1.884	1.503	1.530

#### 4.1.2. Natural vibration analysis of the ship hull

Global vibrations are vibrations of the ship's entire hull in the frequency range from about 0.5 to 20 Hz. Typical large substructures, such as the aft part of the ship, the deckhouse, and the double-bottom, are coupled in a way that they cannot be considered isolated. The global coordinate system of the model is the right hand Cartesian coordinate system: X-direction goes along ship's length pointing to bow; Y-direction goes along ship's breadth pointing to Portside; Z-direction goes along ship's depth pointing to the deck. The structural model and applied loads are in the International System of Units (N, mm, s). The finite element model used in 11400 TEU and 2000 TEU container ship's vibration calculation is built entirely in accordance with the relevant design drawings, and the processing and analysis operations are completed by commercial finite element analysis software Patran and Nastran. All plate structures, such as shell, transverse bulkhead, inner bottom, web frame, and longitudinal bulkheads, etc. are modelled by CQUAD4 and CTRIA3 shell elements. All girders and stiffeners are modelled by an eccentric beam with the appropriate combination. Small structures with a hole are adjusted when finally balancing the quality of the whole ship structure and large structures with holes are modelled according to their actual shape as possible.

In the process of establishing the finite element model, the hull weight and position of the center are controlled by adjusting the material density of some elements and adding the weight structure points. There are two methods of cargo weight model in different load conditions: the first, mass of goods is modelled by rectangular blocks with the corresponding mass, the second, mass of goods is modelled by structure weight points at the corresponding load location and the block points are linked to the surrounding nodes by MPC (Multipoint constraints). The additional weight of the hull is calculated according to the experimental equation. The corresponding vertical and horizontal additional quantities are calculated in each load condition. The added water mass is added to the underwater shell as a concentrated mass point. A more detailed finite-element analysis, in which the entire hull is represented, may be developed by the Nastran computer program [65-69]. Computation of the natural frequencies and mode shapes is to be performed by solving an eigenvalue problem. The natural frequencies and corresponding mode shapes (eigenvectors) of the three-dimensional finite element model can be obtained by solving the following equation of motion:

$$[M]\{\ddot{u}(t)\} + [K]\{u(t)\} = 0, \quad (4.6)$$

$$[K]\{\theta\} = \omega^2 [M]\{\theta\}, \quad (4.7)$$

where:

- $\{\ddot{u}\}$  is column matrix of accelerations,
- $\{u\}$  is column matrix of displacements,
- $[K]$  is symmetrical stiffness matrix,
- $[M]$  is diagonal mass matrix,
- $\{\theta\}$  is column mode shape matrix,
- $\omega$  is natural frequency.

The medium size container ship 2000 TEU and the large size container ship 11400 TEU were modelled and displayed the results in Patran software and analysed in Nastran software. The 3D model in loading condition with water of the medium size container ship

2000 TEU has 25291 elements, 7773 nodes and 44166 degrees of freedom. The 3D model in loading condition with water of the large size container ship 11400 TEU has 84182 elements, 25679 nodes and 153516 degrees of freedom. Numerical software can be analysed for ships of different sizes and capacities. The natural frequency is calculated for the ship in loading condition with and without water.

The 3D model of the medium container ship capacity 2000 TEU in Patran software is presented in Fig. 4.2. The modes of vibration of the medium size container ship capacity 2000 TEU are illustrated as shown in Fig. 4.3÷4.9.

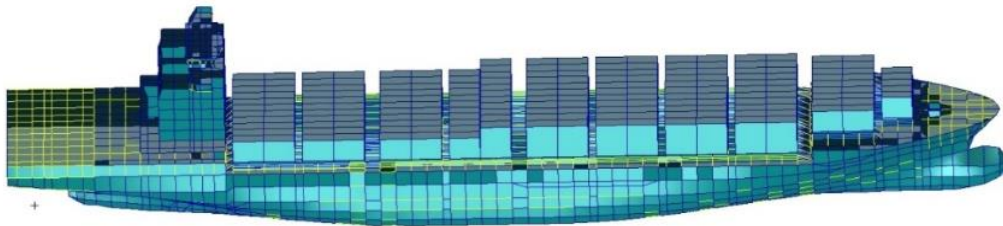


Fig. 4.2. 3D model of the medium size container ship of 2000 TEU

MSC.Patran 2017.0.2 28-Feb-19 16:57:54

Fringe: SUMSR.SC1, Mode 1: Freq. = 1.2068, Eigenvectors, Translational, Magnitude, (NON-LAYEDRED)

Deform: SUMSR.SC1, Mode 1: Freq. = 1.2068, Eigenvectors, Translational,

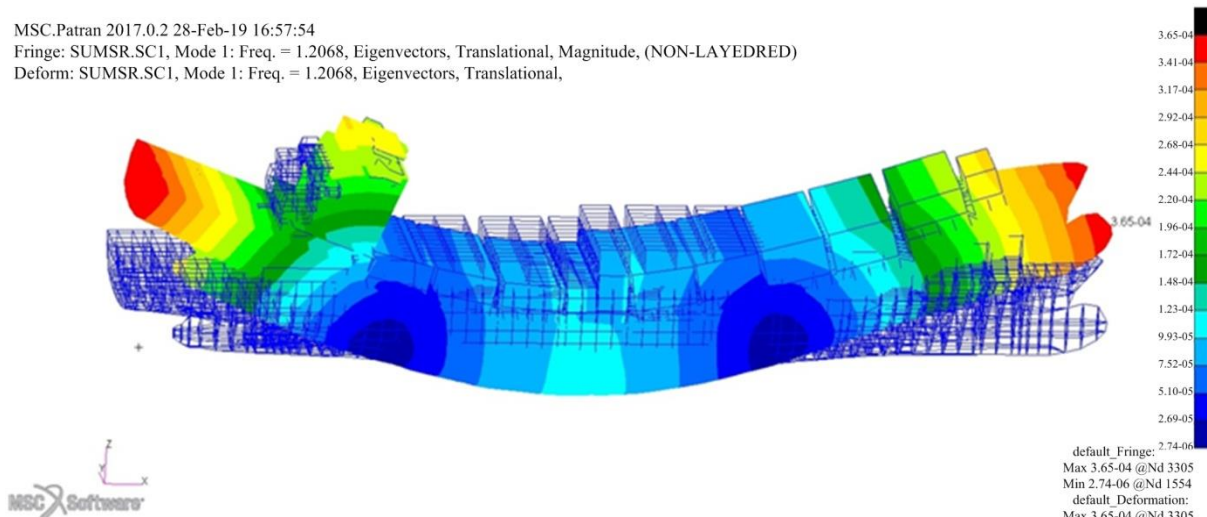


Fig. 4.3. Vertical vibration of 2 nodes of the container ship 2000 TEU with water

MSC.Patran 2017.0.2 28-Feb-19 16:58:10

Fringe: SUMSR.SC1, Mode 2: Freq. = 2.2521, Eigenvectors, Translational, Magnitude, (NON-LAYEDRED)

Deform: SUMSR.SC1, Mode 2: Freq. = 2.2521, Eigenvectors, Translational,

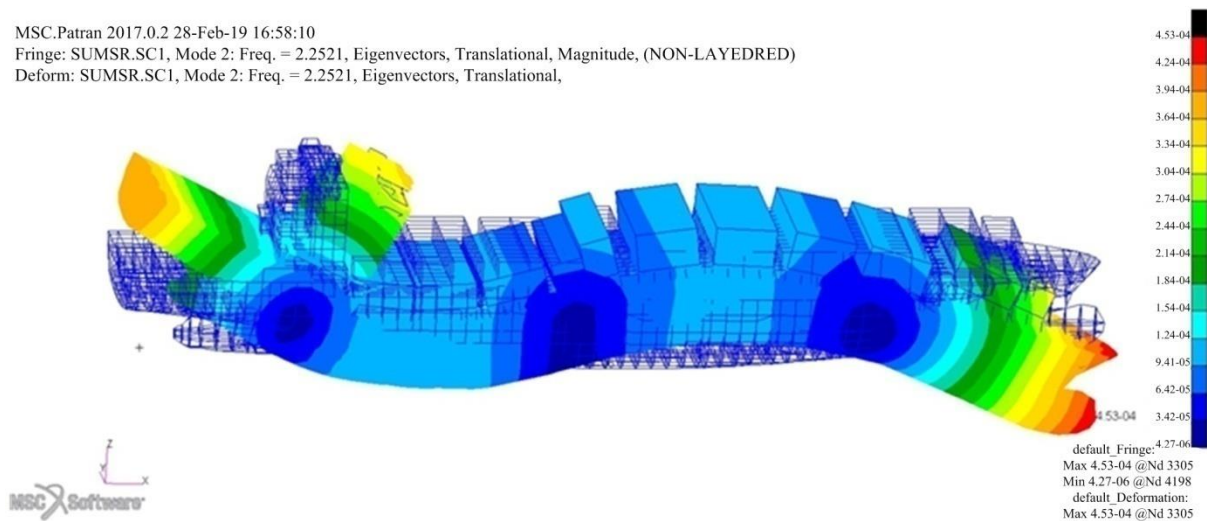


Fig. 4.4. Vertical vibration of 3 nodes of the container ship 2000 TEU with water

## 4. NUMERICAL MODELLING OF SHIP HULL AND SUPERSTRUCTURE

MSC.Patran 2017.0.2 28-Feb-19 16:59:35

Fringe: SUMSR.SC1, Mode 4: Freq. = 3.4223, Eigenvectors, Translational, Magnitude, (NON-LAYEDRED)

Deform: SUMSR.SC1, Mode 4: Freq. = 3.4223, Eigenvectors, Translational,

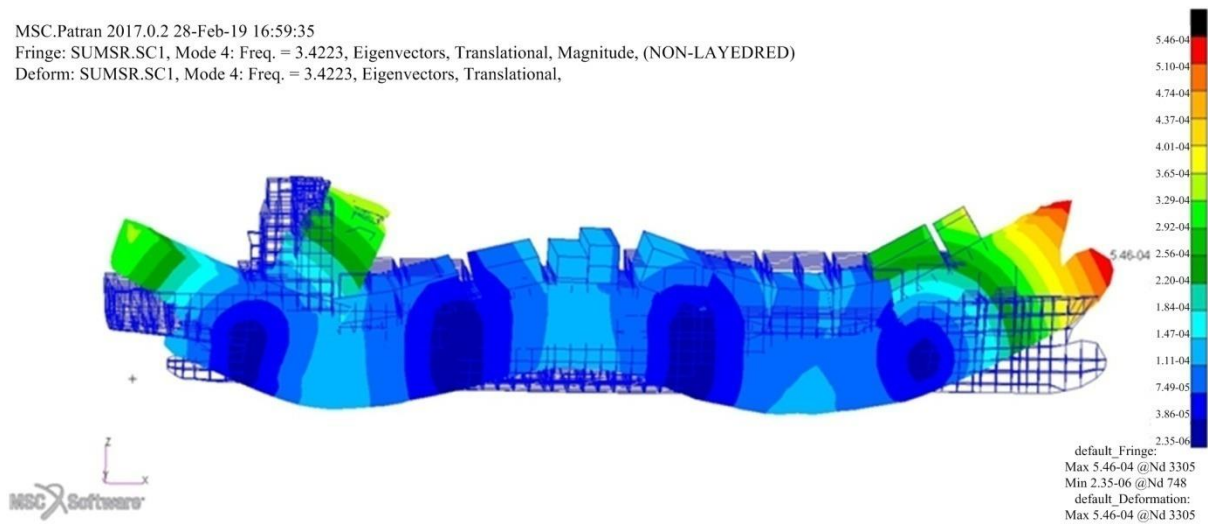


Fig. 4.5. Vertical vibration of 4 nodes of the container ship 2000 TEU with water

MSC.Patran 2017.0.2 28-Feb-19 17:00:22

Fringe: SUMSR.SC1, Mode 3: Freq. = 2.2933, Eigenvectors, Translational, Magnitude, (NON-LAYEDRED)

Deform: SUMSR.SC1, Mode 3: Freq. = 2.2933, Eigenvectors, Translational,

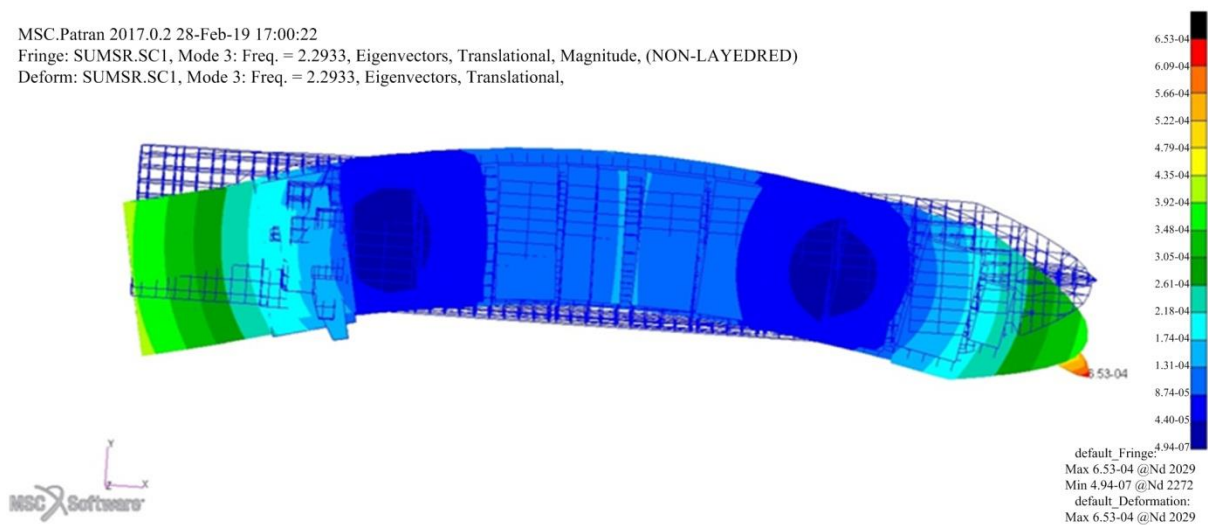


Fig. 4.6. Horizontal vibration of 2 nodes of the container ship 2000 TEU with water

MSC.Patran 2017.0.2 28-Feb-19 17:01:35

Fringe: SUMSR.SC1, Mode 8: Freq. = 4.948, Eigenvectors, Translational, Magnitude, (NON-LAYEDRED)

Deform: SUMSR.SC1, Mode 8: Freq. = 4.948, Eigenvectors, Translational,

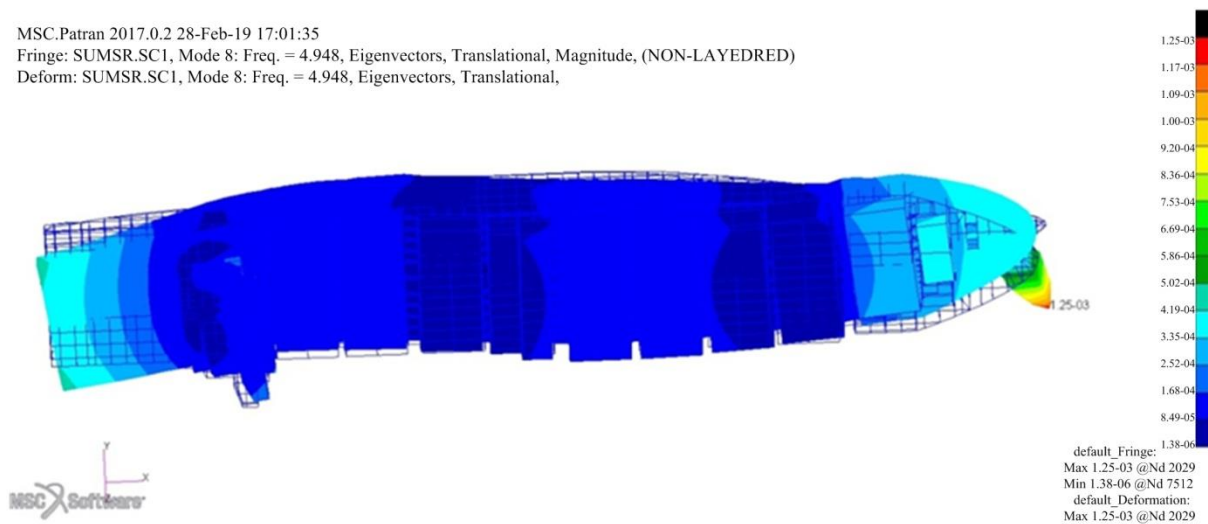


Fig. 4.7. Horizontal vibration of 3 nodes of the container ship 2000 TEU with water

MSC.Patran 2017.0.2 28-Feb-19 17:03:05  
 Fringe: SUMSR.SCI1, Mode 12: Freq. = 6.7009, Eigenvectors, Translational, Magnitude, (NON-LAYEDRED)  
 Deform: SUMSR.SCI1, Mode 12: Freq. = 6.7009, Eigenvectors, Translational,

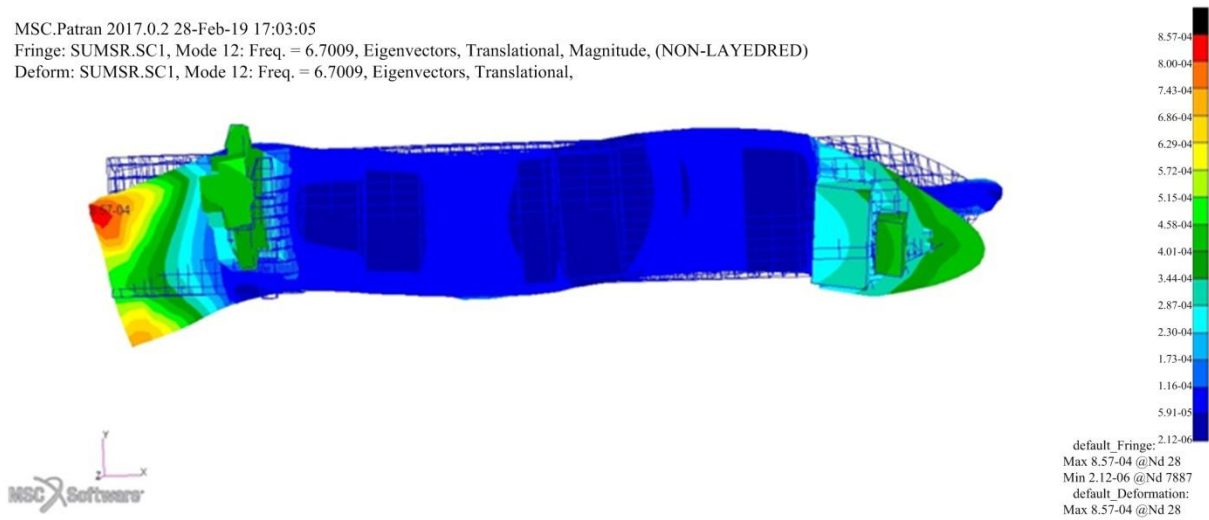


Fig. 4.8. Horizontal vibration of 4 nodes of the container ship 2000 TEU with water

MSC.Patran 2017.0.2 28-Feb-19 17:01:05  
 Fringe: SUMSR.SCI1, Mode 6: Freq. = 4.4095, Eigenvectors, Translational, Magnitude, (NON-LAYEDRED)  
 Deform: SUMSR.SCI1, Mode 6: Freq. = 4.4095, Eigenvectors, Translational,

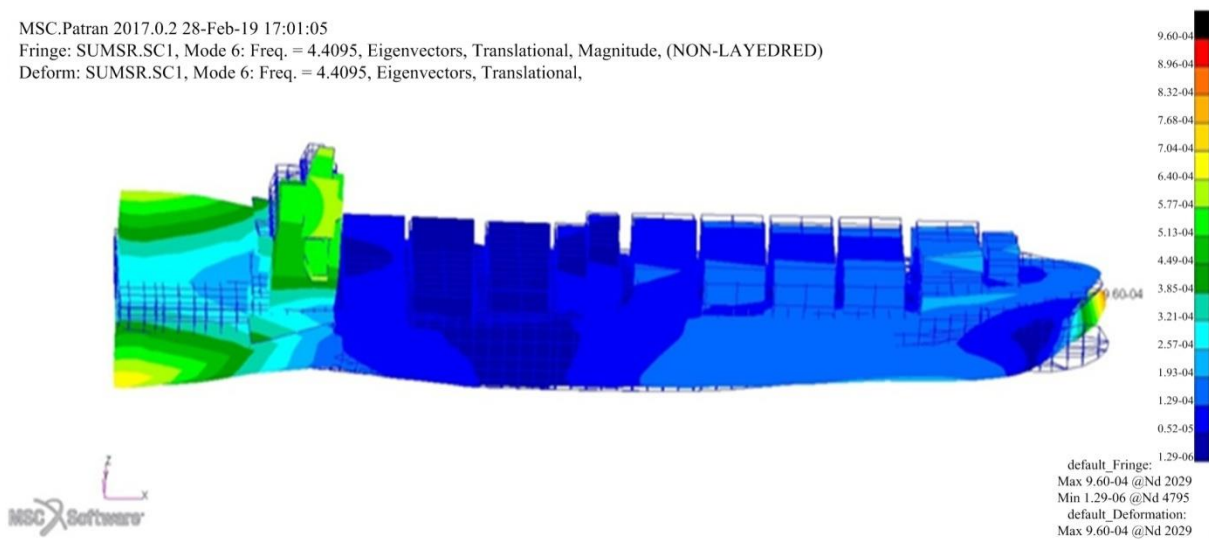


Fig. 4.9. Torsional vibration of the container ship 2000 TEU with water

The natural frequency of the medium size container ship 2000 TEU with water and without water and no-load is illustrated in Fig. 4.10.

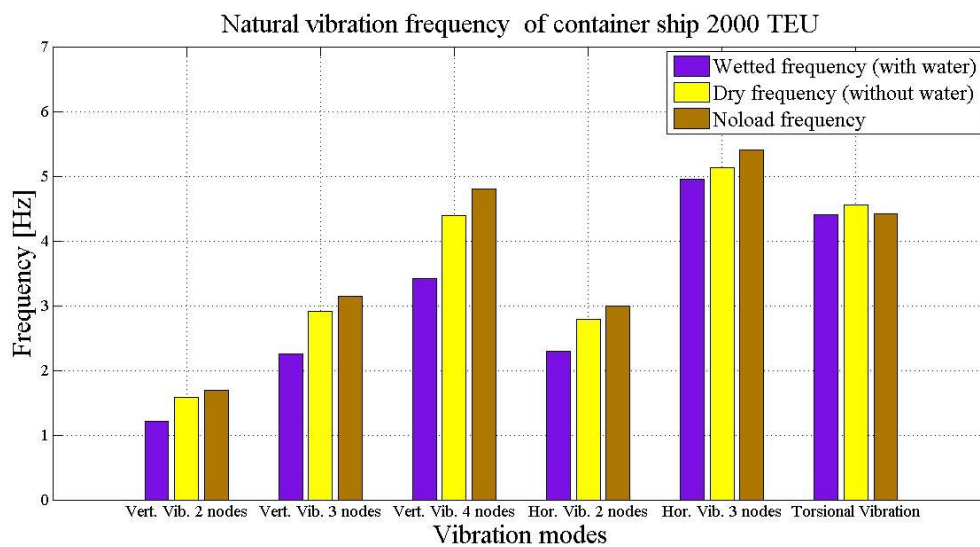


Fig. 4.10. Natural frequency of the medium size container ship 2000 TEU

The 3D model of the large size container ship capacity 11400 TEU in the Patran software is presented in Fig. 4.11. The modes of vibration of the large size container ship capacity 11400 TEU are illustrated as shown in Fig. 4.12÷4.18.

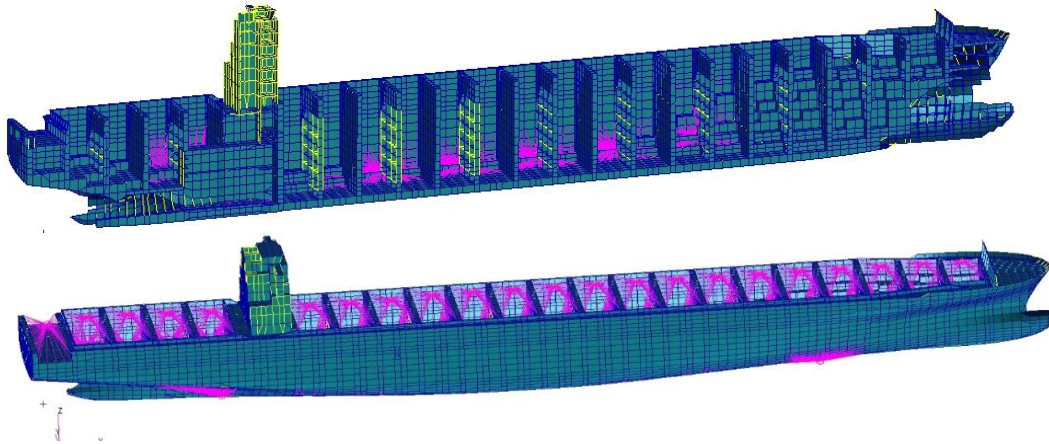


Fig. 4.11. 3D model of the large size container ship of 11400 TEU

MSC.Patran 2017.0.2 18-Feb-19 13:06:39

Fringe: Default.SC1, A2:Mode 9: Freq. = 0.59, Eigenvectors, Translational, Magnitude, (NON-LAYEDRED)

Deform: Default.SC1, A2:Mode 9: Freq. = 0.59, Eigenvectors, Translational,

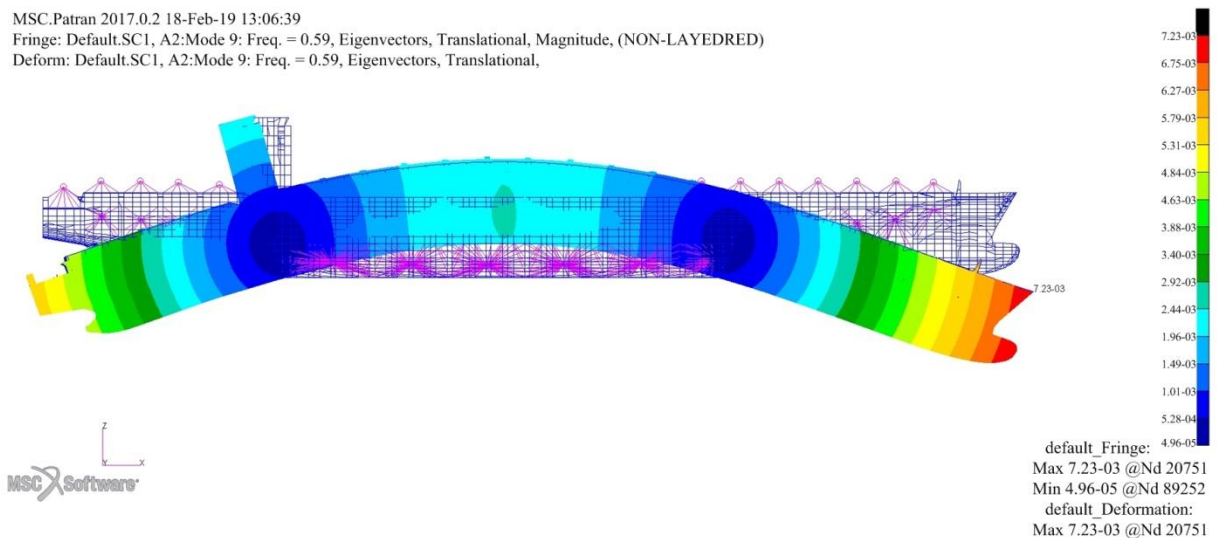


Fig. 4.12. Vertical vibration of 2 nodes of the container ship 11400 TEU with water

MSC.Patran 2017.0.2 18-Feb-19 13:07:57

Fringe: Default.SC1, A2:Mode 11: Freq. = 1.18, Eigenvectors, Translational, Magnitude, (NON-LAYEDRED)

Deform: Default.SC1, A2:Mode 11: Freq. = 1.18, Eigenvectors, Translational,

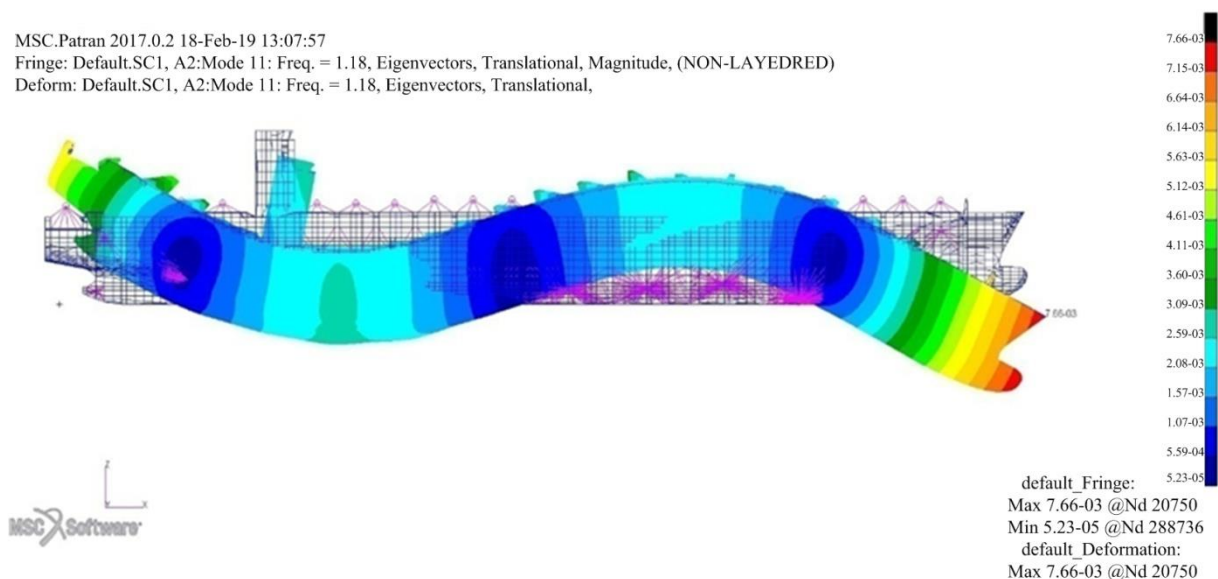


Fig. 4.13. Vertical vibration of 3 nodes of the container ship 11400 TEU with water

MSC.Patran 2017.0.2 18-Feb-19 13:08:14

Fringe: Default.SC1, A2:Mode 14: Freq. = 1.61, Eigenvectors, Translational, Magnitude, (NON-LAYEDRED)

Deform: Default.SC1, A2:Mode 14: Freq. = 1.61, Eigenvectors, Translational,

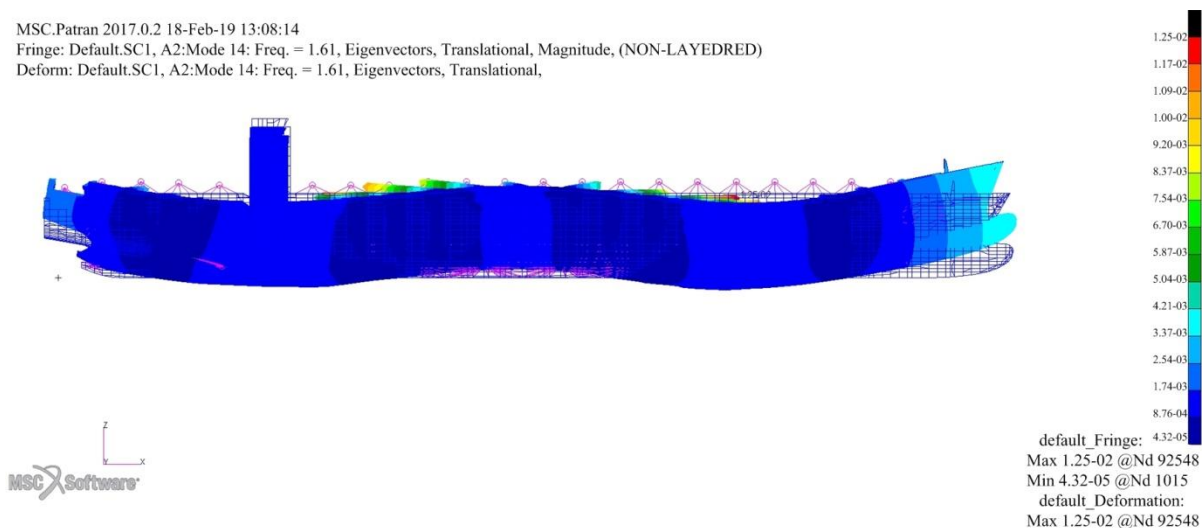


Fig. 4.14. Vertical vibration of 4 nodes of the container ship 11400 TEU with water

MSC.Patran 2017.0.2 18-Feb-19 13:07:37

Fringe: Default.SC1, A2:Mode 7: Freq. = 0.395, Eigenvectors, Translational, Magnitude, (NON-LAYEDRED)

Deform: Default.SC1, A2:Mode 7: Freq. = 0.395, Eigenvectors, Translational,

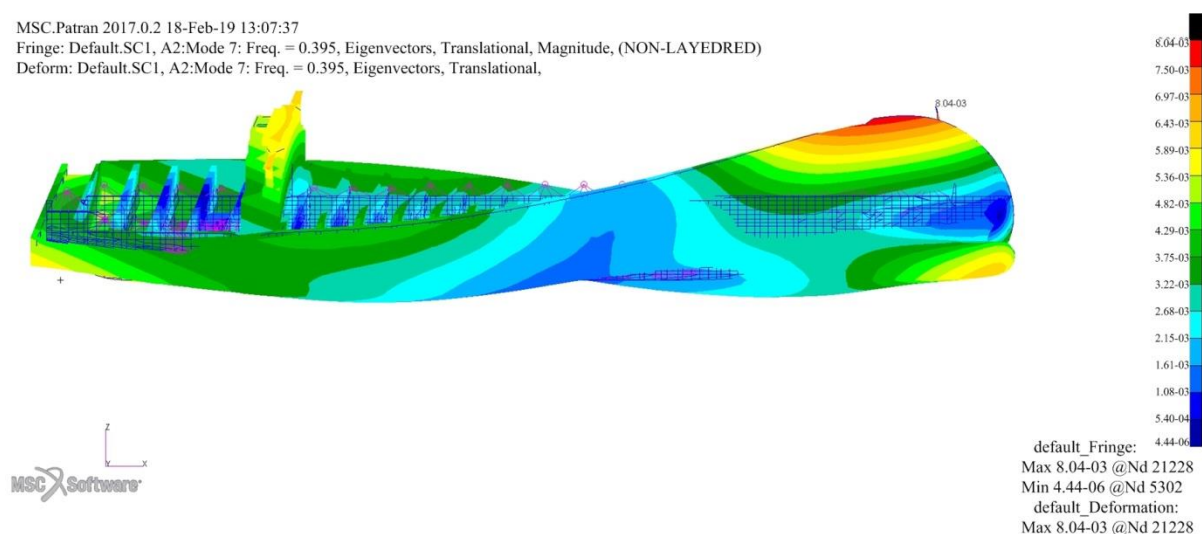


Fig. 4.15. Horizontal vibration of 2 nodes of the container ship 11400 TEU with water

MSC.Patran 2017.0.2 18-Feb-19 13:07:52

Fringe: Default.SC1, A2:Mode 10: Freq. = 0.84, Eigenvectors, Translational, Magnitude, (NON-LAYEDRED)

Deform: Default.SC1, A2:Mode 10: Freq. = 0.84, Eigenvectors, Translational,

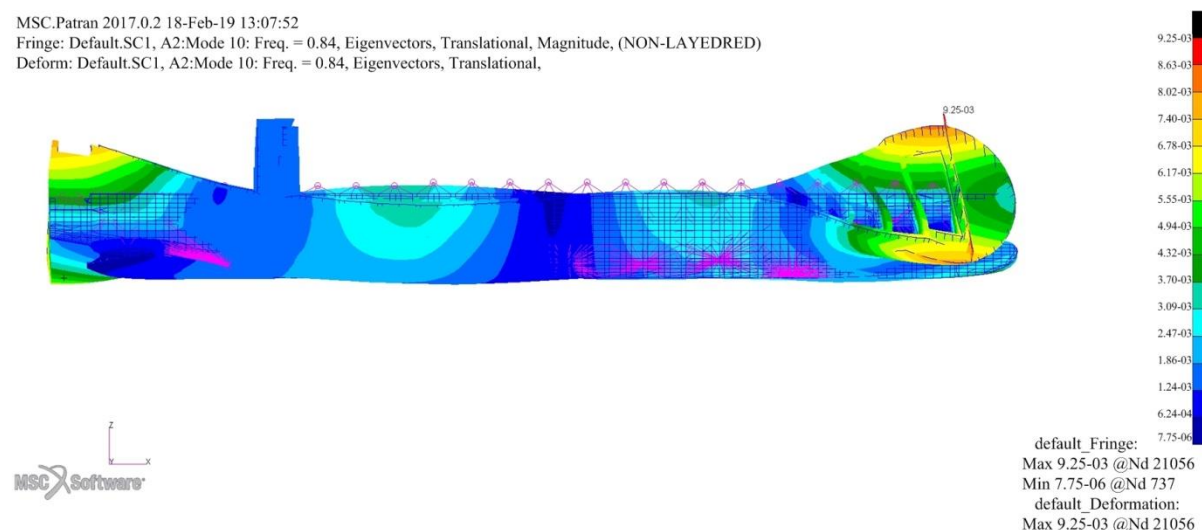


Fig. 4.16. Horizontal vibration of 3 nodes of the container ship 11400 TEU with water

MSC.Patran 2017.0.2 18-Feb-19 13:08:03

Fringe: Default.SC1, A2:Mode 12: Freq. = 1.18, Eigenvectors, Translational, Magnitude, (NON-LAYEDRED)

Deform: Default.SC1, A2:Mode 12: Freq. = 1.18, Eigenvectors, Translational,

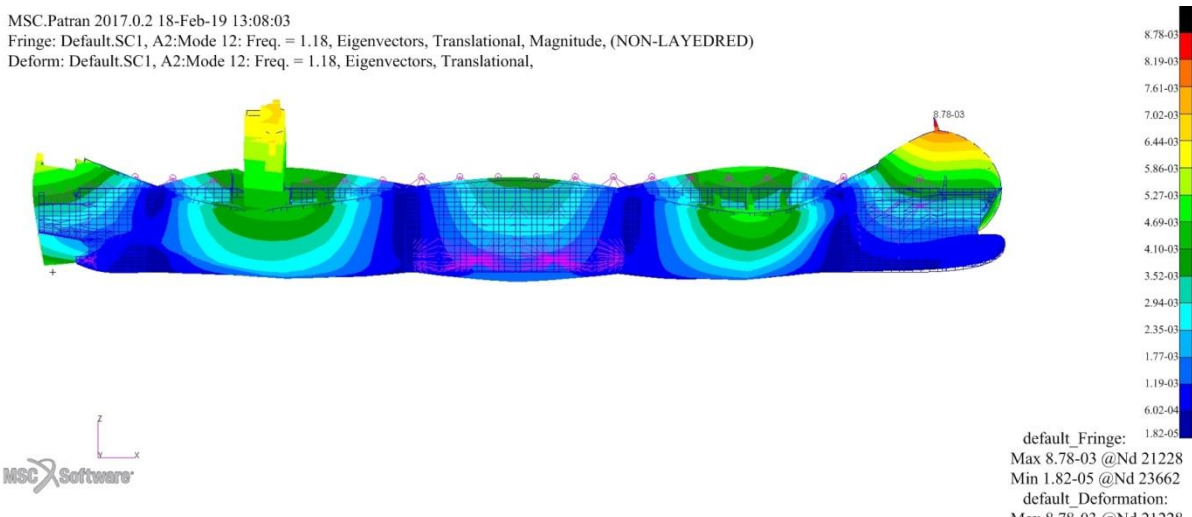


Fig. 4.17. Horizontal vibration of 4 nodes of the container ship 11400 TEU with water

MSC.Patran 2017.0.2 18-Feb-19 13:07:46

Fringe: Default.SC1, A2:Mode 8: Freq. = 0.524, Eigenvectors, Translational, Magnitude, (NON-LAYEDRED)

Deform: Default.SC1, A2:Mode 8: Freq. = 0.524, Eigenvectors, Translational,

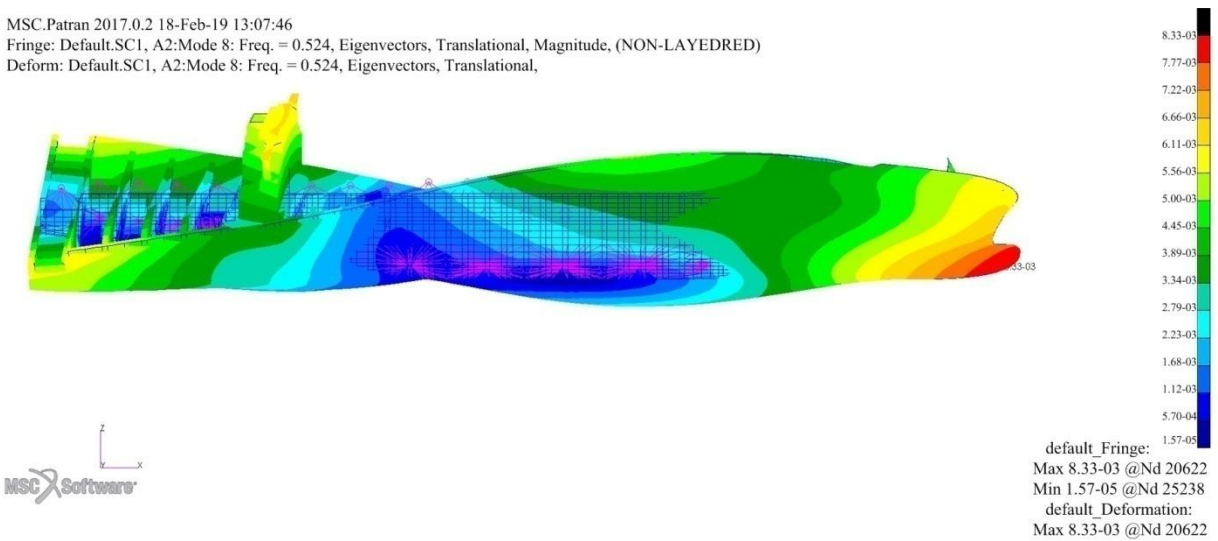


Fig. 4.18. Torsional vibration of the container ship 11400 TEU with water

The natural frequency of the large size container ship 11400 TEU with water and without water and no-load is illustrated in Fig. 4.19.

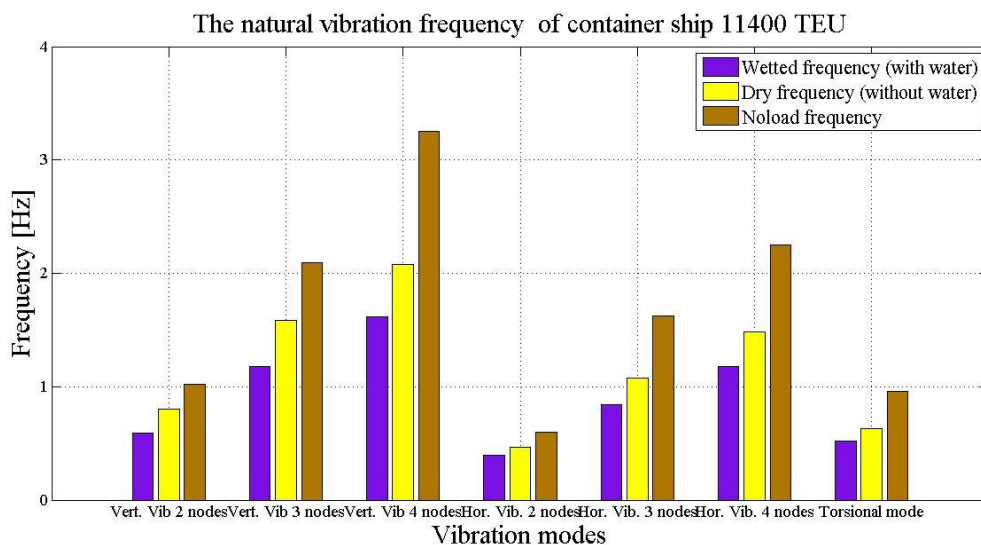


Fig. 4.19. Natural frequency of the large size container ship 11400 TEU

Fig. 4.10 and Fig. 4.19 summarize the natural vibration frequencies of a medium-sized container ship of 2000 TEU and a large size container ship of 11400 TEU for different load cases: case (1) the ship has load and contact with liquid (wetted frequency), the case (2) the ship has load and contact with air (dry frequency), and the case (3) the no-load ship (no-load frequency). These data are compared with the experimentally calculated values in the next section to verify the accuracy and superiority of calculations by numerical models.

#### 4.1.3. Natural vibration analysis of the deckhouses structure

In this section, the free vibration of the deckhouses of the medium size container ship 2000 TEU and the large size container ship 11400 TEU are analysed. The purpose of this analysis is to avoid resonance between the basic vibration modes of deckhouses and the main excitation frequency. The design ensures that the vibration of the deckhouses is within the allowable limits, creating convenient and comfortable conditions for the living and working of the crews. The 3D model of the deckhouses structure of the medium size container ship 2000 TEU in Patran software is shown in Fig. 4.20. The vibration modes of the medium size container ship's deckhouses are illustrated as shown in Fig. 4.21÷4.24.

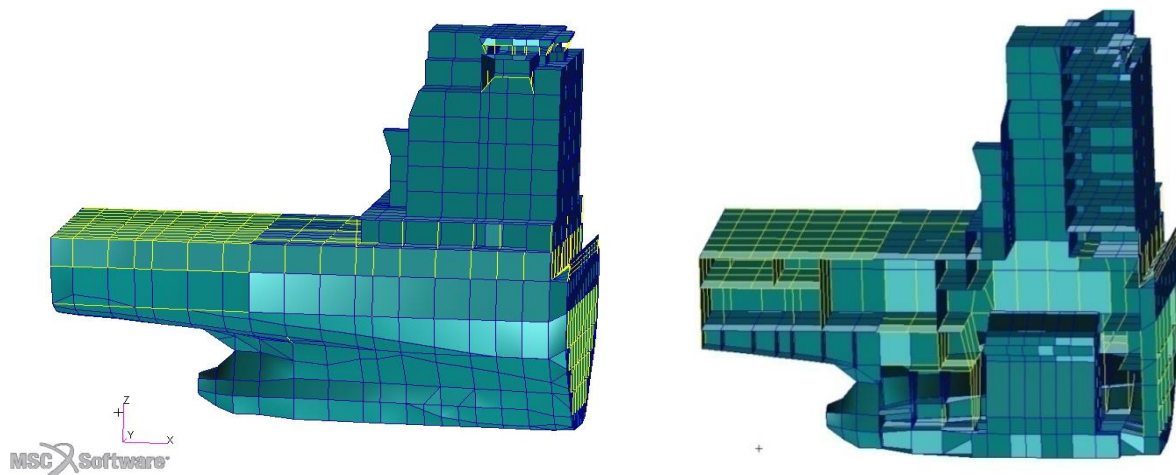


Fig. 4.20. 3D model of the superstructure of the container ship 2000 TEU

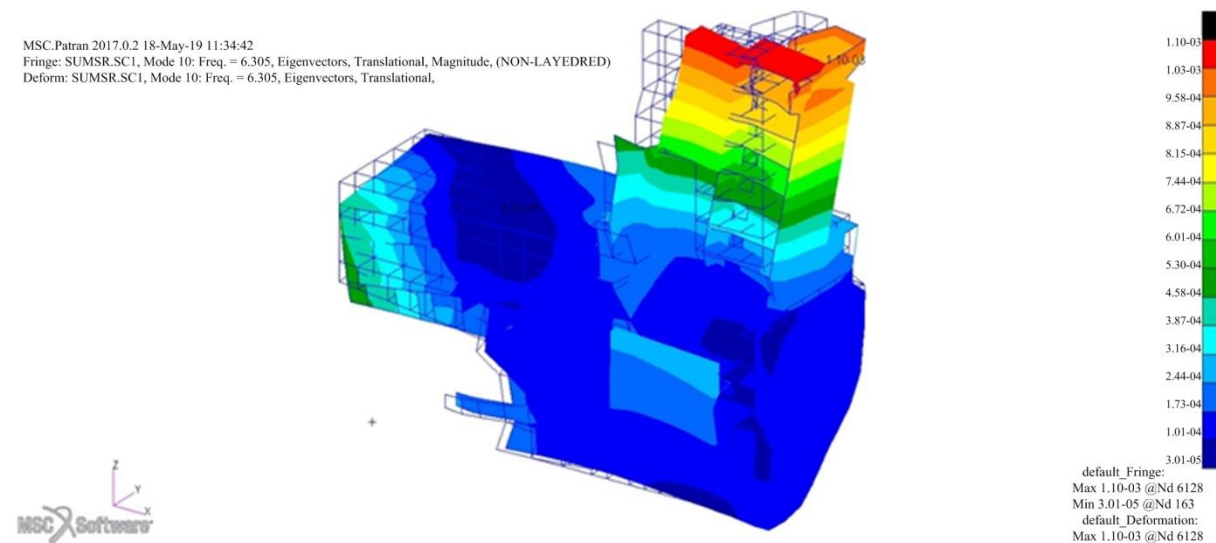


Fig. 4.21. Superstructure mode at 6.305 Hz

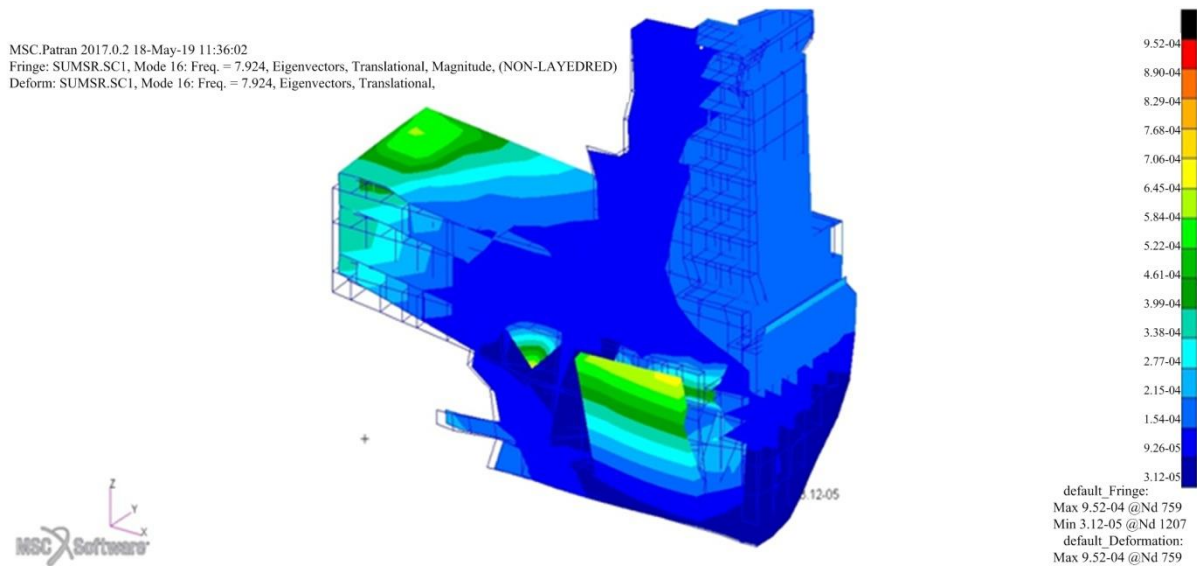


Fig. 4.22. Superstructure mode at 7.924 Hz

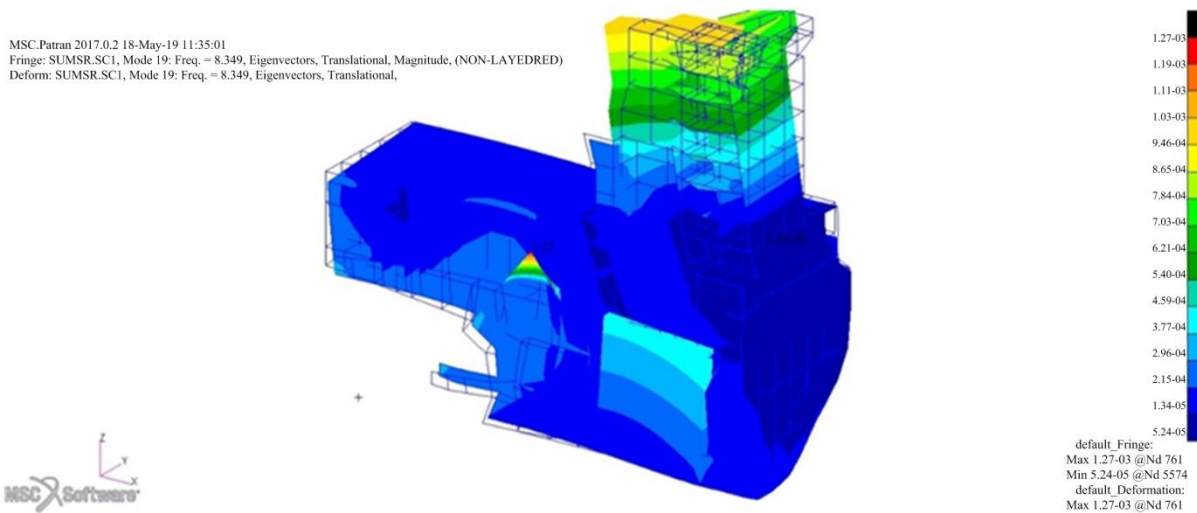


Fig. 4.23. Superstructure mode at 8.349 Hz

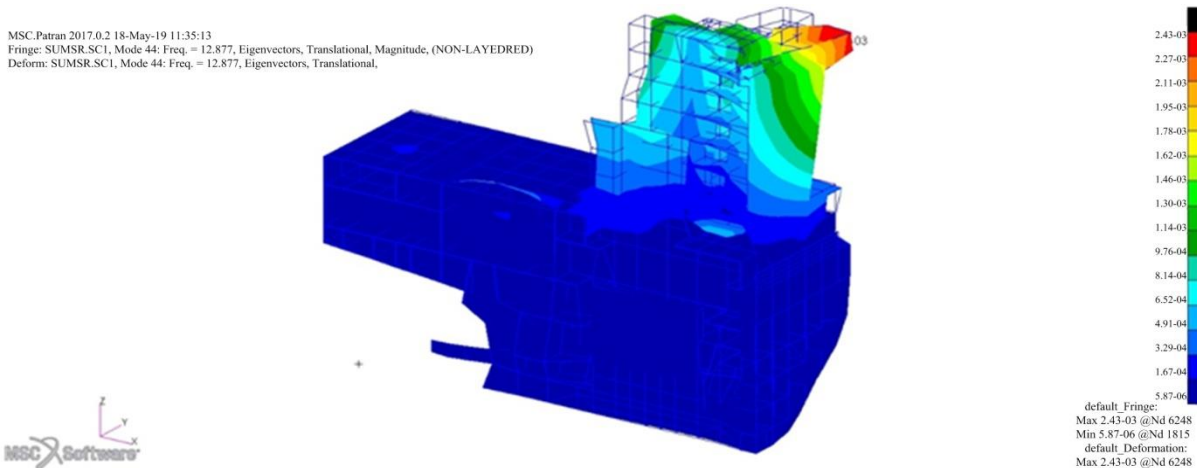


Fig. 4.24. Superstructure mode at 12.877 Hz

The natural frequency of the deckhouse of the medium size container ship 2000 TEU and natural frequency of the entire hull of the medium size container ship of 2000 TEU in the case of load and contact with liquid is illustrated in Fig. 4.25.

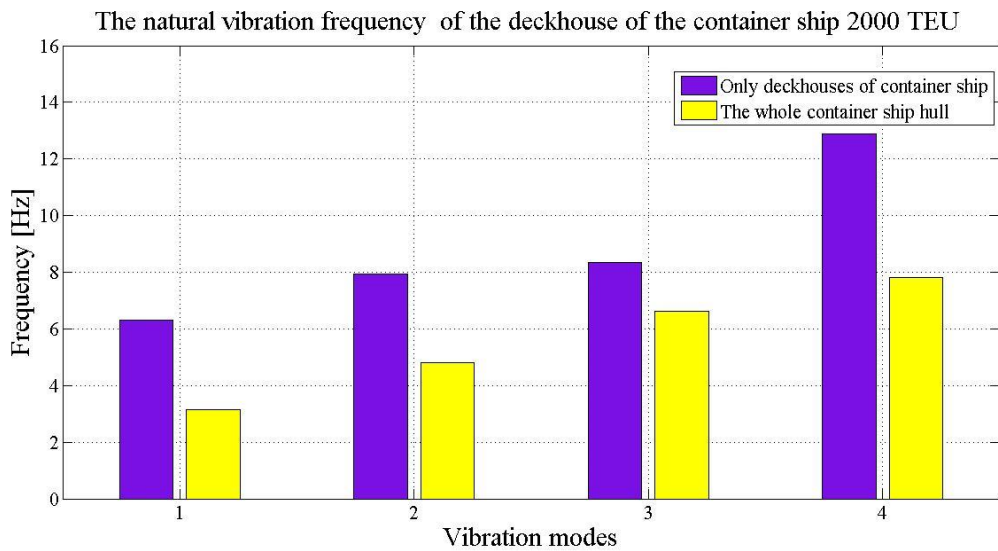


Fig. 4.25. Natural frequency of 2000 TEU container ship's deckhouses

The 3D model of the deckhouses structure of the large size container ship 11400 TEU in Patran software is shown in Fig. 4.26. The vibration modes of the 11400 TEU container ship's deckhouses are illustrated as shown in Fig. 4.27÷4.30.

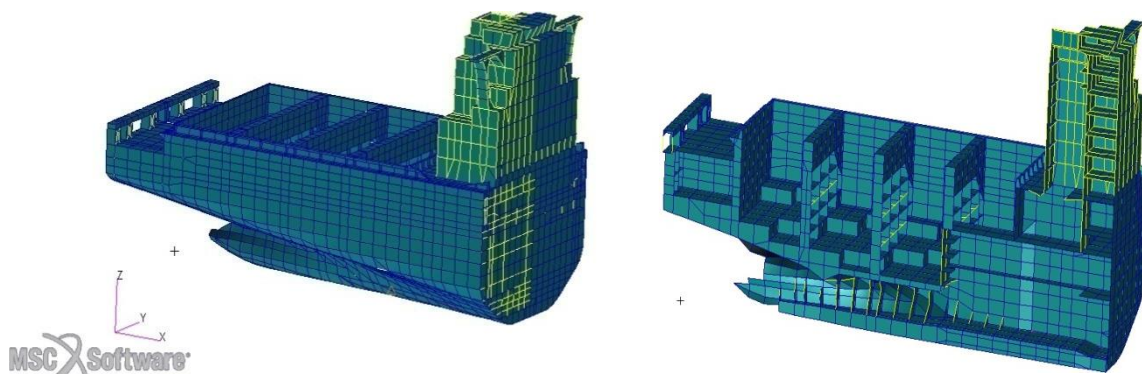


Fig. 4.26. The 3D model of the superstructure of container ship 11400 TEU

MSC.Patran 2017.0.2 21-May-19 11:35:30  
 Fringe: Default, A1. Mode 10: Freq. = 1.722, Eigenvectors, Translational, Magnitude, (NON-LAYEDRED)  
 Deform: Default, A1. Mode 10: Freq. = 1.722, Eigenvectors, Translational,

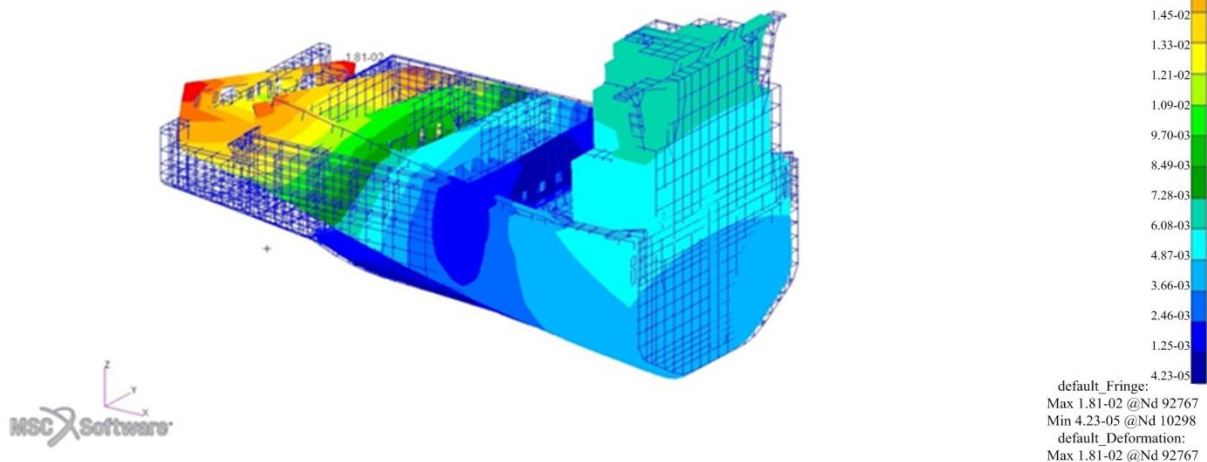
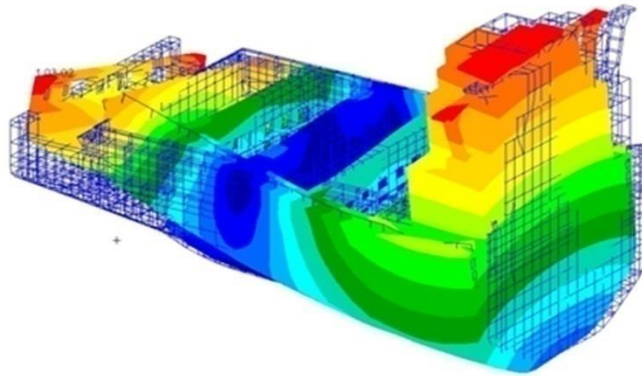


Fig. 4.27. Superstructure mode at 1.722 Hz

## 4. NUMERICAL MODELLING OF SHIP HULL AND SUPERSTRUCTURE

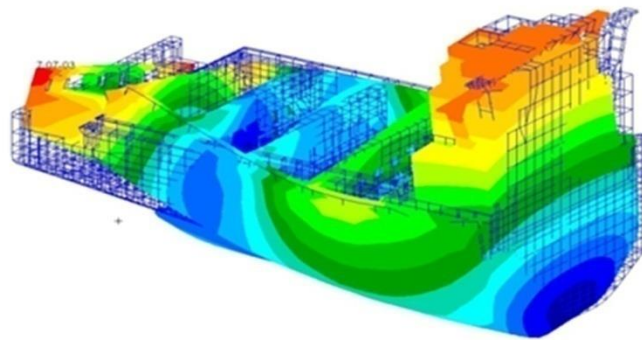
MSC.Patran 2017.0.2 21-May-19 11:35:47  
Fringe: Default, A1. Mode 12: Freq. = 2.398, Eigenvectors, Translational, Magnitude, (NON-LAYEDRED)  
Deform: Default, A1. Mode 12: Freq. = 2.398, Eigenvectors, Translational,



default\_Fringe:  
Max 1.03-02 @Nd 97481  
Min 3.71-05 @Nd 7845  
default\_Deformation:  
Max 1.03-02 @Nd 97481

Fig. 4.28. Superstructure mode at 2.398 Hz

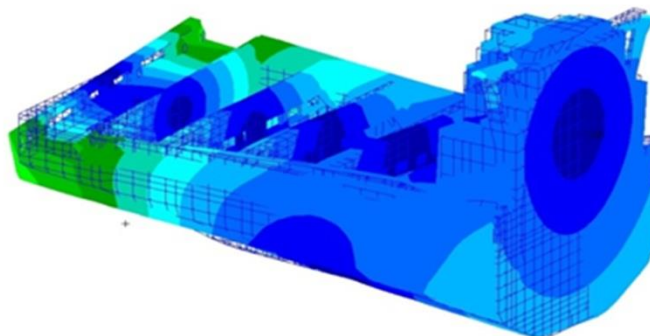
MSC.Patran 2017.0.2 21-May-19 11:36:03  
Fringe: Default, A1. Mode 14: Freq. = 3.465, Eigenvectors, Translational, Magnitude, (NON-LAYEDRED)  
Deform: Default, A1. Mode 14: Freq. = 3.465, Eigenvectors, Translational,



default\_Fringe:  
Max 7.07-03 @Nd 97481  
Min 1.11-05 @Nd 94540  
default\_Deformation:  
Max 7.07-03 @Nd 97481

Fig. 4.29. Superstructure mode at 3.465 Hz

MSC.Patran 2017.0.2 21-May-19 11:36:21  
Fringe: Default, A1. Mode 16: Freq. = 4.115, Eigenvectors, Translational, Magnitude, (NON-LAYEDRED)  
Deform: Default, A1. Mode 16: Freq. = 4.115, Eigenvectors, Translational,



default\_Fringe:  
Max 2.48-02 @Nd 24057  
Min 3.77-05 @Nd 132459  
default\_Deformation:  
Max 2.48-02 @Nd 24057

Fig. 4.30. Superstructure mode at 4.115 Hz

The natural frequency of the deckhouse of the large size container ship 11400 TEU and natural frequency of the entire hull of the large size container ship of 11400 TEU in the case of load and contact with liquid is illustrated in Fig. 4.31.

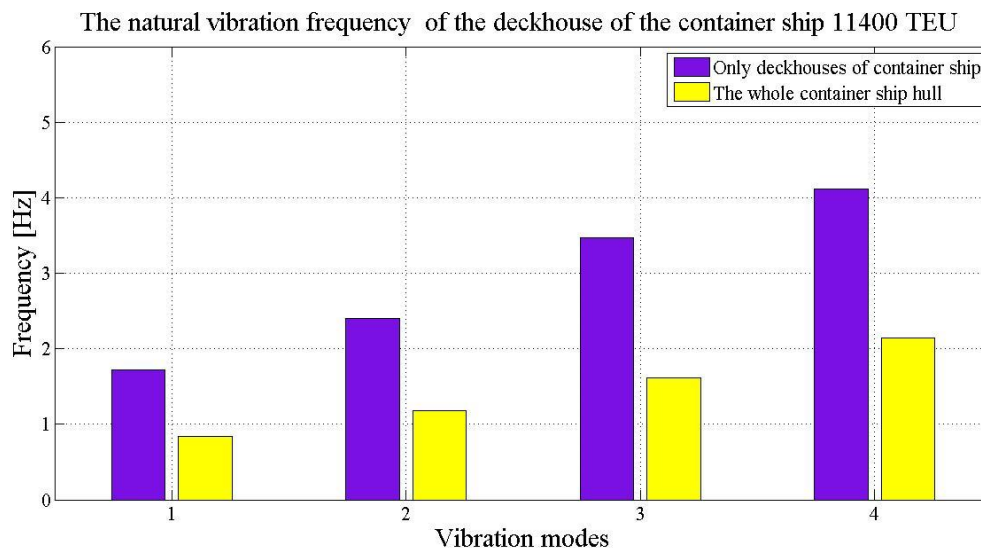


Fig. 4.31. Natural frequency of 11400 TEU container ship's deckhouses

From the natural vibration modes presented in Fig. 4.25 and Fig. 4.31, the natural vibrations of the deckhouses are determined. The natural vibration frequency of container ship 2000 TEU and 11400 TEU is determined for two cases: the first case only considers the superstructure (deckhouses), the second case considers the superstructure (deckhouses) in the whole hull. In the case of container ship 2000 TEU, the vibration frequency between the first case and the second case is quite large, the error ranges from 23% (8.35 Hz and 6.40 Hz) to 50% (6.31 Hz and 3.15 Hz). The container ship 11400 TEU, the frequency of vibration between the first and the second case is within 50% (1.72 Hz and 0.84 Hz). This suggests that the frequency of natural vibrations of the superstructure (deckhouses) under different conditions will be different. Determining the natural vibration frequency of the superstructure will help the designer avoid resonant vibration areas. The superstructure design has vibration within the allowed value, less than 8 mm/s. Small vibration values, creating favorable conditions for sailors to work and live on board.

#### 4.1.4. Compare the natural vibration frequencies of different size container ships

In this section, some comparisons between the results of vertical natural vibration frequency and the horizontal vibration of the medium size container ship of 2000 TEU and the large size container ship of 11400 TEU are obtained by empirical formula and the numerical model method considered. On that basis of assessing the accuracy of the numerical modelling method using the finite element method implemented in the Nastran-Patran software platform applied to the analysis of ship structures.

The natural frequency for vertical bending vibration with the first three modes obtained of the medium size container ship 2000 TEU and the large size container ship 11400 TEU according to the empirical formula and the numerical modelling method is presented in Tab. 4.4.

Tab. 4.4. First three modes of natural frequency of vertical bending vibration

Ship type	Vertical natural vibration frequency / Hz			
	Order	Experimental formula Eq.(2.22)	Experimental formula Eq.(2.24)	Numerical method
Container 2000 TEU	1	1.200	1.1822	1.2068
	2	2.548	2.3444	2.2521
	3	3.937	3.3586	3.4223
Container 11400 TEU	1	0.574	0.5291	0.59004
	2	1.219	1.0492	1.1751
	3	1.884	1.5031	1.6144

The relative error between the vertical natural vibration frequency results of the medium size container ship 2000 TEU and the large size container ship 11400 TEU obtained by the numerical modelling method and the empirical formula is illustrated in Fig. 4.32÷4.33.

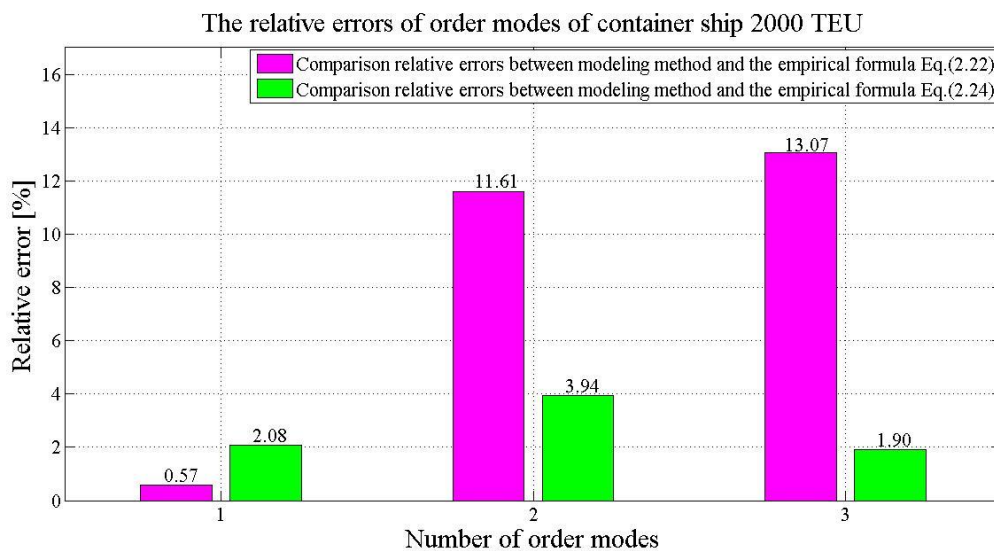


Fig. 4.32. Comparison of vertical natural frequencies of container ship 2000 TEU

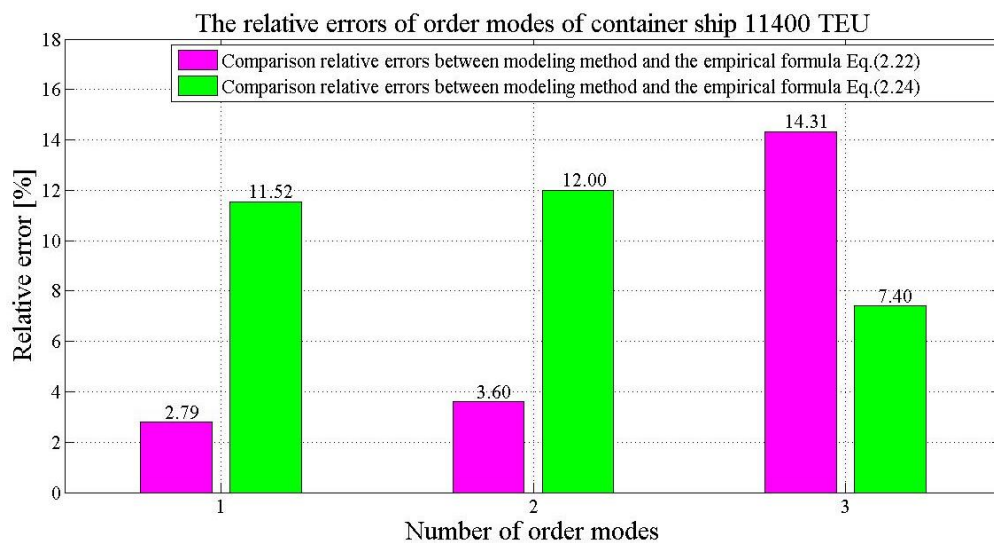


Fig. 4.33. Comparison of vertical natural frequencies of container ship 11400 TEU

From Fig. 4.32 and Fig. 4.33, the empirical formula (2.22) and (2.24) gives relatively accurate results with the numerical modelling method. The smallest error with the medium size container ship 2000 TEU is 0.57%, the large container ship 11400 TEU is 2.79%. The largest error for the medium size container ship 2000 TEU is 13.07%, the large size container ship 11400 TEU is 14.31%. The 3D numerical model based on the finite element method implemented in the Patran-Nastran commercial software platform makes it easier to determine the vibration characteristics of the ship during the design phase. Numerical models can be applied to many ships with complex and different shapes. This helps the shipbuilding designer limit the unwanted effects of ship hull girder vibrations.

Comparison of horizontal natural vibration frequencies of the medium size container ship 2000 TEU and the large size container ship 11400 TEU is conducted. The natural frequency for horizontal vibration with the first three modes obtained according to the empirical formula and the numerical modelling method is presented in Tab. 4.5.

*Tab. 4.5. First three modes of natural frequency of horizontal bending vibration*

Ship type	Horizontal natural vibration frequency / Hz		
	Order	Experimental formula Eq.(4.3)	Numerical method
Container 2000 TEU	1	2.121	2.29
	2	4.252	4.95
	3	6.363	6.7
Container 11400 TEU	1	0.51	0.384
	2	1.02	0.84
	3	1.53	1.180

The relative error between the natural frequency results of horizontal vibration of the medium size container ship 2000 TEU and the large container ship 11400 TEU obtained by the numerical modelling method and the empirical formula is illustrated in Fig. 4.34÷4.35.

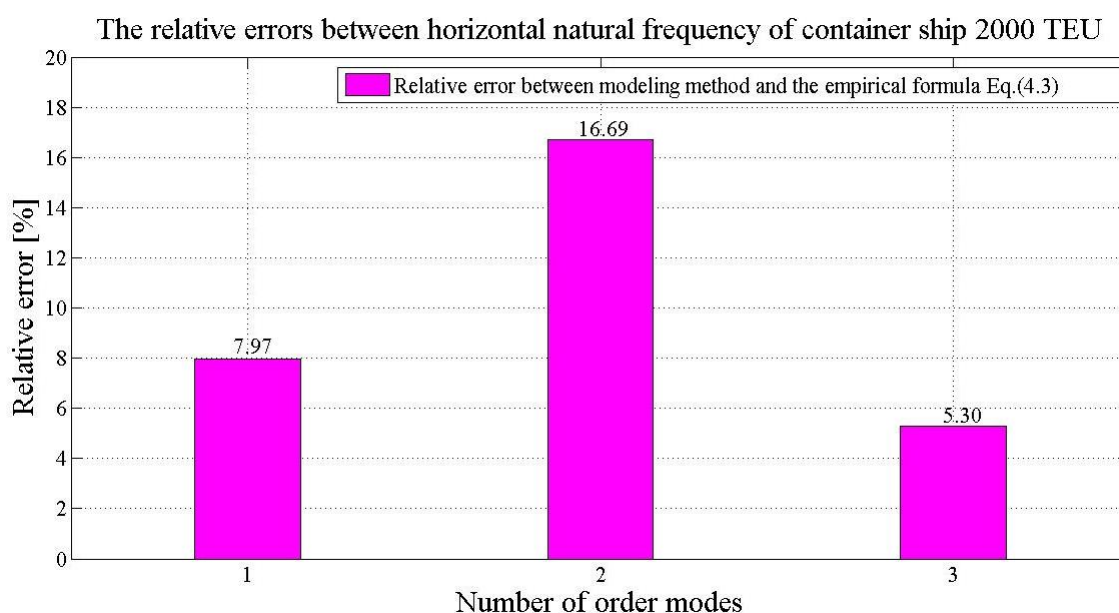


*Fig. 4.34. Comparison of horizontal natural frequencies of container ship 2000 TEU*

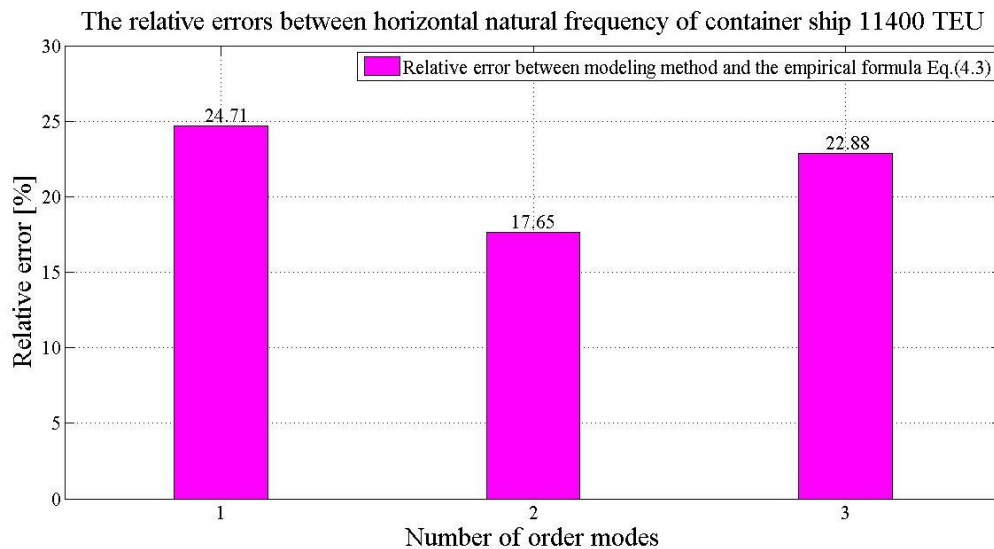


Fig. 4.35. Comparison of horizontal natural frequencies of container ship 11400 TEU

With the horizontal vibration, the first three vibrations are considered. Relative deviations between the result of the container ship 2000 TEU horizontal vibration frequency is obtained by the numerical modelling method and the experimental formula (4.3) for the largest deviation of 16.69%, the minimum deviation of 5.30%. Relative deviations between the result of the container ship 11400 TEU horizontal vibration frequency is obtained by the numerical modelling method and the experimental formula (4.3) for the largest deviation of 24.71%, the minimum deviation of 17.65%. From the above analysis, the difference between the experimental calculation results and the results obtained by the numerical analysis method has a very large error. The larger the ship, the greater the error, the error can reach nearly 30% in the above analysis. Therefore, the application of empirical formulas for predicting the vibration of ships in the design phase has not high accuracy. With rapid and strong development in terms of size, tonnage, and complexity of ship structures, empirical formulas are no longer relevant. The application of numerical modelling for ship vibration analysis provides accurate results, which can be applied to a variety of vessels of different sizes and loads and for many complex structures.

#### 4.1.5. Ship hull vibration threaten using hull resonance diagram

In order to check if the hull girder vibration modes are being excited by the main engine and propeller, designers often use hull resonance diagrams. This is one of the most widely used methods to test threatens of vibration of the ship hull. In this case, not only the vertical modes of hull beam vibration are taken into account, but also the horizontal and torsion modes considered. The hull resonance diagram is also used to determine the number of propeller's blade and the number of main engine's cylinders needed to avoid resonance.

In this section, from the global vibration frequency of the hull and vibration of the superstructure (deckhouses) obtained in section 4.1.2÷4.1.3 together with the parameters of the main engine and the propeller, respective, the author proceeds to draw the hull resonance diagram of the capacity container ship 2000 TEU and 11400 TEU. On that basis, assessing the vibration of the hull and superstructure, the possibility of resonance vibrations can occur and dangerous vibration areas. Provide recommendations for users about dangerous banded ranges and need to pass quickly when operating ships. At these revolutions the resonance

phenomenon occurs, vibration will be large, if a long operation can be harmful to the equipment and structure of the ship, even destroyed.

The medium container ship 2000 TEU has the main engine MAN B7W 8S70MC-C, the normal speed is 91 cycles per minute, the 5-blades propeller. Determine the excitation frequency of the main engine and the propeller. The main engine excitation frequency of container ship 2000 TEU is  $f=12.13$  Hz. The propeller excitation frequency of container ship 2000 TEU is  $f=7.58$  Hz. The vertical axis denotes the natural frequency values of vertical vibrations of the hull ship. The horizontal axis indicates the rotation value at the normal speed condition of the main engine. From the horizontal axis, draw a vertical line at the value of 91 cycles per minute (normal working speed of the main engine). On this line, take two points at frequency values 7.58 Hz and 12.13 Hz. Connecting the origin of the coordinates-axis with the frequency of 12.13 Hz, the author obtains the line for the 8 cylinders' main engine. Connecting the origin of the coordinates-axis with the frequency of 7.58 Hz, the line for the propeller with 5 blades is determined. The hull resonance diagram is illustrated as Fig. 4.36.

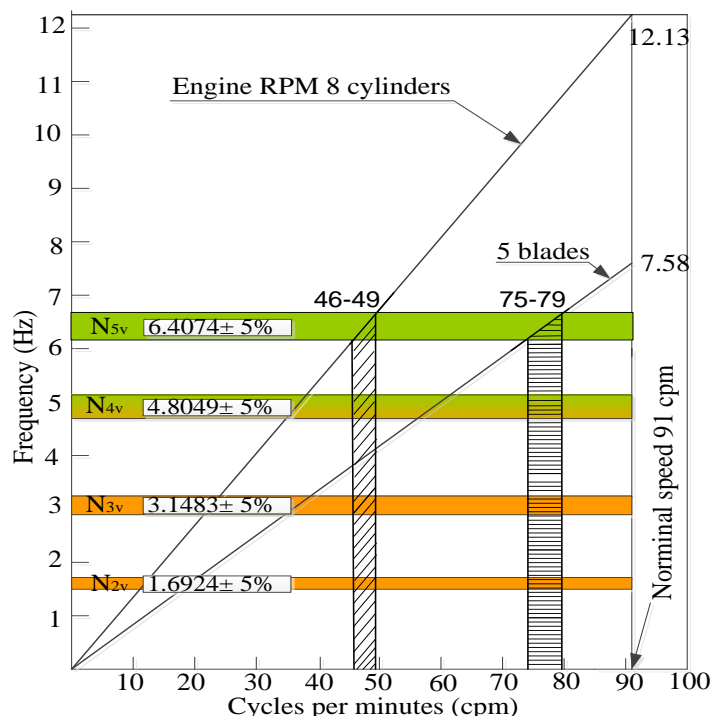


Fig. 4.36. The Hull Resonance Diagram of the container ship 2000 TEU

$N_{2v}$ ,  $N_{3v}$ ,  $N_{4v}$ ,  $N_{5v}$  are the second, third, fourth and fifth modes of vertical hull girder vibration of the container ship 2000 TEU.

Once these values are obtained, they are plotted on the axis, and a tolerance of 5 percent is taken for the factor of safety. So, the shaded bands in the diagram represent each mode with 5 percent tolerance. At 91 rpm, the main engine MAN B7W 8S70MC-C, 8 cylinders, excitation frequency 12.13 Hz, region with higher vibration level within the rotation range of 46÷49 rpm, resonates with vertical vibration 5 nodes of the ship hull - the area with diagonal lines on the hull resonance graph. The area with higher vibration level excitation is determined with the propeller within the rotation range 75÷79 rpm with 5 nodes hull vertical vibration - the area with horizontal lines on the hull resonance graph. With the application of numerical modelling method for vibration analysis of hull girders, the results are relatively accurate, convenient and effective in the calculation.

The large size container ship 11400 TEU has the main engine MAN B&W 12K98ME-(Mk7), the normal speed is 100 cycles per minute, the 6-blades propeller. Determine the excitation frequency of the main engine and the propeller. The main engine excitation frequency of container ship 11400 TEU is  $f=20$  Hz. Propeller excitation frequency of container ship 11400 TEU is  $f=10$  Hz. The vertical axis denotes the natural frequency values of vertical vibrations of the hull girder. The horizontal axis indicates the rotation value at the normal speed condition of the main engine. From the horizontal axis, draw a vertical line at the value of 100 cycles per minute (normal working speed of the main engine). On this line, take two points at frequency values 10 Hz and 20 Hz. Connecting the origin of the coordinates-axis with the frequency of 20 Hz, the author obtains the line for the 12 cylinders' main engine. Connecting the origin of the coordinates-axis with the frequency of 10 Hz, the author obtains the line for the propeller with 6 blades. The hull resonance diagram is illustrated as Fig. 4.37.

$N_{2V}$ ,  $N_{3V}$ ,  $N_{4V}$ ,  $N_{5V}$  are the second, third, fourth and fifth modes of vertical hull girder vibration of the container ship 11400 TEU.

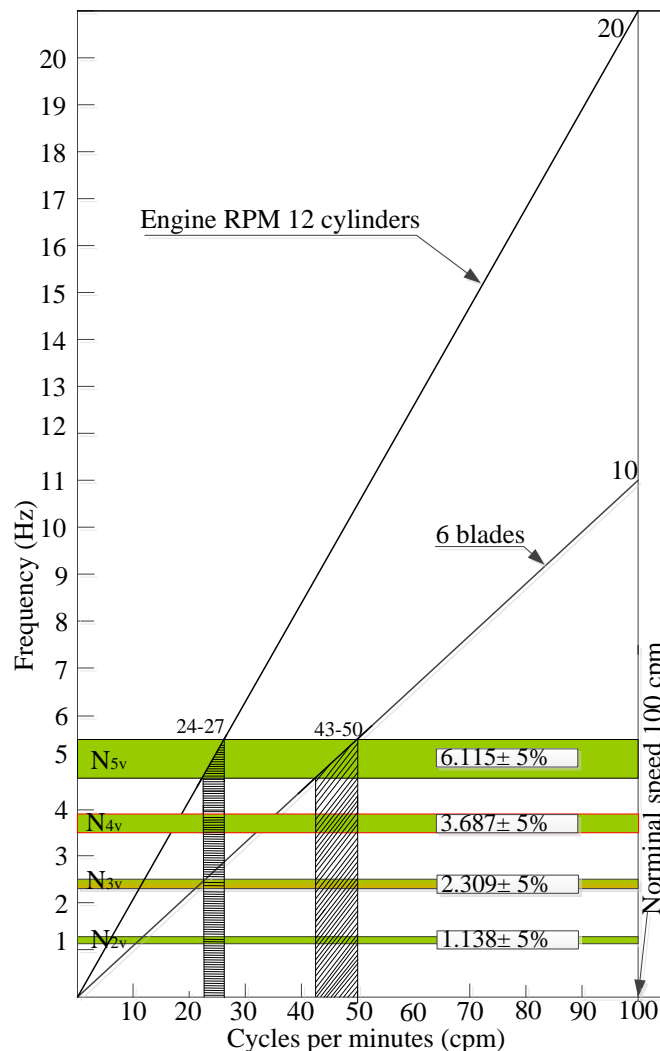


Fig. 4.37. The Hull Resonance Diagram of the container ship 11400 TEU

Once these values are obtained, they are plotted on the axis, and a tolerance of 5 percent is taken for the factor of safety. So, the shaded bands in the diagram represent each mode with 5 percent tolerance. At 100 rpm, the main engine MAN B&W 12K98ME-(Mk7),

12 cylinders, excitation frequency 20 Hz, region with higher vibration level within the rotation range of 24÷27 rpm, resonates with vertical vibration 5 nodes of the ship hull - the area with horizontal lines on the hull resonance graph. The area with higher vibration level excitation comes from the propeller within the rotation range 43÷50 rpm 5 nodes hull vertical vibration - the area with diagonal lines on the hull resonance graph.

## 4.2. Forced vibration analysis

The ship hull structure includes the outer shell plating and all internal members, which collectively provide the necessary strength to satisfactorily perform the design functions in the expected sea environment. The hull structure responds as a free-free beam (both ends free) when subjected to dynamic loads. The vibration induced by the propulsion system is a common source of ship vibration. Vibration from this source manifests itself in several ways: dynamic forces from the shafting system are transmitted to the hull through shaft bearing, the propeller induces fluctuating pressures on the surface of the hull, which induces vibration in the hull structure. The main and auxiliary engines can directly cause vibrations through dynamic forces transmitted through their supports and foundations. The response to this forcing can cause the vibration of the hull girder, deckhouse, deck, and other structures, local structures and equipment. The main engine-induced unbalanced excitations encountered with slow-speed diesel-driven ships are the primary and secondary free engine forces and moments. The engine manufacturer provides the magnitude of these forces and moments. In ship vibrations, the propeller is frequently a source of vibration issues that can cause an excessive ship stern vibration problem.

In this section, forced vibration of 2000 TEU and 11400 TEU container ships are considered. The 2000 TEU and 11400 TEU container ships with the main parameters were presented in Tab. 4.1 and Tab. 4.2. Calculating and analysing forced vibration based on the free vibration of 2000 TEU and 11400 TEU container ships have been calculated. Review and evaluation of possible resonance positions happen. Because ships are a complex structure, there are innumerable natural vibrations of machinery structures, deckhouses, propulsion systems, and auxiliary equipment on board. Therefore, the complete elimination of the resonance phenomenon is impossible. Importantly, vibrations and displacements occur within the allowable limits recommended by social organizations that classify ships. Therefore, in this section, forced vibrations of 2000 TEU and 11400 TEU container ships are represented in the form of forced vibration frequency responses of selected locations (points). Then, these values are compared to the ISO 6954 Standard "Guidelines for the overall evaluation of vibration in merchant values ships".

Forced vibration and frequency response of forced vibration is presented to the representative group of points illustrated in Fig. 4.38 as follows:

- Node 1 is at deck edge on the wheelhouse,
- Node 2 is at the middle point on the wheelhouse,
- Node 3 is at deck transom edge on the main deck,
- Node 4 is at the end of the stern tube shafts,
- Node 5 is at bottom of the superstructure,
- Node 6 is at main engine before cylinder heads,
- Node 7 is at main engine aft cylinder heads,
- Node 8 is at aft top of the superstructure.

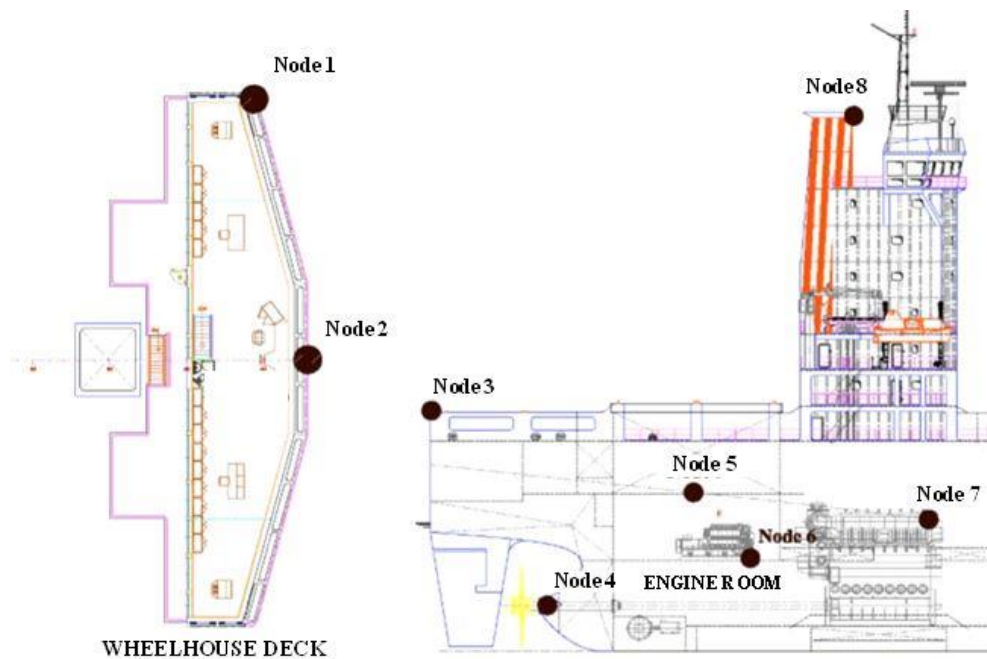


Fig. 4.38. Nodes for forced vibration response

To calculate the forced vibration response of a 2000 TEU and 11400 TEU container ships, the damping value of the structure should be determined. Component damping mainly depends on the floor and deck coverings. Cargo damping mainly depends on the nature of the cargo (container, fluid, bulk, etc.) in calculation usually, the advantage of the damping coefficients obtained from classification societies through a large number of experiments, such as DNV ([Det Norske Veritas-Norway](#)) and GL ([Germanischer Lloyd-Germany](#)) defined the damping coefficients in vibration response calculation, could be used. In this section, the author uses the damping coefficient defined by GL in the vibration response calculation of 2000÷11400 TEU container ship, the dynamic damping coefficient is 25 for all cases.

#### 4.2.1. The unbalanced excitation forces and moments of the main engine

The principle of operation of piston combustion engines causes the formation of unbalanced, external forces and dynamic moments. Marine engines have balanced all external forces and moments of main orders. However, always some of the moments remain unbalanced. They cause longitudinal, transverse and torsion vibrations of the engine body, which are transferred to other ship structures. Unbalanced torque values are given in the engine documentation. The unbalanced moments of the main engine, generated by gas and inertia forces of the piston-crank system. There are internal and external excitation forces and moments of the engine. Internal forces and moments will deform the engine. The most important internal moments for the ship structure vibrations are the lateral X-type moments of a different order. External forces and moments acted on the ship through the foundation. External forces and moments are external moments (order 1 and 2), lateral H-type moments (different order). There are three important vibration modes of the engine: the H-mode, which is the torsion vibration mode around the longitudinal axis, the X-mode, which is the 'twisting' vibration mode around the vertical axis, and the L-mode (see subchapter 2.2.3).

Forced vibration and forced frequency response for the medium-size container ship 2000 TEU are calculated. The main engine excitation forces parameters of the main diesel engine MAN B&W 8S70MC-C are given in Tab. 4.6 [63].

Tab. 4.6. Force and moment of the main engine MAN B&W 8S70MC-C at 91 rpm

External forces [kNm]	Values	Guide forces X-moments in [kNm]	Values
1. Order: Horizontal	0	1. Order:	429
1. Order: Vertical	0	2. Order:	0
2. Order: Vertical	0	3. Order:	1543
4. Order: Vertical	0	4. Order:	816
6. Order: Vertical	0	5. Order:	2203
<b>External moments [kNm]</b>		6. Order:	0
1. Order: Horizontal a)	482	7. Order:	66
1. Order: Vertical a)	482	8. Order:	0
2. Order: Vertical	0	9. Order:	24
4. Order: Vertical	141	10. Order:	0
6. Order: Vertical	0	11. Order:	108
<b>Guide forces H-moments in [kNm]</b>		12. Order:	16
1 x No. of cyl.	905	13. Order:	45
2 x No. of cyl.	78	14. Order:	0
3 x No. of cyl.	-	15. Order:	4

As can be seen from the Engine guide of MAN B&W 8S70MC-C, main engine dynamic forces are most effective at 1<sup>st</sup> order (excitation type L and X), 3<sup>rd</sup> order (excitation type X), 4<sup>th</sup> order (excitation type L and X) and 5<sup>th</sup> order (excitation type X), 8<sup>th</sup> order (excitation type H) of engine rpm of 91 rpm that is 1.52 Hz. Therefore, five loading cases are obtained. The main engine MAN B&W 8S70MC-C has a length of the bedplate is 10.68 m, a width of the bedplate is 4.39 m, height of the bedplate 1.52 m. The excitation moment will be converted into excitation forces based on Eq.(2.6)÷(2.13) (chapter 2), the results are illustrated as a Tab. 4.7÷4.9. The vibration excitation source would be loaded on the center of gravity of the main engine through the junction points of the main engine and the internal bottom plate, the local structure diagram is shown in Fig. 4.39.

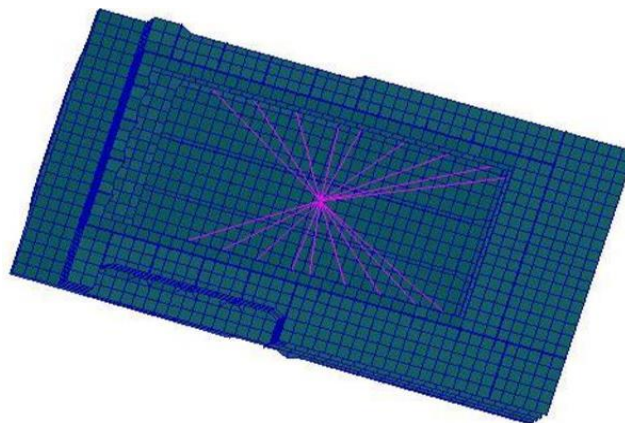


Fig. 4.39. Location diagram of the main engine excitation forces

Tab. 4.7. Axial forced of main diesel engine MAN B&W 8S70MC-C

Order	Hori.couple	Verti.couple	Torque	Lat.moment	Faxi.total
1				14.67	14.67
3				52.72	52.72
4				27.88	27.88
5				75.28	75.28
8				0	0

Tab. 4.8. Horizontal forced of main diesel engine MAN B&W 8S70MC-C

Order	Hori.couple	Verti.couple	Torque	Lat.moment	Fhori.total
1	22.56			6.03	28.59
3				21.67	21.67
4				11.46	11.46
5				30.94	30.94

Tab. 4.9. Vertical forced of main diesel engine MAN B&W 8S70MC-C

Order	Hori.couple	Verti.couple	Torque	Lat.moment	Fvert.total
1	15.63	22.56		7.82	14.75
3				28.12	28.12
4		6.6		14.87	21.47
5				40.15	40.15
8			103.08	0	103.08

The forced frequency response analysis of the medium-size container ship 2000 TEU with a source of excitation by the main diesel engine is carried out by the numerical modelling method in the Patran-Nastran commercial software. The excitation source is shown to change according to the rotation of the main engine as Fig. 4.40.

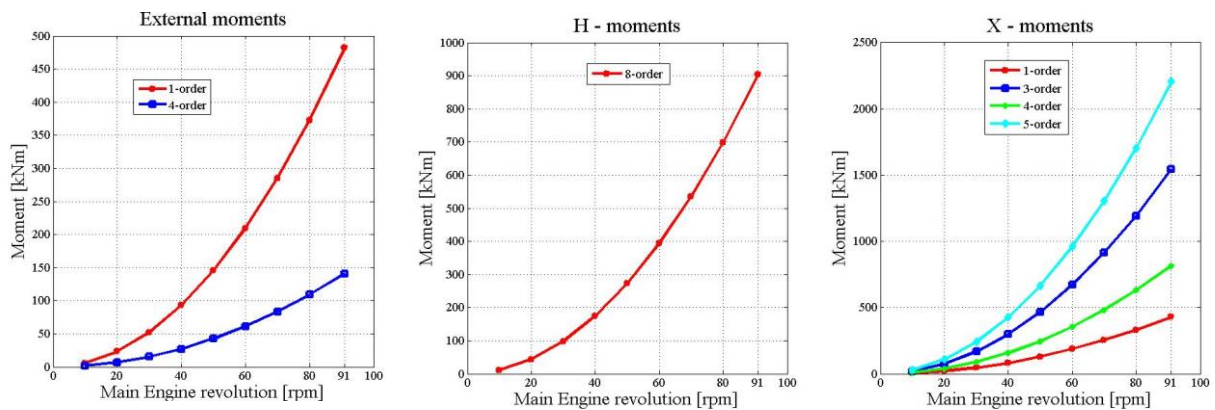


Fig. 4.40. Excitation force graph of the main engine MAN B&W 8S70MC-C

MSC.Patran 2018 11-Jan-20 11:11:34  
 Fringe: SUMSR.SC1, A1: Freq. = 2.7993, Velocities, Translational, Magnitude, (NON-LAYEDRED)  
 Deform: SUMSR.SC1, A1: Freq. = 2.7993, Velocities, Translational,

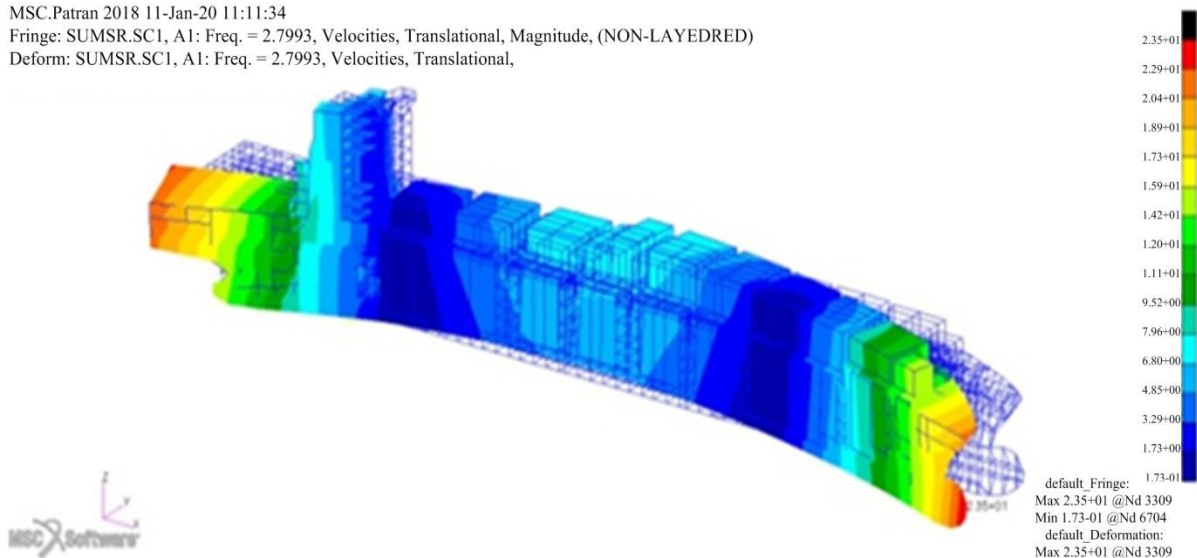


Fig. 4.41. Amplitudes of vibrations forced by the main engine of the container ship 2000 TEU

The vibration analysis of the ship hull and the superstructure of the container ship 2000 TEU are carried out using the finite element method implemented in commercial

software Patran-Nastran 2018. The vibration of the ship hull and superstructure (selected points) as a function of the rotational speed of the drive system, for all directions of the coordinate system and for all considered harmonic components, are shown in Fig. 4.41÷4.45.

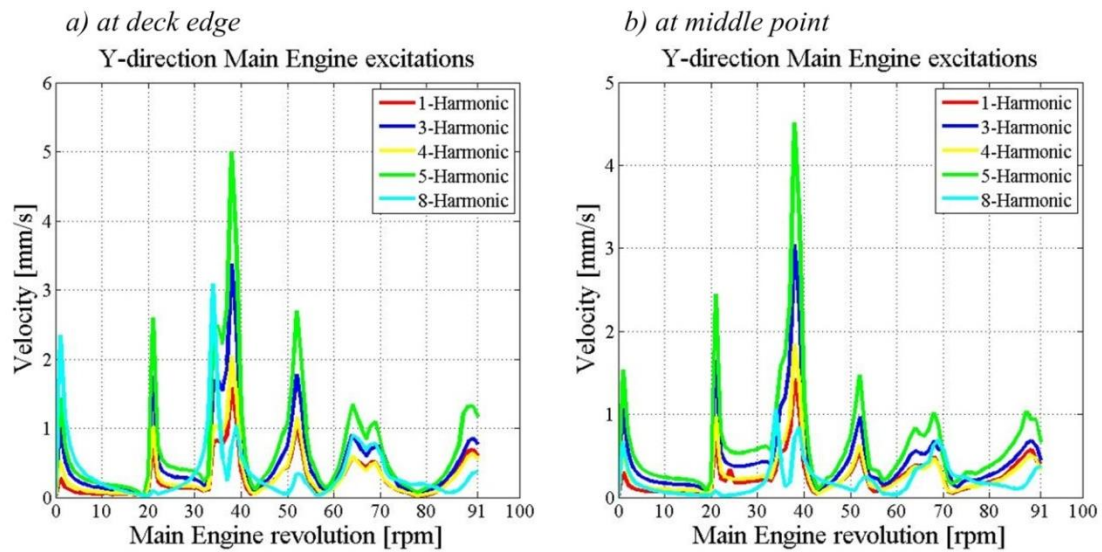


Fig. 4.42. Vibration velocities on the wheelhouse of the container ship 2000 TEU

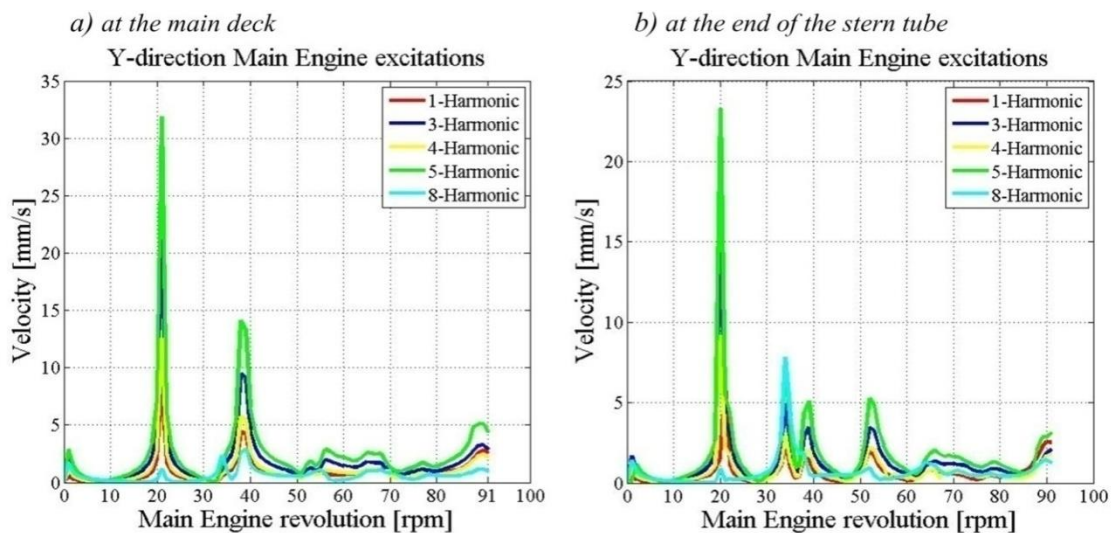


Fig. 4.43. Vibration velocities on main deck and the stern tube shafts of the container ship 2000 TEU

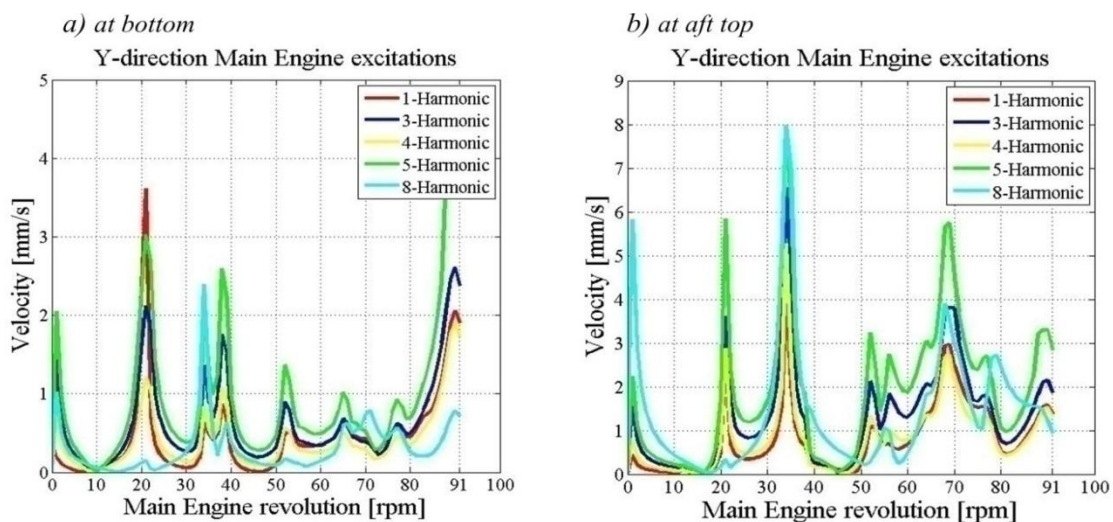


Fig. 4.44. Vibration velocities at bottom of the superstructure of the container ship 2000 TEU

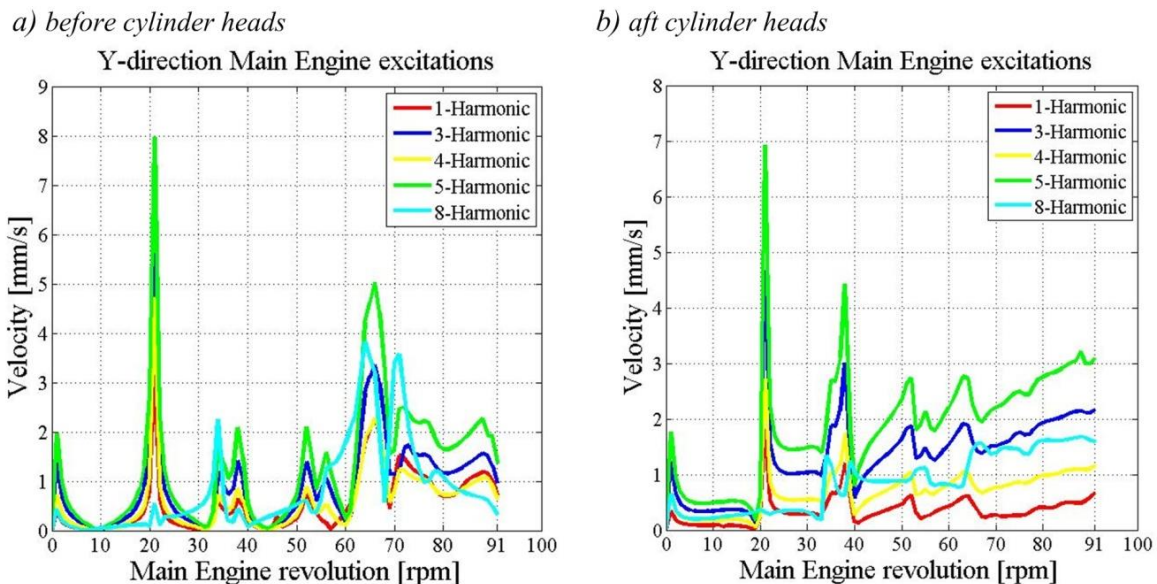


Fig. 4.45. Vibration velocities at main engine of the container ship 2000 TEU

Forced vibration and forced frequency response for container ship 11400 TEU are calculated. The main engine excitation forces parameters of the main diesel engine MAN B&W 12K98ME-C(Mk7) are given in Tab. 4.10 [64].

Tab. 4.10. The force and moment of the main engine MAN B&W 12K98ME-C(Mk7)

External forces [kNm]	Values	Guide forces X-moments in [kNm]	Values
1. Order: Horizontal	0	1. Order:	0
1. Order: Vertical	0	2. Order:	0
2. Order: Vertical	0	3. Order:	4975
4. Order: Vertical	0	4. Order:	2765
6. Order: Vertical	0	5. Order:	0
<b>External moments [kNm]</b>		6. Order:	0
1. Order: Horizontal a)	0	7. Order:	0
1. Order: Vertical a)	0	8. Order:	539
2. Order: Vertical	0	9. Order:	1220
4. Order: Vertical	533	10. Order:	0
6. Order: Vertical	0	11. Order:	0
<b>Guide forces H-moments in [kNm]</b>		12. Order:	0
1 x No. of cyl.	205	13. Order:	0
2 x No. of cyl.	-	14. Order:	0
3 x No. of cyl.	-	15. Order:	277

As can be seen from the Engine guide of MAN B&W 12K98ME-C(Mk7), main engine dynamic forces are most effective at 3<sup>rd</sup> order (excitation type X), 4<sup>th</sup> order (excitation type L and X), 8<sup>th</sup> order (excitation type X), 9<sup>th</sup> order (excitation type X), 12<sup>th</sup> order (excitation type H) and 15<sup>th</sup> order (excitation type X) of engine rpm of 100 rpm that is 1.67 Hz. Propeller RPM is 100 rpm that is 1.67 Hz. The main engine MAN B&W 8S70MC-C has the length of the bedplate is 23.9 m, the width of the bedplate is 6.9 m, height of the bedplate 2.95 m. The excitation moment will be converted into excitation forces based on Eq.(2.6)÷(2.13) (chapter 2) as Tab. 4.11÷4.13. The vibration excitation source would be loaded on the center of gravity of the main engine through the junction points of the main engine and the internal bottom plate.

*Tab. 4.11. Axial forced of main diesel engine MAN B&W 12K98ME-C(Mk7)*

Order	Hori.couple	Verti.couple	Torque	Lat.moment	Faxi.total
3					108.14
4					60.10
8					11.71
9					26.53
12					0.00
15					6.03

*Tab. 4.12. Horizontal forced of main diesel engine MAN B&W 12K98ME-C(Mk7)*

Order	Hori.couple	Verti.couple	Torque	Lat.moment	Fhori.total
3				31.22	31.22
4				17.35	17.35
8				3.38	3.38
9				7.66	7.66
12			14.86	0.00	14.86
15				1.74	1.74

*Tab. 4.13. Vertical forced of main diesel engine MAN B&W 12K98ME-C(Mk7)*

Order	Hori.couple	Verti.couple	Torque	Lat.moment	Fvert.total
3				57.68	57.68
4		11.15		32.06	32.06
8				6.25	6.25
9				14.14	14.14
12				0.00	0.00
15				3.21	3.21

The forced frequency response analysis of a 11400 TEU container ship with a source of excitation by the main diesel engine is carried out by the numerical modelling method in the Patran-Nastran commercial software. The excitation source is shown to change according to the rotation of the main engine as Fig. 4.46.

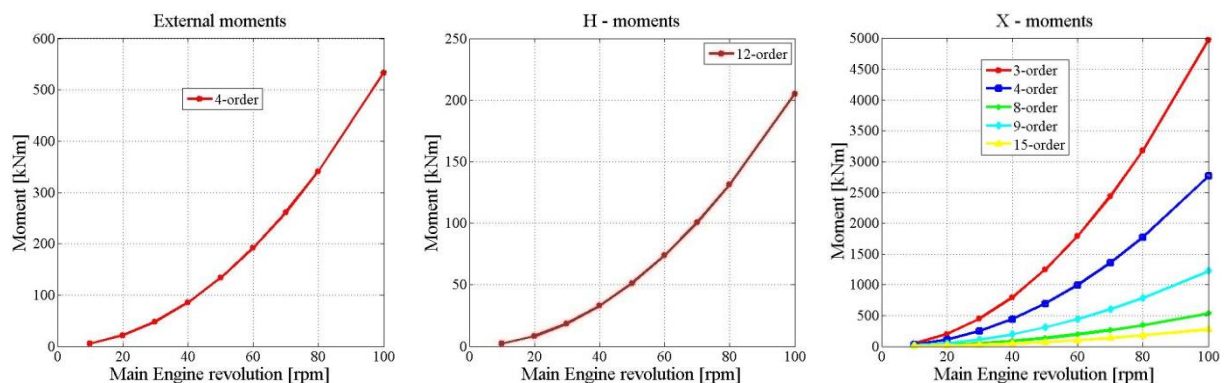


*Fig. 4.46. The excitation force graph of the main engine MAN B&W 12K98ME-C(Mk7)*

The results of the analysis are calculated according to the vibration velocities and rotation speed of the main engine. Then the result of the vibration velocity according to the main engine rotation of the selected points is plotted in the Matlab software. The vibration of the ship hull and superstructure (selected points) as a function of the rotational speed of the

propulsion system, for all directions of the coordinate system and for all considered harmonic components, are shown in Fig. 4.47÷4.51.

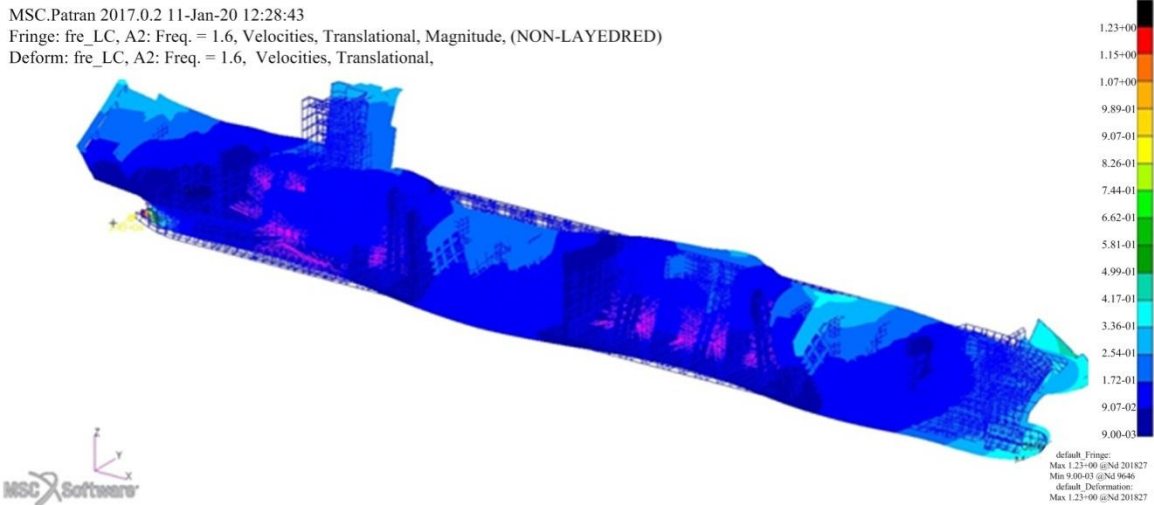


Fig. 4.47. Amplitudes of vibrations forced by the main engine of the container ship 11400 TEU

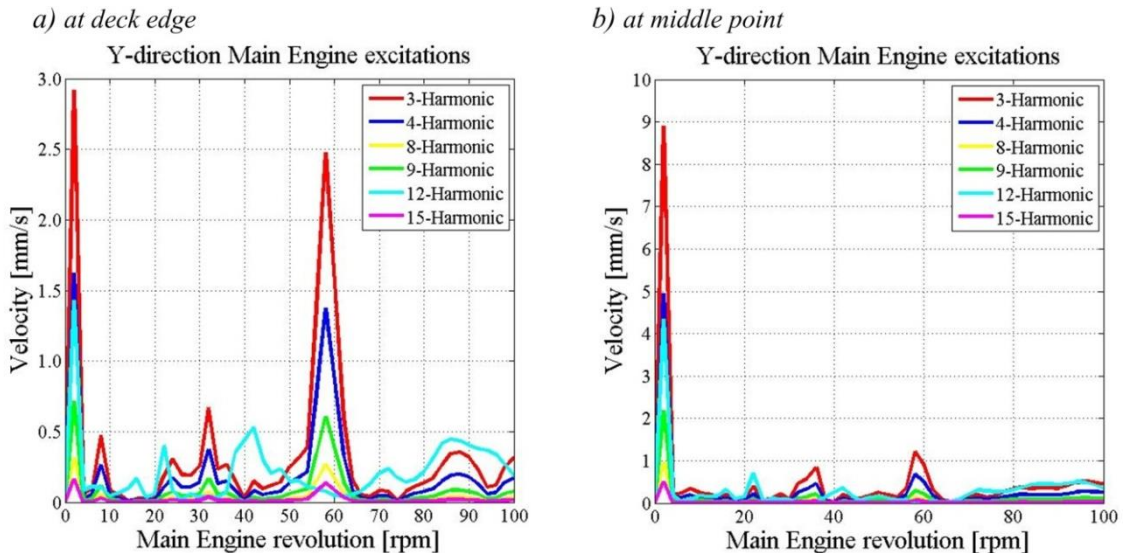


Fig. 4.48. Vibration velocities on the wheelhouse of the container ship 11400 TEU

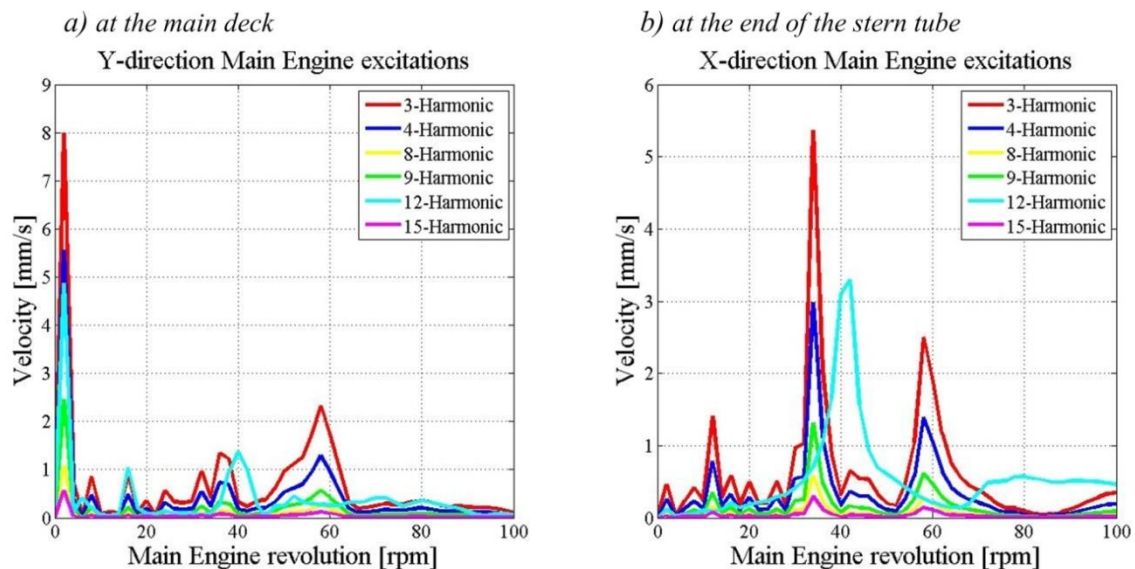


Fig. 4.49. Vibration velocities on main deck and the stern tube shafts of the container ship 11400 TEU

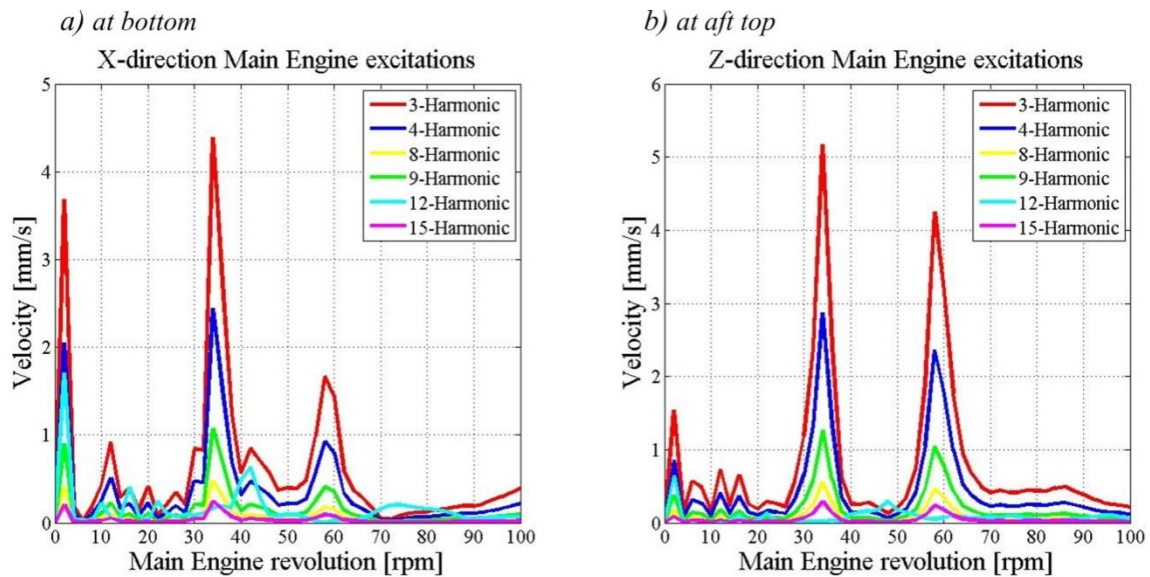


Fig. 4.50. Vibration velocities at bottom of the superstructure of the container ship 11400 TEU

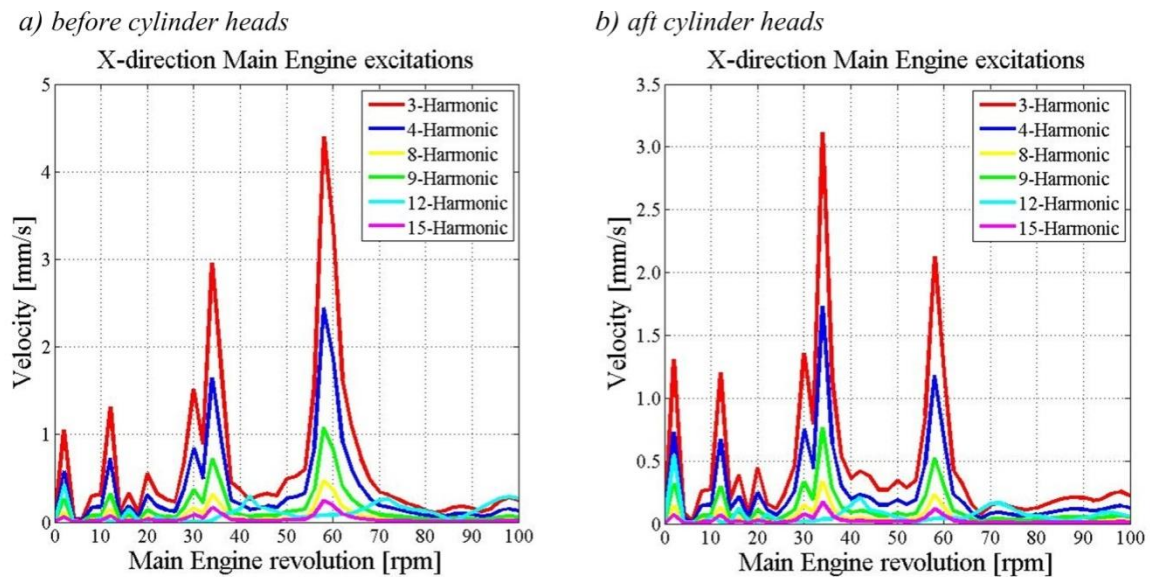
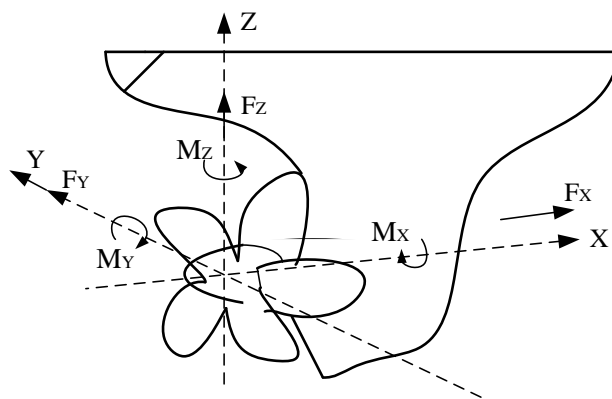


Fig. 4.51. Vibration velocities at main engine of the container ship 11400 TEU

Based on the conducted analyzes, it can be concluded that during the calculation of forced vibrations of the ship, all unbalanced, external moments of the main engine can be of significant importance. Which harmonic components will appear as dangerous is dependent not only on the size of the unbalanced moment but also on its character (there are L, H, and X types) and on the dynamic characteristics of the engine body as well as the ship's hull and superstructure. The first harmonic components (in the medium size container ship 2000 TEU case - 1<sup>st</sup> and 4<sup>th</sup>, in the large size container ship 11400 TEU case - 8<sup>th</sup> and 15<sup>th</sup>) mainly force the global vibrations of the ship's hull. While the higher harmonic components have a larger excitation moment (in the case of the medium size container ship 2000 TEU is the 3<sup>rd</sup> and 5<sup>th</sup> components, the case of the large size container ship 11400 TEU is components 3<sup>rd</sup>, 4<sup>th</sup>, and 9<sup>th</sup>) and the main components related to the number of the ship's cylinders ( in the case of the medium size container ship 2000 TEU is the 8<sup>th</sup> harmonic, in the case of the large size container ship 11400 TEU is the 6<sup>th</sup> and 12<sup>th</sup> harmonic) are responsible for the vibration level of the superstructure and main engine body (structural vibrations).

#### 4.2.2. The forced vibrations with propeller hydrodynamic forces

As a result of the propeller work, forces and hydrodynamic moments are induced on it. By default, during the design of the propulsion system, three components of variables and constant forces (acting in the longitudinal, the transverse and vertical direction of the ship) and three components of hydrodynamic moments are determined and illustrated as Fig. 4.52. Forces and dynamic moments acting in the transverse directions cause flexural vibrations of the shaft lines. The dynamic moment acting around the axis of the shaft line causes torsional vibration of the power transmission system and does not cause direct excitations of vibrations of the ship's hull and superstructure.



X, Y, Z axes are fore aft, athwartship, and vertical axes, respectively,  
 $F_x$  is thrust,  
 $F_y$  is horizontal bearing torque,  
 $F_z$  is vertical bearing torque,  
 $M_x$  is torque,  
 $M_y$  is horizontal bending moment,  
 $M_z$  is vertical bending moment.

Fig. 4.52. Components of hydrodynamic loading on decks

For container ship of 2000 TEU, propellers have five blades, the analysis involved the forced vibration of the fifth harmonic component, i.e. the first harmonic of the propeller. This component is dominant in the propulsion system of the container ship 2000 TEU, the propeller has five blades. During the analyses of vibrations of the superstructure and ship hull forced by hydrodynamic forces, using the approach involves incorporating the power transfer model into the hull model and ship's superstructure, then transverse hydrodynamic forces are applied directly to the propeller model. Propeller RPM is 91 rpm that is 1.52 Hz. Propeller induced hydrodynamic and thrust variations are effective at first blade frequency of 7.6 Hz and the second harmonic of blade frequency of 12.16 Hz. Propeller hydrodynamic forces are illustrated as Tab. 4.14 [105].

Tab. 4.14. Propeller hydrodynamic forces of container ship 2000 TEU

Order	$F_x$ [kN]	$F_y$ [kN]	$F_z$ [kN]
1 order	79.2	31	12.67
	$M_x$ [kNm]	$M_y$ [kNm]	$M_z$ [kNm]
	97.6	177.7	64.9

The analysis of the ship's vibration and the superstructure of the container ship 2000 TEU by excitation hydrodynamic are based on the finite element method implemented in the Patran-Nastran software platform. Then, the result of the vibration velocities according to the main engine rotation of the selected points is drawn in the Matlab software for all directions of the coordinate system and for the 5<sup>th</sup> harmonic component (the first with the propeller), shown in Fig. 4.53÷4.57.

MSC.Patran 2018 11-Jan-20 11:11:34  
 Fringe: Default, A1. Freq. = 2.7993, Velocities, Translational, Magnitude, (NON-LAYEDRED)  
 Deform: Default, A1. Freq. = 2.7993, Velocities, Translational,

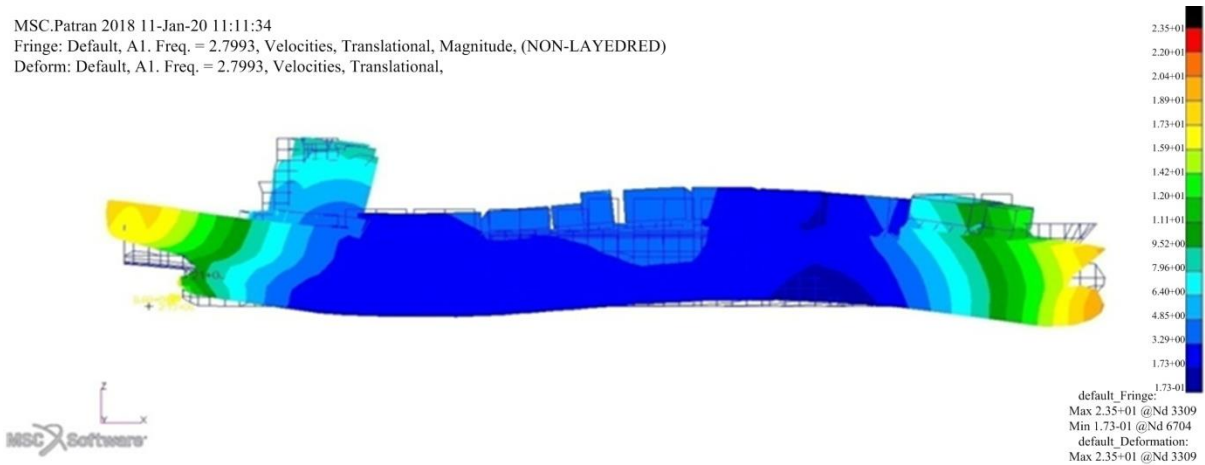


Fig. 4.53. Forced vibration of the container ship 2000 TEU acting by propeller hydrodynamic forces

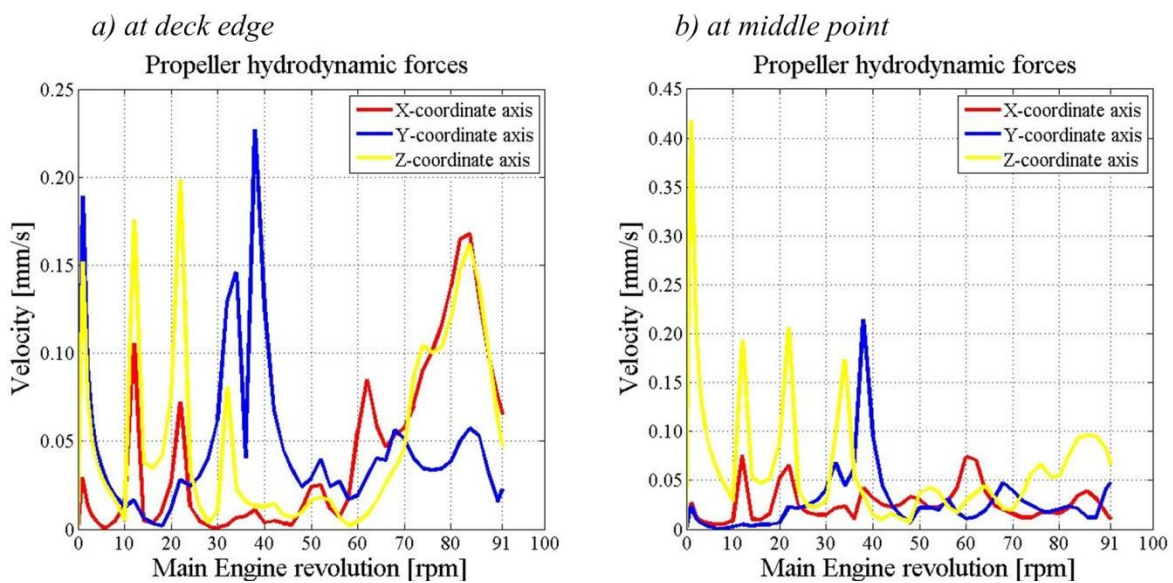


Fig. 4.54. Vibration velocities on the wheelhouse of the container ship 2000 TEU acting by propeller hydrodynamic forces

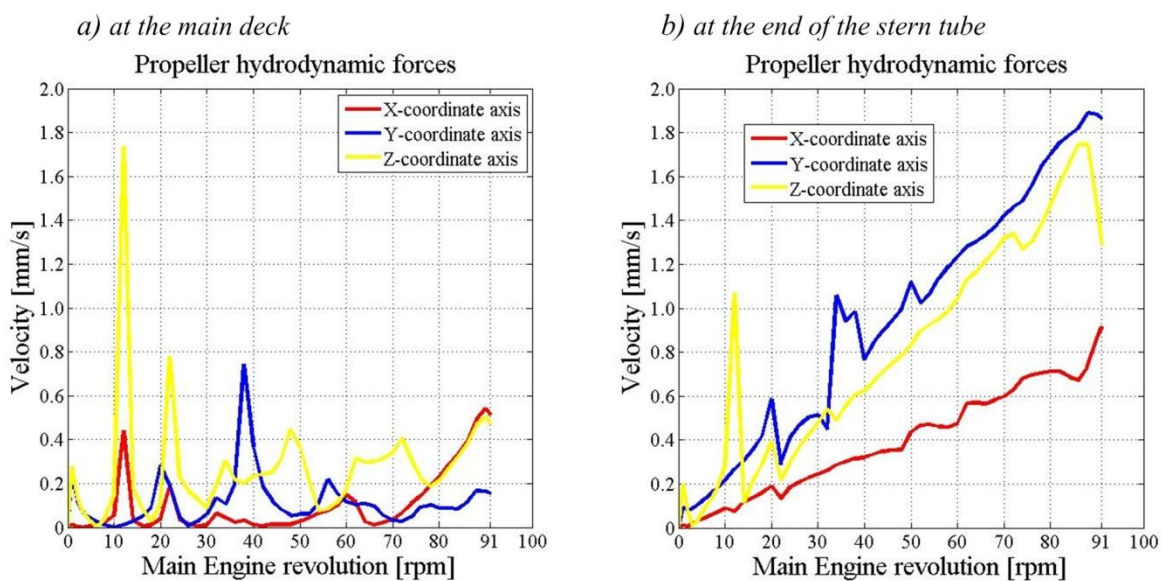


Fig. 4.55. Vibration velocities on the main deck and the stern tube shafts of the container ship 2000 TEU acting by propeller hydrodynamic forces

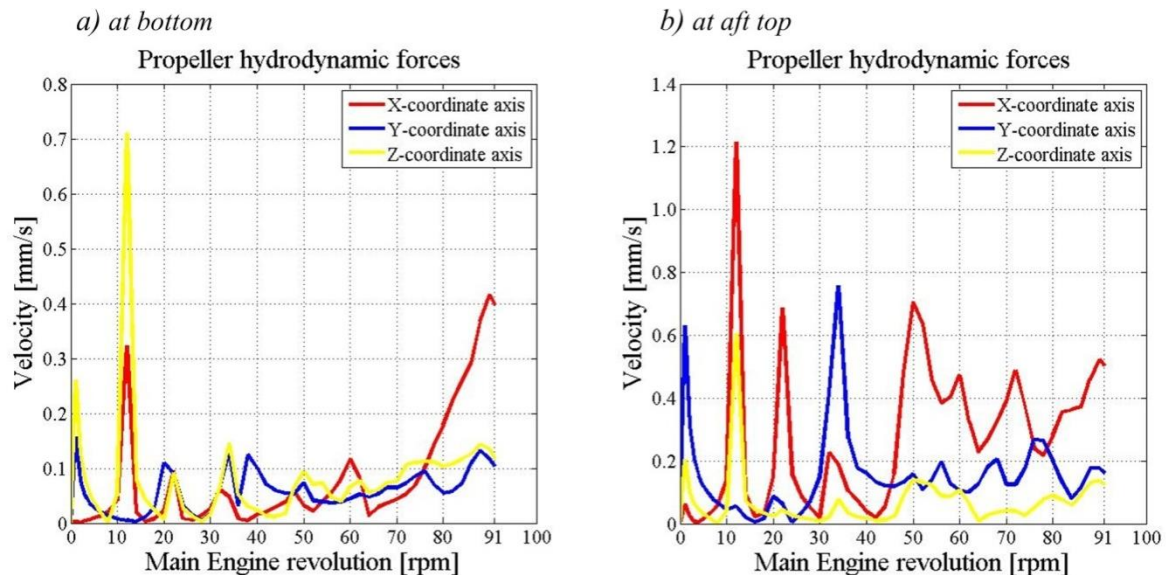


Fig. 4.56. Vibration velocities on the superstructure of the container ship 2000 TEU acting by propeller hydrodynamic forces

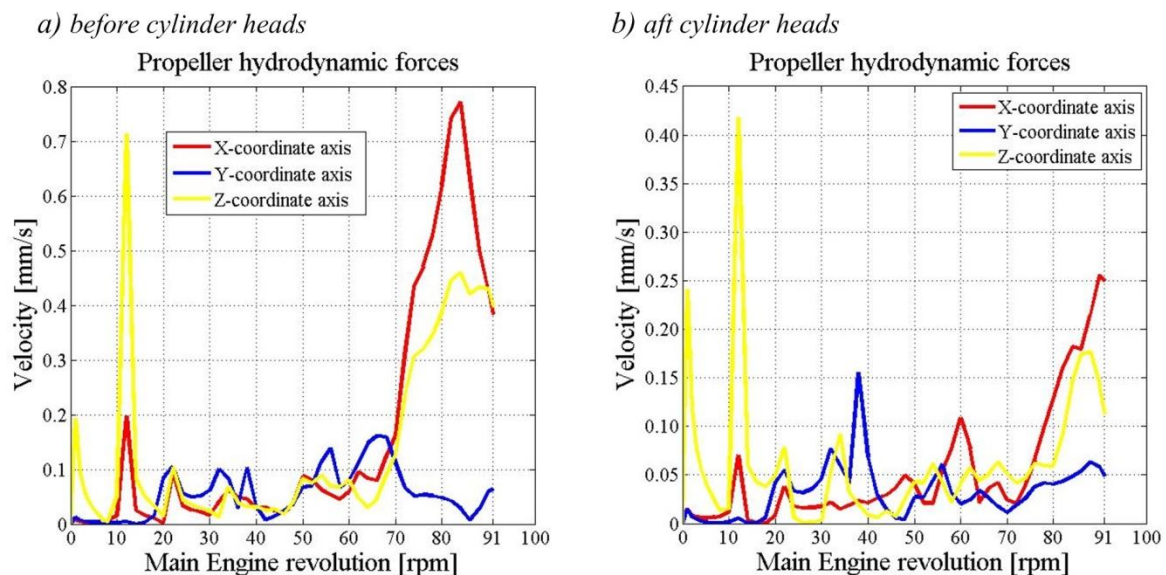


Fig. 4.57. Vibration velocities on the main engine of the container ship 2000 TEU acting by propeller hydrodynamic forces

For container ship of 11400 TEU, propellers have six blades, the analysis involved the forced vibration of the 6<sup>th</sup> and 12<sup>th</sup> harmonic component (the 1<sup>st</sup> and 2<sup>nd</sup> harmonic of the propeller). These components are dominant in the propulsion system of the container ship 11400 TEU, the propeller has six blades. During the analyses of vibrations of the superstructure and ship hull forced by hydrodynamic forces, using the approach involves incorporating the power transfer model into the hull model and ship's superstructure, then transverse hydrodynamic forces are applied directly to the propeller model. Propeller RPM is 100 rpm that is 1.67 Hz. Propeller induced hydrodynamic and thrust variations are effective at first blade frequency of 10 Hz and the second harmonic of blade frequency of 20 Hz. Propeller hydrodynamic forces are illustrated as Tab. 4.15 [105].

Tab. 4.15. Propeller hydrodynamic forces of container ship 11400 TEU

1 order	$F_X$ [kN]	$F_Y$ [kN]	$F_Z$ [kN]
	209.6	82.04	33.53
	$M_X$ [kNm]	$M_Y$ [kNm]	$M_Z$ [kNm]
	258.296	470.28	171.76
2 order	$F_X$ [kN]	$F_Y$ [kN]	$F_Z$ [kN]
	15.53	12.62	4.79
	$M_X$ [kNm]	$M_Y$ [kNm]	$M_Z$ [kNm]
	21.01	75.69	29.64

The analysis of the ship's vibration and the superstructure of container ship 11400 TEU by excitation hydrodynamic are based on the Patran-Nastran software platform. Then, the result of the vibration velocities according to the main engine rotation of the selected points is drawn in the Matlab software for all directions of the coordinate system and for the 6<sup>th</sup> and 12<sup>th</sup> harmonic component (the 1<sup>st</sup> and 2<sup>nd</sup> with the propeller), shown in Fig. 4.58÷4.62.

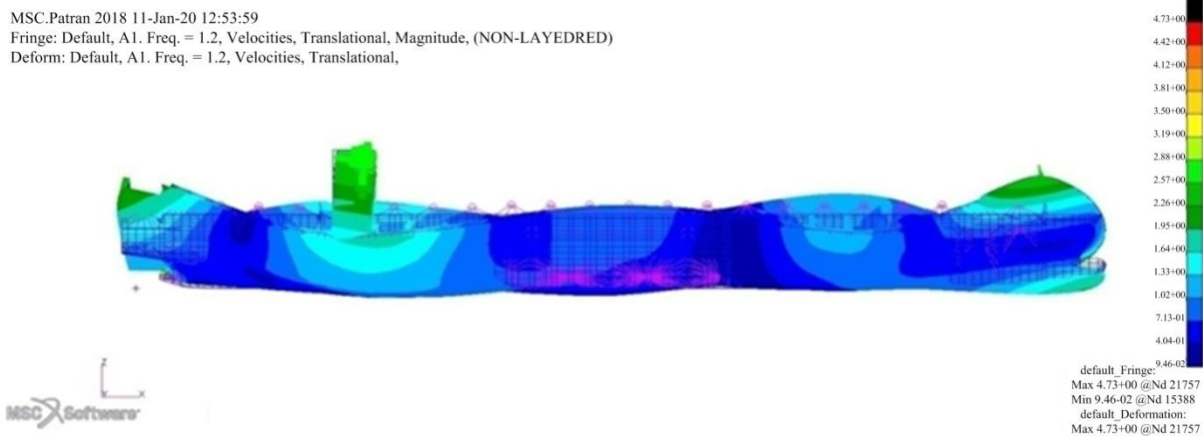


Fig. 4.58. Forced vibration of the container ship 11400 TEU acting by propeller hydrodynamic forces

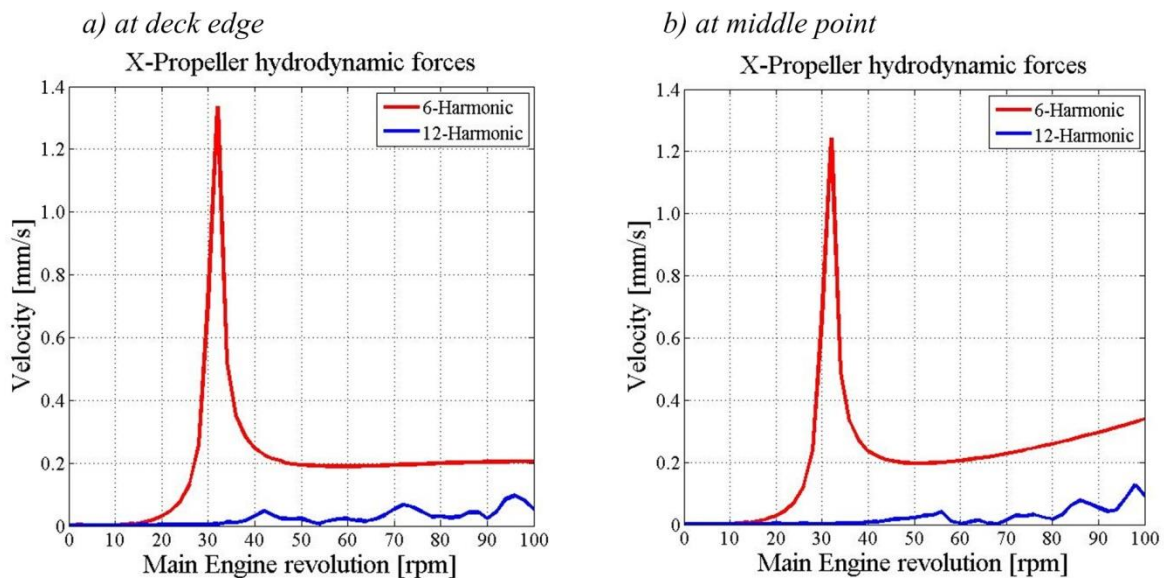


Fig. 4.59. Vibration velocities on the wheelhouse of the container ship 11400 TEU acting by propeller hydrodynamic forces

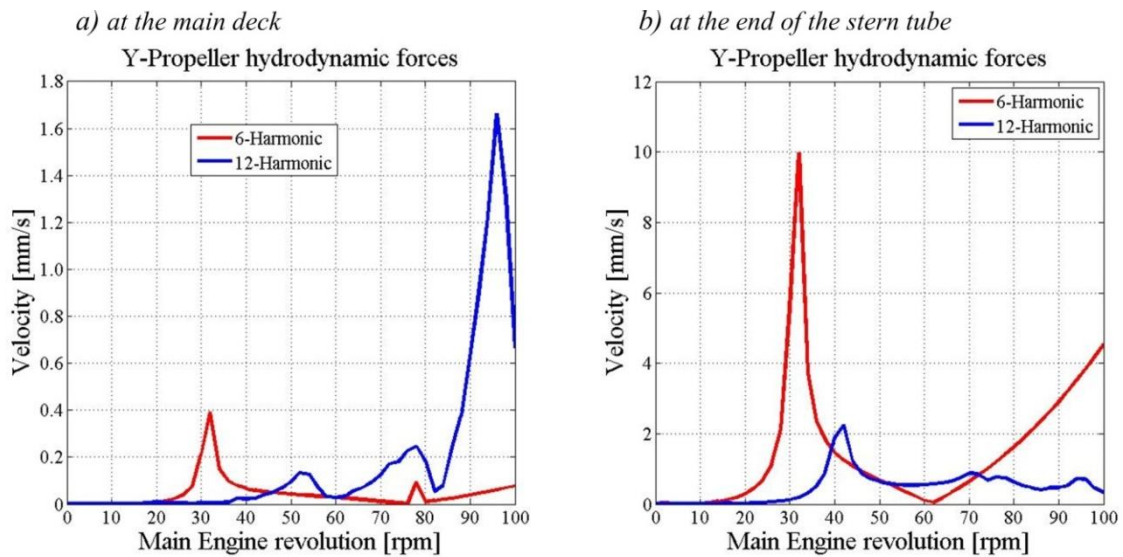


Fig. 4.60. Vibration velocities on the main deck and stern tube shaft of the container ship 11400 TEU acting by propeller hydrodynamic forces

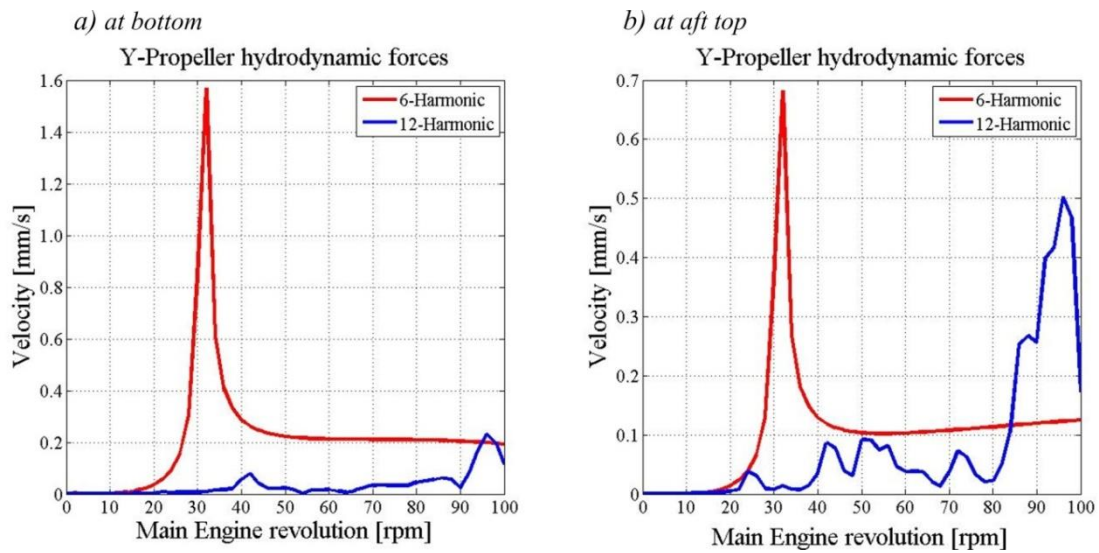


Fig. 4.61. Vibration velocities on the superstructure of the container ship 11400 TEU acting by propeller hydrodynamic forces

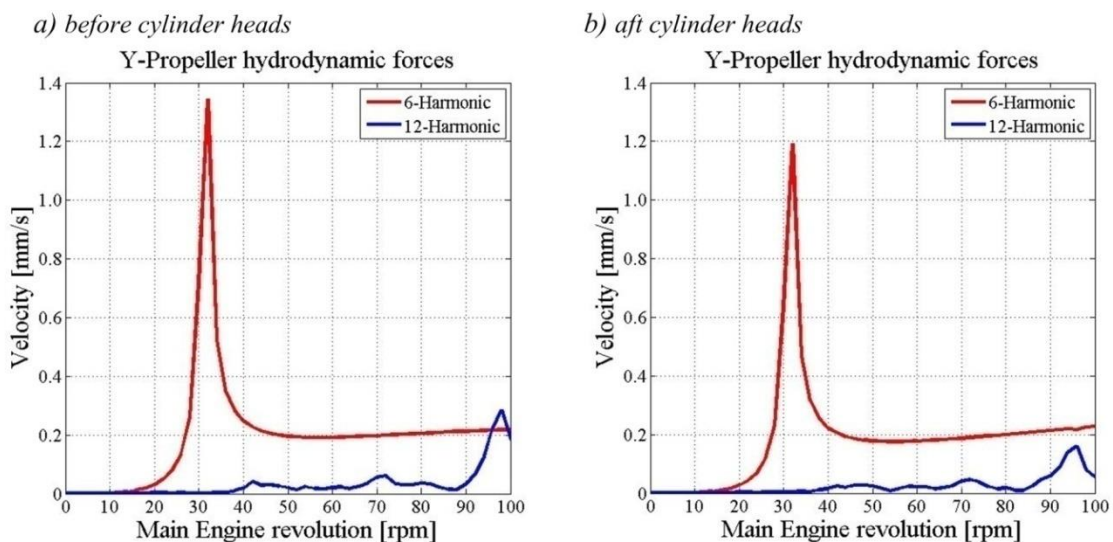


Fig. 4.62. Vibration velocities at main engine of the container ship 11400 TEU acting by propeller hydrodynamic forces

Based on the analysis performed, during the calculation of forced vibration of the medium-sized container ship of 2000 TEU capacity and the large container ship of 11400 TEU capacity by hydrodynamic excitation has some conclusions are as follows: vibration velocity of the propeller hydrodynamic force on the main deck and stern tube shafts of container ship 2000 TEU has a relatively large value, 1.81 mm/s according to Y-coordinate axis for the end of the stern tube end, 0.95 mm/s according to X-coordinate axis at deck transom edge on the main deck. Vibration velocity of the propeller hydrodynamic force on the main deck and stern tube shafts of the medium-size container ship 2000 TEU has a relatively large value, 4.52 mm/s according to Y-coordinate axis for the end of the stern tube end, 1.05 mm/s according to Z-coordinate axis at deck transom edge on the main deck. The remaining positions have smaller vibration velocities.

#### 4.2.3. The forced vibrations with pressure impulses on the transom

The propeller induces a variable pressure field of seawater, which causes the vibration of the transom of the ship's hull (Fig. 4.63). These vibrations are transferred to all ship structure structures. For the 2000 TEU and 11400 TEU container ships, the designer determined the pressure impulses at 11 points of the transom. It was decided to investigate the impact of the modelling accuracy of the transom pressure field on the amplitudes (velocities) of vibrations of the superstructure, main engine and ship's hull.

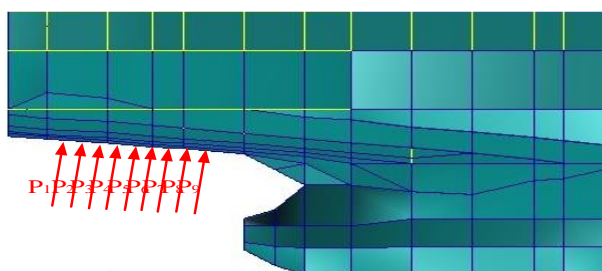


Fig. 4.63. Propeller excitation force acting diagram in loading condition

For container ship of 2000 TEU, propellers have five blades, the analysis involved the forced vibration of the 5<sup>th</sup> harmonic component (1<sup>st</sup> harmonic of the propeller). During the analyses of vibrations of superstructure and ship hull forced by pressure impulses are applied directly to the transom model. Propeller RPM is 91 rpm that is 1.52 Hz. Propeller induced pressure impulses are effective at first blade frequency of 7.6 Hz and the second harmonic of blade frequency of 12.16 Hz. Propeller impulses are illustrated as Tab. 4.16 [105].

Tab. 4.16. Propeller-induced pressure impulses on the transom of container ship 2000 TEU

point	1	2	3	4	5	6	7	8	9	10	11
Xph [m]	0	-0.1	-0.1	-2.6	2.4	-0.1	-0.1	-2.6	-2.6	2.4	2.4
Yph [m]	0	-3.0	3	0	0	-6	6	-3	3	-3	3
Zph [m]	5.6	5.7	5.7	5.2	5.8	6	6	5.4	5.4	6	6
Pressure [kN/m <sup>2</sup> ]	1.43	0.9	1.36	0.97	1.23	0.63	0.55	0.79	1.16	0.61	0.84

The analysis of the ship's vibration and the superstructure of the container ship 2000 TEU by pressure impulses are based on the Patran-Nastran software platform. The result of the vibration velocities according to the main engine rotation of the selected points is drawn

in Matlab software for all directions of the coordinate system and for 5<sup>th</sup> harmonic component (the 1<sup>st</sup> with the propeller), shown in Fig. 4.64÷4.68.

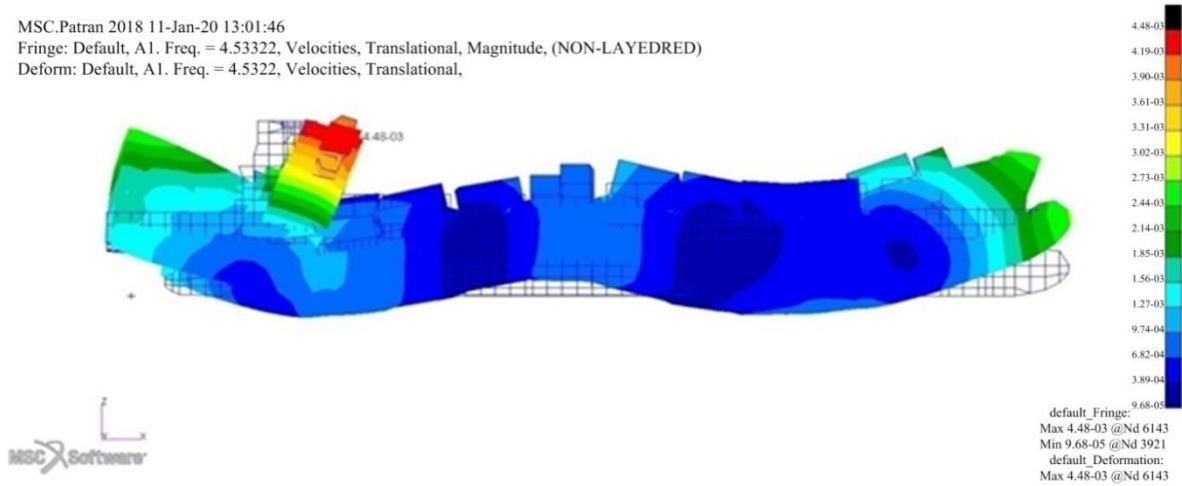


Fig. 4.64. Amplitudes of vibrations forced by pressure impulses of the container ship 2000 TEU

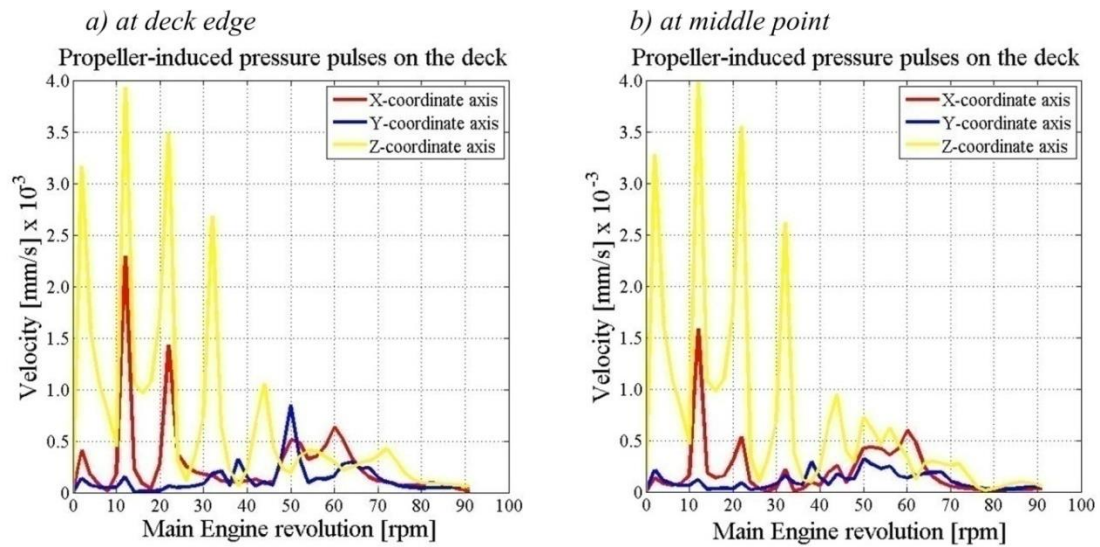


Fig. 4.65. Vibration velocities by pressure impulses on the wheelhouse of the container ship 2000 TEU

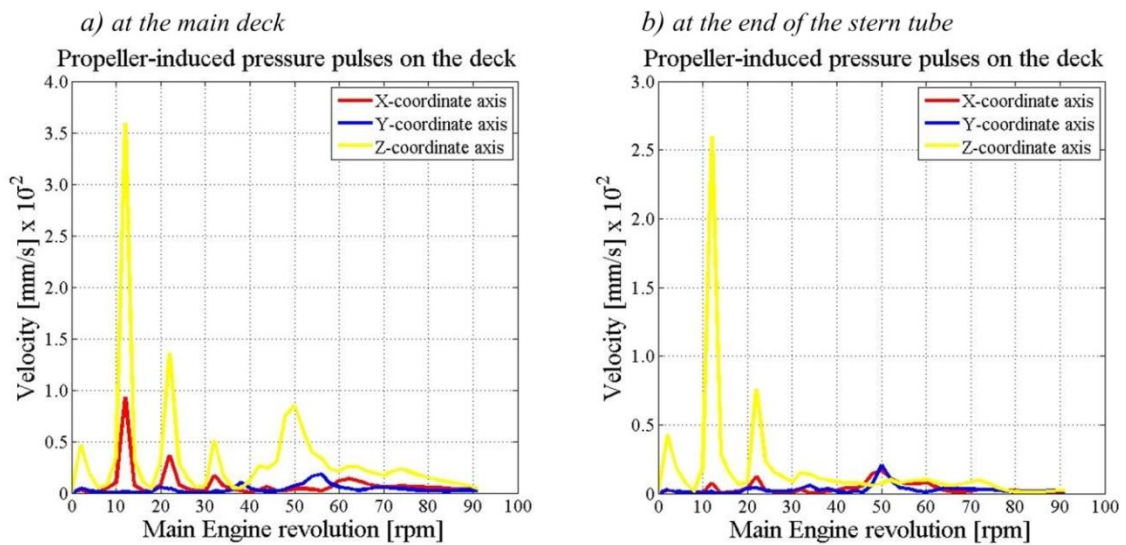


Fig. 4.66. Vibration velocities by propeller pressure impulses on the main deck and the stern tube shafts of the container ship 2000 TEU

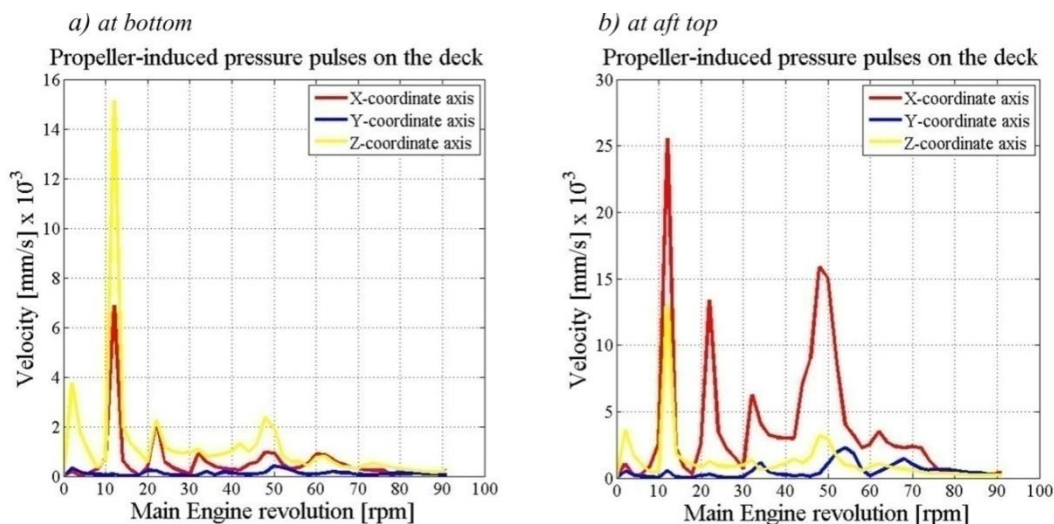


Fig. 4.67. Vibration velocities by propeller pressure impulses on the superstructure of the container ship 2000 TEU

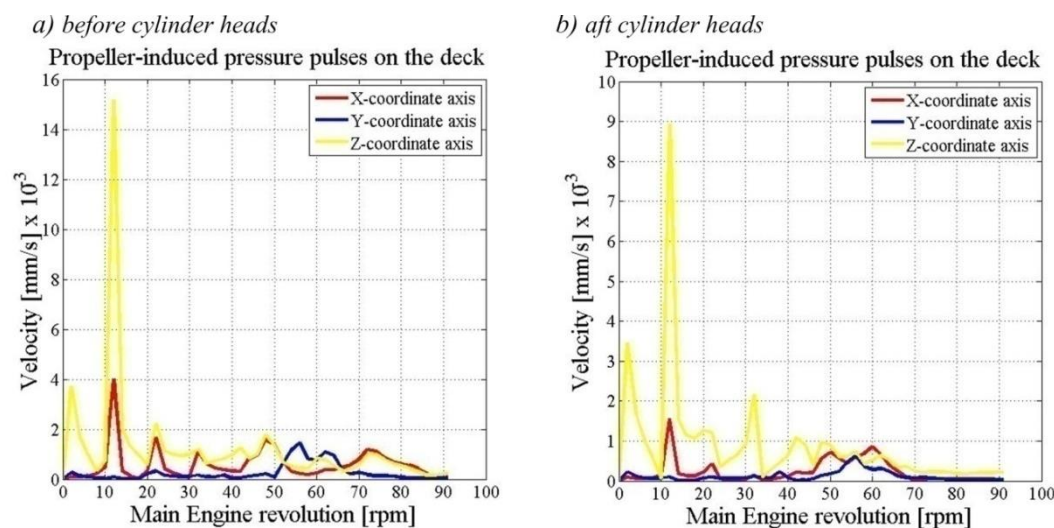


Fig. 4.68. Vibration velocities by propeller pressure on the main engine of container ship 2000 TEU

For container ship of 11400 TEU, propellers have six blades, the analysis involved the forced vibration of the 6<sup>th</sup> and 12<sup>th</sup> harmonic component (the 1<sup>st</sup> and 2<sup>nd</sup> harmonic of the propeller). During the analyses of vibrations of the superstructure and ship hull forced by pressure impulses are applied directly to the transom deck. Propeller RPM is 100 rpm that is 1.67 Hz. The pressure is effective at first blade frequency of 10 Hz and the second harmonic of blade frequency of 20 Hz. Propeller pressure impulses are illustrated as Tab. 4.17 [105].

Tab. 4.17. Propeller-induced pressure pulses on the deck of container ship 11400 TEU

point	1	2	3	4	5	6	7	8	9	10	11
Xph [m]	0.0	-0.26	-0.26	-6.88	6.35	-0.26	-0.26	-6.88	-6.88	6.35	6.35
Yph [m]	0.00	-7.94	7.94	0.00	0.00	-15.9	15.9	-7.94	7.94	-7.94	7.94
Zph [m]	14.8	15.1	15.1	13.8	15.3	15.9	15.9	14.3	14.3	15.9	15.9
Pressure 1 [kN/m <sup>2</sup> ]	3.78	2.38	3.60	2.57	3.25	1.67	1.46	2.09	3.07	1.61	2.22
Pressure 2 [kN/m <sup>2</sup> ]	1.3	0.7	0.7	1.0	0.8	0.4	0.4	0.6	0.7	0.6	0.6

The analysis of the ship's vibration and the superstructure of container ship 11400 TEU by pressure impulses are based on the Patran-Nastran software platform. The results of

the vibration velocities according to the main engine rotation of the selected points is drawn in the Matlab software for all directions of the coordinate system and for the 6<sup>th</sup> and 12<sup>th</sup> harmonic component (the 1<sup>st</sup> and 2<sup>nd</sup> with the propeller), shown in Fig. 4.69÷4.73.

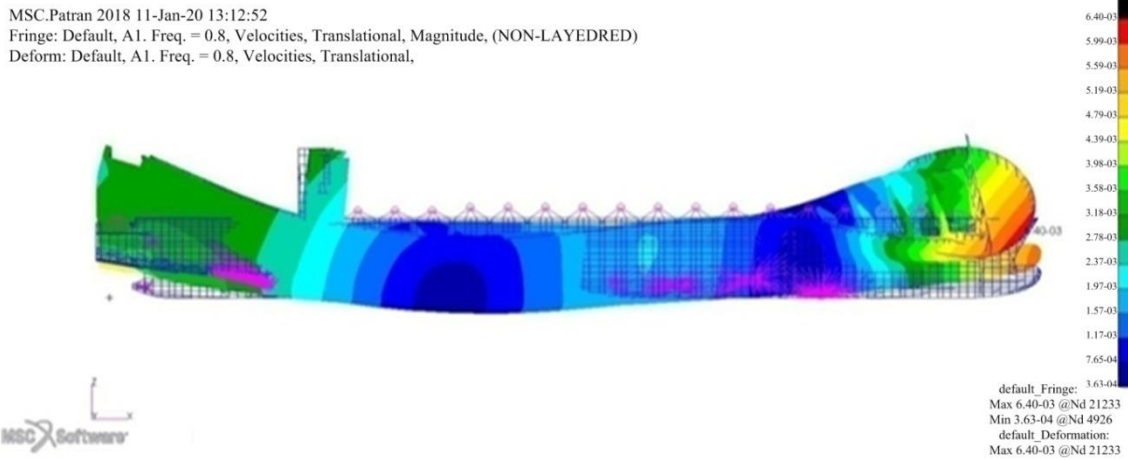


Fig. 4.69. Amplitudes of vibrations forced by pressure impulses of the container ship 11400 TEU

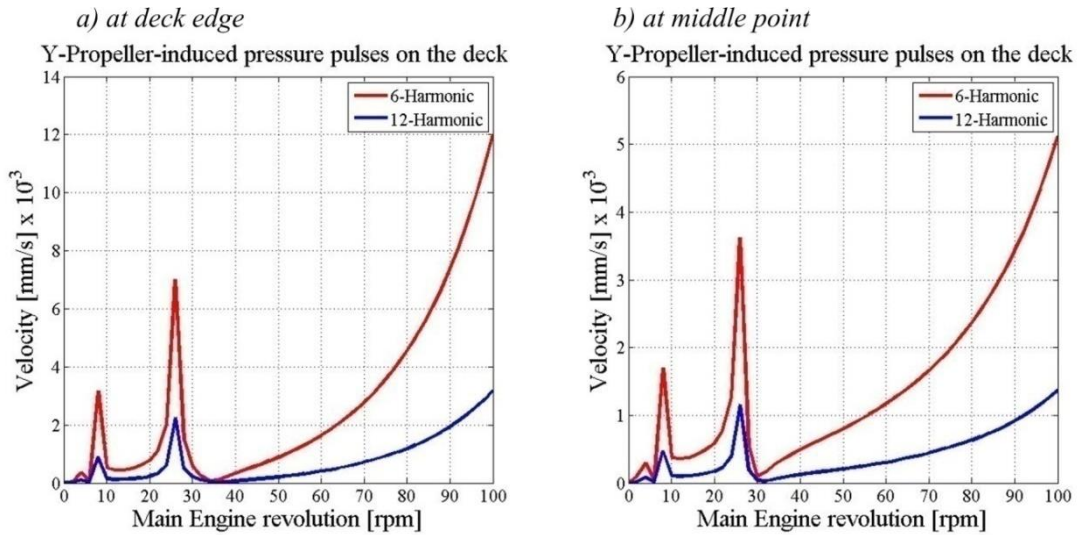


Fig. 4.70. Vibration velocities by propeller pressure impulses at deck edge on the wheelhouse of the container ship 11400 TEU

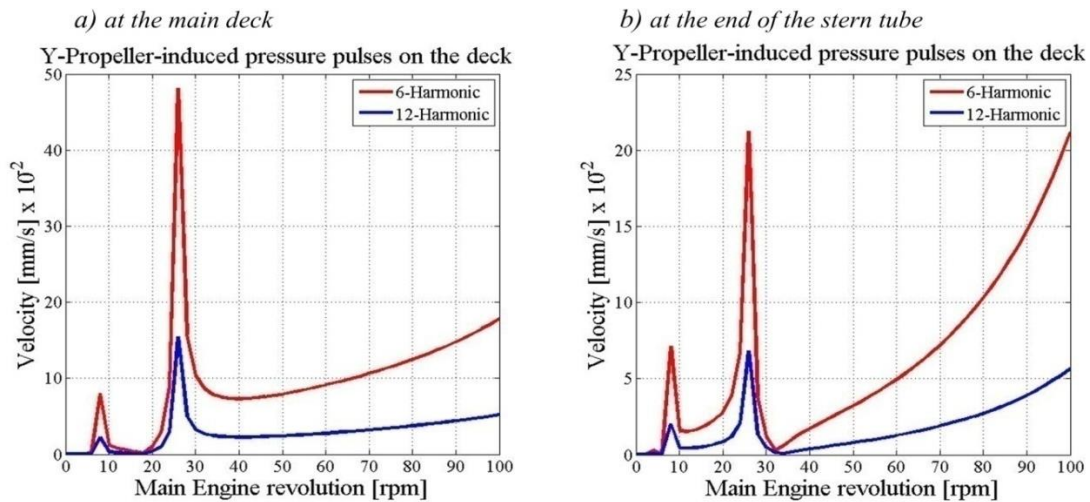


Fig. 4.71. Vibration velocities by propeller pressure impulses on the main deck and stern tube shaft of the container ship 11400 TEU

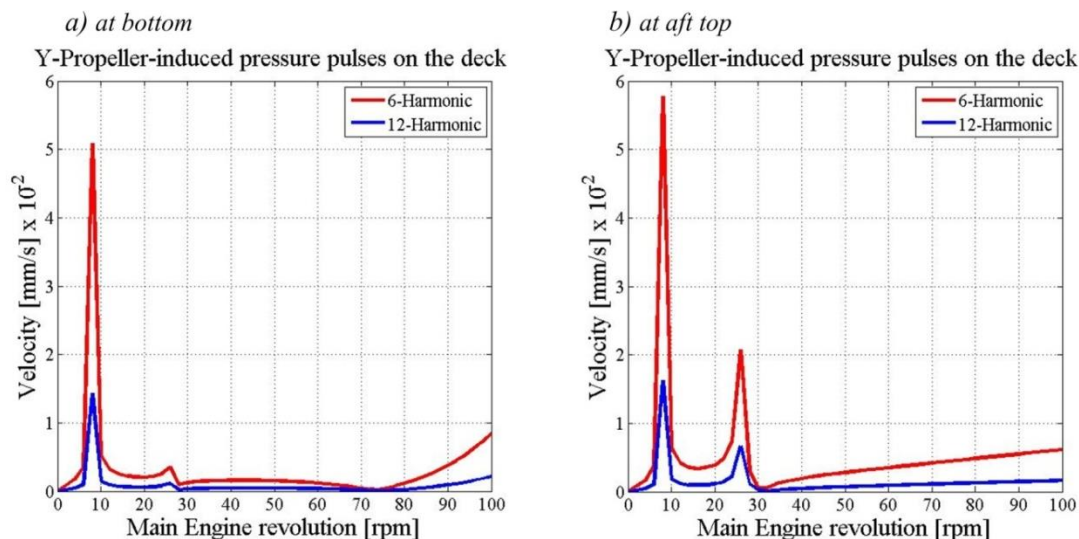


Fig. 4.72. Vibration velocities by propeller pressure impulses at bottom of the superstructure of the container ship 11400 TEU

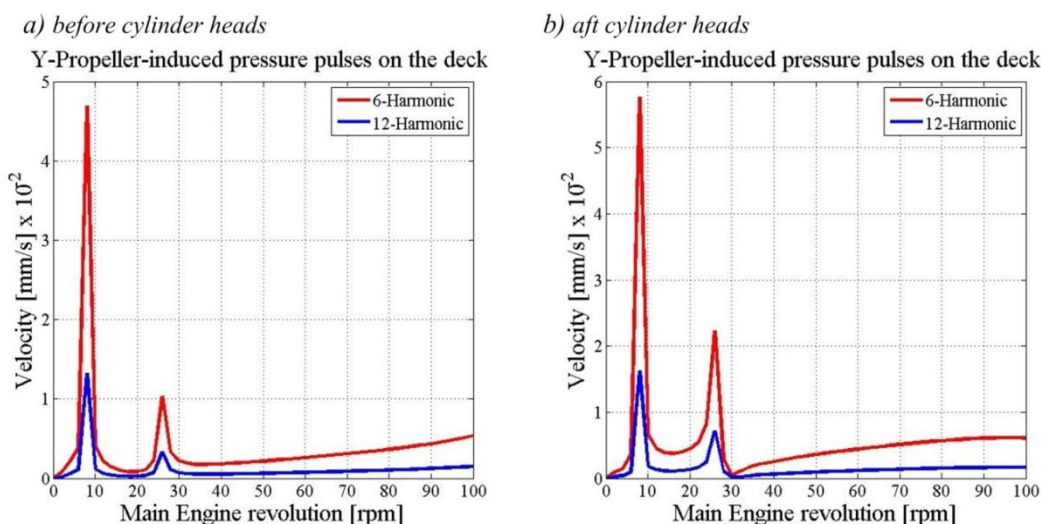


Fig. 4.73. Vibration velocities by propeller pressure impulses at main engine before cylinder heads of the container ship 11400 TEU

Based on the analysis conducted, it can be concluded that during the computation of forced vibration of 2000 TEU and 11400 TEU container ships by pressure impulses. Vibration velocity of the propeller pressure impulses on the 2000 TEU and 11400 TEU container ships have a relatively small value. Vibration velocity of the propeller pressure impulses on the main deck and main engine 0.11 mm/s according to Z-coordinate axis for 12<sup>th</sup> harmonic of the 11400 TEU container ship.

#### 4.2.4. The total excitation forces from the main engine and the propeller

This section evaluates the vibration velocities of container ships of 2000 TEU and 11400 TEU under the influence of total excitation force from the main engine and the propeller. The case for a 2000 TEU container ship is a 5<sup>th</sup> harmonic component (1<sup>st</sup> with a five blades propeller). The case for 11400 TEU container ships is the 6<sup>th</sup> and 12<sup>th</sup> harmonic components (corresponding to the 1<sup>st</sup> and 2<sup>nd</sup> components of the propeller). Vibration velocity values at selected points of 2000 TEU and 11400 TEU container ships were compared with the limited vibration values given by shipbuilding associations and registry societies. The vibration speed of the container ship of 2000 TEU under the effect of the total excitation force

is shown in Fig. 4.74÷4.78. The vibration of the container ship 11400 TEU under the effect of the total excitation force is shown in Fig. 4.79÷4.83.

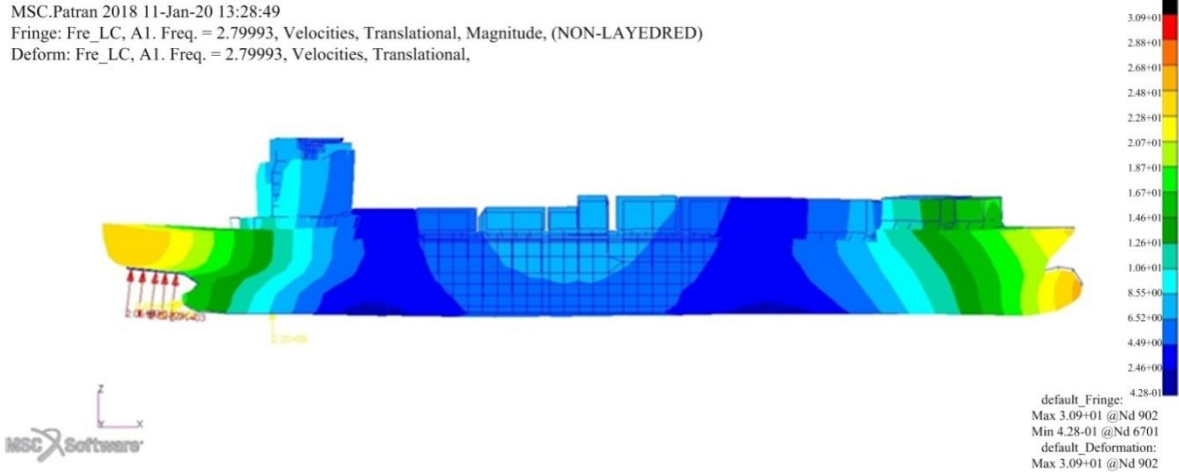


Fig. 4.74. Amplitudes of vibrations forced by total forces of the container ship 2000 TEU

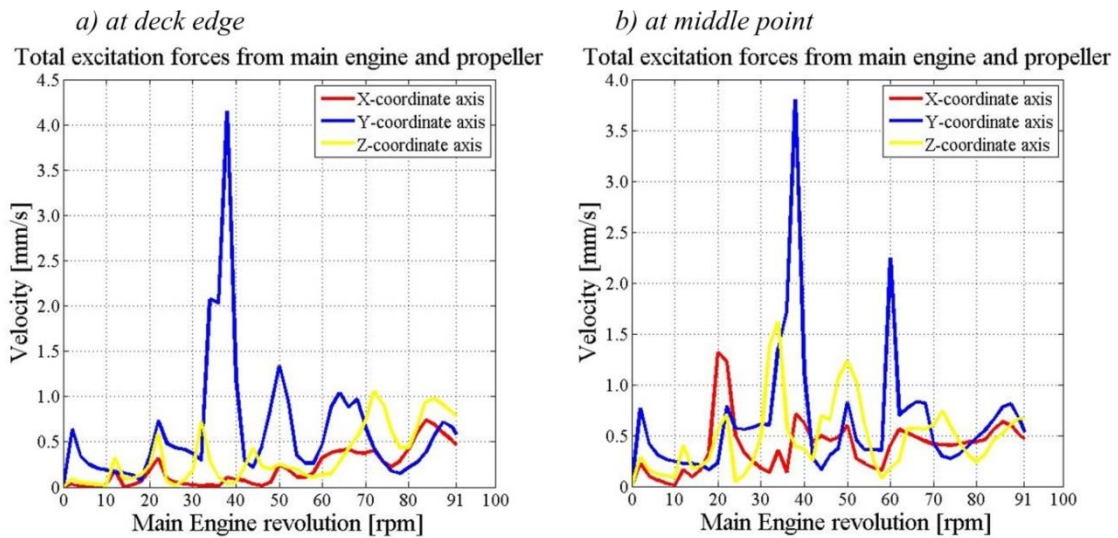


Fig. 4.75. Vibration velocities by total excitation forces from the main engine and the propeller on the wheelhouse of the container ship 2000 TEU

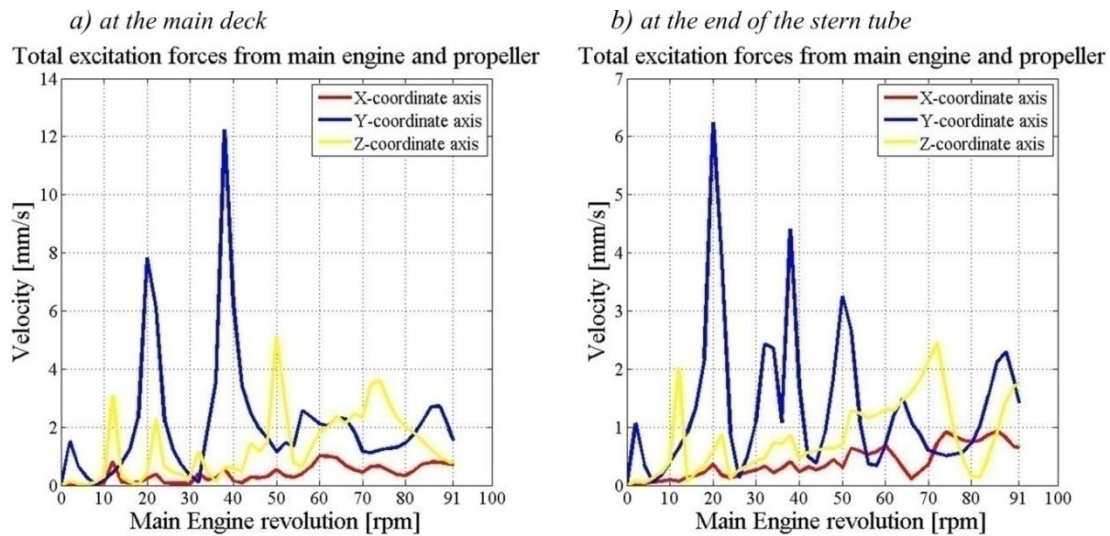


Fig. 4.76. Vibration velocities by total excitation forces from the main engine and the propeller on the main deck and the stern tube shafts of the container ship 2000 TEU

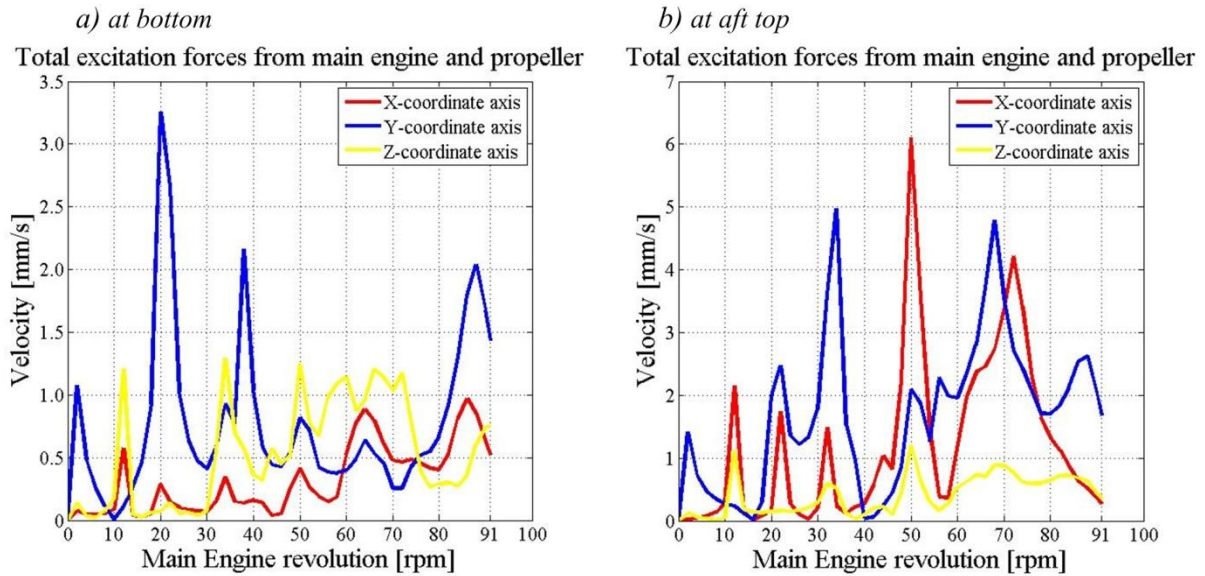


Fig. 4.77. Vibration velocities by total excitation forces from the main engine and the propeller on the superstructure of the container ship 2000 TEU

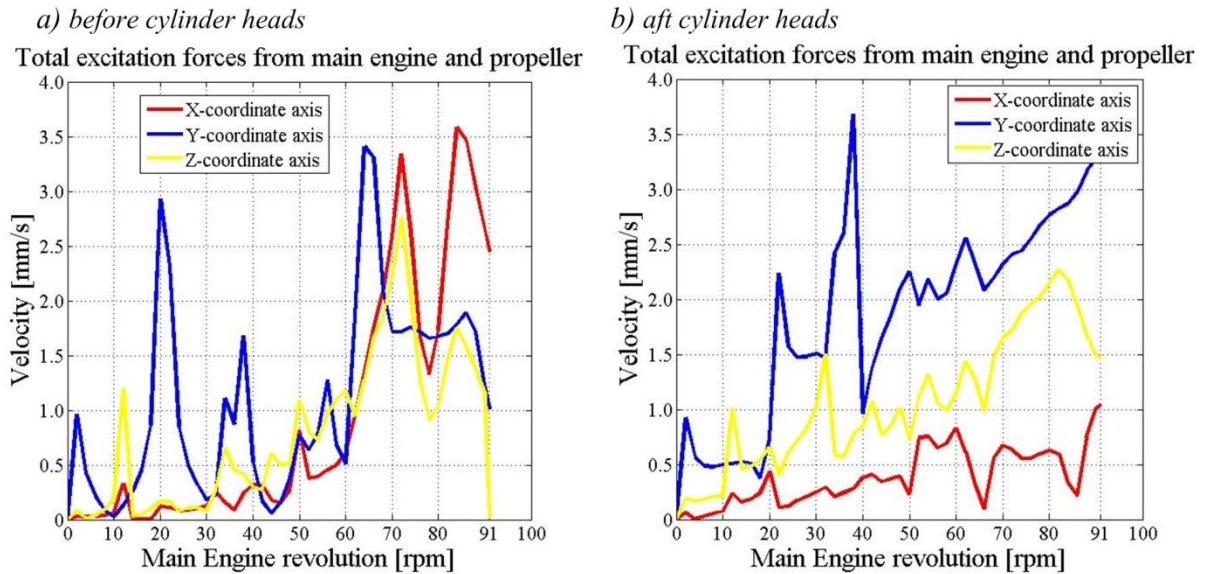


Fig. 4.78. Vibration velocities by total excitation forces from the main engine and the propeller on the main engine of the container ship 2000 TEU

MSC.Patran 2018 11-Jan-20 13:26:17  
 Fringe: Fre\_LC, A1, Freq. = 1.8, Velocities, Translational, Magnitude, (NON-LAYEDRED)  
 Deform: Fre\_LC, A1, Freq. = 1.8, Velocities, Translational,

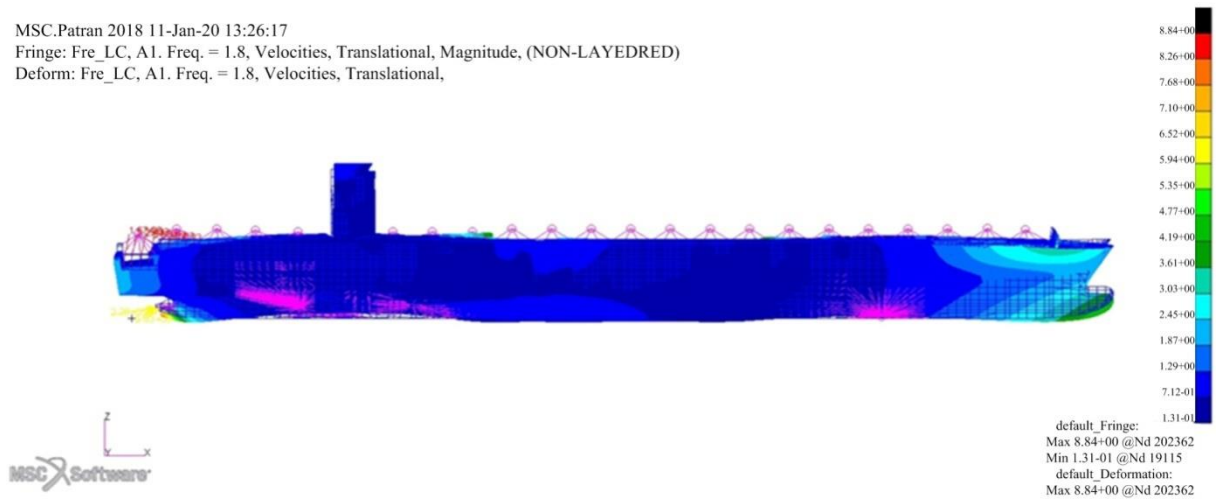


Fig. 4.79. Amplitudes of vibrations forced by total forces of the container ship 11400 TEU

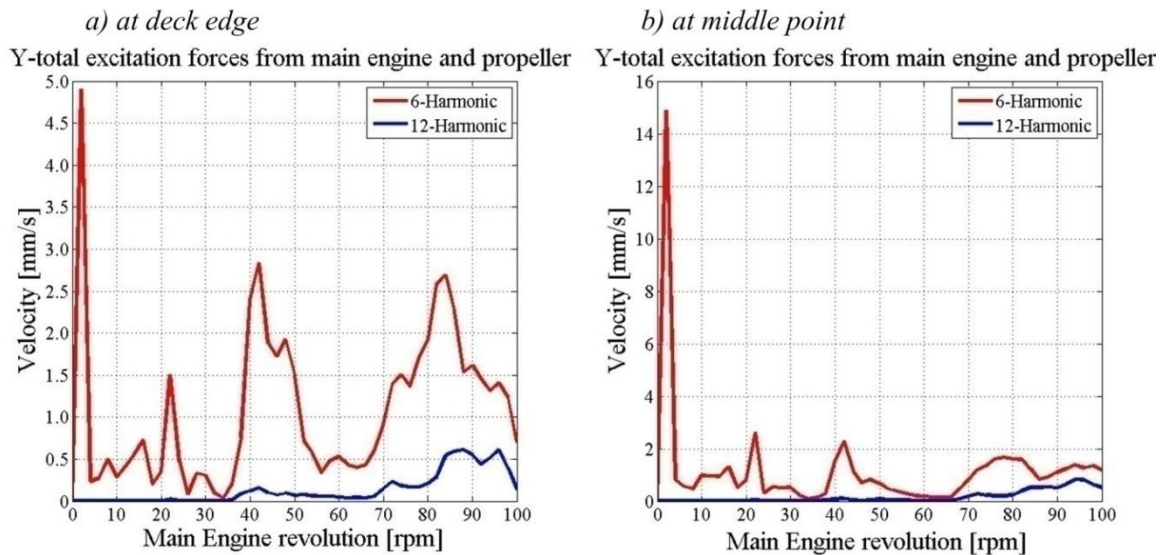


Fig. 4.80. Vibration velocities by total excitation forces from the main engine and the propeller on the wheelhouse of the container ship 11400 TEU

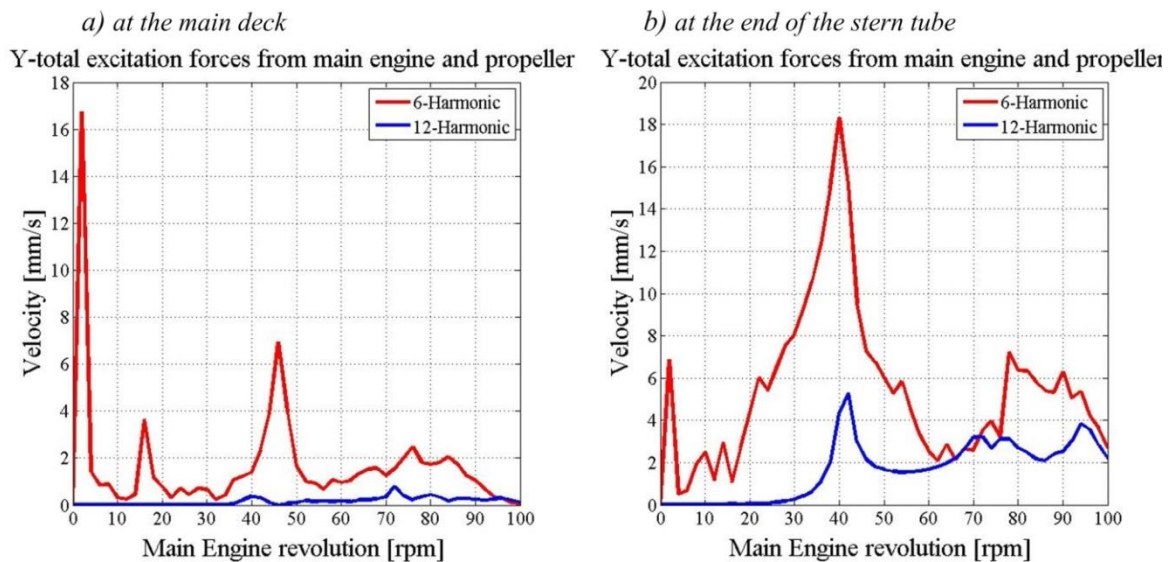


Fig. 4.81. Vibration velocities by total excitation forces from the main engine and the propeller on the main deck and stern tube of the container ship 11400 TEU

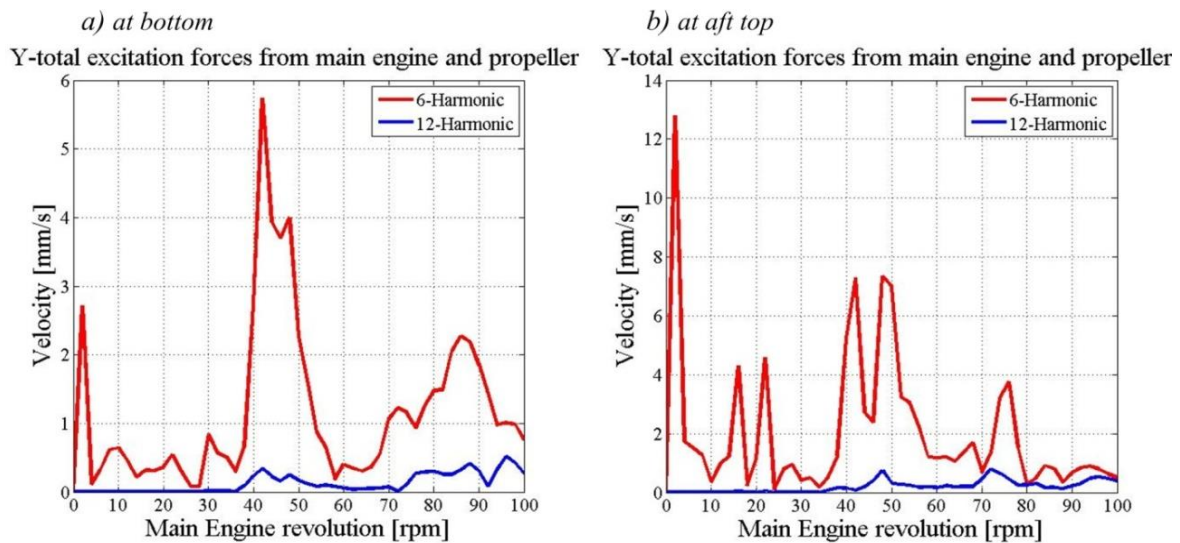


Fig. 4.82. Vibration velocities by total excitation forces from the main engine and the propeller on the superstructure of the container ship 11400 TEU

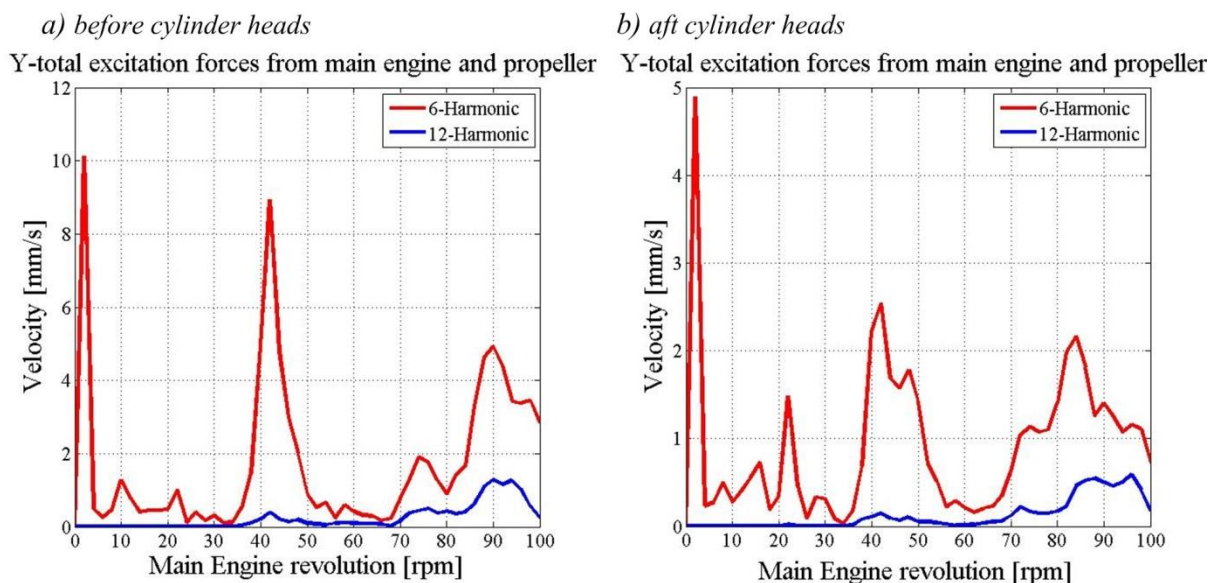


Fig. 4.83. Vibration velocities by total excitation forces from the main engine and the propeller at main engine of the container ship 11400 TEU

Based on the analysis conducted, the source of forced vibration of 2000 TEU and 11400 TEU container ships came from excitation from the main engine and propeller. Vibration velocity of the total excitation force on the transom deck, superstructure and the main engine of the container ship 2000 TEU has a relatively large value, 2.64 mm/s according to Y-coordinate axis for the transom deck, 2.9 mm/s according to Y-coordinate axis on the superstructure, 3.29 mm/s according to Y-coordinate axis on the main engine. Vibration velocity of the total excitation force on the main deck, superstructure and the main engine of the container ship 11400 TEU have a relatively large value, 6.9 mm/s according to Z-coordinate axis for the end of the main deck, 7.0 mm/s according to Y-coordinate axis on the superstructure, 4.94 mm/s according to Y-coordinate axis on the main engine.

### 4.3. Vibration limits for crew, passengers and local structures

The ISO 6954 [53] has been widely used as acceptance criteria for crew habitability and passenger comfort. The criteria are designed to ensure that the vibration levels are below the level at which the crew and the passengers experience discomfort. The ISO 6954 criteria can be transformed into a statement such that for each peak response component (in either the vertical, transverse, or longitudinal direction), at 5 Hz and above, the velocity is acceptable below 4 mm/s and adverse conditions are probably above 9 mm/s. The ISO 6954 [53] has been revised to reflect recent knowledge about human sensitivity to whole-body vibrations. The frequency weighting curves are introduced to represent human sensitivity to multi-frequency vibration for a broad range of frequencies, which are consistent with the combined frequency weighting in ISO 2631-2. The ISO 6954 [54] provides criteria for crew habitability and passenger comfort in terms of overall frequency-weighted RMS values from 1 to 80 Hz for three different areas. The limit vibration is illustrated in Fig. 4.84 and the simplified presentation is shown in Tab. 4.18.

Tab. 4.18. Overall frequency-weighted rms values

Vertical modes	Passenger accommodation (mm/s)	Crew accommodation (mm/s)	Work spaces (mm/s)
A	4	6	8
B	2	3	4

*A is values above which adverse comments are probable; B is values below which adverse comments are not probable*

The vibration level on the engine when installed in the ship must comply with MAN Diesel vibration units as stated in Fig. 4.84 [63, 64].

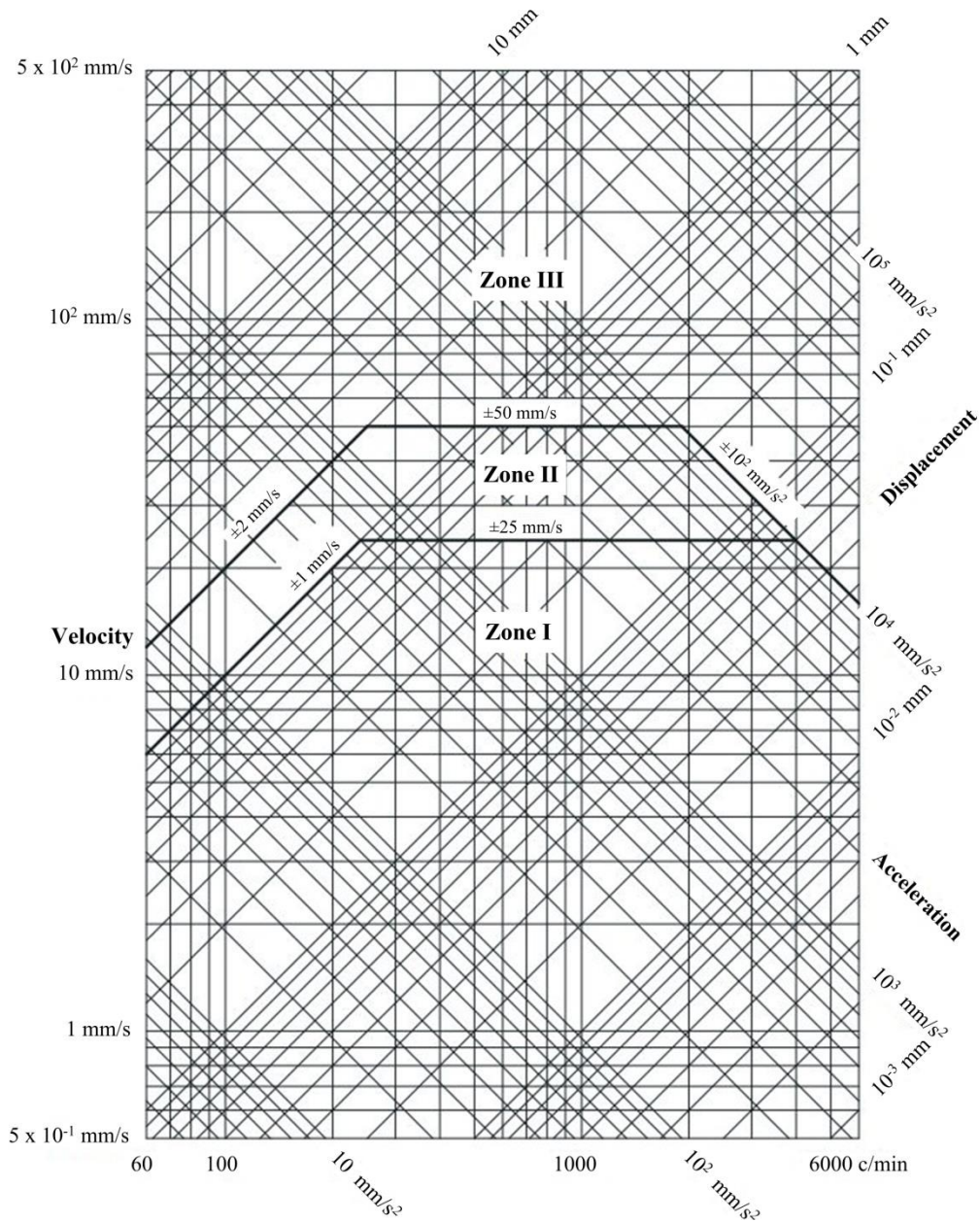


Fig. 4.84. Vibration limits

where:

Zone I is the area where vibration values are accepted,

Zone II is the area where vibration will not damage the main engine, however, under adverse conditions, annoying/harmful vibration responses may appear in the connected structures,

Zone III is the area where vibration values are not accepted.

Based on the forced vibration analysis and the forced vibration frequency response of the medium capacity container ship 2000 TEU and the large capacity 11400 TEU container ship, some results in vibration velocity at some points important calculated and illustrated as Tab. 4.19÷4.20 for the 2000 TEU and 11400 TEU container ships, respectively.

*Tab. 4.19. Forced vibration analyses results – maximum velocities (mm/s) of the container ship 2000 TEU*

Node	1 <sup>st</sup> order	3 <sup>rd</sup> order	4 <sup>th</sup> order	5 <sup>th</sup> order	8 <sup>th</sup> order
Node 1	0.19	0.685	0.338	0.941	0.320
Node 2	0.21	0.654	0.253	0.992	0.701
Node 3	1.26	1.728	1.468	2.639	1.265
Node 4	1.74	2.450	1.521	2.427	1.288
Node 5	1.30	1.781	1.199	2.389	0.927
Node 6	1.02	2.487	1.108	3.056	1.125
Node 7	0.66	2.269	0.515	3.296	0.580
Node 8	1.65	2.378	1.334	2.884	0.876

*Tab. 4.20. Forced vibration analyses results – maximum velocities (mm/s) of the container ship 11400 TEU*

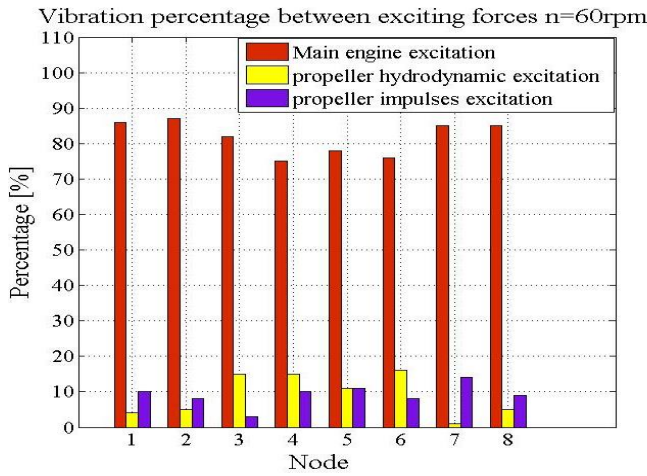
Node	3 <sup>rd</sup> order	4 <sup>th</sup> order	6 <sup>th</sup> order	8 <sup>th</sup> order	9 <sup>th</sup> order	12 <sup>th</sup> order	15 <sup>th</sup> order
Node 1	2.867	1.593	3.003	0.310	0.703	0.192	0.159
Node 2	1.206	0.670	2.784	0.131	0.296	0.490	0.028
Node 3	2.174	1.208	6.880	0.183	0.414	0.672	0.121
Node 4	1.342	0.743	4.299	0.145	0.259	3.269	0.059
Node 5	1.469	0.817	2.836	0.159	0.360	0.373	0.082
Node 6	1.407	0.782	4.944	0.152	0.345	0.307	0.078
Node 7	0.512	0.284	2.394	0.055	0.126	0.169	0.267
Node 8	1.533	0.852	6.993	0.148	0.376	0.213	0.085

where:

- Node 1 is at deck edge on the wheelhouse,
- Node 2 is at the middle point on the wheelhouse,
- Node 3 is at deck transom edge on the main deck,
- Node 4 is at the end of the stern tube shafts,
- Node 5 is at bottom of the superstructure,
- Node 6 is at main engine before cylinder heads,
- Node 7 is at main engine aft cylinder heads,
- Node 8 is at aft top of the superstructure.

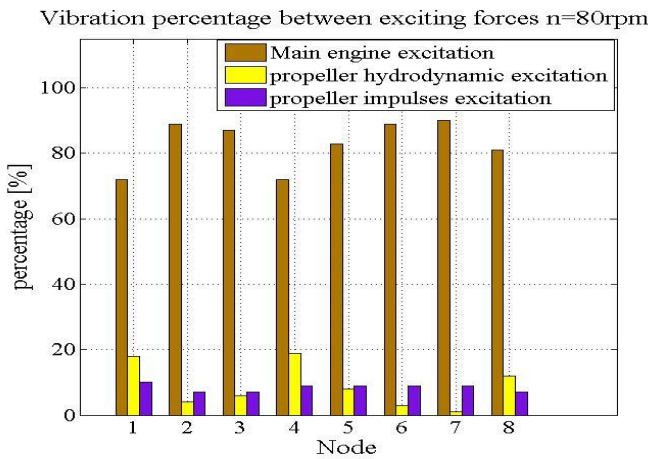
The result of the forced vibration frequency at some important points is compared with the allowable values in Tab. 4.18 and Fig. 4.84 to assess the permissible vibration level at the selected points. The results of the main engine and propeller-induced vibration analysis have shown that the vibration velocities remain under the limits in accommodations but usually exceed the limits in local structures. For container ship of 2000 TEU, node 1÷8 with the maximum vibration velocity of 0.941 mm/s, 0.992 mm/s, 2.639 mm/s, 2.450 mm/s, 2.427 mm/s, 2.389 mm/s, 3.056 mm/s, 3.296 mm/s and 2.884 mm/s, respectively, at the 5<sup>th</sup> harmonic component (1<sup>st</sup> harmonic component for propeller). For the container ship 11400 TEU, node 1÷8 has the largest vibration velocity of 3.003 mm/s, 2.784 mm/s, 6.880 mm/s, 4.229 mm/s, 2.836 mm/s, 4.944 mm/s, 2.394 mm/s and 6.993 mm/s, respectively, at the 6<sup>th</sup> harmonic component (1<sup>st</sup> harmonic component for propeller).

The influence of vibration excitation sources on medium size container ship 2000 TEU and large container ship 11400 TEU are different. The level of vibration depends on the source of excitation from the main diesel engine or from the propulsion system. Fig. 4.85÷4.90 shows different levels of vibration impact from different excitation sources.



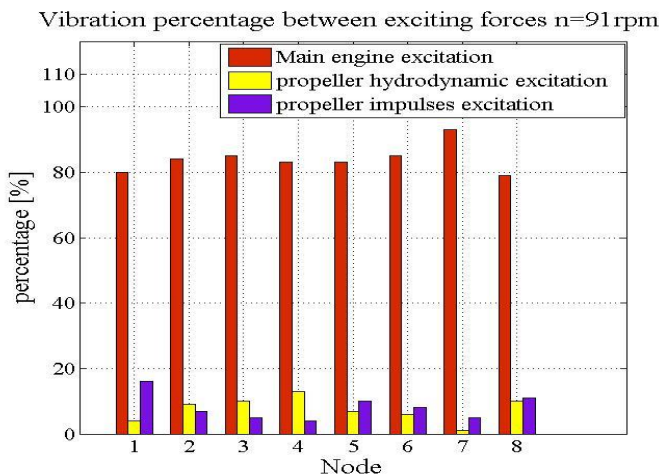
Node 1 is at deck edge on the wheelhouse,  
 Node 2 is at the middle point on the wheelhouse,  
 Node 3 is at deck transom edge on the main deck,  
 Node 4 is at the end of the stern tube shafts,  
 Node 5 is at bottom of the superstructure,  
 Node 6 is at main engine before cylinder heads,  
 Node 7 is at main engine aft cylinder heads,  
 Node 8 is at aft top of the superstructure.

Fig. 4.85. Percentage vibration due to different excitation sources at selected points of the container ship 2000 TEU at n = 60 rpm



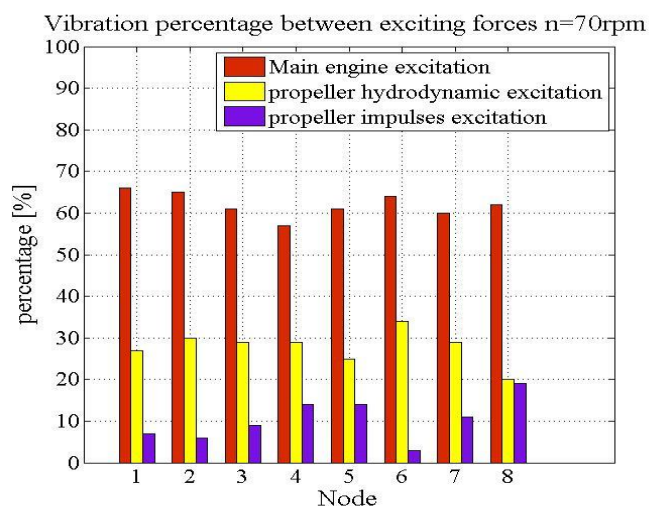
Node 1 is at deck edge on the wheelhouse,  
 Node 2 is at the middle point on the wheelhouse,  
 Node 3 is at deck transom edge on the main deck,  
 Node 4 is at the end of the stern tube shafts,  
 Node 5 is at bottom of the superstructure,  
 Node 6 is at main engine before cylinder heads,  
 Node 7 is at main engine aft cylinder heads,  
 Node 8 is at aft top of the superstructure.

Fig. 4.86. Percentage vibration due to different excitation sources at selected points of the container ship 2000 TEU at n = 80 rpm



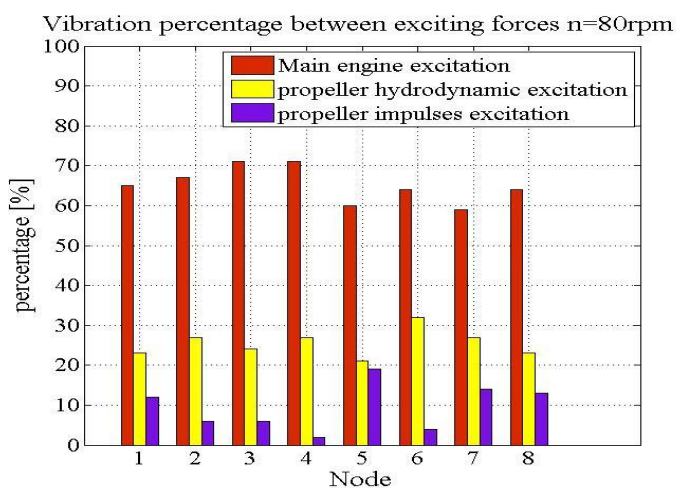
Node 1 is at deck edge on the wheelhouse,  
 Node 2 is at the middle point on the wheelhouse,  
 Node 3 is at deck transom edge on the main deck,  
 Node 4 is at the end of the stern tube shafts,  
 Node 5 is at bottom of the superstructure,  
 Node 6 is at main engine before cylinder heads,  
 Node 7 is at main engine aft cylinder heads,  
 Node 8 is at aft top of the superstructure.

Fig. 4.87. Percentage vibration due to different excitation sources at selected points of the container ship 2000 TEU at n = 91 rpm



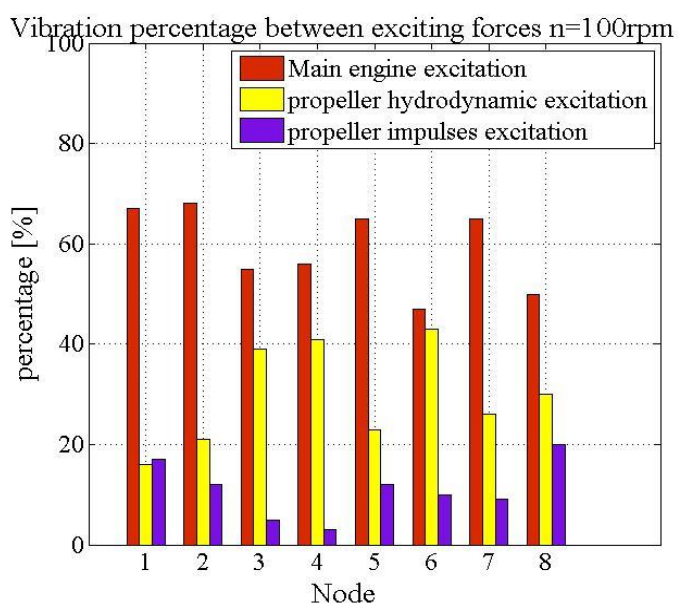
Node 1 is at deck edge on the wheelhouse,  
 Node 2 is at the middle point on the wheelhouse,  
 Node 3 is at deck transom edge on the main deck,  
 Node 4 is at the end of the stern tube shafts,  
 Node 5 is at bottom of the superstructure,  
 Node 6 is at main engine before cylinder heads,  
 Node 7 is at main engine aft cylinder heads,  
 Node 8 is at aft top of the superstructure.

Fig. 4.88. Percentage vibration due to different excitation sources at selected points of the container ship 11400 TEU at n = 70 rpm



Node 1 is at deck edge on the wheelhouse,  
 Node 2 is at the middle point on the wheelhouse,  
 Node 3 is at deck transom edge on the main deck,  
 Node 4 is at the end of the stern tube shafts,  
 Node 5 is at bottom of the superstructure,  
 Node 6 is at main engine before cylinder heads,  
 Node 7 is at main engine aft cylinder heads,  
 Node 8 is at aft top of the superstructure.

Fig. 4.89. Percentage vibration due to different excitation sources at selected points of the container ship 11400 TEU at n = 80 rpm



Node 1 is at deck edge on the wheelhouse,  
 Node 2 is at the middle point on the wheelhouse,  
 Node 3 is at deck transom edge on the main deck,  
 Node 4 is at the end of the stern tube shafts,  
 Node 5 is at bottom of the superstructure,  
 Node 6 is at main engine before cylinder heads,  
 Node 7 is at main engine aft cylinder heads,  
 Node 8 is at aft top of the superstructure.

Fig. 4.90. Percentage vibration due to different excitation sources at selected points of the container ship 11400 TEU at n = 100 rpm

With the medium-sized container ship 2000 TEU, the source of vibration excitation comes mainly from main diesel engines, accounting for over 70%. Meanwhile, the source of vibration caused by the ship's propulsion system is about 20%. The large container ship 11400 TEU, the source of vibration stimulation from the main diesel engine and the ship's propulsion system are not much different. The source of vibration stimulation of the ship from the main engine is about 50-70%, while the source of train vibration stimulation due to the ship's dynamic system can be up to 45%.

### 4.4. Conclusions

The 2000 TEU and 11400 TEU container vessels are modelled in 3D models using the finite element method implemented in Patran-Nastran software to calculate free vibration and forced vibration of the container ships, by adjusting the material density and applying concentrated mass to equal the loading mass distribution in the manual. Added mass is calculated by empirical formula to calculate, and added to the mass points below the waterline.

It is important to determine the natural vibration of the ship and the superstructure in the design stage. This will help designers and shipbuilders avoid dangerous phenomena, resonance vibrations when building ships. The natural vibration of the hull and superstructure is determined by two methods. The first method is based on the most common empirical formulas currently introduced by Todd and Brown [109, 11]. The second method is based on the finite element method, numerical modelling on famous commercial software platform Patran - Nastran. The calculation results between the two methods are compared, thereby assessing the accuracy of the selected numerical method. The finite element method, numerical simulation on the Patran-Nastran software platform gives more accurate results than methods based on existing experimental formulas. The accuracy of the numerical simulation method increases as the density of meshing increases and the finite element type is selected in accordance with the original geometric characteristics of the structure.

From calculating the forced vibration of the ship, the author sees that vibration response amplitude increases with the increase of vibration frequency, the amplitude will reach the maximum value when the excitation frequency approach to the 1st order natural frequency of the hull girder, the resonance will occur at the moment the mode of the forced vibration is close to the 1 order mode. And hull response decreases quickly when the excitation frequency is further increasing, then increases gradually, until the excitation frequency approach to 2 order natural frequency, the amplitude will reach the second peak point, and the second resonance is going to happen, followed by the third-order, fourth-order resonance, etc.

Through the analysis of free vibration and forced vibration of 2000 TEU and 11400 TEU container ships, most of the forced vibration response values of checking points are less than the standard criteria and satisfy the vibration requirements. For medium-sized container ship 2000 TEU, the source of vibration is mainly from the main diesel engine. Large container ship 11400 TEU, the source of vibration excitation comes from the main diesel engine and the ship's propulsion system.

### 5. The operating parameter characteristics of the drive system

The ship's propulsion system, including the ship's main engine, acts as the heart of the ship and creating propulsion that enables the ship to move in the water. Therefore, the identification and alignment of the proper shaft line are one of the most important actions in the design of a ship's propulsion system. It includes the determination of shaft dimensions such as the diameter, length, position of the main drive shaft, intermediate bearing axis and stern tube bearing axis, shaft stiffness. Because the ship's hull has a greater degree of elasticity than the shaft system, and the ship is often surrounded by a hazardous environment that is subject to long periodic loads coming from the continually impacting waves and extreme loads short as violent storms, ocean waves or even collisions. It can cause vibration, cracking, excessive axial deformation, misalignment increase torque, even shaft fracture. Any damage to a marine structure, especially as the propulsion systems, can result in endanger human life, ecological and economic catastrophe. Therefore, the accurate analysis of shaft stiffness, the bearing foundations of the propulsion systems in different conditions (dynamic analysis) right from the design phase will help minimize the risks and increase the safety, reliability as well as the efficiency of ship propulsion systems. A basic propulsion system is shown in Fig. 5.1.

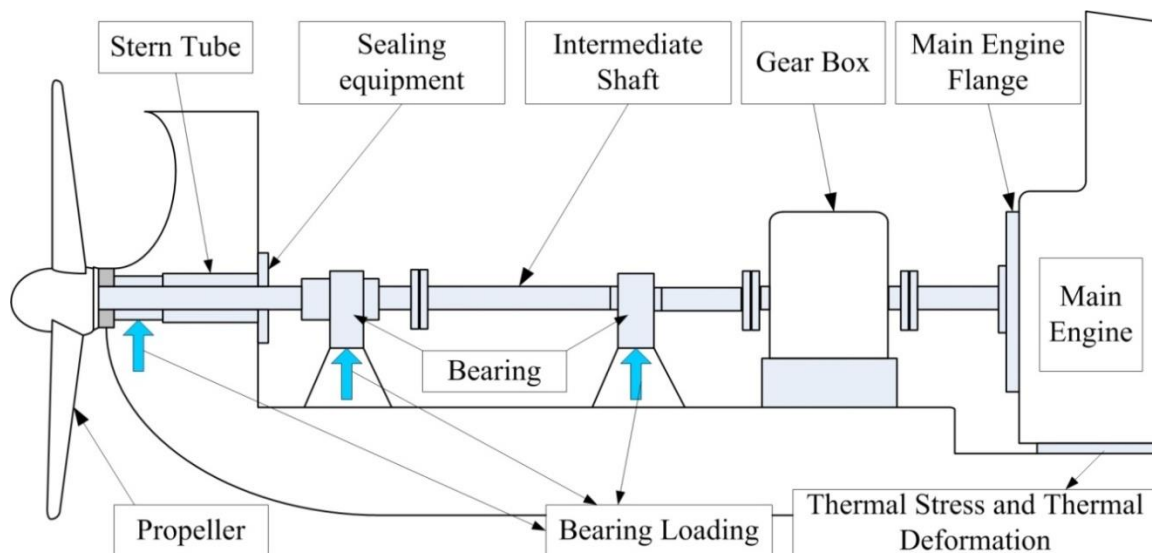


Fig. 5.1. The typical structure sketch map of the marine propulsion system

Vibration is the cause of damage to equipment and machinery on board, reducing the operating life of the equipment. In addition, vibration also causes discomfort for crew members when working onboard. Vibration reduction is an important issue to consider at the design stage of the ship, in order to minimize possible vibration. Vibration can be simply understood as the ratio of the force exerted on the stiffness of equipment and machinery. Mathematically, this is summarized as:

$$K = \frac{F}{\Delta L}, \quad (5.1)$$

where:

- $K$  is stiffness of equipment and machinery,
- $F$  is excitation force,
- $\Delta L$  is displacement.

As Equation Eq.(5.1) shows, vibration can only change as the result of two things: a change in force or a change in stiffness (or both). In other words, vibration is merely a result of other root causes occurring in a machine, equipment or ship's hull. One of those root causes can be changing stiffness, and it is for this reason that a solid grasp of dynamic stiffness is essential for the determination vibration of the ship's hull.

The alignment of the shaft line, as well as the determination of the stiffness of the foundations of the shaft line, has been mentioned in several studies by author Lech Murawski and colleagues [35, 72, 73, 75]. The most common method used to calculate the stiffness of bearings and foundations is the finite element method. The shaft line and crankshaft are modelled by linear beam elements. According to world producers of marine engines, the model of a crankshaft has simplified as beams in the line arrangement (in the model there is no geometry of the cranks). The weight of the propeller and shafts, hydrodynamic forces acting on the propeller and the other forces coming from the propulsion system are modelled by static, nodal forces and moments. The thermal expansion of the main engine body is modelled as a vertical movement of the main bearings. The value of this movement is specified by the engine's manufacturers. Calculations have to be done for all the typical ships' propulsion systems service conditions.

Ship's power transmission systems (crankshaft, shaft line, and propeller) are modelled as isolated from the ship's hull. This is mainly due to difficulties in the accuracy of modelling the propulsion system with the entire ship's hull and superstructure. For this reason, when analyzing propulsion systems, it is very important to correctly map the characteristics of the boundary conditions - the stiffness and damping characteristics of the foundation of the propulsion system in the ship's hull. In this part, an analysis of the propulsion system foundation characteristics was carried out. The stiffness of the support points of the power transmission system in the ship's hull was determined. Main engine body stiffness was calculated at main bearing mounting locations. Stiffness characteristics of the crankshaft were analyzed together with the determination of its coupling coefficients. Next, a multi-variant analysis of the shaft line alignment was made, taking into account the ship's hull compliance, bearing clearances and the relative deflection line of the ship's shaft and hull.

The calculation method is based on the finite element method implemented in the Patran-Nastran software, the popular commercial software. The numerical model is applied to two types of container ships with different sizes: the first for the medium-sized container ship 2000 TEU with length 182.85 m, width 28 m, MAN B&W 8S70MC-C engine with the power of 24840 kW and a rotational speed of 91 rpm and a five-wing propeller with a diameter of 7.6 m, the second, the second for large size container ship 11400 TEU with parameters length 364.7 m, width 45.6 m, MAN B&W 12K98ME-C (Mk7) engine with the power of 72240 kW and a rotational speed of 100 rpm and a six-wing propeller with a diameter of 8.9 m. From there, evaluate the accuracy of the applied numerical modelling method, as well as evaluate the influence of the numerical modelling method on the accuracy of the analysis results, the applicability to all types of other ships. The author also conducted the shaft line alignment analysis of the typical propulsion system of the medium container ship of 2000 TEU, using the finite element method implemented in the Patran - Nastran software platform, verifying and evaluating the accuracy of the numerical method already applied. Evaluation of wide applicability of numerical modelling method, improve the reliability and confidence of engineers when applying numerical modelling methods for the analysis of ship structures.

### 5.1. Stiffness characteristics of the ship's hull

In this section, the foundation stiffness of the ship propulsion system and the double bottom is determined for the medium-sized container ships of 2000 TEU and the large-sized container ship of 11400 TEU. The hull beam is often more flexible than the shaft line. The reason is the aspiration of designers to optimize the weight and cost of the hull structure while increasing the power of the propulsion system. For this reason, the correct determination of the stiffness characteristics of the propulsion's bearing is very important due to the accuracy of the calculation of the static alignment of the shaft lines and the flexural vibrations and even longitudinal. The determination of static-dynamic stiffness characteristics of the propulsion's bearing can be successfully carried out with the help of good the finite element method. For dynamic calculations (forced vibrations) the direct method was used. In this case, first, determine the frequencies and forms of natural vibrations. The natural vibration frequency and vibration modes of medium-sized container ship of 2000 TEU and large container ship of 11400 TEU were determined in chapter 4. For the types of propulsion systems discussed, the predominant switching frequencies do not exceed 20 Hz. Therefore, in the calculation of frequency response to determine the stiffness of the bearing foundation, the frequency range is limited to this frequency level.

The author has calculated stiffness of the bearing foundation of the shaft line and the double bottom. Computational analysis of different types of ships was carried out using various mathematical models. Ship power transmission systems (crankshaft, shaft line, and propeller) are modelled as isolated from the ship's hull. The calculations were carried out for medium-sized container ship 2000 TEU, length 182.85 m, width 28 m, MAN B&W 8S70MC-C engine with the power of 24840 kW and a rotational speed of 91 rpm and a five-wing propeller with a diameter of 7.6 m) and large-sized container ship 11400 TEU, length 364.7 m, width 45.6 m, MAN B&W 12K98ME-C(Mk7) engine with the power of 72240 kW and a rotational speed of 100 rpm and a six-wing propeller with a diameter of 8.9 m using FEM model of the entire aft part of the hull. Most often it is sufficient to model the entire aft part of the hull along with the deckhouse and funnel of the ship. A medium-sized container model 2000 TEU, 182.85 m length with support positions for stiffness calculation is shown in Fig. 5.2. A large container model 11400 TEU, 364.7 m length with support positions for stiffness calculation is shown in Fig. 5.3.

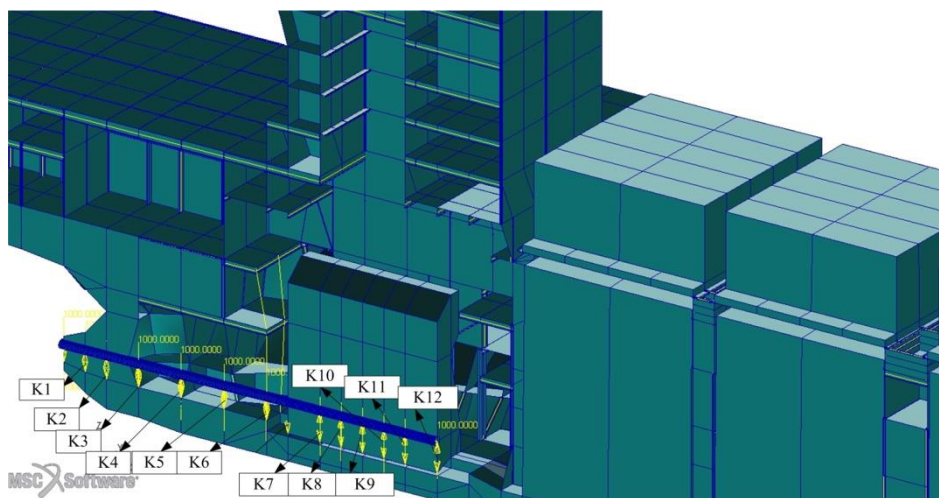


Fig. 5.2. Cross-section of the container ship 2000 TEU with the support positions

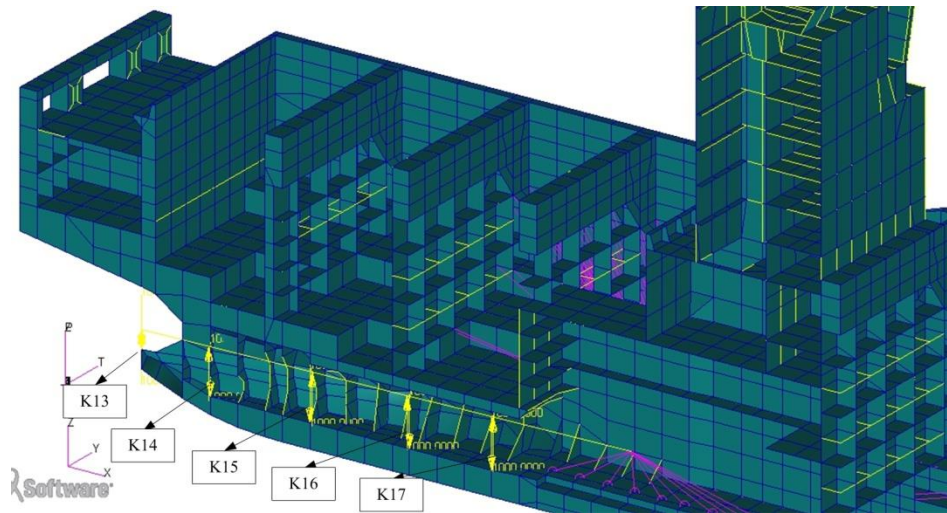


Fig. 5.3. Cross-section of the container ship 11400 TEU with the support positions

Calculations of the stiffness of the foundation bearing were carried out for some of the support points of the propulsion system in the ship's hull: the stern tube bearing, intermediate bearings and the main engine bearings. When determining the stiffness characteristics of the propulsion system foundation of the container ship 2000 TEU, the assumption was made to analyze the stern part of the ship's hull. Forces were applied in two directions (vertical and horizontal) on the stern bearing and in the geometrical center of the intermediate bearing and on all main bearings of the engine. The excitation frequency was changed in steps of 1 Hz, supplemented with all-natural frequencies in the range of 1÷20 Hz. Particular attention was paid to the basic frequencies of the propulsion system excitation. With the medium-sized container ship 2000 TEU has the nominal rotational speed of the propulsion system is 91 rpm, five-wing propeller, and eight-cylinder engine, so 12.13 Hz is the engine's main excitation frequency, the propeller's main excitation frequency is equal 7.58 Hz. The model of the container ship 2000 TEU, 182.85 m length is presented in Fig. 5.2. The model contains 19000 degrees of freedom. The excitation forces are placed at the stern tube bearing (K1), intermediate bearing no.1 (K2), intermediate bearing no.2 (K3), intermediate bearing no.3 (K4), intermediate bearing no.4 (K5) intermediate bearing no.5 (K6), from the side of the propeller. Some of the forms of forced vibrations by horizontal and vertical forces, for basic excitation frequencies, are shown in Fig. 5.4÷5.6.

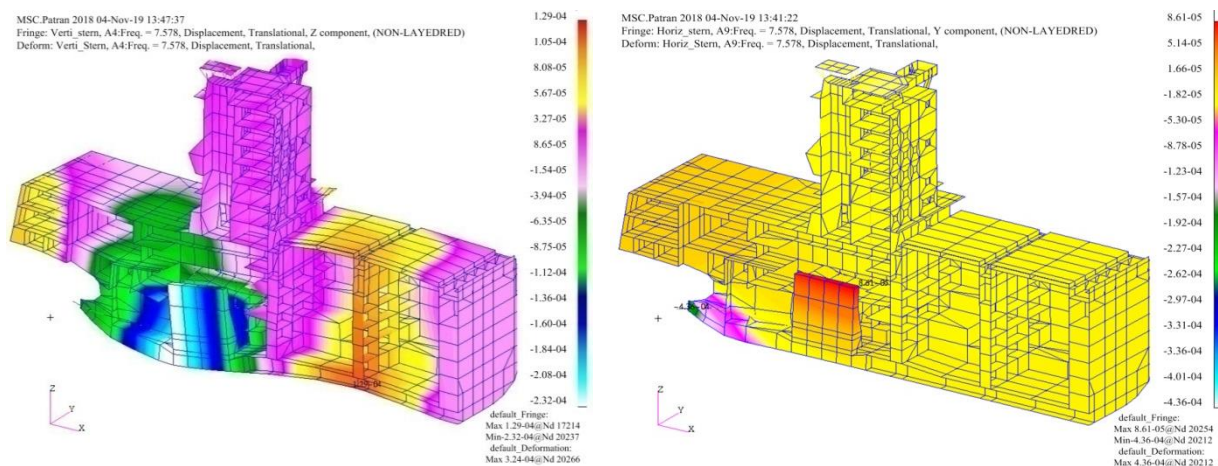


Fig. 5.4. Amplitudes of vibrations forced by the first excitation frequency of the propeller at the stern bearing according to horizontal and vertical

## 5. THE OPERATING PARAMETER CHARACTERISTICS OF THE DRIVE SYSTEM

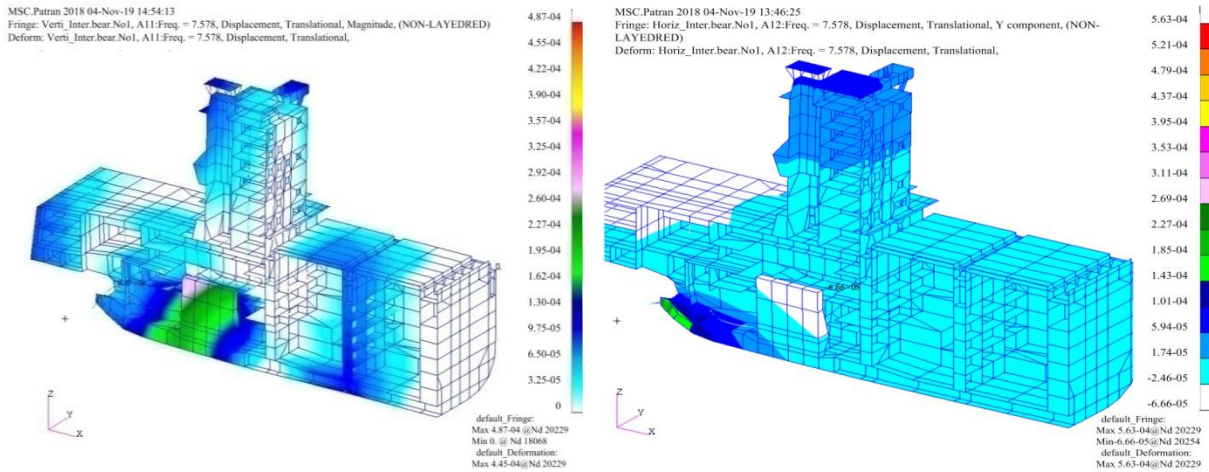


Fig. 5.5. Amplitudes of vibrations forced by the first excitation frequency of the propeller at the intermediate bearing No.1 according to horizontal and vertical

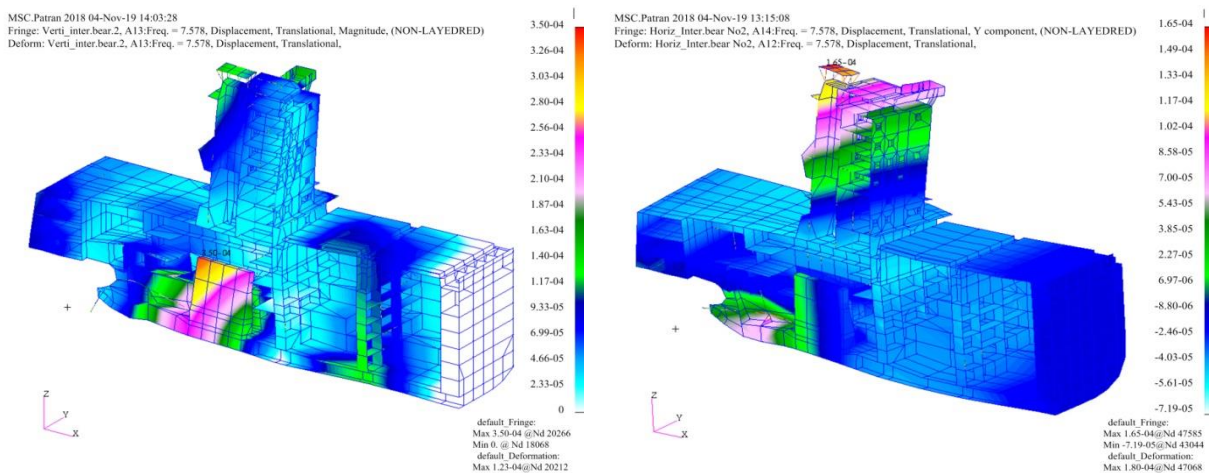


Fig. 5.6. Amplitudes of vibrations forced by the first excitation frequency of the propeller at the intermediate bearing No.2 according to horizontal and vertical

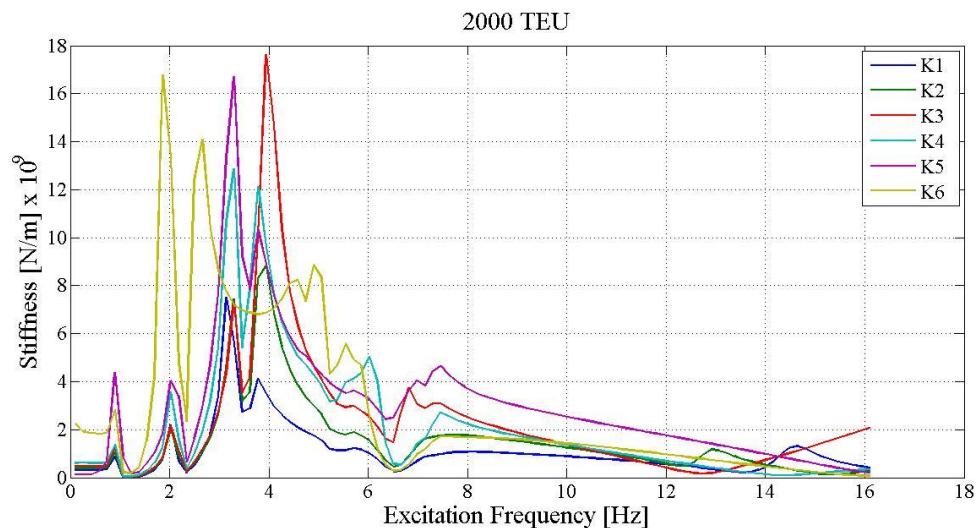


Fig. 5.7. Vertical, dynamic stiffness characteristics of the container ship 2000 TEU

The Fig. 5.7 and Fig. 5.9 show the vertical and horizontal dynamic stiffness characteristics of the foundation of the propulsion system of the container ship 2000 TEU at the stern tube bearing, intermediate bearings. While Fig. 5.8 and Fig. 5.10 present the stiffness characteristics of these points at basic excitation frequencies of the propulsion system according to the length of the shaft line. In Tab. 5.1 and 5.2, Fig. 5.11÷5.12 summarizes the

numerical values of the stiffness of all bearings of the power transmission system for the basic excitation frequencies of the propulsion system of the container ship 2000 TEU.

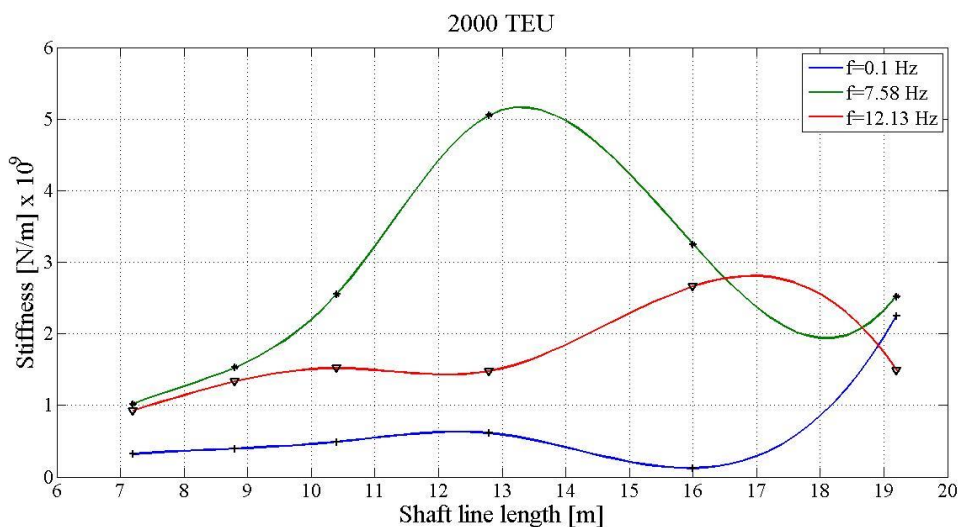


Fig. 5.8. Vertical, stiffness characteristics of the container ship 2000 TEU at basic excitation frequencies  $f = 0.1, 7.58$  and  $12.13$  Hz

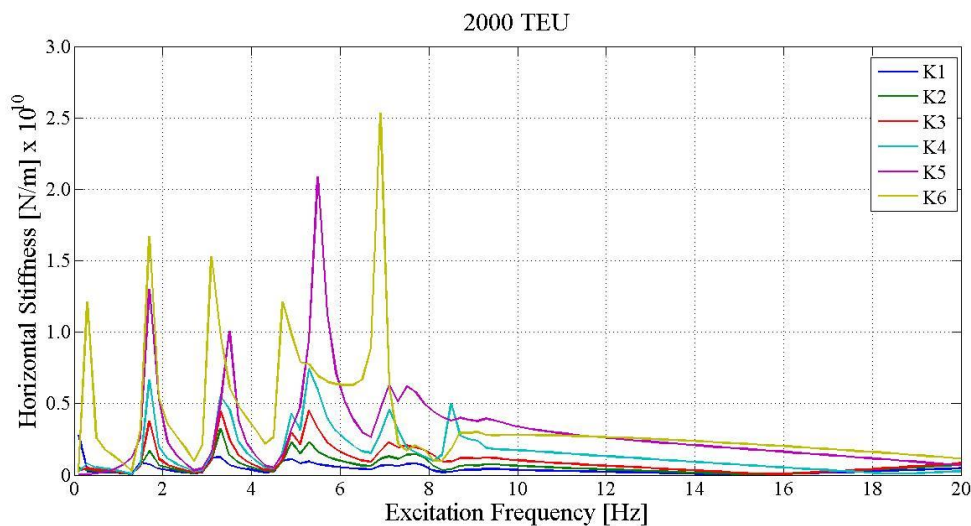


Fig. 5.9. Horizontal, stiffness characteristics of the container ship 2000 TEU

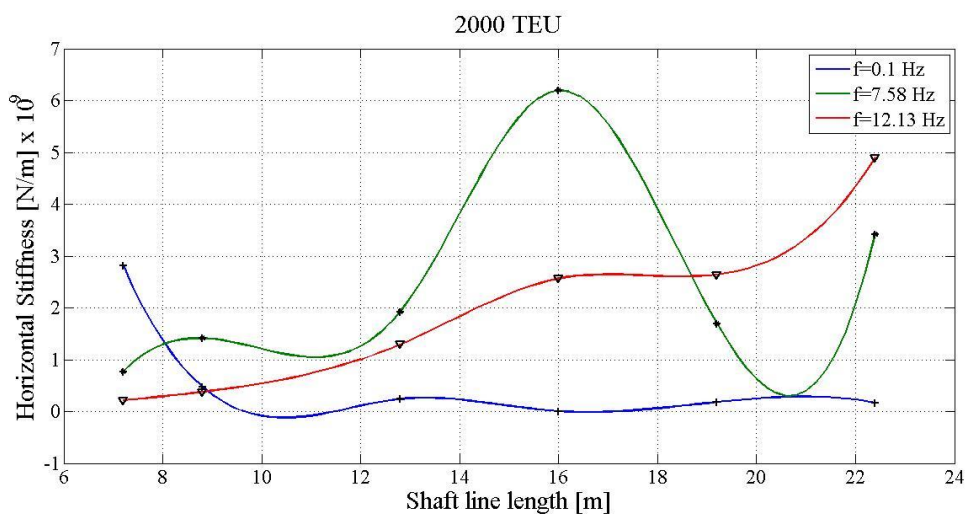


Fig. 5.10. Horizontal stiffness characteristics of the container ship 2000 TEU at basic excitation frequencies  $f = 0.1, 7.58$  and  $12.13$  Hz

## 5. THE OPERATING PARAMETER CHARACTERISTICS OF THE DRIVE SYSTEM

*Tab. 5.1. Vertical Stiffness of the bearing foundation of the container ship 2000 TEU*

STIFFNESS FOR FORCED VIBRATIONS						
Frequency [Hz]	Bearings					
	Stern - K1	Intermediate No.1 - K2	Intermediate No.2 - K3	Intermediate No.3 - K4	Intermediate No.4 - K5	Intermediate No.5 - K6
	Stiffness [N/m]					
0.1	$0.319 \times 10^9$	$0.395 \times 10^9$	$0.49 \times 10^9$	$0.613 \times 10^9$	$0.123 \times 10^9$	$2.25 \times 10^9$
7.58	$1.02 \times 10^9$	$1.53 \times 10^9$	$2.55 \times 10^9$	$5.05 \times 10^9$	$3.25 \times 10^9$	$2.52 \times 10^9$
12.13	$0.925 \times 10^9$	$1.33 \times 10^9$	$1.52 \times 10^9$	$1.48 \times 10^9$	$2.66 \times 10^9$	$1.49 \times 10^9$

*Tab. 5.2. Horizontal Stiffness of the bearing foundation of the container ship 2000 TEU*

STIFFNESS FOR FORCED VIBRATIONS						
Frequency [Hz]	Bearings					
	Stern - K1	Intermediate No.1 - K2	Intermediate No.2 - K3	Intermediate No.3 - K4	Intermediate No.4 - K5	Intermediate No.5 - K6
	Stiffness [N/m]					
0.1	$2.82 \times 10^9$	$0.473 \times 10^9$	$0.296 \times 10^9$	$0.239 \times 10^9$	$0.04 \times 10^9$	$0.179 \times 10^9$
7.58	$0.765 \times 10^9$	$1.41 \times 10^9$	$2.06 \times 10^9$	$1.92 \times 10^9$	$6.2 \times 10^9$	$1.7 \times 10^9$
12.13	$0.213 \times 10^9$	$0.367 \times 10^9$	$0.63 \times 10^9$	$1.3 \times 10^9$	$2.56 \times 10^9$	$2.64 \times 10^9$

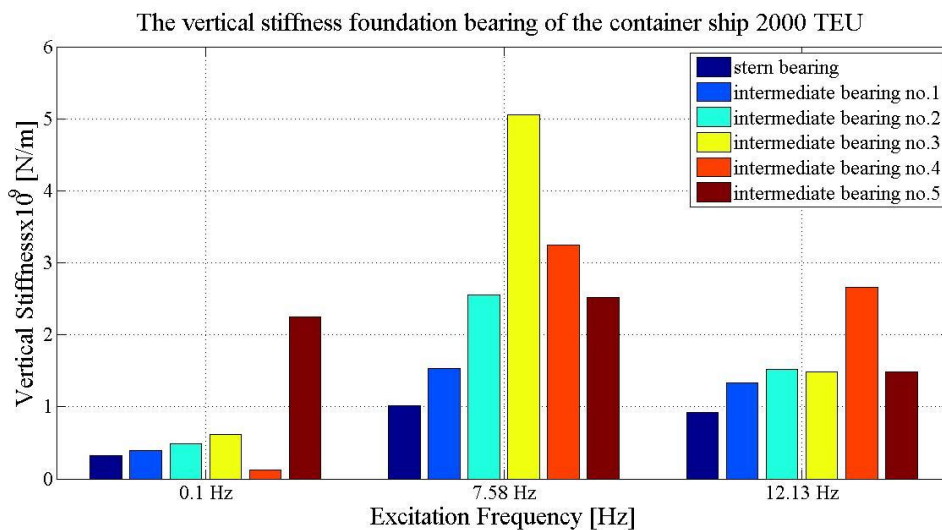


*Fig. 5.11. Vertical stiffness of container ship 2000 TEU for shaft line foundation*

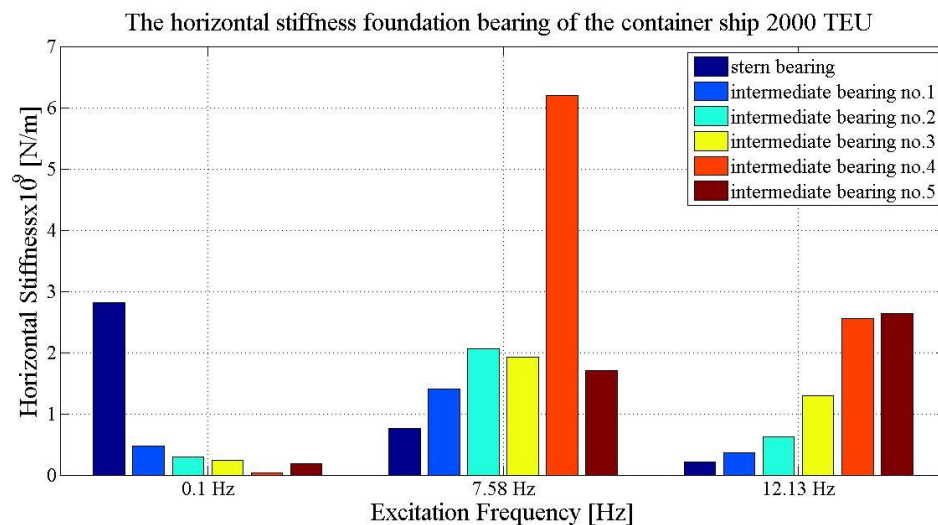


*Fig. 5.12. Horizontal stiffness of the container ship 2000 TEU for shaft line foundation*

From the data, Fig. 5.11÷5.12 and Tab. 5.1÷5.2, the stiffness of bearings at support positions has an approximate form such as a quadratic polynomial, peaking at a number of support positions. Vertical stiffness of foundation of the bearing peaked at intermediate bearing number 3 at the excitation frequency 7.58 Hz with  $K_4 = 5.05 \times 10^9$  N/m, and horizontal stiffness of foundation of the bearing peaked at the intermediate bearing number 4 at the excitation frequency 7.58 Hz with  $K_5 = 6.2 \times 10^9$  N/m, respectively.

Calculations of the stiffness of the main bearing were carried out for the support points as main bearing no.1 (K7), main bearing no.2 (K8), main bearing no.3 (K9), main bearing no.4 (K10), main bearing no.5 (K11), main bearing no.6 (K12) for the main engine, from the side of the propeller. Dynamic, vertical and horizontal stiffness characteristics of the main bearing foundation for the main engine are shown in Fig. 5.13÷5.14.

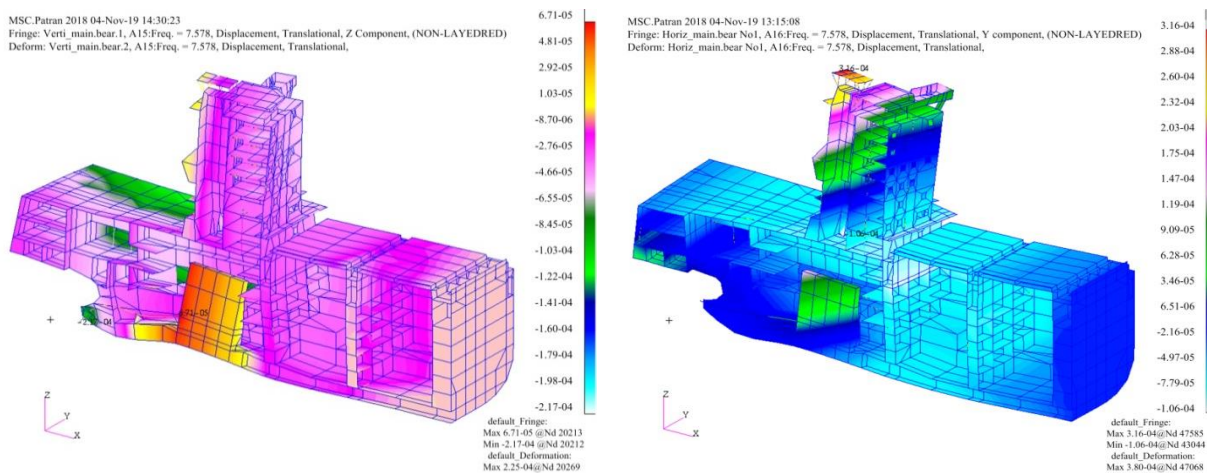


Fig. 5.13. Amplitudes of vibrations forced by the first excitation frequency of the propeller at the main bearing No.1 according to horizontal and vertical

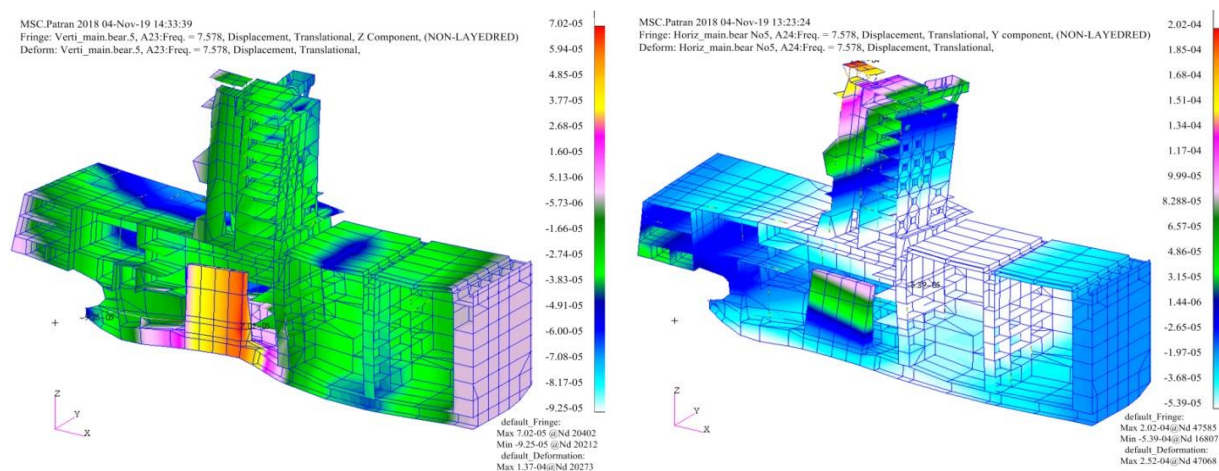


Fig. 5.14. Amplitudes of vibrations forced by the first excitation frequency of the propeller at the main bearing No.5 according to horizontal and vertical

The Fig. 5.15 and Fig. 5.17 show the vertical and horizontal dynamic stiffness characteristics of the main bearing of the container ship 2000 TEU. While Fig. 5.16 and Fig. 5.18 present the stiffness characteristics of these points at basic excitation frequencies of the propulsion system according to the length of the shaft line. In Tab. 5.3÷5.4, Fig. 5.19÷5.20 summarizes the numerical values of the stiffness of main bearings for the basic excitation frequencies of the propulsion system of the container ship 2000 TEU.

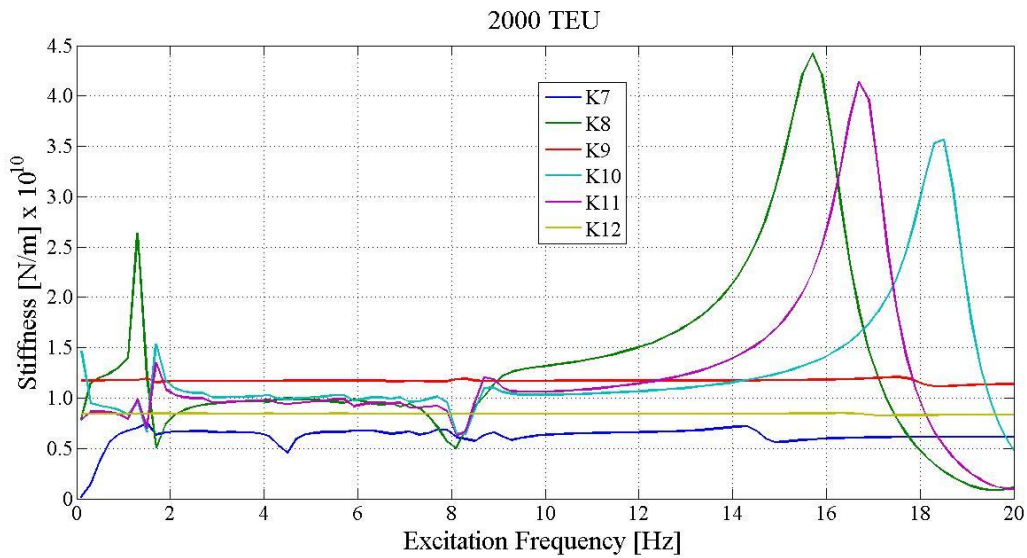


Fig. 5.15. Vertical, dynamic stiffness characteristics of the container ship 2000 TEU for main bearings

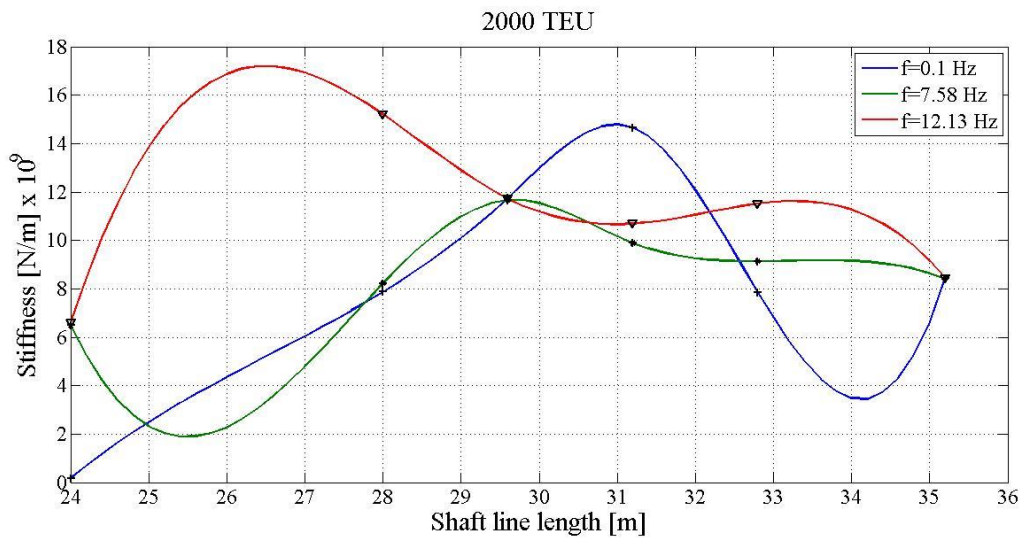


Fig. 5.16. Vertical, dynamic stiffness characteristics of the container ship 2000 TEU for main bearings at basic excitation frequencies  $f = 0.1, 7.58$  and  $12.13$  Hz

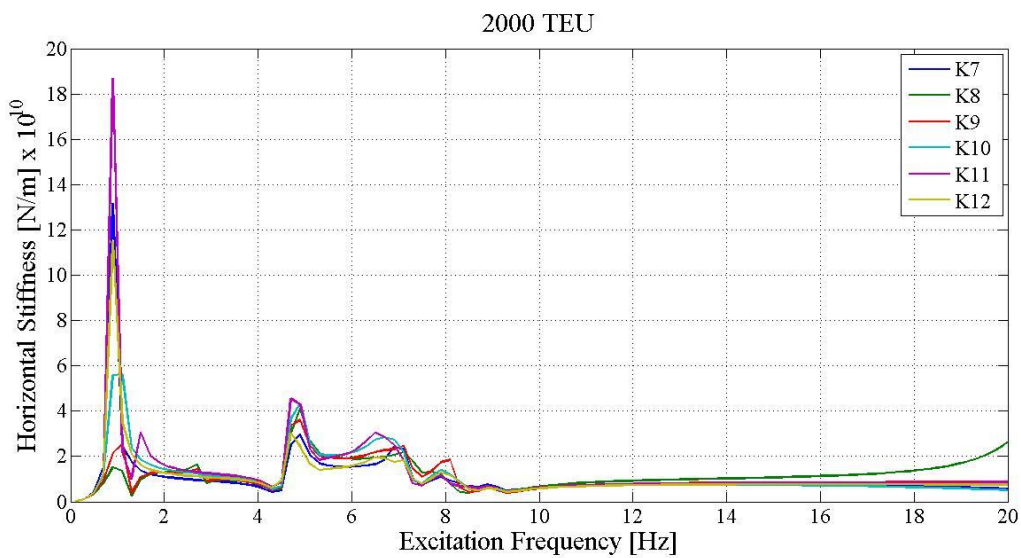


Fig. 5.17. Horizontal, dynamic stiffness characteristics of the container ship 2000 TEU for main bearings

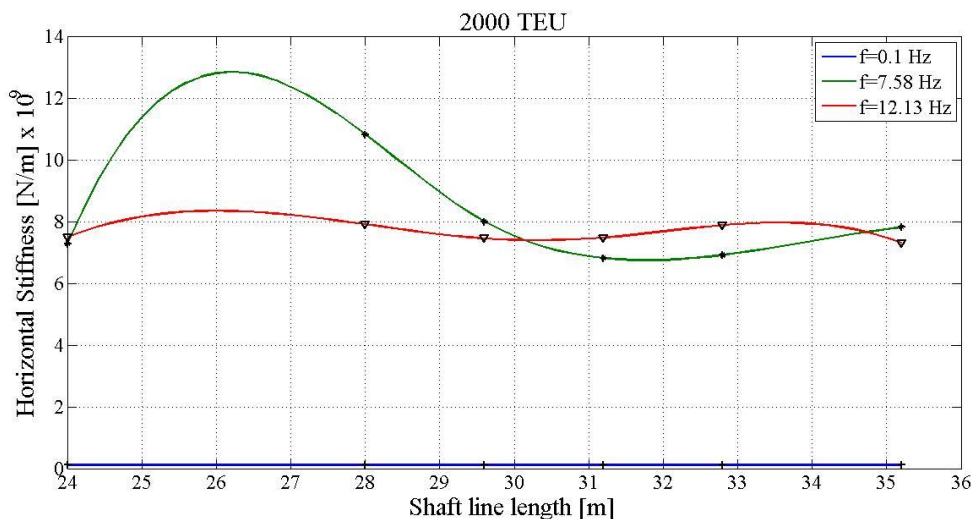


Fig. 5.18. Horizontal, dynamic stiffness characteristics of the container ship 2000 TEU for main bearings at  $f = 0.1$  Hz,  $f = 7.58$  Hz,  $f = 12.13$  Hz

Tab. 5.3. Vertical Stiffness of the main bearing of the container ship 2000 TEU

STIFFNESS FOR FORCED VIBRATIONS						
Frequency [Hz]	Bearings					
	Bearing No.1 – K7	Bearing No.2 – K8	Bearing No.3 – K9	Bearing No.4 – K10	Bearing No.5 – K11	Bearing No.6 – K12
	Stiffness [N/m]					
0.1	$0.164 \times 10^9$	$7.87 \times 10^9$	$11.75 \times 10^9$	$14.66 \times 10^9$	$7.84 \times 10^9$	$8.44 \times 10^9$
7.58	$6.48 \times 10^9$	$8.22 \times 10^9$	$11.7 \times 10^9$	$9.89 \times 10^9$	$9.13 \times 10^9$	$8.42 \times 10^9$
12.13	$6.62 \times 10^9$	$15.19 \times 10^9$	$11.72 \times 10^9$	$10.68 \times 10^9$	$11.51 \times 10^9$	$8.43 \times 10^9$

Tab. 5.4. Horizontal Stiffness of the main bearing of the container ship 2000 TEU

STIFFNESS FOR FORCED VIBRATIONS						
Frequency [Hz]	Bearings					
	Bearing No.1 – K7	Bearing No.2 – K8	Bearing No.3 – K9	Bearing No.4 – K10	Bearing No.5 – K11	Bearing No.6 – K12
	Stiffness [N/m]					
0.1	$0.118 \times 10^9$	$0.116 \times 10^9$	$0.117 \times 10^9$	$0.116 \times 10^9$	$0.115 \times 10^9$	$0.115 \times 10^9$
7.58	$7.27 \times 10^9$	$10.82 \times 10^9$	$7.99 \times 10^9$	$6.81 \times 10^9$	$6.91 \times 10^9$	$7.81 \times 10^9$
12.13	$7.49 \times 10^9$	$7.90 \times 10^9$	$7.45 \times 10^9$	$7.48 \times 10^9$	$7.88 \times 10^9$	$7.31 \times 10^9$

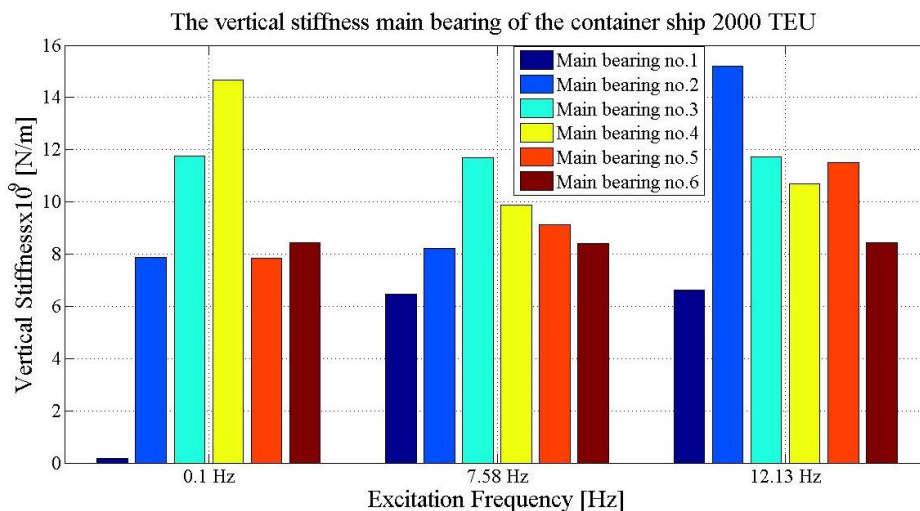


Fig. 5.19. Vertical stiffness of container ship 2000 TEU for main bearing

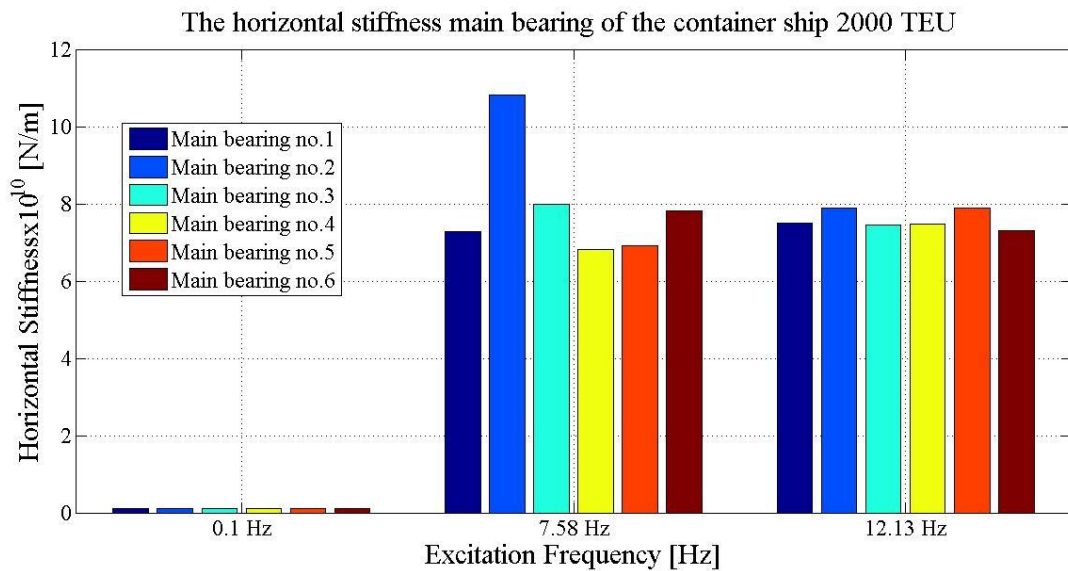


Fig. 5.20. Horizontal stiffness of container ship 2000 TEU for main bearing

From the figures, Fig. 5.19÷5.20 and Tab. 5.3÷5.4, the stiffness of the main bearings of diesel engines has a similarity value between support positions when the excitation frequency changes. There are some support positions the value of the magnitude of the bearing stiffness is significantly different from the rest. Vertical stiffness of the bearing peaked at the main bearing number 2 at the excitation frequency 12.13 Hz with  $K_8 = 15.19 \times 10^9$  N/m and horizontal stiffness of the bearing peaked at the main bearing number 2 at the excitation frequency 7.58 Hz with  $K_8 = 10.82 \times 10^9$  N/m, respectively.

The container ship 11400 TEU has the nominal rotational speed of the propulsion system is 100 rpm, six-wing propeller, and twelve-cylinder engine, so 20 Hz is the engine’s main excitation frequency, the propeller’s main excitation frequency is equal 10 Hz. The model of the container ship 11400 TEU, 364.7 m length is presented in Fig. 5.2. The model contains 154170 degrees of freedom. The excitation forces are placed at the stern tube bearing (K13) and intermediate bearing no.1 (K14), intermediate bearing no.2 (K15), intermediate bearing no.3 (K16), intermediate bearing no.4 (K17). The form of forced vibrations by horizontal and vertical forces, for basic excitation frequencies, is shown in Fig. 5.21.

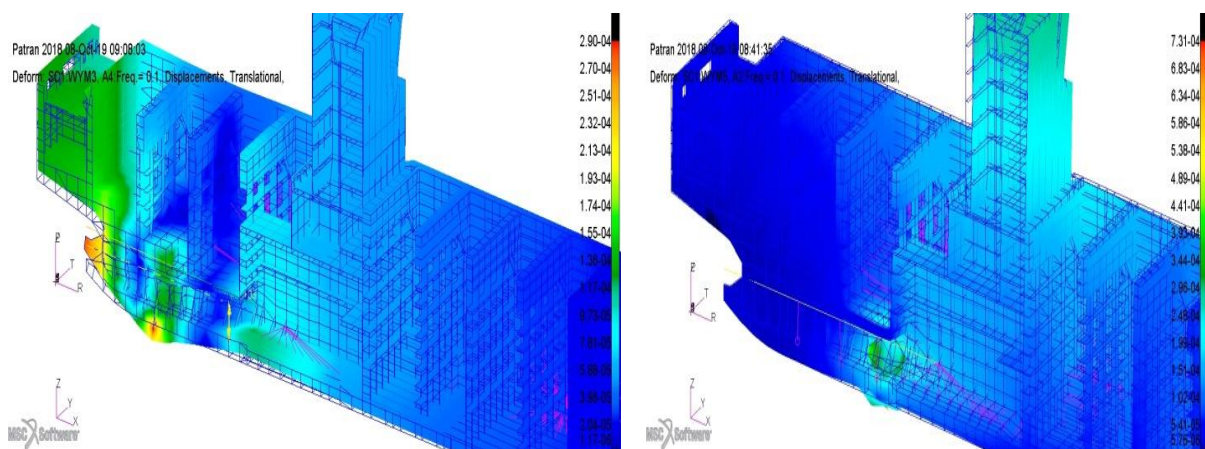


Fig. 5.21. Amplitudes of forced vibrations of the container ship 11400 TEU

The Fig. 5.22 and Fig. 5.24 show the vertical and horizontal dynamic stiffness characteristics of the foundation bearing of the container ship 11400 TEU. While Fig. 5.23 and Fig. 5.25 present the stiffness characteristics of these points at basic excitation

frequencies of the propulsion system according to the length of the shaft line. In Tab. 5.5÷5.6 and Fig. 5.26÷5.27 summarize the numerical values of the stiffness of foundation bearings for the basic excitation frequencies of the propulsion system of the container ship 11400 TEU.

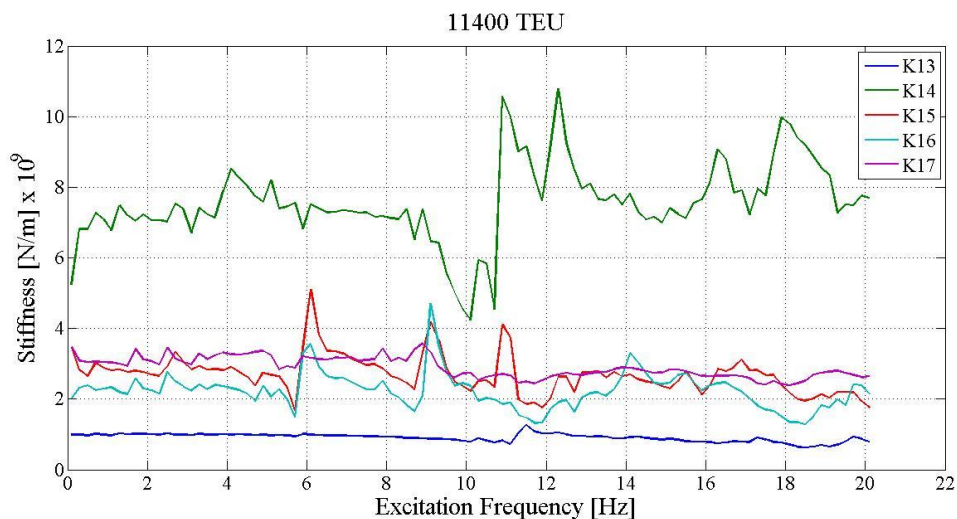


Fig. 5.22. Vertical, dynamic stiffness characteristics of the container ship 11400 TEU

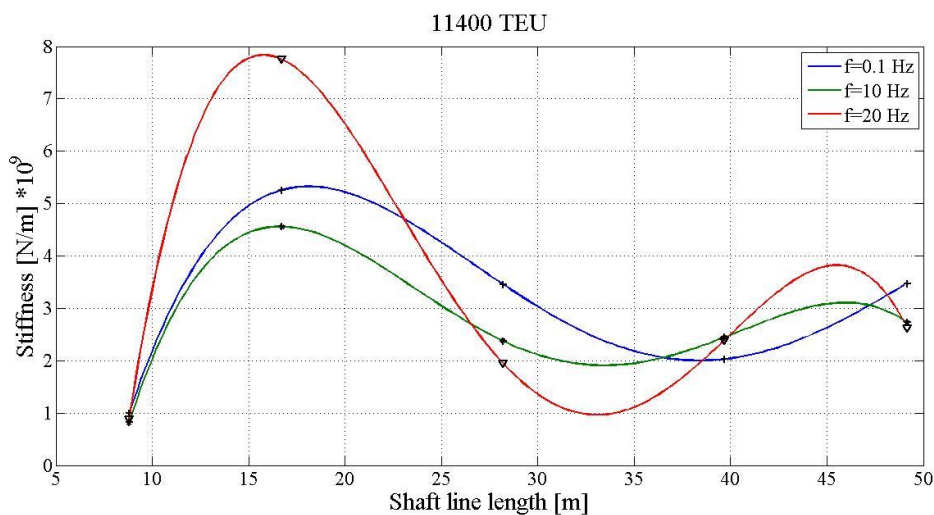


Fig. 5.23. Vertical, dynamic stiffness characteristics of the container ship 11400 TEU at  $f = 0.1$  Hz,  $f = 10$  Hz,  $f = 20$  Hz

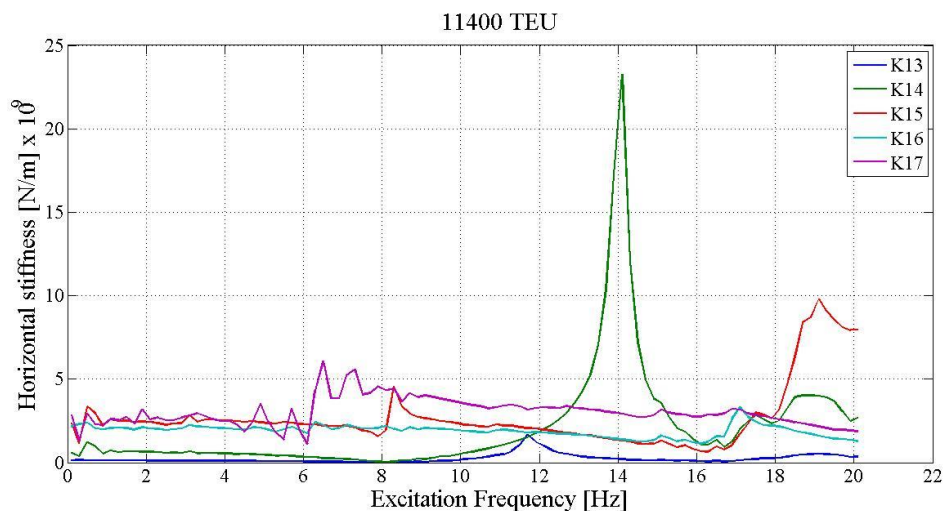


Fig. 5.24. Horizontal, dynamic stiffness characteristics of the container ship 11400 TEU

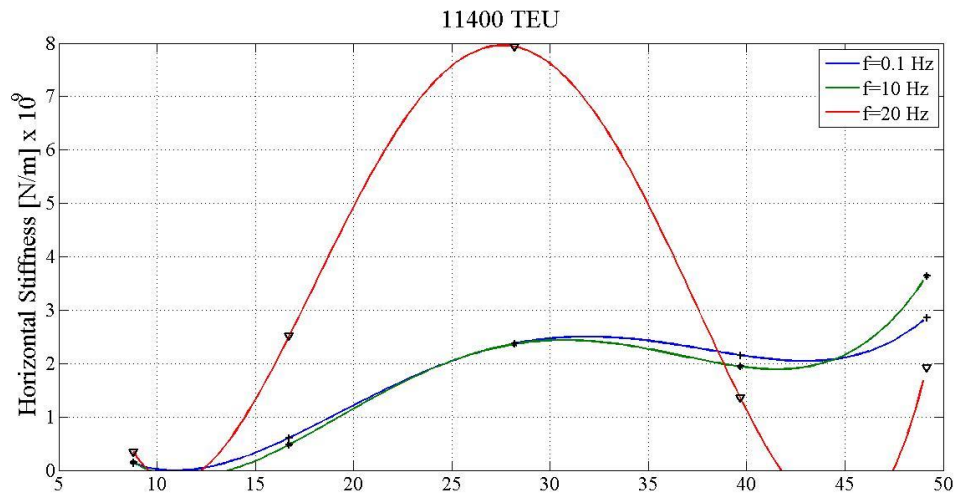


Fig. 5.25. Horizontal, dynamic stiffness characteristics of the container ship 11400 TEU at  $f = 0.1 \text{ Hz}$ ,  $f = 10 \text{ Hz}$ ,  $f = 20 \text{ Hz}$

Tab. 5.5. Vertical Stiffness of the foundation bearing of the container ship 11400 TEU

STIFFNESS FOR FORCED VIBRATIONS					
Frequency [Hz]	Bearings				
	Stern tube K13	Intermediate No.1 – K14	Intermediate No.2 – K15	Intermediate No.3 – K16	Intermediate No.4 – K17
	Stiffness [N/m]				
0.1	$0.99 \times 10^9$	$5.26 \times 10^9$	$3.45 \times 10^9$	$2.03 \times 10^9$	$3.47 \times 10^9$
10	$0.817 \times 10^9$	$4.56 \times 10^9$	$2.37 \times 10^9$	$2.44 \times 10^9$	$2.73 \times 10^9$
20	$0.877 \times 10^9$	$7.75 \times 10^9$	$1.94 \times 10^9$	$2.39 \times 10^9$	$2.62 \times 10^9$

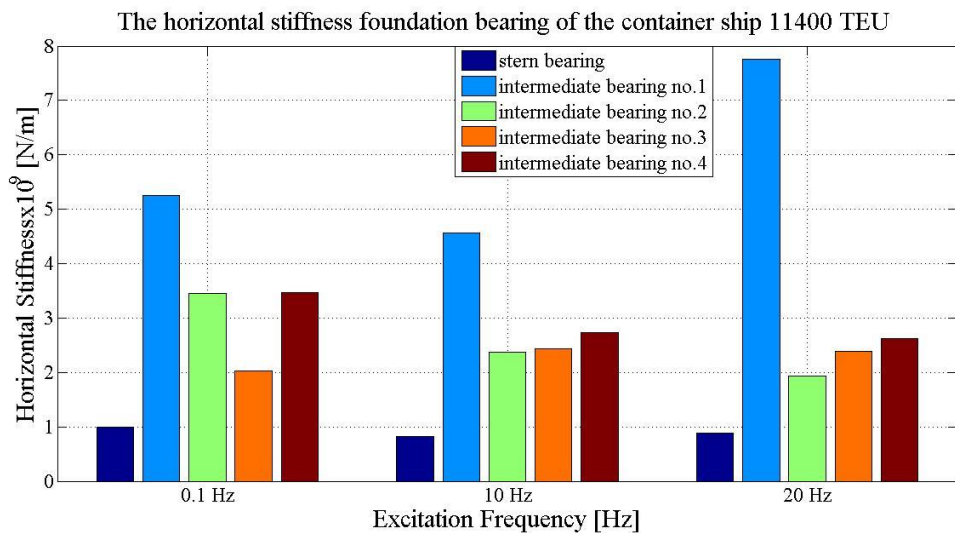


Fig. 5.26. Vertical stiffness of container ship 11400 TEU for shaft line foundation

Tab. 5.6. Horizontal Stiffness of the foundation bearing of the container ship 11400 TEU

STIFFNESS FOR FORCED VIBRATIONS					
Frequency [Hz]	Bearings				
	Stern tube K13	Intermediate No.1 – K14	Intermediate No.2 – K15	Intermediate No.3 – K16	Intermediate No.4 – K17
	Stiffness [N/m]				
0.1	$0.126 \times 10^9$	$0.609 \times 10^9$	$2.38 \times 10^9$	$2.16 \times 10^9$	$2.86 \times 10^9$
10	$0.142 \times 10^9$	$0.479 \times 10^9$	$2.36 \times 10^9$	$1.94 \times 10^9$	$3.64 \times 10^9$
20	$0.339 \times 10^9$	$2.51 \times 10^9$	$7.94 \times 10^9$	$1.35 \times 10^9$	$1.91 \times 10^9$

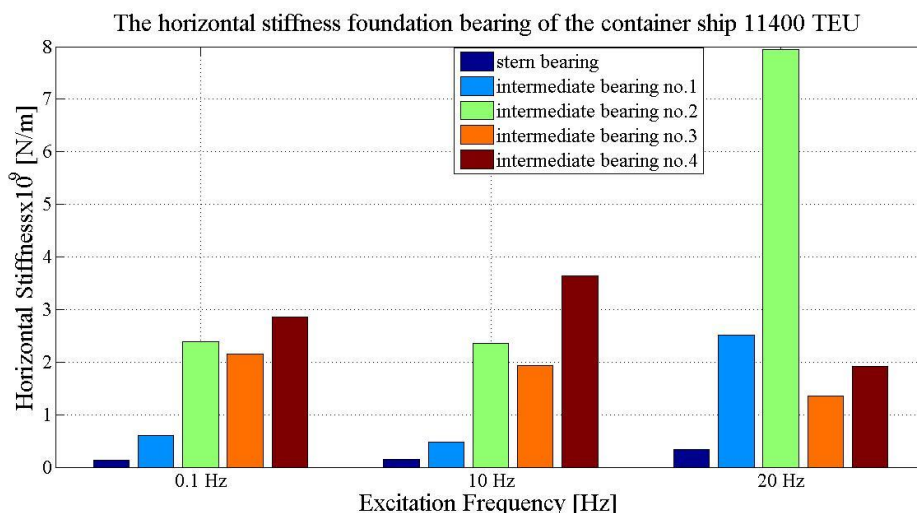


Fig. 5.27. Bar graph for horizontal stiffness of container ship 11400 TEU for shaft line foundation

From Fig. 5.26÷5.27 and Tab. 5.5÷5.6, the stiffness of the foundation bearings of large container ships capacity of 11400 TEU has the highest value at intermediate bearing No.1, at  $K_{14} = 7.75 \times 10^9$  N/m corresponds to the excitation frequency value of 20 Hz, in the vertical direction. In the horizontal direction, the maximum stiffness value is at intermediate bearing No.2,  $K_{15} = 7.94 \times 10^9$  N/m, which corresponds to the excitation frequency of 20 Hz.

Next, the author proceeds to determine the local stiffness of the double bottom at locations corresponding to the locations calculated for the stiffness of the foundation bearings. Evaluate the stiffness of the double bottom (local stiffness) with the stiffness of the foundation bearings at the support positions (considered as whole stiffness). First, with the medium-sized container ship 2000 TEU, the model and the location of the stiffness calculation of the double bottom are described in Fig. 5.28. The result of the local stiffness calculation is summarized in Tab. 5.7 and shown in Fig. 5.29.

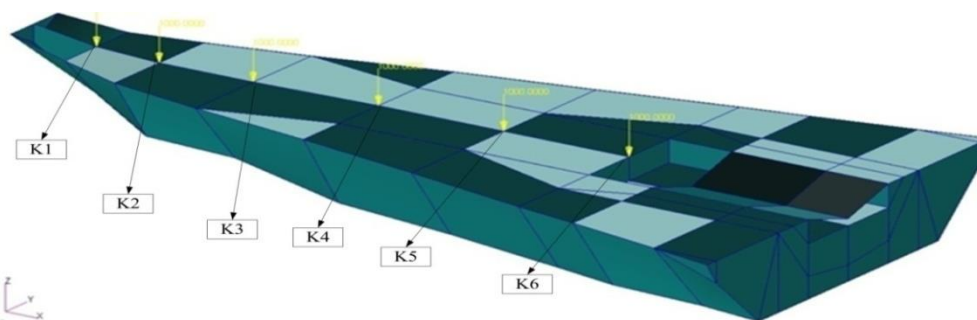


Fig. 5.28. Model and support positions for local stiffness calculation of container ship 2000 TEU

Tab. 5.7. Local stiffness of the container ship 2000 TEU at the basic excitation frequencies

Position	Excitation Frequencies [Hz]			
	F = 7.58 Hz		F = 12.13 Hz	
	Whole hull	Local hull	Whole hull	Local hull
K1 - Intermediate bearing No.1	$1.53 \times 10^9$	$1.83 \times 10^9$	$1.33 \times 10^9$	$1.43 \times 10^9$
K2 - Intermediate bearing No.2	$2.55 \times 10^9$	$2.75 \times 10^9$	$1.52 \times 10^9$	$2.31 \times 10^9$
K3 - Intermediate bearing No.3	$5.05 \times 10^9$	$3.07 \times 10^9$	$1.48 \times 10^9$	$3.64 \times 10^9$
K4 - Intermediate bearing No.4	$3.25 \times 10^9$	$3.03 \times 10^9$	$2.66 \times 10^9$	$5.47 \times 10^9$
K5 - Intermediate bearing No.5	$2.52 \times 10^9$	$2.88 \times 10^9$	$1.49 \times 10^9$	$6.78 \times 10^9$
K6 - Intermediate bearing No.6	$7.75 \times 10^9$	$2.66 \times 10^9$	$3.46 \times 10^9$	$5.57 \times 10^9$

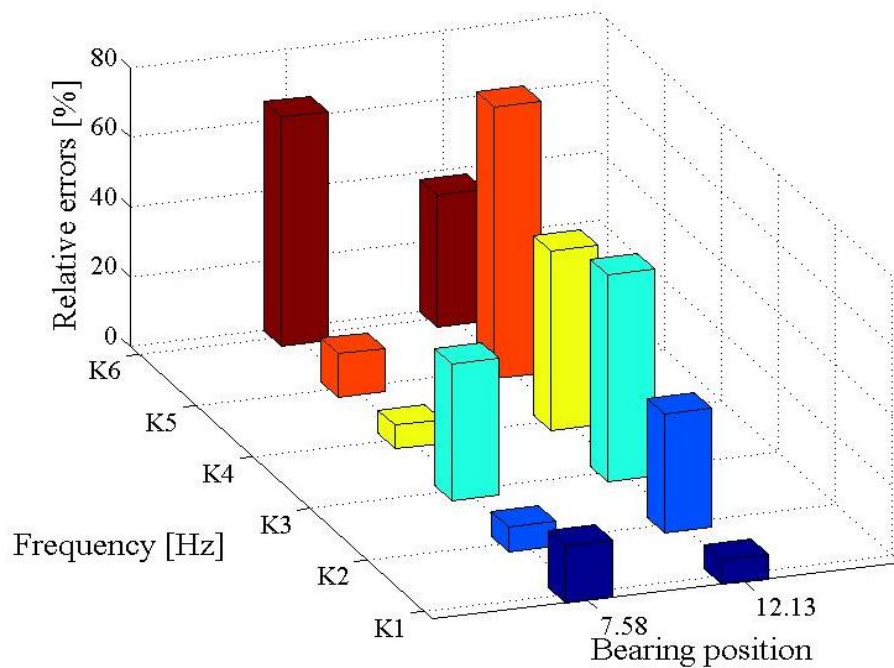


Fig. 5.29. Compare between local stiffness and whole stiffness of the container ship 2000 TEU at  $f = 7.58$  Hz and  $12.13$  Hz

The stiffness of the hull is usually more flexible than the ship's shaft system. With current ship structures, the bottom of the ship is often constructed as a double bottom to increase the stiffness of the structures. From the data in Tab. 5.7 and Fig. 5.29, with the first excitation frequency of propeller  $f = 7.58$  Hz, the local stiffness of the double bottom and the bearing stiffness is higher at some positions, such as K3 - intermediate bearings No.3 and K6 - intermediate bearings No.6, respectively 39.21% and 65.68%. At the first excitation frequency of the diesel engine  $f = 12.13$  Hz, the local stiffness of the double bottom and the stiffness of the bearing have higher deviations in some positions such as K3 - intermediate bearings No.3, K4 - Intermediate bearing No. 4, K5 - Intermediate bearing No.5, respectively 59.34%, 51.37%, and 78.02%. These locations have a large deviation because in these areas bulkheads are not modelled in simple models.

The large-sized container ship 11400 TEU, the model and the location of the stiffness calculation of the double bottom are described in Fig. 5.30. The result of the local stiffness calculation is summarized in Tab. 5.8 and shown in Fig. 5.31.

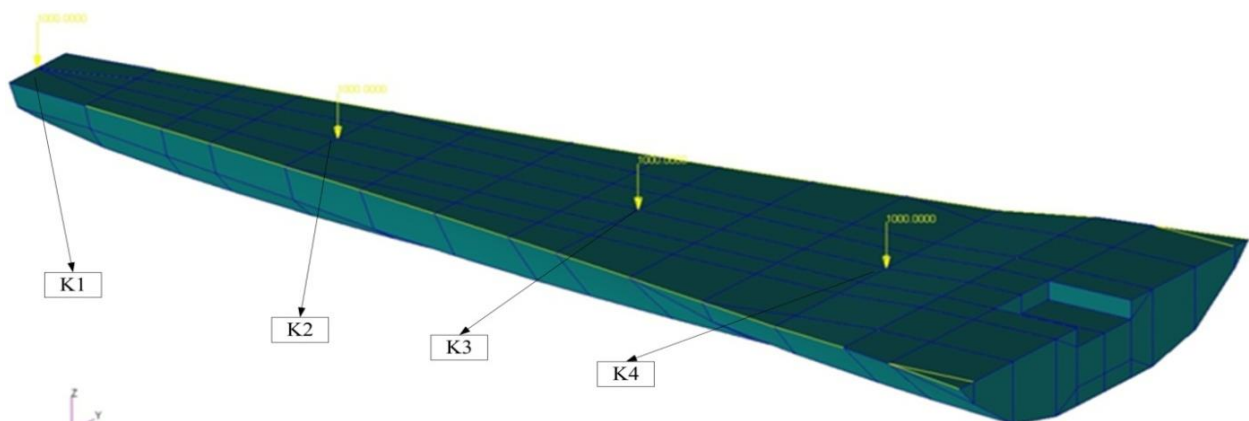


Fig. 5.30. Model and support positions for local stiffness calculation of container ship 11400 TEU

Tab. 5.8. Local stiffness of the container ship 11400 TEU at the basic excitation frequencies

Position	Excitation Frequencies [Hz]			
	F = 10 Hz		F = 20 Hz	
	Whole hull	Local hull	Whole hull	Local hull
	Vertical Stiffness [N/m]			
K1 - Intermediate bearing No.1	$4.56 \times 10^9$	$7.01 \times 10^9$	$7.75 \times 10^9$	$4.58 \times 10^9$
K2 - Intermediate bearing No.2	$2.37 \times 10^9$	$1.02 \times 10^9$	$1.94 \times 10^9$	$2.96 \times 10^9$
K3 - Intermediate bearing No.3	$2.44 \times 10^9$	$1.85 \times 10^9$	$2.39 \times 10^9$	$2.91 \times 10^9$
K4 - Intermediate bearing No.4	$2.73 \times 10^9$	$1.63 \times 10^9$	$2.62 \times 10^9$	$3.82 \times 10^9$

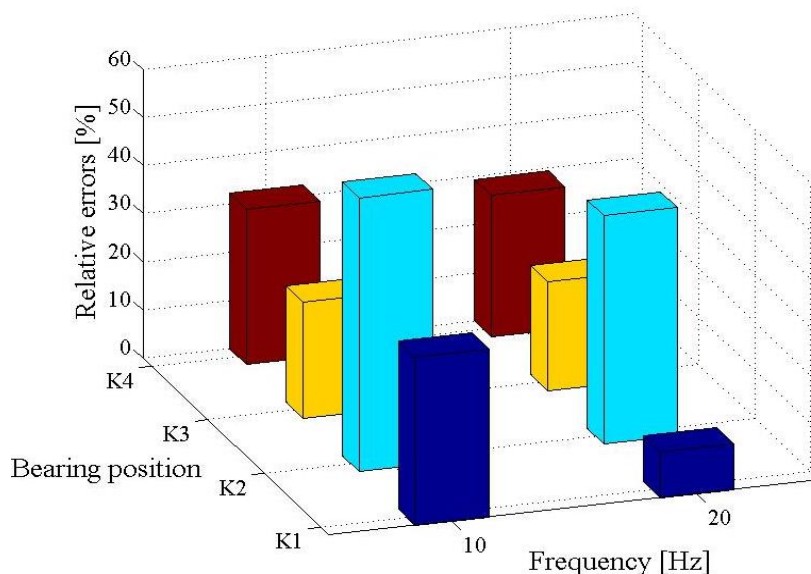


Fig. 5.31. Compare between local stiffness and whole stiffness of the container ship 11400 TEU at  $f = 10$  Hz and 20 Hz

The local structure stiffness and whole hull stiffness of the large container ship 11400 TEU at the basic excitation frequency of propeller and diesel engine are compared. With data from Tab. 5.8 and Fig. 5.31, at the first excitation frequency of the propeller,  $f = 10$  Hz, and the first excitation frequency of the diesel engine  $f = 20$  Hz, the deviation between the local stiffness and the whole stiffness is the largest at position K2 - intermediate bearing No. 2, are 56.96% and 47.42%, respectively. This deviation is due to some complex structures that are not taken into account when the structure model of the whole ship.

Tab. 5.9. Local stiffness of the two container ships at the basic excitation frequencies

Ship type	Excitation Frequency [Hz]	Bearing positions			
		Inter. bearing No.1	Inter. bearing No.2	Inter. bearing No.3	Inter. bearing No.4
		Stiffness [N/m]			
2000 TEU	7.58	$1.53 \times 10^9$	$2.55 \times 10^9$	$5.05 \times 10^9$	$3.25 \times 10^9$
11400 TEU		$7.2 \times 10^9$	$2.9 \times 10^9$	$2.27 \times 10^9$	$3.11 \times 10^9$
2000 TEU	10	$1.74 \times 10^9$	$2.50 \times 10^9$	$2.21 \times 10^9$	$3.61 \times 10^9$
11400 TEU		$4.56 \times 10^9$	$2.37 \times 10^9$	$2.44 \times 10^9$	$2.73 \times 10^9$
2000 TEU	12.13	$1.33 \times 10^9$	$1.52 \times 10^9$	$1.48 \times 10^9$	$2.66 \times 10^9$
11400 TEU		$9.09 \times 10^9$	$2.34 \times 10^9$	$1.75 \times 10^9$	$2.65 \times 10^9$
2000 TEU	20	$2.56 \times 10^9$	$2.05 \times 10^9$	$0.32 \times 10^9$	$2.25 \times 10^9$
11400 TEU		$7.75 \times 10^9$	$1.94 \times 10^9$	$2.39 \times 10^9$	$2.62 \times 10^9$

Comparing the stiffness between a medium-sized container ship 2000 TEU and a large container ship 11400 TEU at the basic excitation frequencies is considered. The stiffness values of the two containers are summarized in Tab. 5.9, and Fig. 5.32.

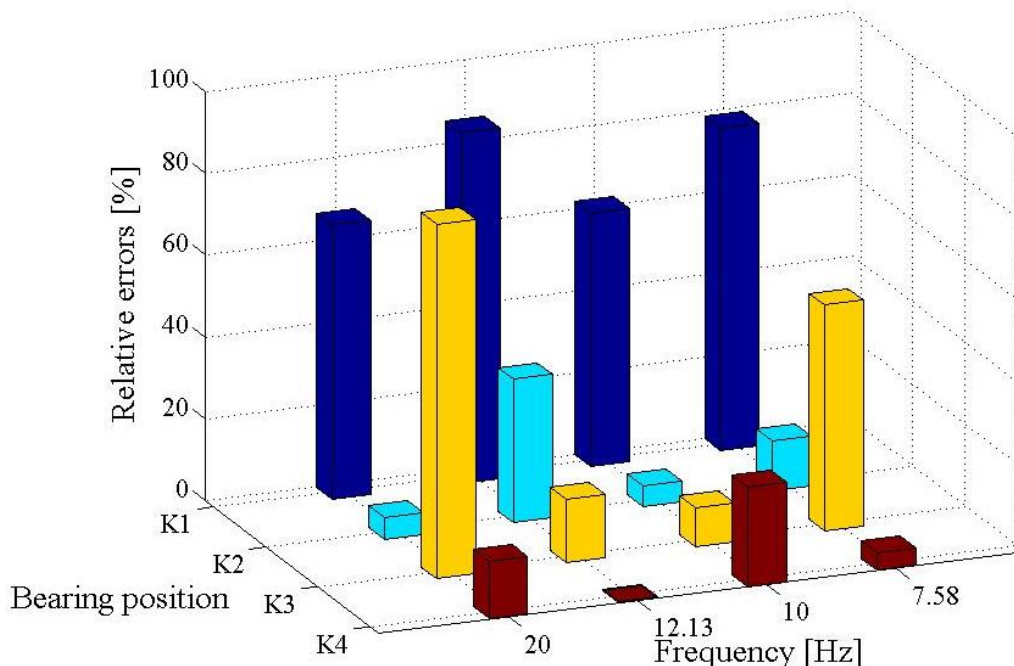


Fig. 5.32. Compare the stiffness between the two container ships 2000 TEU and 11400 TEU at the basic excitation frequencies

The large container ship has a capacity of 11400 TEU, so it has the stiffness more than the medium-sized container ship of 2000 TEU. The evaluation of the rigidity analysis of the two vessels is clearly shown in Tab. 5.9 and Fig. 5.32 at all the basic excitation frequencies of the propeller and diesel engine.

In this section, the author has calculated stiffness of the foundation bearings of the propulsion system and the main bearings of two containers with different capacity, medium-sized 2000 TEU and large-sized 11400 TEU. Calculate and compare bearing stiffness with local stiffness at respective support positions was determined. In addition, the author also compared the stiffness of the different ships at the basic excitation frequencies to have a more comprehensive view of the ship's stiffness. The analysis has made some statements as follows: ships with greater capacity, the stiffness of it is also larger, respectively, the stiffness of the foundation bearings changes according to the frequency of excitation.

## 5.2. Shaft line alignment

In this section, the calculation of the alignment of the shaft line for the medium-size container ship of 2000 TEU (length 182.85 m) will be presented. Calculations are performed in many different mathematical models, from which to select the most optimal mathematical model for detailed calculations. Calculating shaft deflections, reaction forces at bearings, bending stress, shear forces, bending moment, SAG and GAP are considered. The calculations are made based on the finite element method. The calculation results are verified to evaluate the accuracy of the numerical method applied and ability to apply this numerical method to many different types of ships.

The correct alignment of the shaft line is one of the most important elements during the design and assembly of the marine propulsion system. The main task is to correctly align the radial bearing axis of the power transmission system. Usually, the base is the crankshaft line (main bearings) of the engine. The task of the correct arrangement of the shaft line is to move (usually vertical) intermediate and stern bearings in such a way that the operating parameters of the propulsion system (especially bearings) are correct. The analysis of the shaft line alignment has a number of objectives that must be simultaneously fulfilled in all operating conditions of the propulsion system. First of all, the load on shaft line bearings (aft and intermediate) must be within the specified range. In the event of a low bearing load, the dynamic load level must also be checked (based on bending vibration analysis of the shaft lines). If the amplitude of the dynamic load is higher than the static one, a dangerous phenomenon called "hammering" may occur, which is a short time that leads to the destruction of the bearing sliding surfaces. With the optimal arrangement of the shaft line, all bearings are evenly loaded. The best parameter for even loading is the equality of Sommerfeld numbers for all bearings. The Sommerfeld number is described by equation Eq.(5.2).

$$S = \frac{R}{\eta \cdot U} \cdot \left( \frac{d}{c} \right)^2, \quad (5.2)$$

where:

- S is the Sommerfeld number,
- R is bearing's loading unitary force,
- $\eta$  is lubricating oil absolute viscosity,
- U is peripheral speed of the shaft,
- d is diameter of shaft journal,
- c is bearing clearance.

In typical drive systems (without gears), the circumferential speed of the journals of all bearings is identical. Similarly, usually, the viscosity of the lubricating oil is the same for all bearings. Under such assumptions, the reaction quotient of the compared bearings should meet Eq.(5.3). A low load is especially dangerous for intermediate bearings. The reason is the deformation of the ship's hull beam in various loading conditions and on the regular wave, which is often the reason for additional relief for intermediate bearings. For this reason, the Sommerfeld number of these bearings should be 30÷50% larger than other bearings (especially the stern bearing)

$$\frac{R_1}{R_2} = \frac{L_1}{L_2} \cdot \frac{d_2}{d_1} \cdot \left( \frac{c_1}{c_2} \right)^2 \cdot \frac{S_1}{S_2}, \quad (5.3)$$

where L is bearing length.

The second purpose of correctly positioning the shaft line is to evenly distribute the stern bearing's load. The stern bearing is the heaviest loaded radial bearing. Its load is strongly asymmetrical due to one-sided loading with a massive propeller, which additionally induces constant and variable hydrodynamic forces. Due to the magnitude of the load, the stern bearing is relatively long. It is important that the lift is distributed over the entire length of the bearing. The correct load distribution can be checked analytically by reducing the reaction to

the two extreme bearing edges and comparing their values. The condition for correct bearing operation is that both reactions are positive, even after taking into account their dynamic components. An alternative method may be to check the relative displacement of the pivot axis and the sheath of the bearing. This displacement must be smaller than the total bearing clearance. When using this method, it is necessary to take into account both the deformation of the shaft line and the local deformation of the ship's hull (based on the stiffness of the double bottom - section 5.1).

Another element that should be met is the appropriate load on the crankshaft by shear forces and bending moments of the shaft line. All main engine manufacturers define the allowable crankshaft load field. An example of the permissible field of shear forces and bending moments are shown in Fig. 5.33. Generalized forces from the shaft line must be within this field for all operating conditions of the propulsion system.

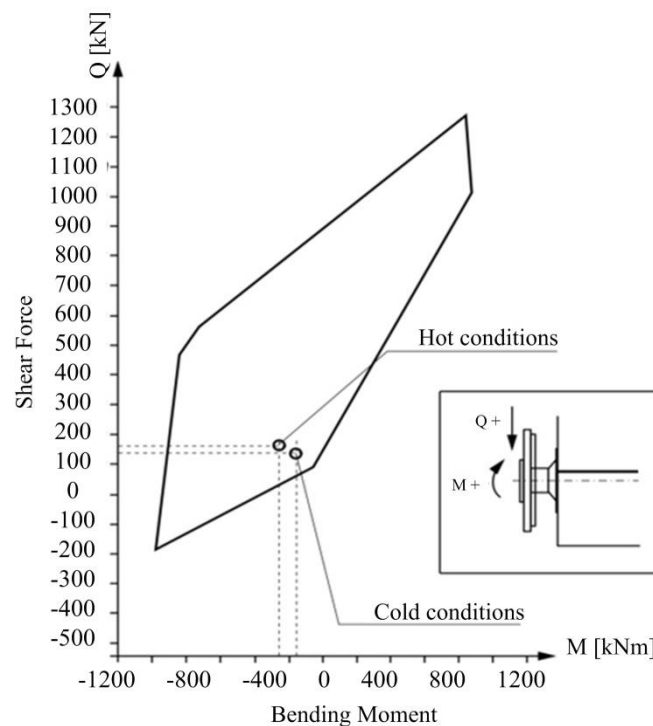


Fig. 5.33. Example of an acceptable crankshaft load field

The last element that should be checked is the bending and shear stress in the shaft line elements. Usually, for typical drive systems, these stresses are not too high for all operating conditions. The reason is the relatively large diameters of the shaft lines, which are determined by the stress originating from the torsional vibrations of the propulsion system. On the other hand, the limits for allowable bending stress cannot be too high precisely because of the expected high level of torsional stress. Ship's power transmission systems are modeled using linear beam elements. In accordance with engine manufacturers' recommendations, the crankshaft model for the static-dynamic analysis of shaft line arrangement is simplified. It consists of several beam elements located in the axis of the crankshaft, without taking into account its cranks. The thermal deformation of the motor body (arising during continuous operation of the propulsion system) should be modelled as a given, vertical displacement of the main bearings. Engine manufacturers provide the estimated size of this displacement. The forces and moments modelling the propeller interaction on the shaft line should take into account its weight along with buoyancy force and generalized

hydrodynamic forces (their constant components). It should be noted that the amount of hydrodynamic forces strongly depends on the cargo state of the ship. The intermediate and stern tube bearings can be modelled as point support with given foundation elastic.

Calculation analyzes should be performed for all typical operating states of the propulsion system and the ship. The most important variant occurs at the nominal operating parameters of the propulsion system: hot main engine and active hydrodynamic forces in a given loading condition of the ship. Shaft alignment parameters must also be checked for the inoperative drive system in hot and cold conditions. A separate analysis should be carried out for the propulsion system during its assembly - for disconnected shafts (crankshaft, intermediate and propeller shaft). These calculations allow the mutual displacement of shaft flanges to be determined. These values can be used as an auxiliary in determining the correctness of shaft line assembly.

During the static-dynamic analysis of the ship's propulsion system, its power transmission system is isolated from the ship's hull structure. For this reason, the correctness of mapping the boundary conditions is essential from the point of view of the correctness of the calculations performed. The necessary scope to take into account various factors of boundary conditions is still being discussed in global shipbuilding. There is a clear tendency to extend the analysis of boundary conditions - the recommendations of classification societies are extended. However, due to analytical difficulties, there is in the literature regarding the calculation methods and typical values that could be accepted for preliminary analyzes. According to the author of the dissertation, when analyzing the arrangement of the shaft line, it is necessary to take into account the rigidity of the ship's hull (chapter 5.1). When determining the rigidity of the shaft line foundation, it is also beneficial to determine the compliance of the main engine body (section 5.1).

### **5.2.1. Influence of assumptions on the alignment of the shaft line**

This part of the dissertation considers the impact of the most important assumptions of the mathematical model on the results of calculations of the arrangement of the shaft line. The effect of various propulsion system operating conditions on the power transmission system operating parameters were also examined. The influence of boundary conditions and finite elements (one dimensional -1D and three dimensional - 3D) on the results of the shaft line alignment calculation using the finite element method. From that, choose the most optimal model applied for the calculation of basic axis system alignment for the average container ship of 2000 TEU (length 182.85 m).

The FEM model of the propulsion system of the container ship 2000 TEU with model 1D (one-dimensional) consists of 27 beam elements and one continuous support (stern bearing) and four point supports (intermediate and main bearings of the engine). The shaft line is mainly loaded with hydrodynamic forces. The weight of the propeller and its buoyancy were also taken into account. The calculations were carried out in the vertical plane of the shaft line, for the nominal operating conditions of the propulsion system - the engine in the "hot" state and hydrodynamic forces. A typical propulsion system of a medium-sized container ship with a load capacity of 2000 TEU (standard containers) was analyzed. The mathematical model of the power transmission system, for the most complex variant No. 4 (see below), is shown in Fig. 5.34÷5.35.



Fig. 5.34. Beam model of the shaft line, 3d view

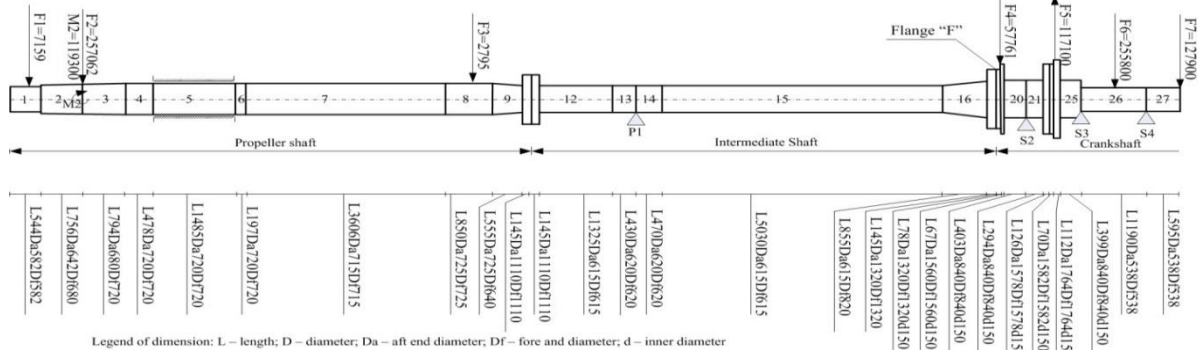


Fig. 5.35. FEM mathematical model of the container ship's power transmission system

The calculations were made for the alignment of the shaft lines and the propulsion system under nominal operating conditions. Analyzes were carried out for the following four variants with model one-dimensional (1D) (for four different mathematical models):

1. Variant 1 - all bearings are modelled as a points-wise, ideal stiff support,
2. Variant 2 - a model similar to the model 1 for variant 1, the stern tube bearing is modelled by one spring, with the equivalent stiffness,
3. Variant 3 - all bearings are modelled as spring with supports' elasticity; stern tube bearing is modelled similar to model 2 for variant 2,
4. Variant 4 - all bearings are modelled the same model 3 for variant 3, but the stern tube bearing is modelled by two springs.

The results of the analysis of the alignment of the shaft line for the above variants of the mathematical model are shown in Fig. 5.36÷5.37 (the absolute deformation of the shaft line) and in Fig. 5.38 (magnitude of bearing reactions). The following numbering of the bearings was adopted: No. 1 and 2 - the stern bearing (its aft and forward stern tube bearing); No. 3 - intermediate bearing; No. 4, 5 and 6 - the first three main bearings of the engine.

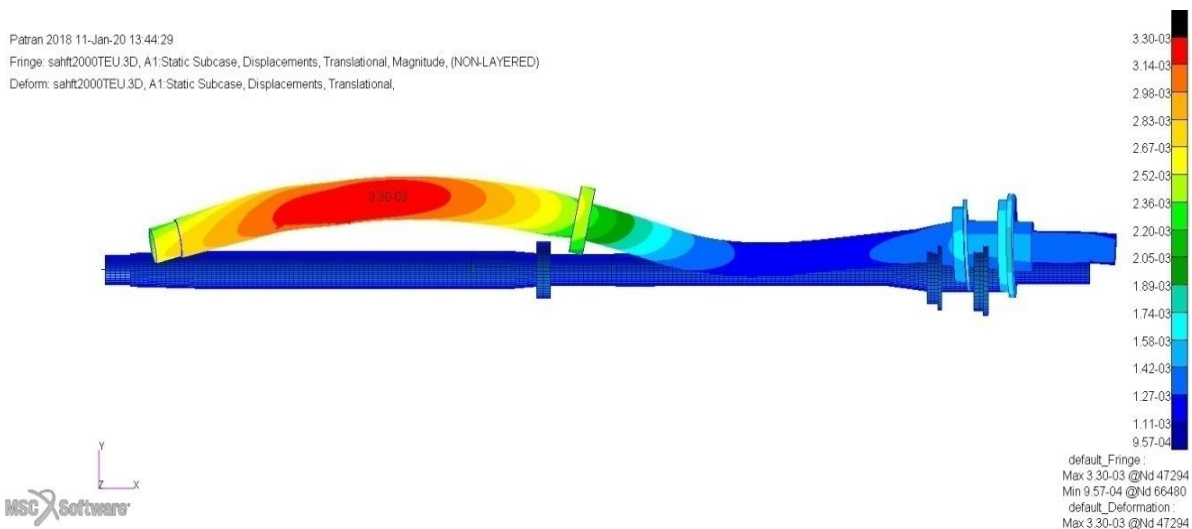


Fig. 5.36. Three-dimensional vibration model of a ship's propulsion system

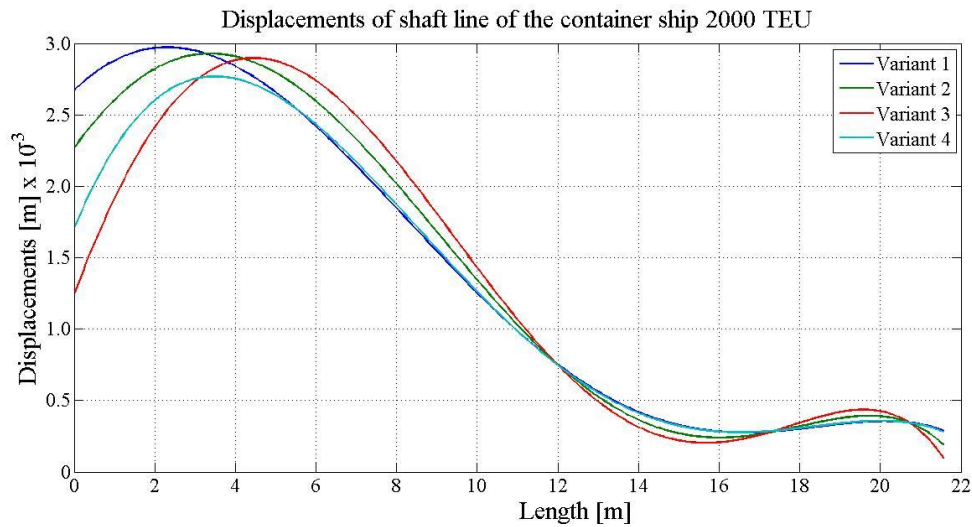


Fig. 5.37. Shaft line deflections under various assumptions of the mathematical model

Tab. 5.10. The deflection for variants model of the propulsion system

Bearing's position	Number variant			
	Variant 1	Variant 2	Variant 3	Variant 4
Aft stern tube bearing	2.95	2.775	2.874	2.67
Forward Stern bearing	3.05	3.119	3.215	3.01
Intermediate Bearing	1.455	1.457	1.459	1.45

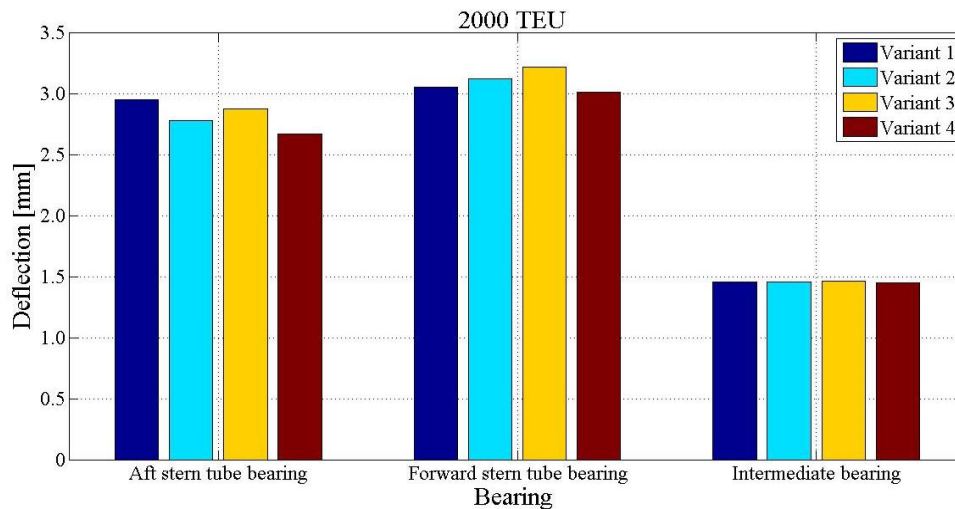


Fig. 5.38. Bearing deflections under various assumptions of a mathematical model

Because the load and moment caused at the propeller shaft and the intermediate shaft are larger than the crankshaft, the deflections for the stern tube bearing and intermediate shaft bearings are considered. Tab. 5.10 and Fig. 5.38 summarize the shaft deflection results at stern tube bearings and intermediate bearings for various mathematical models. From this summary, the author finds that the 4<sup>th</sup> mathematical model is the most optimal this model will be applied to the next calculations and analysis of the typical propulsion system.

The ship propulsion system is modelled with one-dimensional (1D) beam elements, which makes the modelling and calculation simpler while ensuring accuracy. In this section, the author models the propulsion system of the ship is similar to mathematical model No. 4 using three-dimensional (3D) elements (hex8) to mesh the elements. The ship's propulsion system has 49765 nodes and 47905 elements. Results of deflections of the shaft line at the bearing between the 1-D element model and 3-D element model are shown in Fig. 5.39÷5.40.

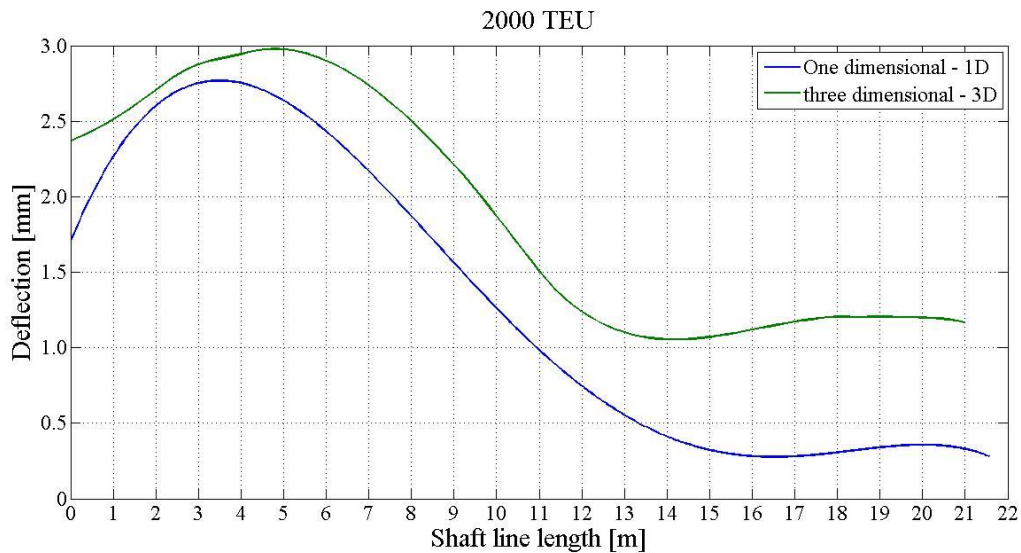


Fig. 5.39. Deflection of shaft line with model 1D and 3D

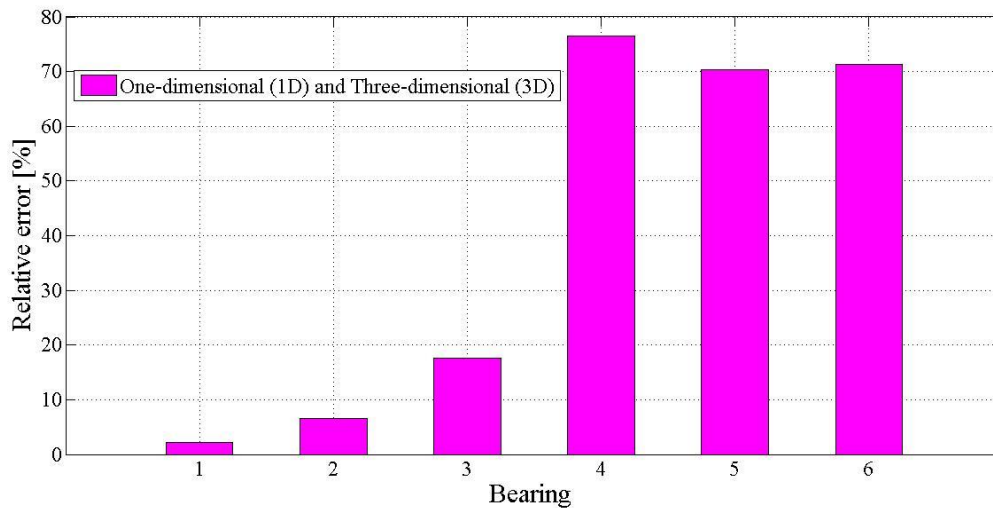


Fig. 5.40. Compare the deflection of the shaft line between 1-D and 3-D model

Obviously, with the summary result from Fig. 5.38÷5.39, the shaft deflection at bearings of the 1D element model is smaller. The 3D models require longer computation times and higher device configurations. This results in economical and time-consuming costs for analysts and designers. While the propulsion system model with 1D elements gives results with acceptable accuracy. Therefore, the model of the propulsion system is usually modelled by 1D element in the analysis and alignment of the shaft line.

### 5.2.2. Analysis of a typical propulsion system

In the next step, the influence of various operating conditions on the parameters of the shaft line alignment was examined. The propulsion system of a medium container ship capacity of 2000 TEU (182.5 m in length) has been analyzed the model of the medium size container ship with its parameters is shown in Fig. 5.35 (section 5.2.1). As analyzed above, the best model according to option 4 was used for analysis the shafts were modelled as one-dimensional beam elements. The bearings are modelled as spring with supports' elasticity the stern tube bearing is modelled by two springs. The calculations were made for the following cases of propulsion system operation:

1. Variant 1 - The operating system in nominal conditions: hot main engine and interacting nominal hydrodynamic forces,
2. Variant 2 - Propulsion system shortly after stopping (propulsion system just stopped): hot main engine without hydrodynamic forces,
3. Variant 3 - Propulsion system before starting (propulsion system stopped for a long time): cold main engine without hydrodynamic forces.

The analysis of the propulsion system of a 2000 TEU medium-sized container ship with different operating conditions (hot and cold) was calculated based on the finite element method on the well-known commercial software platform Patran - Nastran. In the calculation taking into account the influence of the stiffness of the bearings and foundations, ignoring the hull deformation, due to the model of the propulsion system is modelled separately. In the hot condition engine case, the engine is warmed up to 55 °C. Main engine bearings, due to thermal displacement, are offset in the vertical direction by 0.33 mm compared to the case with a cold engine. The shifted value was provided by the manufacturer for a specific engine model with the main engine 8S70 MC-C [63].

The reactions of shaft bearings, shaft deviations, bending moments and bending stresses with different operating conditions of the propulsion system of the medium-sized container ship 2000 TEU will be calculated. The deformation of the propulsion system, bending moment, bending stress of a medium-sized container ship system with hot conditions is described as Fig. 5.41÷5.43. The results of the calculation for all shafts connected - with different operating conditions as summarized as Tab. 5.11÷5.13.

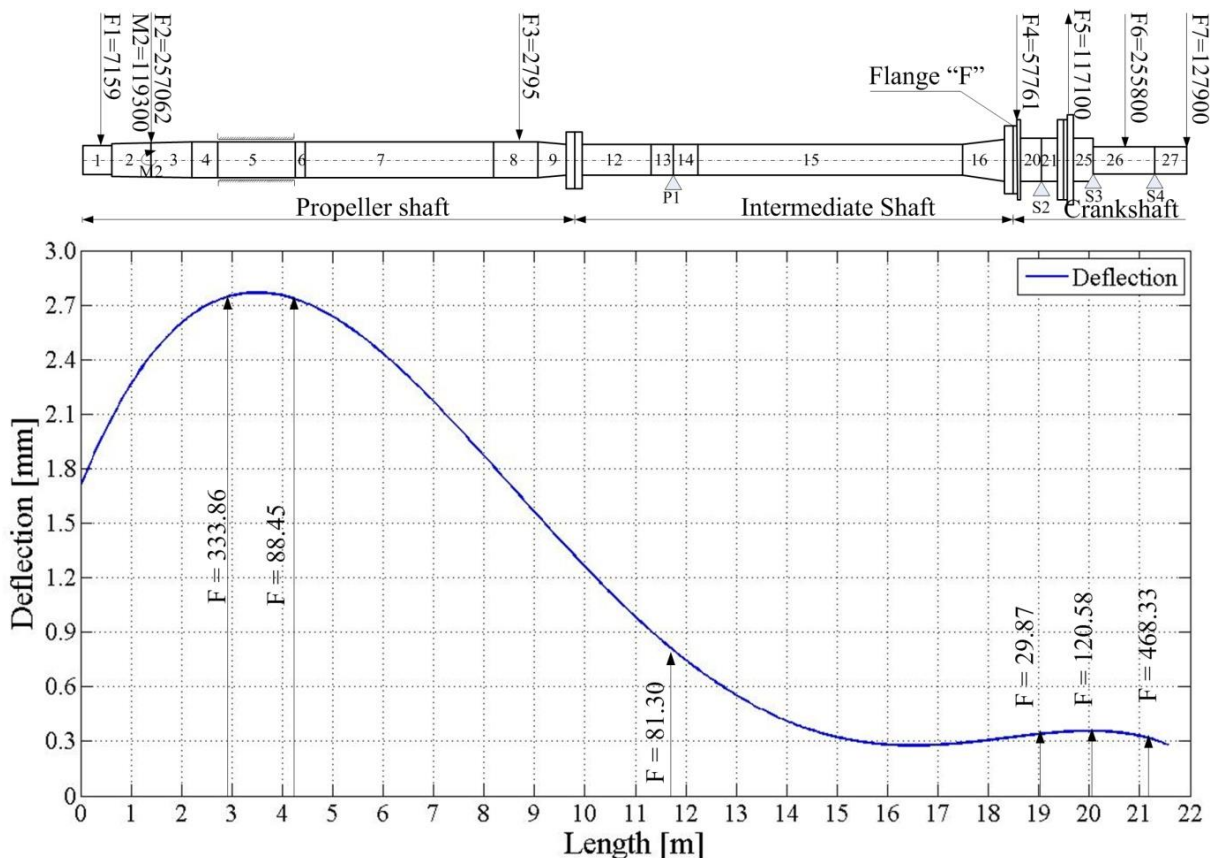


Fig. 5.41. Deflections for all shaft line – hot condition, with hydrodynamic forces

## 5. THE OPERATING PARAMETER CHARACTERISTICS OF THE DRIVE SYSTEM

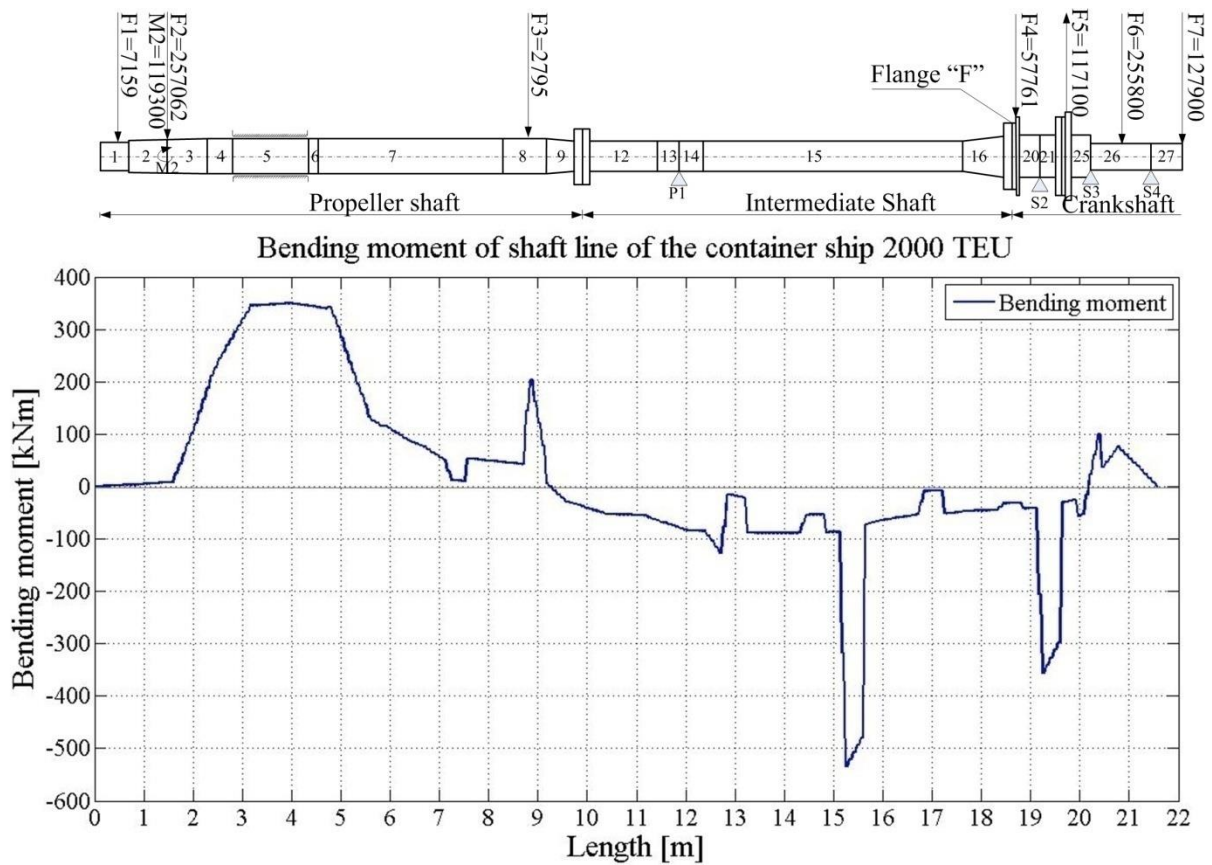


Fig. 5.42. Bending moments for all shafts connected – hot condition, with hydrodynamic forces

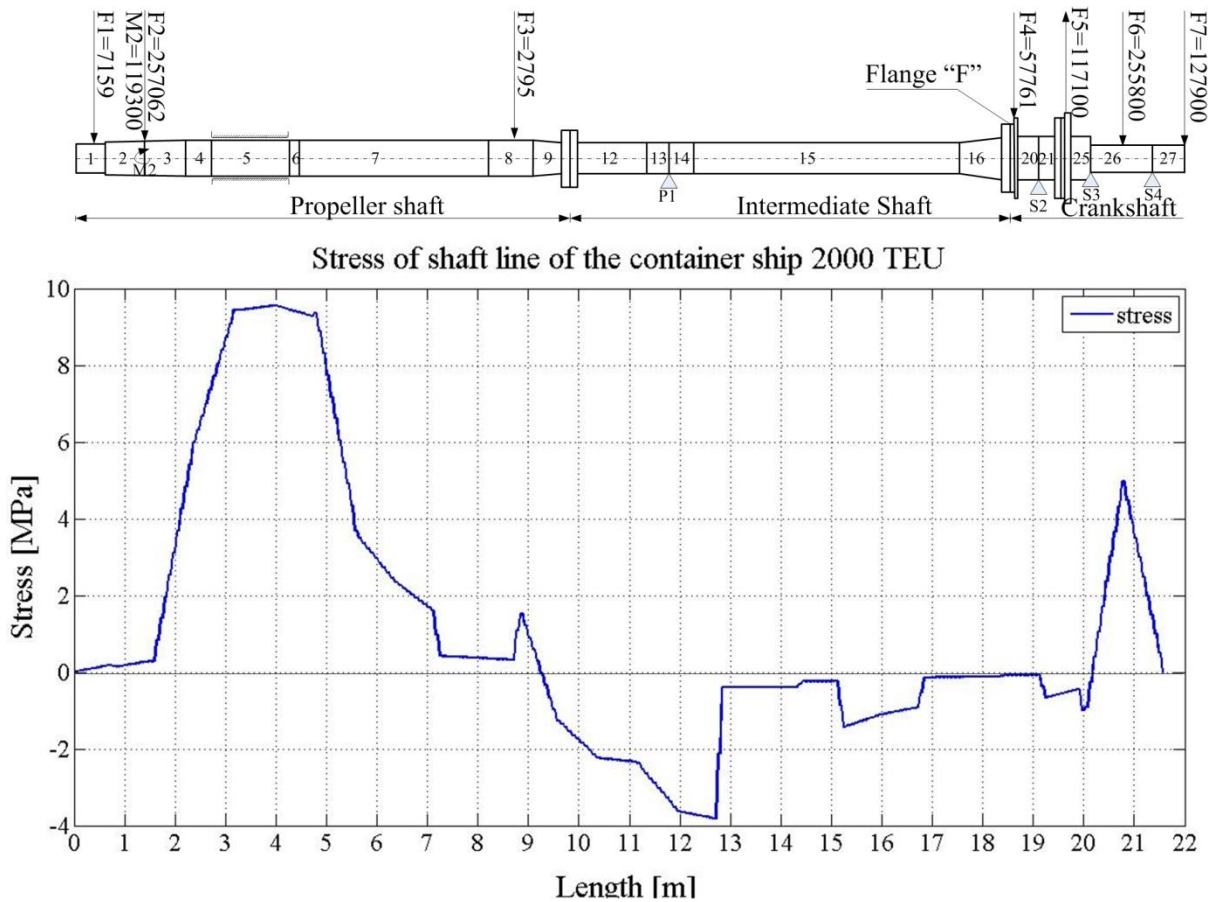


Fig. 5.43. Bending stress for all shafts connected – hot condition, with hydrodynamic forces

*Tab. 5.11. Summary the results of the calculation for all shafts connected-hot condition, with hydrodynamic forces*

No. of bearing	Deflection	Reaction	Bending moment	Shear force	Inclination
--	mm	kN	kNm	kN	mm/m
Aft stern tube bearing	2.774	274.68	345.22	368.55	-0.191
Forward stern tube bearing	3.019	105.37	349.98	-136.47	0.023
Intermediate bearing	1.450	48.18	-52.36	86.01	-0.310
Section "F" /flange/	0.341	0	-88.47	85.32	-0.012
Main bearing No.1	0.330	11.88	-64.31	-102.77	0.004
Main bearing No.2	0.330	43.73	-57.55	55.18	-0.028
Main bearing No.3	0.330	467.80	76.06	-168.95	0.016

*Tab. 5.12. Summary the results of the calculation for all shafts connected-hot condition, without hydrodynamic forces*

No. of bearing	Deflection	Reaction	Bending moment	Shear force	Inclination
--	mm	kN	kNm	kN	mm/m
Aft stern tube bearing	2.810	121.15	345.22	264.31	-0.252
Forward stern tube bearing	3.282	236.77	557.57	-187.05	-0.082
Intermediate bearing	1.412	99.84	-114.42	343.76	-1.471
Section "F" /flange/	0.331	0	-56.39	38.59	-0.024
Main bearing No.1	0.330	65.28	-24.34	-58.10	0.002
Main bearing No.2	0.330	81.83	-55.09	-68.01	0.024
Main bearing No.3	0.330	466.94	76.06	-170.43	0.016

*Tab. 5.13. Summary the results of the calculation for all shafts connected-cold condition*

No. of bearing	Deflection	Reaction	Bending moment	Shear force	Inclination
--	mm	kN	kNm	kN	mm/m
Aft stern tube bearing	3.532	253.91	424.30	322.01	-0.309
Forward stern tube bearing	3.875	161.23	535.58	-170.11	-0.059
Intermediate bearing	1.468	86.70	-104.04	351.67	-1.769
Section "F" /flange/	0.000	0	-99.04	155.74	0.002
Main bearing No.1	0.000	11.22	-71.41	-260.66	0.040
Main bearing No.2	0.000	36.95	-57.99	100.38	0.020
Main bearing No.3	0.000	467.96	76.06	-170.43	0.017

The maximum permissible load at the aft flange of the main engine crankshaft and the calculated values are compared with the allowable values normally provided by the engine manufacturer [13]. The diesel engine manufacturers precisely determine the bending moment values  $M$  and the shear force  $F$ , derived from the axis, can act on the crankshaft, more precisely the flange of the crankshaft. From the values of bending moment  $M$  and shear force  $F$ , for each different diesel engine, there is a maximum loading boundary that allows the operating range of the load to act on the flange of the crankshaft. After calculating the bending moment values and shear stress at the flange of the "flange F" crankshaft with different operating conditions (hot and cold). These values will be presented on the same

## 5. THE OPERATING PARAMETER CHARACTERISTICS OF THE DRIVE SYSTEM

graph as the maximum allowable load curve graph at the flange of the crankshaft provided by the manufacturer, thereby evaluating the condition of the shaft line alignment. The maximum load graph on the flange of a crankshaft consists of two axes: the x-axis describes the value of the bending moment  $M$ , the y-axis describes the value of the shear force and weight of the flywheel ( $F$  shear forces,  $G$  weight of the flywheel  $G = 57.761$  kN). The boundary values for the maximum allowable load area of the 8S70MC-C8 engine are described in Tab. 5.14 [13].

Tab. 5.14. Boundary conditions of bending moment and shear forces acting on the crankshaft flange for the B&W 8S70MC engine

Boundary conditions	Bending moment $M$ [kNm]	Shear forces and weight of the flywheel $F + G$ [kN]
1	150,5	-89,5
2	-442,0	292,4
3	-442,0	663,0
4	-163,5	483,5

With the allowable boundary condition values of the bending moment  $M$  and the shear force  $F$ , the allowable load area graph applied to the flange of the crankshaft is determined. From the values of bending moments and shear force at the flange of crankshaft were calculated and described as in Tab. 5.11÷5.13. The load values of bending moment and shear force for the different operating conditions of the 2000 TEU medium vessel propulsion system are determined. All values the maximum load under different operating conditions shall be within the permissible load area. The diagram of crankshaft loading with shearing force and bending moment is shown in Fig. 5.44.

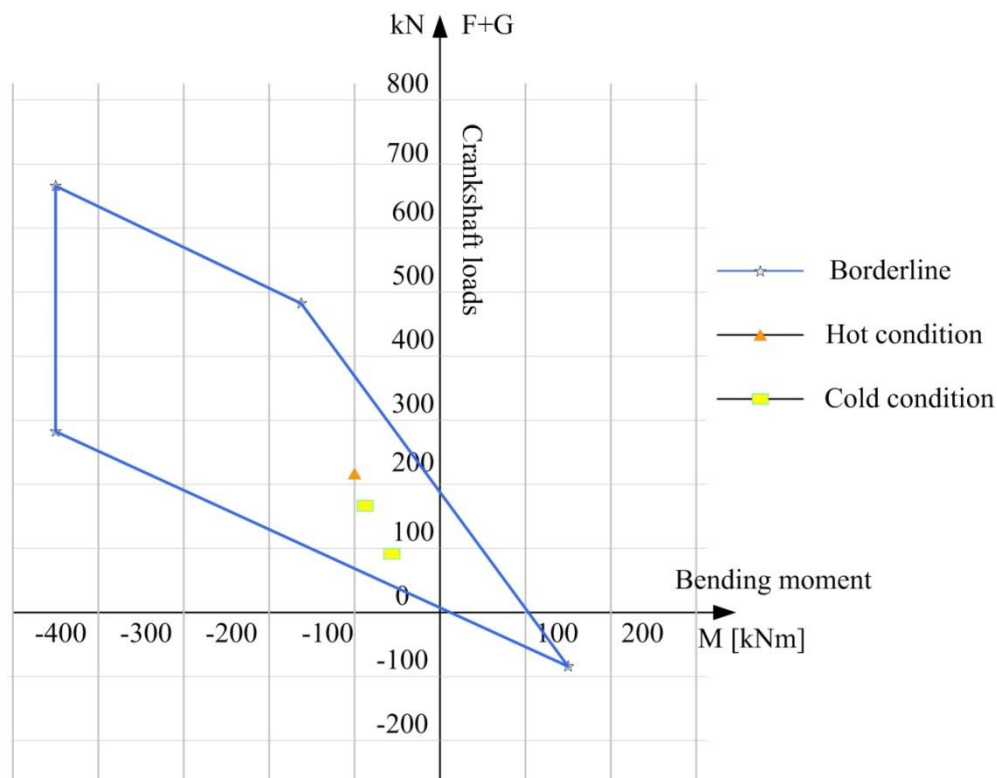


Fig. 5.44. Field of allowable crankshaft loads for various operating conditions, graphic interpretation of results

Under various operating conditions of the thrust system, the values of shear force and bending moment are in the boundary field. These values are important because the thrust bearing mainly drives the longitudinal (axial) force. Excessive values of shear force and bending moment outside the permissible operating condition area may cause the propulsion system to malfunction and damage.

### 5.2.3. Analytical the shaft line alignment for measurement authentication

Then, necessary adjustments of the height of each supports, including possible temporary supports, are made to ensure that the calculated “GAP” and “SAG” between the connecting flanges are realized. Therefore, the determination method "GAP" and "SAP" are often used to verify the accuracy of the installation and alignment of shaft lines. The last stage of determining the parameters of the shaft line alignment consists of determining the relative deflection of the shaft line flanges and the crankshaft after disconnection. In this section, the deformation of the propulsion system consists of two parts: the first part of the propeller shaft and the intermediate shaft, the second part of the crankshaft, will be considered individually with cold conditions. First, the deformation of the propeller shaft and intermediate shaft were analyzed. Next, the deformation of the crankshaft was calculated. The analyses were carried out for the propulsion system of the medium size container ship of 2000 TEU (182.85 m). The analyses were based on the finite element method. The graphs of deformation of the propeller shaft, intermediate shaft, and crankshaft under cold operating conditions are shown in Fig. 5.45÷5.46. The results of deformation calculations are summarized in Tab. 5.15÷5.16.

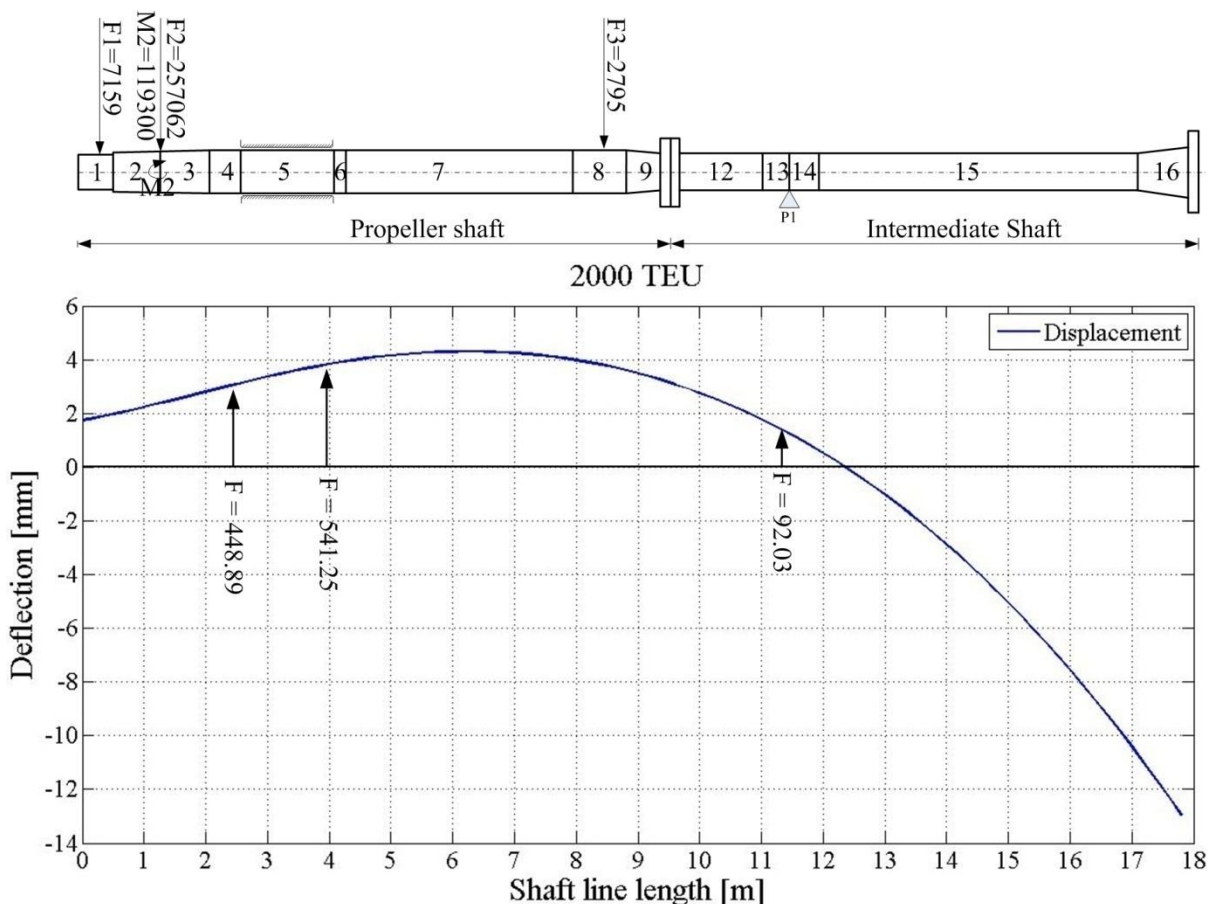


Fig. 5.45. Deflection for shafting disconnected from M.E. – Cold condition

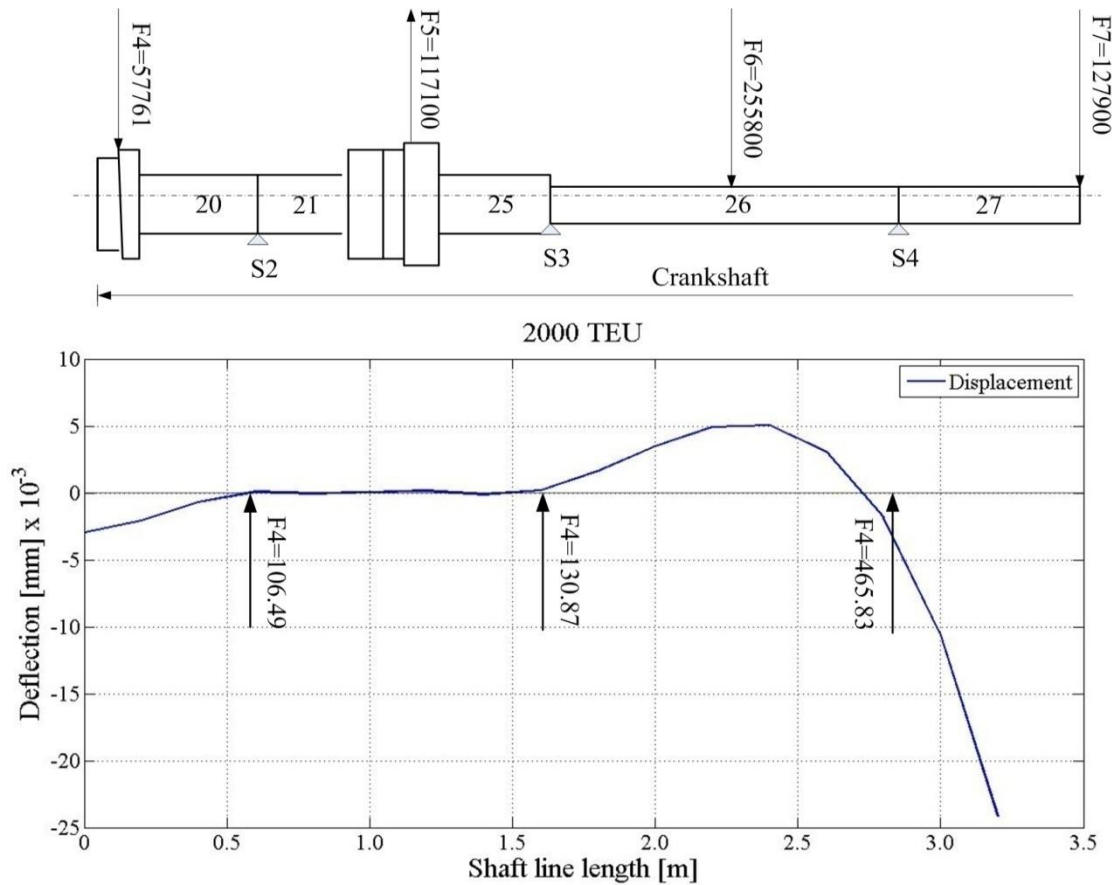


Fig. 5.46. Deflection for crankshaft disconnected from shafting – Cold condition

Tab. 5.15. Summary the results of the calculation of shafting alignment for disconnected main engine (propeller shaft + intermediate shaft) – Cold condition

No. of bearing	Deflection	Reaction	Bending moment	Shear force	Inclination
--	mm	kN	kNm	kN	mm/m
Aft stern tube bearing	3.125	448.89	424.30	319.07	-0.446
Forward stern tube bearing	3.855	541.25	439.03	-83.52	-0.206
Intermediate bearing	1.412	92.03	0	0	0
Section "F" /flange/	-12.996	0	0	0	2.567

Tab. 5.16. Summary the results of M.E. crankshaft alignment for main engine disconnected from shafting – Cold condition

No. of bearing	Deflection	Reaction	Bending moment	Shear force	Inclination
--	mm	kN	kNm	kN	mm/m
Section "F" /flange/	-0.003	0	0	0	0.006
Main bearing No.1	0	106.49	27.11	81.67	-0.002
Main bearing No.2	0	130.87	-51.92	101.82	0.016
Main bearing No.3	0	465.83	76.06	-170.43	0.017

With the results of the deflection at the shafting flange and crankshaft flange of the propulsion system as shown in Tab. 5.15÷5.16, the values of SAG and GAP were determined. The offset value of the crankshaft and the deviation between the flange of the shaft and the crankshaft flange are shown in Fig. 5.47.

$$\text{SAG} = 12.996 - 0.003 = 12.993 \text{ mm}$$

$$\text{GAP} = 1.320 \times 2.567 + 1.320 \times 0.006 = 3.39636 \text{ mm}$$

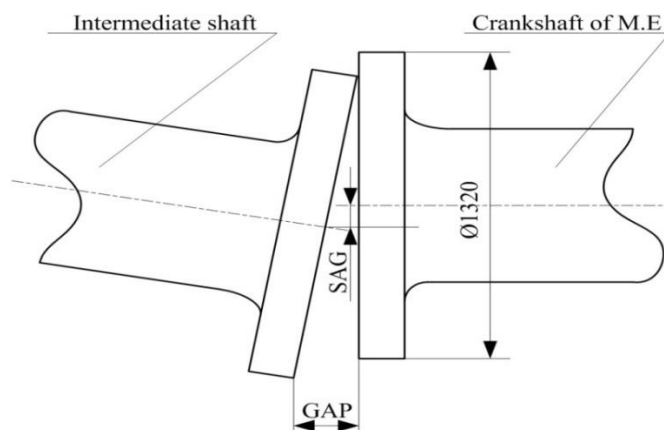


Fig. 5.47. Relative position of intermediate shaft flange and main engine crankshaft flange in cold condition

In this section, the author has calculated and analyzed the alignment of the propulsion system of the medium-size container ship of 2000 TEU. The analysis and calculation are done by the finite element method. Calculating and analyzing shaft line alignment is done with many different mathematical model assumptions, different finite elements (one dimensional - 1D and three dimensional - 3D) as well as different operating conditions so that assess the accuracy of the selected numerical modelling method, as well as select the most optimal modelling for propulsion system analysis and alignment. With the above results, the author can draw some conclusions as follows:

- Modelling propulsion systems with 1D beam elements are often used for shaft line analysis and alignment, due to its simplicity, and the results achieved accuracy within the permitted range.

- The application of the finite element method implemented on the Patran - Nastran software platform can easily calculate and align the propulsion system with many assumptions, many elements, and different operating conditions. This will help align the shaft line system to ensure greater accuracy under various operating conditions.

- The numerical modelling method is based on the finite element method, implemented in the Patran-Nastran numerical software platform, for relatively easy calculations and accuracy within the accepted range.

### 5.3. Dynamic shaft line alignment

Bending vibrations of the shaft lines are usually treated as one of the elements (next to torsional and longitudinal vibrations) of vibrations of marine power transmission systems. The bending vibration calculations are recommended (but not required) by classification societies. Such analyses should be carried out especially for long, flexible shaft lines (e.g. warships [29]) or when the ship's hull (double bottom) has relatively low stiffness [13]. According to the author of the dissertation, bending vibrations should be named and treated as a dynamic arrangement of the shaft lines. Dynamic components of bearing reactions and generalized forces loading the crankshaft can be important for the correct positioning of the shaft line [74].

Similarly to the analyses of the static arrangement of shaft lines, in the bending vibration calculations the power transmission system is modelled as isolated from the ship's hull. Standard methods of modelling the boundary conditions of the propulsion system have not yet been developed in global shipbuilding. Therefore, a comparative analysis was carried out on the influence of methods for creating a mathematical model of the propulsion system on the results of bending vibration calculations of shaft lines. The analyses were carried out for a typical container ship with a carrying capacity of 2000 TEU and a length of 182.85 m. The mathematical model of the shaft line is similar to the one presented in Fig. 5.35. The model of the propulsion system located in the ship's hull (for calculations by the Nastran program) is shown in Fig. 5.48.

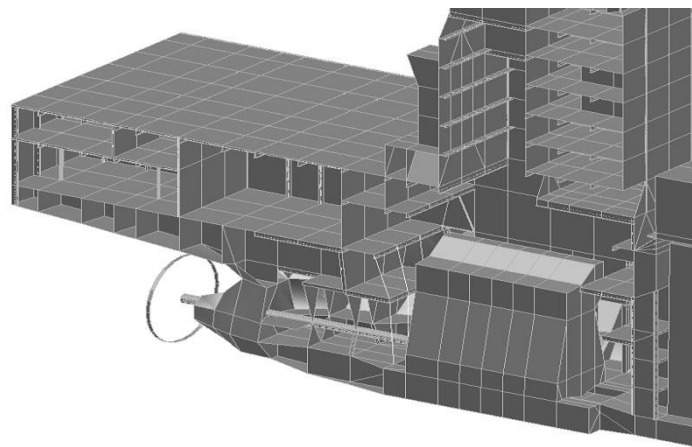


*Fig. 5.48. Model of the aft part of the 2000 TEU container ship with the propulsion system*

The following three calculation options were carried out with the Nastran program:

1. Variant 1 - shaft line isolated from the hull, infinitely rigid support, stern tube bearing modelled by two support points, other bearings - one support point,
2. Variant 2 - model equivalent to variant 1, except for the stern bearing tube modelled by one support point,
3. Variant 3 - model equivalent to variant 1, other bearings are modelled as spring with supports' elasticity.

An example of horizontal and vertical eigenvibration forms of the propulsion system, determined according to variant No.3, is shown in Fig. 5.49.

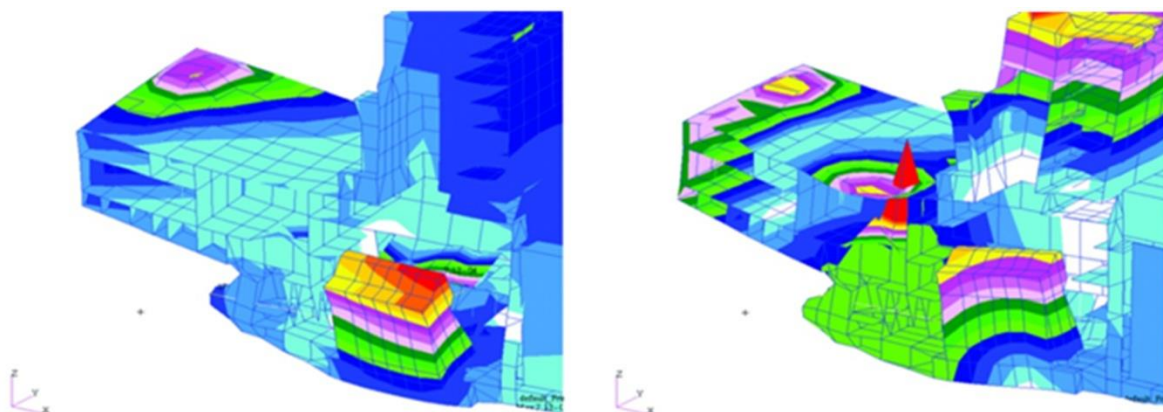


*Fig. 5.49. Horizontal and vertical natural vibrations of the container ship 2000 TEU propulsion system*

The summary of natural vibration calculations determined in accordance with the above variants is presented in Tab. 5.17. The comparison of forms of free vibrations of the shaft lines is presented in Fig. 5.50. The modelling of the stern bearing has the greatest influence on the bending vibrations of the propulsion system. When modelling the stern tube bearing as point support, there are doubts: how many support points should be used and where are they to be placed. It is recommended that support points be placed on the edges of the bearing or in its center. The most common recommendation is to place the fulcrum at a distance of the propeller shaft radius from the stern edge. According to the author of the dissertation, various methods of modelling the stern bearing using point supports can only be used for approximate calculations. The calculation error of such analyzes is difficult to determine because the correct position of the support point is different for different propulsion systems and different for subsequent forms of natural vibrations.

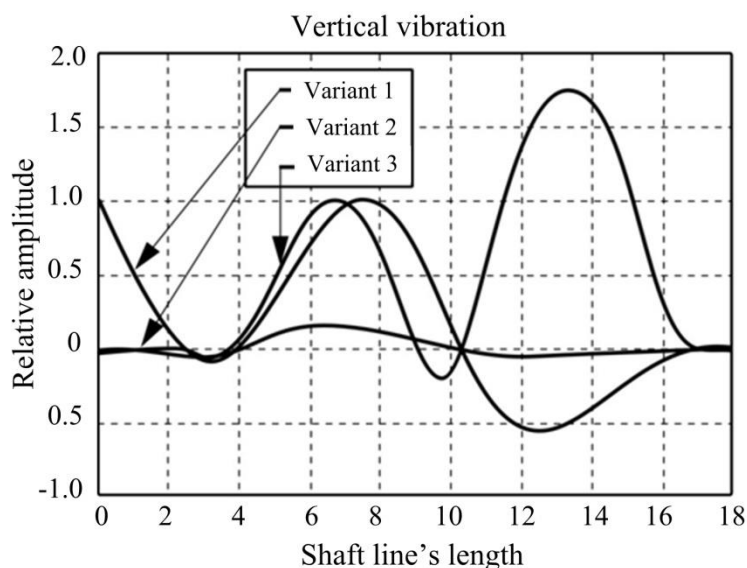


Fig. 5.50. Vertical free vibrations of the drive system

Tab. 5.17. Natural frequencies of the container ship 2000 TEU propulsion system determined using various mathematical models

Analysis variant	Horizontal vibration [Hz]	Vertical vibration [Hz]
Variant 1; isolated system; stiffness support; two-point aft stern bearing.	14.686	16.171
Variant 2; isolated system; stiffness support; single point stern bearing.	8.993	9.636
Variant 3; isolated system; flexible support; two-point aft stern bearing.	7.126	7.359

Based on comparative analyses, it can be stated that bending vibrations can be determined using a power transmission system model isolated from the ship's hull, provided that the stiffness and damping characteristics of the propulsion system foundation (boundary conditions) are well determined. According to the authors of the dissertation, it is necessary to determine the stiffness of the ship's hull and all bearings. Not only the absolute values of stiffness and damping are important, also their distribution is important, especially for the stern bearing.

## Conclusions and objectives of further research

The objective of the doctoral thesis is to evaluate the influence of numerical modeling methods on errors and dispersion of the results of analysis and development of optimal numerical modeling methods for chosen marine structures and machines. The analytical parameters are mainly based on the vibration analysis of chosen marine machines and structures. The author has proved that it is possible to limit dispersions and errors in numerical modelling of the marine structures and machines to an acceptable level and consistent with empirical research. Mathematical models of selected maritime structures and machines are built in the finite element method implemented in famous Patran-Nastran digital software. In the dissertation, two methods, the numerical modelling method, and measurement method are used in parallel to support each other, to determine the accuracy of the numerical modelling method applied. Although the measurement method itself has its own errors which comes from measuring instruments measurement techniques, and the person conducting the measurement. But the error of measurement methods is a task in another topic. In this thesis, the target of interest is the influence of the numerical modelling method, namely the numerical model method based on the finite element method implemented in the Patran-Nastran software platform, to the error and dispersion of the results of the analysis of chosen maritime machines and structures.

The basic method for reducing analysis error and dispersion is the use of correlation and mutual support between the numerical modelling method and the measurement method. In the doctoral thesis, the causes of computational errors and dispersion results are considered, depending on the model of the chosen marine machines and structures. Methods to minimize them are also analyzed. The influence of computational conditions such as boundary conditions, density of meshing, type of finite elements, etc. on calculation imperfections are considered. The assessments are based on a comparison between results obtained from a numerical model and results obtained based on a number of empirical formulas verified by measurement methods. Based on the obtained results, the author asserts that the thesis has solved some initial contents of the thesis as follows:

1. Mathematical models of the small basic parts that make up the hull and superstructure such as beams, thin plates, stiffened plates has built. Analysis of selected structures takes into account factors that may cause errors and dispersion in calculations such as boundary conditions, density and finite element type to be applied. The structures are also calculated and analysed in two cases of liquid contact and non-liquid contact. The results obtained are compared with the results from some experience formulas and verified by a measurement method based on the measurements performed in the laboratory of Gdynia Maritime University.
2. Building the mathematical model for two container vessels of different sizes: an average container ship of 2000 TEU and a large container ship of 11400 TEU. One of the most important parameters analysed is the ship's vibration. Global vibrations of the entire hull and local vibrations of the superstructure and main engine body are determined. The results obtained by numerical models are compared with the empirical formulas given by Brown and F. M. Lewis and F. H. Todd and some other authors. Since then, confirming the accuracy and advantages of the numerical modelling method based on the finite element method, the ability to applied numerical

modelling methods to other structures in the maritime field. The reliability and confidence of engineering calculations was improved when applying numerical modelling methods for structural calculations and analysis.

3. Finally, the author has applied the numerical modelling method to the ship's propulsion system. The mathematical models for the ship's propulsion system with many different assumptions are built to choose the most optimal ship propulsion model. Determined (point 2) stiffness of ship hull is used as the boundary conditions of the power transmission system. Apply the most optimal mathematical model of the ship propulsion system to analyse and align the shaft line of the typical ship propulsion system. Static and dynamic calculations analysis of the propulsion system is carried out and compared with allowed values.

In summary, the thesis has studied the effect of the numerical modelling method, namely the numerical modelling method based on the finite element method implemented in the Patran-Nastran software platform on errors and dispersion of results analysis of selected machinery and marine structures. From the analysis, this study the author can make some following assertions:

1. The impact of calculation assumptions on errors and dispersion of analysis results in individual types of analyses (static, normal modes, forced vibrations) was estimated.
2. An optimal methodology for carrying out computational analyses using the finite element method was developed for the ship's hull structure (including its superstructure and main engine body), taking into account the purpose of the calculations (static strength calculations, vibration analysis, thermal calculations, etc.).
3. An optimal methodology for conducting calculations using the finite element method was developed for the ship's power transmission system, taking into account the purpose of the calculations.
4. The developed calculation methods were verified by comparing them with experimental tests of selected elements of ship systems, together with determining the levels of measurement dispersions.

The author of the dissertation plans to develop the research of the dissertation in the future which is presented mainly through an effort to build a library of vibration data of all maritime structures and machines. This includes the construction of a library of vibration data that occurs when maritime structures and machinery are damaged and encounter problems from actual exploitation data of ship owners as well as shipping companies. From there, the author can build a reference data library when making comparisons between the results obtained from the construction of numerical models of maritime structures and machines and actual data. The software package will build to optimize the calculation model of the maritime structures taking into account the effects of the computational conditions such as vibration, thermal influence, ship strength of marine machines and structures. Construction software packages can become part of the structural health monitoring (SHM) system of marine structures, predict, diagnosed failures and the remaining working time of equipment.

## References

- [1] Aktan A. E., Helmicki A. J. and Hunt, V. J.: *Issues in Health Monitoring for Intelligent Infrastructure*, Smart Materials and Structures, Vol. 7, No.5, pp. 674-692, 1998.
- [2] Anderson T. L.: *Fracture Mechanics: Fundamentals and Applications*, 3rd ed. CRC Press; 2005.
- [3] Argyris J. H.: *Recent Advances in Matrix Methods of Structural Analysis*, Pergamon Press, Elmsford, NY, 1954.
- [4] Baker A. J.: *A Finite Element Computational Theory for the Mechanics and Thermodynamics of a Viscous Compressible Multi-Species Fluid*, Bell Aerospace Research Dept. 9500-920200, 1971.
- [5] Baker A. J.: *Finite Element Computational Fluid Mechanics*, Hemisphere Pub. Corp., Washington, D.C, 1983.
- [6] BAŠIĆ J., PARUNOV J.: *Analytical and numerical computation of added mass in ship vibration analysis*, Brodogradnja, 64:1-11, 2013.
- [7] Bardetsky A., Lee A.: *Analytical prediction of progressive structural failure of a damaged ship for rapid response damage assessment*, Proc. ASME 2014 33rd Int. Conf. Ocean. Offshore Arct. Eng., 2016, p. 1–9.
- [8] Becker E. G., Carey G. F., and Oden J. T.: *Finite Elements, an introduction*, Volume I, Prentice-Hall, Inc., Englewood Cliffs, NJ, 1981.
- [9] Becker A. J.: *An introductory guide to finite element analysis*, ASME Press, NY, 2004.
- [10] Bickford W. B.: *A First Course in the Finite Element Method*, Richard D. Irwin, Inc., Homewood, IL, 1990.
- [11] Brown, T. W. F.: *Vibration Problems from the Marine Engineering Point of View*, N. E. C. I., 1939.
- [12] Bulletin T., Che M., Science I., Moesli M., Science M., Science H. N., et al.: *Failure Analysis of A Marine Vessel Shaft Coupling*, 2012.
- [13] Camisetti C., Molinari R.: *Vertical and axial vibration of a ship propulsion system*. Quaderno no 49, pp. 16÷28, Genova 1982.
- [14] Chandrupatla T. R., and Belegundu A. D.: *Introduction to finite elements in engineering*, Prentice Hall, Upper Saddle River, NJ, 2002.
- [15] Chen Y. H., Bertran I. M.: *Parametric study of ship - hull vibrations*, International Shipbuilding Progress, Vol. 37, No 410, July 1990.
- [16] Clough, R. W.: *The Finite Element Method in Plane Stress Analysis*, Proc. 2nd Conf. Electronic Computations, ASCE, Pittsburgh, PA, pp. 345-378, 1960.
- [17] COWPER G. R.: *The shear coefficient in Timoshenko's beam theory*, Journal of Applied Mechanics, 33: 335-340, 1966.
- [18] Cook, R. D., Malkus, D. S., Plesha, M. E., and Witt, R. J.: *Concepts and Applications of Finite Element Analysis*, 4th ed., Wiley, New York, 2002.
- [19] Cui W. A.: *State of the art review on fatigue life prediction methods for metal structures*, J Mar Sci Technol 2002; 7:43–56.
- [20] Darcis, Ph., Lassen, T., Recho N.: *Fatigue Behaviour of Welded Joints Part 2 : Physical Modelling of the Fatigue Process*, Weld J 2006:19–26.

- [21] Desai, C. S.: *Elementary Finite Element Method*, Prentice-Hall, Inc., Englewood Cliffs, NJ, 1979.
- [22] Department of the Navy, Bureau of Ships, Interim Design Data Sheets, DDS-4301, "Propulsion Shafting," 1 Jan., 1960.
- [23] DE Technology for Design Engineering. Femap Used by Evektor in Aircraft Design and Development. <http://www.deskeng.com/articles/aaajps.htm>, July 2008.
- [24] Demidovich B. P., and Maron I. A.: *Computational mathematics*, MIR publisher, Moscow, 1982, translated from the Russian by G. Yankovski.
- [25] Det Norske Veritas. Fatigue Assessment of Ship Structures 2014.
- [26] Det Norske Veritas. Fatigue Methodology of Offshore Ships 2007.
- [27] Det Norske Veritas.: *Prevention of Harmful Vibration in Ships*, Printed in Norway by Det Norske Veritas, Oslo Norway, 1983.
- [28] Dimarogonas A.: *Vibration Engineering*, We, st Publishing, saint Paul, MN, 1976.
- [29] Djodjo B., Hofman M., Radojcic D., Motok M., Pejicic M.: *A case of excessive lateral vibrations of patrol boat shafting: Failures, analysis and solution*. Marine Technology and SNAME News, vol. 35, pp. 242÷256, October 1998.
- [30] Doebling, S. W., Farrar, C. R. and Prime, M. B.: *A summary review of vibration-based damage identification methods*, The Shock and Vibration Digest Vol. 30, Vol. 2, pp. 91–105, 1998.
- [31] Doebling S., Farrar C., Prime M., Daniel W.: *Damage identification and health monitoring of structural and mechanical systems from changes in their vibration characteristics: a literature review*. LA-13070-MS, May, 1996.
- [32] Doan. D. V., Murawski. L.: *The errors of the numerical calculations of the dynamic characteristics of cantilever beam mounted on the plate*, Journal of KONES Powertrain and Transport, Vol. 25, No.1, 2018.
- [33] Doan D. V., Szeleziński A., Murawski L., Muc A.: *Finite element method in modelling of ship structures part I – theoretical background*. Zeszyt Naukowe Akademii Morskiej w Gdyni, Vol.100, pp. 51-62, 2017.
- [34] Doan D. V., Szeleziński A., Murawski L., Muc A.: *Finite element method in modelling of ship structures part II – practical analysis example*. Zeszyt Naukowe Akademii Morskiej w Gdyni, Vol. 105, pp. 19-31, 2018.
- [35] Doan D. V., Murawski L.: *Vibration in marine power transmission system*, Scientific Journal of Gdynia Maritime University, Nr 100, pp. 37–50, 2017.
- [36] Doan D. V., Szeleziński A., Murawski L., Muc A.: *Modelling method of dynamic characteristics of marine thin-walled structure*, Journal of KONES Powertrain and Transport, Vol. 26, No. 4, pp. 39÷46, 2019.
- [37] Ern A., and Guermond, J. L.: *Theory and practice of finite elements*, Springer-Verlag, NY, 2004.
- [38] Finlayson, B.A.: *The Method of Weighted Residuals and Variational Principles*, Academic Press, NY, (1972).
- [39] Fitzgerald R. W.: *Mechanics of Materials* (2<sup>nd</sup> ed.), Addison-Wesley, Reading, MA, 1982.
- [40] Fletcher C. A. J.: *Computational Galerkin Methods*, Springer-Verlag, NY, 1984.
- [41] Galerkin B. G.: *Series Occurring in Some Problems of Elastic Stability of Rods and Plates*, Eng. Bull., Vol. 19, pp. 897-908, 1915.

- [42] Germanischer Lloyd, *Ship vibration*, Issue No. 5/2001.
- [43] Golub G. H. and Van Loan C. F.: *Matrix computations*, the Johns Hopkins University, 1996.
- [44] Gopalakrishnan S., Ruzzene M., Hanagud S.: *Computational Techniques for Structural Health Monitoring*, Springer-Verlag London Limited, 2011.
- [45] Guddati M. N., Yue B.: *Modified integration rules for reducing dispersion error in finite element methods*, *Comput. Methods Appl. Mech. Engrg.* 193 pp. 275–287, 2004.
- [46] Harris C. M.: *Shock and Vibration Handbook* (3<sup>rd</sup> ed.), McGraw-Hill, New York, 1988.
- [47] Heuser J.: "Finite Element Method for Thermal Analysis," NASA Technical Note TN-D-7274, Goddard Space Flight Center, Greenbelt, MD, 1972.
- [48] Hirowatari T.: *On the Natural Frequencies of Ships* (Part 2), *Journal of the Society of Naval Architects of Japan*, 92: 91-102, 1957.
- [49] Hollig K.: *Finite elements with B-splines*, *Society of Industrial and Applied Mathematics*, Philadelphia, PA, 2003.
- [50] Huebner K. H.: *Finite Element Method for Engineers*, John Wiley & Sons, NY, 1975.
- [51] Hutton D. V.: *Fundamentals of Finite Element Analysis*, McGraw-Hill, Boston, MA, 2004.
- [52] Hughes O. F.: *Ship structural design*, Jersey city New Jersey Society of Naval Architects and Marine Engineers 1988.
- [53] ISO 6954 (1984) Mechanical vibration and shock - guidelines for the overall evaluation of vibration in merchant ships.
- [54] ISO 6954 (2000) Mechanical vibration - guidelines for the measurement, reporting and evaluation of vibration with regard to habitability on passenger and merchant ships.
- [55] JIN X. D., ZHAO D.Y.: *Ship vibration*, Shanghai Jiaotong University Press, Shanghai, 2000.
- [56] Johnson C.: *Numerical Solution of Partial Differential Equations by the Finite Element Method*, Cambridge University Press, Cambridge, UK, 1987.
- [57] Juntunen J. S. and Tsiboukis T. D.: *Reduction of Numerical Dispersion in FDTD Method Through Artificial Anisotropy*, *IEEE Transactions on Microwave theory and techniques*, Vol. 48, No. 4, pp. 582-589, April 2000.
- [58] KUMAI T.: *On the estimation of natural frequencies of vertical vibration of ships*, *Journal of the Society of Naval Architects of Japan*, 121:175-182, 1967.
- [59] Lassen T., Darcis Ph., Recho N.: *Fatigue Behaviour of Welded Joints Part 1 - Statistical Methods for Fatigue Life prediction*, *Weld J*, 183–7, 2005.
- [60] Liu, G. R. and Quek, S. S.: *The finite element method: A practical course*, Butterworth-Heinemann, Boston, MA, 2003.
- [61] LR. Design and Construction, *Fatigue Design Assessment, Level 3 Procedure, Guidance on direct calculations* 2009:70.
- [62] Marie I., Andersen V., Jensen J. J.: *Hull Girder Fatigue Damage Estimations of a Large Container Vessel by Spectral Analysis*, pp. 557–65, 2013.
- [63] MAN B&W S70MC-C8, *Project Guide*, 1st Edition, May 2014.
- [64] MAN B&W 12K98ME-C(Mk7), *Project Guide*, 2nd Edition, April 2014.
- [65] MSC.Software. MSC Nastran: Industry Leading Multidisciplinary FEA Solution. <http://www.mscsoftware.com/product/msc-nastran>, 2016.

- [66] MSC.Software. MSC Nastran 2017: *Dynamic Analysis User's Guide*. MSC.Software Corporation, Santa Ana, CA 92707 USA, revision 0. November 25, 2016.
- [67] MSC.Software. MSC Nastran 2008, Quick reference guide. MSC.Software Corporation, Santa Ana, CA 92707 USA, 2008.
- [68] MSC.Software. MSC Nastran: Industry Leading Multidisciplinary FEA Solution. <http://www.mscsoftware.com/product/msc-nastran>, December 2012.
- [69] MSC.Software. MSC.Nastran 2018, *Quick Reference Guide*. MSC.Software Corporation, Santa Ana, CA 92707 USA, December 7, 2017.
- [70] Murawski L.: *Axial vibrations of a propulsion system taking into account the couplings and the boundary conditions*, Journal of Marine Science and Technology 2004; 9 (4):171-181.
- [71] Murawski L.: *Shaft line whirling vibrations: effects of numerical assumptions on analysis results*, Marine Technology and SNAME News; 42 (2), pp. 53-61, 2005.
- [72] Murawski L., Charchalis A.: *Analysis methods of crankshaft's stiffness characteristics*, Journal of KONES Powertrain and Transport, Vol. 20, No. 1, 2013.
- [73] Murawski L.: *Stiffness characteristics of main bearings foundation of marine engine*, Journal of KONES Powertrain and Transport, Vol. 23, No. 1, 2016.
- [74] Murawski L.: *Influence of journal bearing modelling method on shaft line alignment and whirling vibrations*. PRADS – Eighth International Symposium on Practical Design of Ships and Other Floating Structures, pp. 1205÷1212, Shanghai-China, Elsevier 2001.
- [75] Murawski L., *Shaft line alignment analysis taking ship construction flexibility and deformations into consideration*, Marine Structures Volume 18, Issue 1, , Pages 62-84, January 2005
- [76] Murawski. L.: *Forces exciting vibrations of ship's hull and superstructure*, POLISH MARITIME RESEARCH, No 4/2005, pp 15-21.
- [77] Murawski L., Charchalis A.: *Simplified method of torsional vibration calculation of marine power transmission system*, Marine Structures; Vol 39, pp. 335-349, 2014.
- [78] Muravin, B., Muravin, G., Lezvinsky, L.: *The Fundamentals of Structural Health Monitoring by the Acoustic Emission Method*, Proceedings of the 20th International Acoustic Emission Symposium, November 17-19, 2010, Kumamoto, Japan, pp. 253-258.
- [79] NAGAMOTO R.: *On the Natural Frequency of Main Hull Vibration*, Journal of the Society of Naval Architects of West Japan, 35, pp. 131-155, 1968.
- [80] Nestorides E. J.: *A handbook on torsional vibration*, Cambridge University Press, Cambridge 1958.
- [81] Noonan, E. F.: *Propeller Shaft Bending Stresses on the S.S. Esso Jamestown*, Journal of the A. S. N. E., August, 1961.
- [82] Oden, J. T.: *Finite Elements of Nonlinear Continua*, McGraw-Hill Book Publishers, NY, (1972).
- [83] OKADA Y.: *Shipbuilding design handbook*, The Kansai Society of Naval Architects, Tokyo, 1983.
- [84] Owen, D. R. J., and Hinton, E.: *A Simple Guide for Finite Elements*, Pineridge Press Limited, Swansea, UK, 1980.
- [85] Paulling J. R.: *Strength of Ships*, in "Principles of Naval Architecture", Vol. I, SNAME, 1988.

- [86] Prikšaitis J., Mažeika L., Barauskas R., Žukauskas E., Krišpinjnas A.: *Influence of the numerical dispersion effects in the modelling of ultrasonic measurements*, Physics Procedia 70, pp. 532 – 536, International Congress on Ultrasonics, ICU Metz, 2015.
- [87] Rao S. S.: *Mechanical Vibrations*, Addison-Wesley Publishing Company, 2000.
- [88] Rayleigh J. W. S.: *Theory of Sound*, 1st Revised edition, Dover Publishers, NY, 1877.
- [89] Reddy J. N.: *Introduction to the Finite Element Method*, McGraw-Hill Book Company, NY, 1993.
- [90] Reddy J. N.: *An introduction to nonlinear finite element analysis*, Oxford University Press, Oxford, UK, 2004.
- [91] Ritz, W.: "Über eine Neue Methode zur Lösung Gewisser Variations-Probleme der Mathematischen Physik," J. Reine Angew. Math., Vol. 135, pp. 1-61, 1909.
- [92] Richardson L. F.: *The approximate arithmetical solution by finite differences of physical problems*, Philosophical Transactions of the Royal Society A 210:307–357, 1910.
- [93] Ritchie R. O., Engineering M., Lankford J., Antonio S.: *Small Fatigue Cracks: A Statement of the Problem nad Potential Solutions*; 84:11–6, 1986.
- [94] Roache P. J.: *Computational Fluid Mechanics*, Hermosa Publishers, Albuquerque, NM, 1972.
- [95] Santos F. M., Temarel P., Guedes Soares C.: *Modal analysis of a fast patrol boat made of composite material*, *Ocean Engineering*, 36:179-192, 2009.
- [96] SENJANOVIĆ I., TOMAŠEVIĆ S., GRUBIŠIĆ R.: *Coupled horizontal and torsional vibrations of container ships*, *Brodogradnja*, 58:365-377, 2007.
- [97] SENJANOVIĆ I., GRUBIŠIĆ R.: *Coupled horizontal and torsional vibration of a ship hull with large hatch openings*, *Computers & Structures*, 41: 213-226, 1991.
- [98] SENJANOVIĆ I., ĆATIPOVIĆ I., TOMAŠEVIĆ S.: *Coupled horizontal and torsional vibrations of a flexible barge*, *Engineering Structures* 30:93-109, 2008.
- [99] Sea N., Centre L., Technology M.: *Fatigue fracture mechanics analysis of offshore structures*, 52–60, 1981.
- [100] Segerlind, L. J.: *Applied Finite Element Analysis*, John Wiley & Sons, NY, 1984.
- [101] Shama M.A.: *Marine Structural Safety and Economy*, *Mar Struct Insp Maintence Monit Symp*; 1:1–8, 1991.
- [102] Shang D., Yao W., Wang D.: *fatigue crack initiation size*, 20:683–7, 1998.
- [103] Smith, I. M.: *Programming the Finite Element Method*, John Wiley & Sons, NY, 1982.
- [104] Southwell, R. V.: *Relaxation Methods in Theoretical Physics*, Clarendon Press, 1946.
- [105] Syrocki M. Sc.: *Prediction of cavitation and propeller - induced excitations for propeller design No. RH-2000/T-153E*, Gdansk, October 2000.
- [106] Solin P., Segeth K., and Dolezel I.: *Higher-order finite element methods*, Chapman and Hall/CRC, Boca Raton, FL, 2004.
- [107] Szeleziński A., Muc A., Murawski L., Doan D. V.: *Introduction to the examination of thin-walled structures using the vibrodiagnostic method*, *Journal of KONES Powertrain and Transport*, Vol. 26, No. 4, pp. 241÷248, 2019.
- [108] Turner M., Clough R. W., Martin H. and Topp L.: "Stiffness and Deflection of Complex Structures," *J. Aero Sci.*, Vol. 23, pp. 805-823, 1956.
- [109] Todd F. H.: *Ship hull vibration*. London, Edward Arnold Ltd, 1961.

- [110] Weckner O., Brunk G.: *Numerical Dispersion Error in Finite Methods, Exemplified by the Perfectly Straight Beam Undergoing Bending Oscillations*, Technical Mechanics, Vol. 22, Issue 4, (2002), pp. 247-258.
- [111] WENG C.J.: *Estimation of natural frequency of free vibration for riverboat*, Journal of Wuhan University of Technology (Transportation Science & Engineering), 2:45-52, 1978.
- [112] Wilson W. K.: *Practical solution of torsional vibration problems*, Chapman and Hall Ltd, London 1963.
- [113] Yucel A., Arpacı A.: *Free and forced vibration analyses of ship structures using the finite element method*, Journal of Marine Science and Technology, 18:324-338, 2013.
- [114] Yumei Y., Hongyu C., Deyou Z., Ming H.: *Predicting method of natural frequency for ship's overall vertical vibration*, Shipbuilding Volume 65 Number 3, 2014.
- [115] Zienkiewicz O. C. and Cheung Y. K.: "*Finite Elements in the Solution of Field Problems*," The Engineer, Vol. 220, pp. 507-510, 1965.
- [116] Zienkiewicz O. C., Taylor R. L., and Zhu J. Z.: *The finite element method: Its basis and fundamentals*. Elsevier Butterworth-Heinemann, USA, sixth edition, 2005.
- [117] ZHAO D. Y.: *On the approximate calculation of the natural frequency of vertical modes of main hull vibrating*, Journal of Dalian University of Technology, 18:113-126, 1979.
- [118] ZHAO D. Y., LI Z. Y., HONG M.: *Practical approach to calculation of natural frequency of ship hull vibration*, Journal of Dalian University of Technology, 30:325-332, 1990.
- [119] ZHANG Y.M.: *Mechanical vibration*, Tsinghua University Press, Beijing, 2007.
- [120] ZHAO D. Y.: *Calculation method of natural frequency for ship's overall vibration*, China Biaozhun Publishing House, Beijing, 1993.

## List of figures

Fig. 1.1.	Modelling of real objects with their verification.....	10
Fig. 1.2.	A frequent view of engineers for computational and measurement errors.....	11
Fig. 1.3.	Dispersion of calculating a forced vibration empty tank and filled with water.....	11
Fig. 1.4.	Calculations and measurements of forced vibrations of the drive system.....	12
Fig. 1.5.	The results of strength calculations of the T-beam with different finite elements.....	15
Fig. 1.6.	Beam modelled without offset and with offset .....	15
Fig. 1.7.	Finite element model: superstructure, main engine body, and crankshaft.....	16
Fig. 1.8.	History of numerical methods.....	16
Fig. 1.9.	Typical elements using in the FE analysis.....	19
Fig. 1.10.	Geometry error of discretization for the domain bounded by a curve.....	23
Fig. 1.11.	MSC.Nastran solution flow.....	25
Fig. 1.12.	Workflow and files of the Patran and Nastran software.....	25
Fig. 1.13.	Main menu and figure depicting the origin point and the geometry Icon.....	26
Fig. 1.14.	Determination of material properties.....	26
Fig. 1.15.	Determination of material properties of elements.....	27
Fig. 1.16.	Create finite element mesh in the Patran software.....	27
Fig. 1.17.	Creating the loads and boundary conditions for the element.....	28
Fig. 1.18.	Determining analysis form and submitting analysis.....	29
Fig. 1.19.	Attaching the results from the Nastran file to the Patran software.....	29
Fig. 1.20.	Post-processing in the Patran-Nastran software.....	30
Fig. 1.21.	Equipment for testing stiffened plates using vibration methods.....	31
Fig. 1.22.	B&K calibrator [www.bksv.com access time 20.12.2018].....	32
Fig. 2.1.	Static load components on hull.....	37
Fig. 2.2.	Interaction of Weight and Buoyancy.....	37
Fig. 2.3.	Positive and negative stability.....	38
Fig. 2.4.	Bending moment development of a rectangular barge in still water.....	39
Fig. 2.5.	Wave bending moment in a regular wave.....	39
Fig. 2.6.	Typical transverse and longitudinal strength members.....	41
Fig. 2.7.	Main excitation sources (taken from [27]).....	44
Fig. 2.8.	Description of bearing forces and moments.....	44
Fig. 2.9.	Description of hull pressure forces and moments.....	45
Fig. 2.10.	Superstructure longitudinal vibration.....	46
Fig. 2.11.	Shaft line alignment for the container ship.....	47
Fig. 2.12.	Longitudinal vibration of shafting system.....	48
Fig. 2.13.	Torsional vibration of typical shafting system.....	49
Fig. 2.14.	Whirling vibration of shafting.....	49
Fig. 2.15.	External horizontal moments.....	50
Fig. 2.16.	External vertical moments.....	51
Fig. 2.17.	Lateral H-type moments.....	51
Fig. 2.18.	Lateral X-type moments.....	52
Fig. 2.19.	Overall process of Structural Health Monitoring.....	65
Fig. 3.1.	Mathematical model of the undamaged beam mounted on the plate.....	68
Fig. 3.2.	Model for calculating the moment of inertia of the beam cross section	68
Fig. 3.3.	A beam in bending.....	69
Fig. 3.4.	Beam property analysis by Patran software.....	73
Fig. 3.5.	Modes of vibration for the undamaged aluminium T-beam of 1D model.....	73
Fig. 3.6.	Modes of vibration for the undamaged aluminium T-beam of 2D model.....	73
Fig. 3.7.	Modes of vibration for the undamaged aluminium T-beam of 3D model.....	73
Fig. 3.8.	Mathematical model of the damaged beam with an open gap.....	75

Fig. 3.9.	Modes of vibration for T-beam of two-dimensional model.....	75
Fig. 3.10.	Modes of vibration for T-beam of three-dimensional model.....	75
Fig. 3.11.	The relative error of the natural frequencies of the undamaged beams with different boundary conditions.....	76
Fig. 3.12.	The relative error of the natural frequencies of the undamaged beam models with different mesh densities.....	77
Fig. 3.13.	The relative error of the natural frequencies of the undamaged beam models with the different finite elements.....	78
Fig. 3.14.	The relative error of the natural frequencies of the damaged beam models with different finite element.....	79
Fig. 3.15.	Computational models of the thin plate, respectively: 2D, 2-3D, 3-D and 3-D det.....	80
Fig. 3.16.	Natural vibration modes of analytical thin plates without water.....	83
Fig. 3.17.	Natural frequencies of the thin plate without water.....	83
Fig. 3.18.	Natural vibration modes of analytical thin plates coupled with fluid.....	87
Fig. 3.19.	Natural frequency of the thin plate coupled with fluid.....	88
Fig. 3.20.	Photograph of measuring model of thin plate, a) without water, b) with water....	89
Fig. 3.21.	Location of the transmitters during the tests.....	89
Fig. 3.22.	Response of the acceleration spectrum vibrates with the impact of the hammer of thin plate without water.....	89
Fig. 3.23.	Response of the acceleration spectrum vibrates with the impact of the hammer of thin plate coupled with water.....	90
Fig. 3.24.	Relative errors of calculations of the natural frequency of the thin plate without water.....	91
Fig. 3.25.	Relative errors of calculations of the natural frequency of the thin plate coupled with water.....	92
Fig. 3.26.	Computational models of the stiffened plate, respectively: 2D, 2-3D, 3-D and 3-D det.....	94
Fig. 3.27.	Natural vibration modes of analytical stiffened plates without fluid.....	97
Fig. 3.28.	Natural frequency of the stiffened plate without fluid.....	97
Fig. 3.29.	Natural vibration modes of analytical stiffened plates coupled with fluid.....	100
Fig. 3.30.	Natural frequency of the analysed stiffened plate coupled with water.....	101
Fig. 3.31.	Photograph of measuring model of stiffened plate.....	101
Fig. 3.32.	Location of the transmitters during the tests for stiffened plate.....	102
Fig. 3.33.	Response of the acceleration spectrum vibrates with the impact of the hammer of stiffened plate without water.....	102
Fig. 3.34.	Response of the acceleration spectrum vibrates with the impact of the hammer of stiffened plate coupled with water.....	103
Fig. 3.35.	Relative errors of calculations of the natural frequency of the stiffened plate without water.....	103
Fig. 3.36.	Relative errors of calculations of the natural frequency of the stiffened plate with water.....	104
Fig. 4.1.	Real model of the container ships, a) 2000 TEU, b) 11400 TEU.....	108
Fig. 4.2.	3D model of the medium size container ship of 2000 TEU.....	111
Fig. 4.3.	Vertical vibration of 2 nodes of the container ship 2000 TEU with water.....	111
Fig. 4.4.	Vertical vibration of 3 nodes of the container ship 2000 TEU with water.....	111
Fig. 4.5.	Vertical vibration of 4 nodes of the container ship 2000 TEU with water.....	112
Fig. 4.6.	Horizontal vibration of 2 nodes of the container ship 2000 TEU with water.....	112
Fig. 4.7.	Horizontal vibration of 3 nodes of the container ship 2000 TEU with water.....	112
Fig. 4.8.	Horizontal vibration of 4 nodes of the container ship 2000 TEU with water.....	113
Fig. 4.9.	Torsional vibration of the container ship 2000 TEU with water.....	113
Fig. 4.10.	Natural frequency of the medium size container ship 2000 TEU.....	113

LIST OF FIGURES

---

Fig. 4.11.	3D model of the large size container ship of 11400 TEU.....	114
Fig. 4.12.	Vertical vibration of 2 nodes of the container ship 11400 TEU with water.....	114
Fig. 4.13.	Vertical vibration of 3 nodes of the container ship 11400 TEU with water.....	114
Fig. 4.14.	Vertical vibration of 4 nodes of the container ship 11400 TEU with water.....	115
Fig. 4.15.	Horizontal vibration of 2 nodes of the container ship 11400 TEU with water.....	115
Fig. 4.16.	Horizontal vibration of 3 nodes of the container ship 11400 TEU with water.....	115
Fig. 4.17.	Horizontal vibration of 4 nodes of the container ship 11400 TEU with water.....	116
Fig. 4.18.	Torsional vibration of the container ship 11400 TEU with water.....	116
Fig. 4.19.	Natural frequency of the large size container ship 11400 TEU.....	116
Fig. 4.20.	3D model of the superstructure of the container ship 2000 TEU.....	117
Fig. 4.21.	Superstructure mode at 6.305 Hz.....	117
Fig. 4.22.	Superstructure mode at 7.924 Hz.....	118
Fig. 4.23.	Superstructure mode at 8.349 Hz.....	118
Fig. 4.24.	Superstructure mode at 12.877 Hz.....	118
Fig. 4.25.	Natural frequency of 2000 TEU container ship's deckhouses.....	119
Fig. 4.26.	The 3D model of the superstructure of container ship 11400 TEU.....	119
Fig. 4.27.	Superstructure mode at 1.722 Hz.....	119
Fig. 4.28.	Superstructure mode at 2.398 Hz.....	120
Fig. 4.29.	Superstructure mode at 3.465 Hz.....	120
Fig. 4.30.	Superstructure mode at 4.115 Hz.....	120
Fig. 4.31.	Natural frequency of 11400 TEU container ship's deckhouses.....	121
Fig. 4.32.	Comparison of vertical natural frequencies of container ship 2000 TEU.....	122
Fig. 4.33.	Comparison of vertical natural frequencies container ship of 11400 TEU .....	122
Fig. 4.34.	Comparison of horizontal natural frequencies container ship of 2000 TEU .....	123
Fig. 4.35.	Comparison of horizontal natural frequencies of container ship 11400 TEU.....	124
Fig. 4.36.	The hull resonance diagram of the container ship 2000 TEU.....	125
Fig. 4.37.	The hull resonance diagram of the container ship 11400 TEU.....	126
Fig. 4.38.	Nodes for forced vibration response.....	128
Fig. 4.39.	Location diagram of the main engine excitation forces.....	129
Fig. 4.40.	Excitation force graph of the main engine MAN B&W 8S70MC-C.....	130
Fig. 4.41.	Amplitudes of vibrations forced by the main engine of the container ship 2000 TEU.....	130
Fig. 4.42.	Vibration velocities on the wheelhouse of the container ship 2000 TEU .....	131
Fig. 4.43.	Vibration velocities main deck and the stern tube shafts of the container ship 2000 TEU.....	131
Fig. 4.44.	Vibration velocities at bottom of the superstructure of the container ship 2000 TEU .....	131
Fig. 4.45.	Vibration velocities at main engine of the container ship 2000 TEU.....	132
Fig. 4.46.	The excitation force graph of the main engine MAN B&W 12K98ME-C(Mk7)..	133
Fig. 4.47.	Amplitudes of vibrations forced by the main engine of the container ship 11400 TEU.....	134
Fig. 4.48.	Vibration velocities on the wheelhouse of the container ship 11400 TEU.....	134
Fig. 4.49.	Vibration velocities main deck and the stern tube shafts of the container ship 11400 TEU .....	134
Fig. 4.50.	Vibration velocities at bottom of the superstructure of the container ship 11400 TEU.....	135
Fig. 4.51.	Vibration velocities at main engine of the container ship 11400 TEU.....	135
Fig. 4.52.	Components of hydrodynamic loading on decks.....	136
Fig. 4.53.	Forced vibration of the container ship 2000 TEU acting by propeller hydrodynamic forces.....	137

Fig. 4.54.	Vibration velocities on the wheelhouse of the container ship 2000 TEU acting by propeller hydrodynamic forces.....	137
Fig. 4.55.	Vibration velocities on the main deck and the stern tube shafts of the container ship 2000 TEU acting by propeller hydrodynamic forces.....	137
Fig. 4.56.	Vibration velocities on the superstructure of the container ship 2000 TEU acting by propeller hydrodynamic forces.....	138
Fig. 4.57.	Vibration velocities on the main engine of the container ship 2000 TEU acting by propeller hydrodynamic forces.....	138
Fig. 4.58.	Forced vibration of the container ship 11400 TEU acting by propeller hydrodynamic forces.....	139
Fig. 4.59.	Vibration velocities on the wheelhouse of the container ship 11400 TEU acting by propeller hydrodynamic forces.....	139
Fig. 4.60.	Vibration velocities on the main deck and stern tube shaft of the container ship 11400 TEU acting by propeller hydrodynamic forces.....	140
Fig. 4.61.	Vibration velocities on the superstructure of the container ship 11400 TEU acting by propeller hydrodynamic forces.....	140
Fig. 4.62.	Vibration velocities at main engine of the container ship 11400 TEU acting by propeller hydrodynamic forces.....	140
Fig. 4.63.	Propeller excitation force acting diagram in loading condition.....	141
Fig. 4.64.	Amplitudes of vibrations forced by pressure impulses of the container ship 2000 TEU.....	142
Fig. 4.65.	Vibration velocities by pressure impulses on the wheelhouse of the container ship 2000 TEU.....	142
Fig. 4.66.	Vibration velocities by propeller pressure impulses on the main deck and the stern tube shafts of the container ship 2000 TEU.....	142
Fig. 4.67.	Vibration velocities by propeller pressure impulses on the superstructure of the container ship 2000 TEU.....	143
Fig. 4.68.	Vibration velocities by propeller pressure on the main engine of container ship 2000 TEU.....	143
Fig. 4.69.	Amplitudes of vibrations forced by pressure impulses of the container ship 11400 TEU.....	144
Fig. 4.70.	Vibration velocities by propeller pressure impulses at deck edge on the wheelhouse of the container ship 11400 TEU.....	144
Fig. 4.71.	Vibration velocities by propeller pressure impulses on the main deck and stern tube shaft of the container ship 11400 TEU.....	144
Fig. 4.72.	Vibration velocities by propeller pressure impulses at bottom of the superstructure of the container ship 11400 TEU.....	145
Fig. 4.73.	Vibration velocities by propeller pressure impulses at main engine before cylinder heads of the container ship 11400 TEU.....	145
Fig. 4.74.	Amplitudes of vibrations forced by total forces of the container ship 2000 TEU..	146
Fig. 4.75.	Vibration velocities by total excitation forces from the main engine and the propeller on the wheelhouse of the container ship 2000 TEU.....	146
Fig. 4.76.	Vibration velocities by total excitation forces from the main engine and the propeller on the main deck and the stern tube shafts of the container ship 2000 TEU.....	146
Fig. 4.77.	Vibration velocities by total excitation forces from the main engine and the propeller on the superstructure of the container ship 2000 TEU.....	147
Fig. 4.78.	Vibration velocities by total excitation forces from the main engine and the propeller on the main engine of the container ship 2000 TEU.....	147
Fig. 4.79.	Amplitudes of vibrations forced by total forces of the container ship 11400 TEU	147
Fig. 4.80.	Vibration velocities by total excitation forces from the main engine and the propeller on the wheelhouse of the container ship 11400 TEU.....	148

## LIST OF FIGURES

---

Fig. 4.81.	Vibration velocities by total excitation forces from the main engine and the propeller on the main deck and stern tube of the container ship 11400 TEU.....	148
Fig. 4.82.	Vibration velocities by total excitation forces from the main engine and the propeller on the superstructure of the container ship 11400 TEU.....	148
Fig. 4.83.	Vibration velocities by total excitation forces from the main engine and the propeller at main engine of the container ship 11400 TEU.....	149
Fig. 4.84.	Vibration limits.....	150
Fig. 4.85.	Percentage vibration due to different excitation sources at selected points of the container ship 2000 TEU at $n = 60$ rpm.....	152
Fig. 4.86.	Percentage vibration due to different excitation sources at selected points of the container ship 2000 TEU at $n = 80$ rpm.....	152
Fig. 4.87.	Percentage vibration due to different excitation sources at selected points of the container ship 2000 TEU at $n = 91$ rpm.....	152
Fig. 4.88.	Percentage vibration due to different excitation sources at selected points of the container ship 11400 TEU at $n = 70$ rpm.....	153
Fig. 4.89.	Percentage vibration due to different excitation sources at selected points of the container ship 11400 TEU at $n = 80$ rpm.....	153
Fig. 4.90.	Percentage vibration due to different excitation sources at selected points of the container ship 11400 TEU at $n = 100$ rpm.....	153
Fig. 5.1.	The typical structure sketch map of the marine propulsion system.....	155
Fig. 5.2.	Cross-section of the container ship 2000 TEU with the support positions.....	157
Fig. 5.3.	Cross-section of the container ship 11400 TEU with the support positions.....	158
Fig. 5.4.	Amplitudes of vibrations forced by the first excitation frequency of the propeller at the stern bearing according to horizontal and vertical.....	158
Fig. 5.5.	Amplitudes of vibrations forced by the first excitation frequency of the propeller at the intermediate bearing No.1 according to horizontal and vertical.....	159
Fig. 5.6.	Amplitudes of vibrations forced by the first excitation frequency of the propeller at the intermediate bearing No.2 according to horizontal and vertical.....	159
Fig. 5.7.	Vertical, dynamic stiffness characteristics of the container ship 2000 TEU .....	159
Fig. 5.8.	Vertical, stiffness characteristics of the container ship 2000 TEU at basic excitation frequencies $f = 0.1, 7.58$ and $12.13$ Hz.....	160
Fig. 5.9.	Horizontal, stiffness characteristics of the container ship 2000 TEU.....	160
Fig. 5.10.	Horizontal stiffness characteristics of the container ship 2000 TEU at basic excitation frequencies $f = 0.1, 7.58$ and $12.13$ Hz.....	160
Fig. 5.11.	Vertical stiffness of container ship 2000 TEU for shaft line foundation.....	161
Fig. 5.12.	Horizontal stiffness of container ship 2000 TEU for shaft line foundation.....	161
Fig. 5.13.	Amplitudes of vibrations forced by the first excitation frequency of the propeller at the main bearing No.1 according to horizontal and vertical.....	162
Fig. 5.14.	Amplitudes of vibrations forced by the first excitation frequency of the propeller at the main bearing No.5 according to horizontal and vertical.....	162
Fig. 5.15.	Vertical, dynamic stiffness characteristics of the container ship 2000 TEU for main bearings.....	163
Fig. 5.16.	Vertical, dynamic stiffness characteristics of the container ship 2000 TEU for main bearings at basic excitation frequencies $f = 0.1, 7.58$ and $12.13$ Hz.....	163
Fig. 5.17.	Horizontal, dynamic stiffness characteristics of the container ship 2000 TEU for main bearings.....	163
Fig. 5.18.	Horizontal, dynamic stiffness characteristics of the container ship 2000 TEU for main bearings at $f = 0.1$ Hz, $f = 7.58$ Hz, $f = 12.13$ Hz.....	164
Fig. 5.19.	Vertical stiffness of container ship 2000 TEU for main bearing.....	164
Fig. 5.20.	Horizontal stiffness of container ship 2000 TEU for main bearing.....	165
Fig. 5.21.	Amplitudes of forced vibrations of the container ship 11400 TEU.....	165
Fig. 5.22.	Vertical, dynamic stiffness characteristics of the container ship 11400 TEU .....	166

Fig. 5.23.	Vertical, dynamic stiffness characteristics of the container ship 11400 TEU .....	166
Fig. 5.24.	Horizontal, dynamic stiffness characteristics of the 11400 TEU container's ship.	166
Fig. 5.25.	Horizontal, dynamic stiffness characteristics of the 11400 TEU container's ship.	167
Fig. 5.26.	Vertical stiffness of container ship 11400 TEU for shaft line foundation.....	167
Fig. 5.27.	Bar graph for horizontal stiffness of container ship 11400 TEU for shaft line foundation.....	168
Fig. 5.28.	Model and support positions for local stiffness calculation of container ship 2000 TEU .....	168
Fig. 5.29.	Compare between local stiffness and whole stiffness of the container ship 2000 TEU.....	169
Fig. 5.30.	Model and support positions for local stiffness calculation of container ship 11400 TEU.....	169
Fig. 5.31.	Compare between local stiffness and whole stiffness of the container ship 11400 TEU.....	170
Fig. 5.32.	Compare the stiffness between the two container ships 2000 TEU and 11400 TEU at the basic excitation frequencies.....	171
Fig. 5.33.	Example of an acceptable crankshaft load field.....	173
Fig. 5.34.	Beam model of the shaft line, 3D view.....	175
Fig. 5.35.	FEM Mathematical model of the container ship's power transmission system....	175
Fig. 5.36.	Three-dimensional vibration model of a ship's propulsion system.....	175
Fig. 5.37.	Shaft line deflections under various assumptions of the mathematical model.....	176
Fig. 5.38.	Bearing deflections under various assumptions of a mathematical model.....	176
Fig. 5.39.	Deflection of shaft line with model 1D and 3D.....	177
Fig. 5.40.	Compare the deflection of the shaft line between 1-D and 3-D model.....	177
Fig. 5.41.	Deflections for all shaft line – hot condition, with hydrodynamic forces.....	178
Fig. 5.42.	Bending moments for all shafts connected – hot condition, with hydrodynamic forces.....	179
Fig. 5.43.	Bending stress for all shafts connected – hot condition, with hydrodynamic forces.....	179
Fig. 5.44.	Field of allowable crankshaft loads for various operating conditions, graphic interpretation of results.....	181
Fig. 5.45.	Deflection for shafting disconnected from M.E. – Cold condition.....	182
Fig. 5.46.	Deflection for crankshaft disconnected from shafting – Cold condition.....	183
Fig. 5.47.	Relative position of intermediate shaft flange and main engine crankshaft flange in cold condition.....	184
Fig. 5.48.	Model of the aft part of the container ship 2000 TEU with the propulsion system	185
Fig. 5.49.	Horizontal and vertical natural vibrations of the container ship 2000 TEU propulsion system.....	185
Fig. 5.50.	Vertical free vibrations of the drive system.....	186

## List of tables

Tab. 2.1.	Coefficient $A_n$ of natural of the ship overall vertical vibration.....	55
Tab. 2.2.	Coefficient $C_n$ of natural of the ship overall vertical vibration.....	56
Tab. 3.1.	Geometric properties of the T-beam model mounted on the plate.....	68
Tab. 3.2.	Common boundary conditions for the transverse vibration of a beam.....	72
Tab. 3.3.	Natural frequencies of the beam with different boundary conditions in theory....	72
Tab. 3.4.	Natural frequencies of the undamaged beam with different boundary conditions according to the numerical model-FEM.....	74
Tab. 3.5.	Natural frequencies of the undamaged beam with different mesh densities according to the numerical model-FEM.....	74
Tab. 3.6.	Natural frequencies of the undamaged aluminium beam with the different finite element according to the numerical model-FEM.....	74
Tab. 3.7.	Natural frequencies of the damaged aluminium beam with 2D and 3D elements according to the numerical model-FEM.....	75
Tab. 3.8.	Relative errors of natural frequencies of the undamaged beam with different boundary conditions.....	76
Tab. 3.9.	Relative error of natural frequencies of the undamaged beam with different mesh densities.....	77
Tab. 3.10.	Relative error of natural frequencies of the undamaged beam with the different finite element.....	77
Tab. 3.11.	Error of natural frequencies of the damaged beam with different finite element...	78
Tab. 3.12.	Geometric properties of the thin plate.....	80
Tab. 3.13.	Natural frequencies of calculation models without water (in the air).....	84
Tab. 3.14.	Natural frequencies of the thin plate coupled with fluid.....	88
Tab. 3.15.	Parameters of calculation model for the thin plate without water.....	91
Tab. 3.16.	Parameters of calculation model for the thin plate with water.....	91
Tab. 3.17.	Geometric properties of the stiffened plate.....	93
Tab. 3.18.	Natural frequencies of the stiffened plate without fluid.....	97
Tab. 3.19.	Natural frequencies of the stiffened plate coupled with fluid.....	100
Tab. 3.20.	Parameters of calculation model for the stiffened plate without water.....	103
Tab. 3.21.	Parameters of calculation model for the stiffened plate with water.....	104
Tab. 4.1.	Properties of the modelled ship 2000 TEU.....	107
Tab. 4.2.	Properties of the modelled ship 11400 TEU.....	107
Tab. 4.3.	Natural frequency of two container ships 2000 TEU and 11400 TEU.....	109
Tab. 4.4.	First three modes of natural frequency of vertical bending vibration.....	122
Tab. 4.5.	First three modes of natural frequency of horizontal bending vibration.....	123
Tab. 4.6.	Force and moment of the main engine MAN B&W 8S70MC-C at 91 rpm.....	129
Tab. 4.7.	Axial forced of main diesel engine MAN B&W 8S70MC-C.....	129
Tab. 4.8.	Horizontal forced of main diesel engine MAN B&W 8S70MC-C.....	130
Tab. 4.9.	Vertical forced of main diesel engine MAN B&W 8S70MC-C.....	130
Tab. 4.10.	The force and moment of the main engine MAN B&W 12K98ME-C(Mk7).....	132
Tab. 4.11.	Axial forced of main diesel engine MAN B&W 12K98ME-C(Mk7).....	133
Tab. 4.12.	Horizontal forced of main diesel engine MAN B&W 12K98ME-C(Mk7).....	133
Tab. 4.13.	Vertical forced of main diesel engine MAN B&W 12K98ME-C(Mk7).....	133
Tab. 4.14.	Propeller hydrodynamic forces of container ship 2000 TEU.....	136
Tab. 4.15.	Propeller hydrodynamic forces of container ship 11400 TEU.....	139
Tab. 4.16.	Propeller-induced pressure impulses on the transom of container ship 2000 TEU	141
Tab. 4.17.	Propeller-induced pressure pulses on the deck of container ship 11400 TEU.....	143
Tab. 4.18.	Overall frequency-weighted rms values.....	150
Tab. 4.19.	Forced vibration analyses results – maximum velocities (mm/s) of the container ship 2000 TEU .....	151

Tab. 4.20.	Forced vibration analyses results – maximum velocities (mm/s) of the container ship 11400 TEU .....	151
Tab. 5.1.	Vertical stiffness of the bearing foundation of the container ship 2000 TEU.....	161
Tab. 5.2.	Horizontal stiffness of the bearing foundation of the container ship 2000 TEU...	161
Tab. 5.3.	Vertical stiffness of the main bearing of the container ship 2000 TEU.....	164
Tab. 5.4.	Horizontal stiffness of the main bearing of the container ship 2000 TEU.....	164
Tab. 5.5.	Vertical stiffness of the foundation bearing of the container ship 11400 TEU.....	167
Tab. 5.6.	Horizontal stiffness of the foundation bearing of the container ship 11400 TEU	167
Tab. 5.7.	Local stiffness of the container ship 2000 TEU at the basic excitation frequencies.....	168
Tab. 5.8.	Local stiffness of the container ship 11400 TEU at the basic excitation frequencies.....	170
Tab. 5.9.	Local stiffness of the two container ships at the basic excitation frequencies.....	170
Tab. 5.10.	The deflection for variants model of the propulsion system.....	176
Tab. 5.11.	Summary the results of the calculation for all shafts connected-hot condition, with hydrodynamic forces.....	180
Tab. 5.12.	Summary the results of the calculation for all shafts connected-hot condition, without hydrodynamic forces.....	180
Tab. 5.13.	Summary the results of the calculation for all shafts connected-cold condition....	180
Tab. 5.14.	Boundary conditions of bending moment and shear forces acting on the crankshaft flange for the B&W 8S70ME engine.....	181
Tab. 5.15.	Summary the results of the calculation of shafting alignment for disconnected main engine (propeller shaft + intermediate shaft) – Cold condition.....	183
Tab. 5.16.	Summary the results of M.E. crankshaft alignment for main engine disconnected from shafting – Cold condition.....	183
Tab. 5.17.	Natural frequencies of the container ship 2000 TEU propulsion system determined using various mathematical models.....	186